Separation of Carbon Dioxide from Flue Gas (Post-Combustion Capture) via Gas Hydrate Crystallization

by

PRAVEEN LINGA

Bachelor of Technology (Chem. Eng.), University of Madras, 2000
Master of Technology (Chem. Eng.), Indian Institute of Technology, Kharagpur, 2002

A THESIS SUBMITTED IN PARTIAL FULFILLMENT OF THE REQUIREMENTS FOR THE DEGREE OF

DOCTOR OF PHILOSOPHY

in

THE FACULTY OF GRADUATE STUDIES

(Chemical and Biological Engineering)

THE UNIVERSITY OF BRITISH COLUMBIA
(Vancouver)

April 2009

ABSTRACT

This thesis examines the prospect of employing hydrate crystallization in a gas/liquid stirred vessel for separation of carbon dioxide (CO_2) from a flue gas mixture. A treated flue gas mixture contains CO_2, O_2 and N_2. Because O_2 and N_2 form hydrate at approximately same pressure-temperature conditions a model gas mixture to work with consists of 17 mol % CO_2 and 83 mol % N_2.

Gas hydrates were formed in a 323 cm^3 vessel at 273.7 K and constant pressures. The data enabled us to propose a process based on three hydrate stages coupled with a membrane separation stage. Two metrics, CO_2 recovery and separation factor were introduced to evaluate the efficiency of the process. The operating pressures were found to be 10, 5 and 2.5 MPa for the three stages. The high operating pressure required for the first stage necessitated the use of an additive to lower the pressure. Tetrahydrofuran (THF) was chosen and relevant thermodynamic and kinetic data were obtained and reported. The efficiency of the separation was also determined. It was concluded that a stream containing 96% CO_2 can be obtained from of a medium-pressure process consisting of three hydrate stages. The three stages operate at 2.5 MPa and 273.75 K without compromising the separation efficiency obtained without the addition of THF.

A new apparatus was designed and built to demonstrate the hydrate process at a larger scale. The results showed an improvement in the kinetics and the separation efficiency. Finally, the kinetics of the hydrate crystallization were also studied using a fixed bed of silica sand particles and the results were compared with those obtained in the gas/liquid systems. The gas uptake was found to be significantly higher for the systems involving water dispersed in silica sand.

TABLE OF CONTENTS

ABSTRACT ..... **ii**

TABLE OF CONTENTS ..... **iii**

LIST OF TABLES ..... **vii**

LIST OF FIGURES ..... **ix**

NOMENCLATURE ..... **xv**

ACKNOWLEDGEMENTS ..... **xvi**

DEDICATION ..... **xvii**

CO-AUTHORSHIP STATEMENT ..... **xviii**

1. LITERATURE REVIEW **1**

1.1. CO_2 capture and storage (CCS) 1

1.2. Background on gas hydrates 11

1.2.1. CO_2, N_2 and CO_2/N_2 mixed hydrates 17

1.3. Research objectives 23

1.4. Thesis organization 24

1.5. References 27

2. KINETICS OF HYDRATE FORMATION FROM A FLUE GAS MIXTURE **37**

2.1. Introduction 37

2.2. Experimental section 38

2.2.1. Materials 38

2.2.2. Apparatus and procedure 39

2.2.3. Calculation of the amount of gas consumed 41

2.2.4. Gas phase analysis 43

2.3. Results and discussion 43

2.4. Conclusions 53

2.5. References 54

3. THE CLATHRATE HYDRATE PROCESS FOR POST COMBUSTION CAPTURE OF CO_2 58

3.1. Introduction 58

3.2. The clathrate hydrate process 59

3.3. CO_2 recovery and separation factor 62

3.4. Results and discussion 63

3.5. Conclusions 68

3.6. References 70

4. THE MEDIUM-PRESSURE CLATHRATE HYDRATE/MEMBRANE HYBRID PROCESS FOR POST COMBUSTION CAPTURE OF CO_2 72

4.1. Introduction 72

4.2. Experimental section 72

4.3. Results and discussion 74

4.3.1. Phase equilibrium measurements 74

4.3.2. Gas uptake measurements 77

4.3.3. Proposed medium pressure hybrid process 86

4.3.4. Membrane unit for CO_2/N_2 separation 88

4.3.5. Comparison of hydrate process with membrane separation 90

4.3.6. Justification of the hybrid process 91

4.4. Conclusions 93

4.5. References 94

5. A NEW LARGE SCALE APPARATUS TO TEST CO_2 CAPTURE PROCESS VIA HYDRATE CRYSTALLIZATION 99

5.1. Introduction 99

5.2. Experimental section 101

5.2.1. A new large scale hydrate apparatus 101

5.2.2. Hydrate formation procedure for "batch operation" 105

5.2.3. Hydrate formation procedure for "semi-batch operation" 105

5.3. Results and discussion 106

5.4. Conclusions 123

5.5. References 125

6. ENHANCED RATE OF GAS HYDRATE FORMATION IN A SILICA SAND MATRIX COMPARED TO A STIRRED VESSEL 127

6.1. Introduction 127

6.2. Experimental section 129

6.2.1. Materials 129

6.2.2. Apparatus 129

6.2.3. Procedure for hydrate formation 130

6.2.4. Calculation of the amount of gas consumed during hydrate formation 132

6.3. Results and discussion 133

6.3.1. CH_4/water system 134

6.3.2. CH_4/C_3H_8/water system 138

6.3.3. CH_4/C_2H_6/water system 139

6.3.4. CO_2/water system 144

6.3.5. $CO_2/H_2/C_3H_8$/water system 145

6.3.6. CO_2/N_2/1.0 mol% THF system 146

6.4. Conclusions 150

6.5. References 152

7. CONCLUSIONS, CONTRIBUTION TO KNOWLEDGE AND RECOMMENDATIONS FOR FUTURE WORK 154

7.1. Conclusions 154

7.2. Contribution to the knowledge 156

7.3. Recommendations for future work 157

7.4. References 159

APPENDIX A 160

APPENDIX B 166

APPENDIX C 168

APPENDIX D 178

LIST OF TABLES

Table 1-1: Total carbon dioxide emissions (Mt) from fossil fuels in 1997, added by 2020 (Source: World Energy Outlook 2000) 2

Table 1-2: Worldwide capacity of potential CO_2 storage sites (Herzog, 2001). 6

Table 1-3: Structural properties of hydrates. 14

Table 1-4: Size ratio for CO_2 and N_2. 15

Table 2-1: Experimental conditions along with measured induction times and hydrate formation rates for $CO_2/N_2/H_2O$ system at 273.7 K. 47

Table 2-2: Vapor phase composition during hydrate formation from CO_2/N_2 mixture. .. 51

Table 3-1: Split fraction and separation factors for the three stages for CO_2/N_2 separation. 68

Table 4-1: Incipient equilibrium hydrate formation conditions for CO_2/N_2/THF/water system. 75

Table 4-2: Experimental conditions along with measured induction times and hydrate formation rates for CO_2/N_2/THF/H_2O system at 273.7 K. The CO_2/N_2 composition of the mixture was 16.9 mol % CO_2 and balance N_2. 80

Table 4-3: Vapor phase composition during hydrate formation from CO_2/N_2/THF system. 82

Table 4-4: Experimental conditions along with measured induction times and hydrate formation rates for hydrate formation from CO_2/N_2 mixtures corresponding to the initial gas phase composition for the three process stages at 273.7 K. 85

Table 4-5: Comparison of energy penalty between membrane separation process and hydrate process..... 90

Table 5-1: Experimental conditions along with measured induction times and hydrate formation rates for $CO_2/N_2/THF/H_2O$ system at 273.7 K. The CO_2/N_2 composition of the mixture was 16.9 mol % CO_2 and balance N_2. 110

Table 5-2: CO_2 composition at start and end of the experiment as analyzed by gas chromatography. 112

Table 5-3: Split fraction or CO_2 recovery and separation factor. 114

Table 5-4: Comparison of CO_2 recovery or split fraction between small and the new large scale apparatus. Both experiments run for 7 hours. 120

Table 6-1: Summary of experimental conditions along with the induction time and percent conversion of water to hydrates achieved at the end of the experiment. 151

LIST OF FIGURES

Figure 1-1: Methods for storing CO_2 in deep underground geological formations, Courtesy of Intergovernmental Panel on Climate Change, Special report on CO_2 Capture and Storage (IPCC, 2005). 8

Figure 1-2: Gas hydrate cavity structures. 13

Figure 1-3: Equilibrium hydrate formation conditions for pure carbon dioxide hydrate. 19

Figure 1-4: Equilibrium hydrate formation conditions for pure nitrogen hydrates. 20

Figure 1-5: Equilibrium hydrate formation conditions for $CO_2 - N_2$ mixtures. 21

Figure 2-1: Apparatus. 40

Figure 2-2: Incipient equilibrium hydrate formation conditions for CO_2/N_2 gas mixture.44

Figure 2-3: A typical gas uptake measurement curve together with the temperature profile in the aqueous phase (experiment 3, table 3-1)..... 45

Figure 2-4: Memory effect on hydrate formation for experiment carried out at 9.0 MPa and 273.7 K. 49

Figure 2-5: Rate of hydrate formation vs experimental pressure for the kinetic experiments given in Table 2-1..... 50

Figure 2-6: Mole consumption and molar ratio for the $CO_2/N_2/H_2O$ system at 11 MPa. 52

Figure 2-7: Mole consumption and molar ratio for the $CO_2/N_2/H_2O$ system at 10 MPa.. 53

Figure 3-1: Hydrate based gas separation. 60

Figure 3-2: Block diagram of the experimental methods for the hydrate formation kinetic and separation experiments. 62

Figure 3-3: Hydrate based separation for CO_2 (16.9 mol %) – N_2 (83.1 mol %) gas mixture (Temperature = 273.7 K, 120 Minutes growth). 64

Figure 3-4: Gas uptake measurement curve for the second stage (Pressure = 5.0 MPa & Temperature = 273.7K)..... 65

Figure 3-5: Gas uptake measurement curve for the third stage (Pressure = 2.5 MPa & Temperature = 273.7K)..... 66

Figure 3-6: Composition changes due to stage-wise hydrate formation from CO_2/N_2 mixtures..... 67

Figure 3-7: A hybrid hydrate-membrane process for CO_2 recovery from flue gas. 69

Figure 4-1: Incipient equilibrium hydrate formation conditions for 16.9 % CO_2 and rest N_2 gas mixture..... 76

Figure 4-2: Temperature-Composition equilibrium data for THF + water system (not isobaric condition). The symbols H_{II}, S, L, and G stand for s-II THF hydrate, solid (ice Ih), aqueous solution, and gas phases, respectively. The subscript 1 means that the THF composition is lower than the stoichiometric ratio of s-II THF hydrate, and 2 means a composition greater than the stoichiometric ratio (stoichiometric ratio of s-II THF hydrate is 5.56 mol%). Reprinted ("Adapted") with permission from Makino et al. (2005). Copyright 2005 American Chemical Society. 77

Figure 4-3: Gas uptake measurement for the CO_2/N_2/THF hydrate at 273.7 K and 2.2 MPa in the presence of 0.5 mol% THF (experiment 1). 78

Figure 4-4: Gas uptake measurement curves for 0.5, 1.0 and 1.5 mol% THF fresh solutions carried out at a driving force of 1.2 MPa or at a pressure of 2.15, 1.55 and 1.4 MPa, respectively. 81

Figure 4-5: Gas uptake measurement curves for 0.5, 1.0 and 1.5 mol% THF memory solutions carried out at a driving force of 2.2 MPa or at a pressure of 3.15, 2.55 and 2.35 MPa, respectively. 81

Figure 4-6: Gas uptake curves for 1.0 mol% THF concentration solutions with memory at 273.7 K and different pressures. 83

Figure 4-7: CO_2 content in the gas phase (initial composition), hydrate phase and residual gas phase (final composition) for the three process stages all operating at 2.5MPa and 273.7 K. 85

Figure 4-8. Gas uptake curves for hydrate formation with flue gas mixtures corresponding to the initial gas phase composition of the three process stages at 2.5 MPa and 273.7 K (the initial gas phase compositions are shown in Figure 4-7). 86

Figure 4-9: A hybrid hydrate-membrane process for CO_2 recovery from flue gas in the presence of THF as additive. Hydrate formation is carried out at 273.75 K and 2.5 MPa in the three stages. 87

Figure 4-10: Membrane separation process for flue gas separation, Reprinted from Herzog et al. (1991) with permission of John Wiley & Sons, Inc., Copyright 1991..... 89

Figure 5-1: Schematic of the apparatus. 102

Figure 5-2: Top and side view of the crystallizer with dimensions. 103

Figure 5-3: Cross section of the crystallizer with the stirrer and nozzle arrangement. .. 104

Figure 5-4: Effect of stirring rate on hydrate formation at 273.7 K and 2.5 MPa. The experiment was performed under a batch mode. 106

Figure 5-5: A typical gas uptake measurement curve carried out at 2.5 MPa and 273.7 K (experiment 3). 108

Figure 5-6: Gas uptake measurement curves for 1.0 and 1.5 mol% THF memory solutions carried out at a driving force of 2.2 MPa or at 2.5 and 2.3 MPa respectively. 109

Figure 5-7: Gas uptake curves for 1.0 mol% THF concentration solutions with memory at 273.7 K and different pressures. 113

Figure 5-8: Hydrate growth for a typical hydrate formation experiment (experiment 5) along with the calculated average rates for 20 min. 115

Figure 5-9: Rate of hydrate formation vs driving force for the kinetic experiments carried with 1.0mol% memory solutions. 116

Figure 5-10: Comparison of gas uptake for hydrate formation for 1.0 mol% (Pressure = 2.5 MPa, Temperature = 273.7 K). 118

Figure 5-11: Schematic of the mass transfer resistance encountered in the lab scale apparatus described in Chapter 2. 118

Figure 5-12: Comparison of the gas consumption for the lab scale apparatus and the new apparatus on a water free basis plotted against experimental pressure. 119

Figure 5-13: The normalized rate of gas supply calculated by taking into account of amount of water (equation 5.3) for the experiments conducted in the presence of 1.0 mol% THF in the lab-scale apparatus (Linga et al., 2008) and the new large scale apparatus plotted against the experimental pressure. 121

Figure 5-14: The normalized rate of gas supply calculated by taking into account of the volume of reactor (equation 5.4) for the experiments conducted in the

presence of 1.0 mol% THF in the lab-scale apparatus (Linga et al., 2008) and the new large scale apparatus plotted against the experimental pressure. 122

Figure 6-1: Schematic of the experimental apparatus..... 130

Figure 6-2: Comparison of gas uptake (hydrate growth) measurement curves for CH_4/water hydrate formation experiments. Time zero in the graph is induction time for the corresponding experiment (given in Table 6-1). 135

Figure 6-3: Comparison of the rate of methane uptake per mol of water for CH_4/water system. 135

Figure 6-4: Comparison of gas uptake (hydrate growth) measurement curves for CH_4/water hydrate formation experiment conducted in the same apparatus with and without the presence of silica sand. 137

Figure 6-5: Comparison of gas uptake (hydrate growth) for CH_4 (90.5%)/C_3H_8 (9.5%)/water system. Time zero in the graph is induction time for the corresponding experiment (given in Table 6-1)..... 138

Figure 6-6: Comparison of the rate of gas uptake for CH_4 (90.5%)/C_3H_8 (9.5%)/water system. 139

Figure 6-7: Comparison of gas uptake (hydrate growth) for CH_4 (91.0%)/C_2H_6 (9.0%)/water system. Time zero in the graph is induction time for the corresponding experiment (given in Table 6-1)..... 140

Figure 6-8: Comparison of gas consumption for all the three hydrocarbon containing systems. The experimental time is the same for both experiments carried for each system. 141

Figure 6-9: Comparison of temperature profiles and gas uptake for CH_4 (90.5%)/C_3H_8 (9.5%)/water system. 142

Figure 6-10: Comparison of temperature profiles and gas uptake for CH_4 (91.0%)/C_2H_6 (9.0%)/water system. 143

Figure 6-11: Comparison of gas uptake (hydrate growth) for CO_2/water system (Temperature = 1.0 C, Pstart = 3.1 MPa). Time zero in the graph is induction time for the corresponding experiment (given in Table 6-1). 144

Figure 6-12: Comparison of gas uptake (hydrate growth) for CO_2 (38.1%)/H_2 (59.4%)/C_3H_8 (2.5%)/water system (Temperature = 1.0 C, Pstart = 5.1 MPa). Time zero in the graph is induction time for the corresponding experiment (given in Table 6-1). 146

Figure 6-13: Comparison of gas uptake (hydrate growth) for CO_2 (16.9%)/N_2 (83.1%)/1.0 mol% THF system (Temperature = 1.9 C, Pstart = 2.5 MPa). Time zero in the graph is induction time for the corresponding experiment (given in Table 6-1). 147

Figure 6-14: Comparison of gas uptake (hydrate growth) for CO_2 (16.9%)/N_2 (83.1%)/1.0 mol% THF system (Temperature = 1.9 C, Pstart = 5.0 MPa). Time zero in the graph is induction time for the corresponding experiment (given in Table 6-1). 148

Figure 6-15: Comparison of gas consumption for all the three hydrocarbon containing systems. The experimental time is the same for both experiments carried for each system. 149

NOMENCLATURE

n_T	total number of moles
CR	crystallizer
SV	supply vessel
n_H	moles of the gas in Hydrate + Water phase of CR
n_G	moles of gas in gas phase of CR
n_{SV}	moles of gas in SV
Δn_H^i	mole consumption for *i* component in hydrate + liquid phase
t_{ind}	induction time (min)
V_G	volume of gas phase in CR
V_{SV}	volume of supply vessel
y_i	mole fraction in gas phase
$n_{CO_2}^{Feed}$	number of moles of CO_2 in feed gas
$n_{CO_2}^{H}$	number of moles of CO_2 in hydrate phase
$n_{N_2}^{H}$	number of moles of N_2 in the hydrate phase
$n_{CO_2}^{gas}$	number of moles of CO_2 in the gas phase at the end of the kinetic experiment
$n_{N_2}^{gas}$	number of moles of N_2 in the gas phase at the end of kinetic experiment
z	compressibility factor
THF	tetrahydrofuran
P	pressure
T	temperature
R	gas constant
IGCC	Integrated Gasification Combined Cycle

ACKNOWLEDGEMENTS

I would like to acknowledge the following people and organizations that helped me in various ways throughout the duration of this project.

Firstly, I am very grateful to my supervisor, Professor Peter Englezos for his support, skilful guidance and encouragement throughout my doctoral studies to accomplish this challenging research project. I would also like to extend my gratitude to Dr. John A. Ripmeester with whom I had meaningful discussions and encouragement when he visited our lab at UBC.

I would also like to thank Natural Science and Engineering Research Council of Canada (NSERC), Canada Foundation for Innovation (CFI) and Natural Resources Canada (NRCan) for providing funding for this project.

I would also like to extend this acknowledgement to my colleagues and friends in the gas Hydrate and PPC labs: Rajnish Kumar, Shivamurthy Modgi, Rajeev Chandraghatgi, Dr. Judong Lee, Robin Susilo, Professor Myungho Song, Hui-Jie Wu, Dr. Xiaosen Li, Nayef Al-Saifi, Adebola Adeyemo, Dr. Sung-Chan Nam, Cef Haligva, Jeffry Yoslim and Nagu Daraboina for their help and support. A special thanks to Rajnish Kumar for all the discussion and fun I had with him while working together in the lab. Last but not least, I would like to thank my family, particularly my wife, Sandhya for being patient and supportive during difficult times during my research work.

Dedicated to my parents

and

To my wife and my brother

CO-AUTHORSHIP STATEMENT

The work of this thesis consists of six different manuscripts which correspond to chapters two to six. The authors include Linga P., Kumar R., Adeyemo A., Haligva C., Ripmeester, J.A., and Englezos P. Professor Peter Englezos is my principal research supervisor at the University of British Columbia. During the course of my research, I was fortunate enough to hold meaningful discussions with Dr. John A. Ripmeester who is a principal research officer at SIMS, National Research Council Ottawa. Kumar R. (Ph.D.), Adeyemo A. (MASc) and Haligva C. (MASc) are fellow researchers in our lab.

The literature review, experimental design, performing experiments and data analysis were done extensively by P. Linga under supervision of Professor P. Englezos. In some part of the work R. Kumar, A. Adeyemo and C. Haligva provided assistance with the experiments. Finally, I did the final preparation for each manuscript after careful revision and approval of my research supervisor.

1. LITERATURE REVIEW

1.1. CO_2 capture and storage (CCS)

Carbon dioxide and other chemicals such as methane (CH_4), nitrous oxide (N_2O) and chlorofluorocarbons (CFCs) are known collectively as greenhouse gases because of their ability to absorb infrared radiation that leads to a rise in atmospheric temperature (global warming). CO_2 has the highest concentration in the atmosphere and hence it is considered the dominant greenhouse gas. Global warming is likely to induce large climatic changes with many consequences. Consequently, global warming has become an enormously serious problem (Shindo and Komiyama, 1994). Thus, the urgent need to prevent carbon emissions produced by human activities from reaching the atmosphere.

Energy related activities are by far the largest source of greenhouse gas emissions. The energy sector includes emissions of all greenhouse gases from the production of fuels and their combustion for power generation. Though estimates vary, world total primary energy consumption is projected to increase by 57 percent between 1997 and 2020. Under the Reference scenario of the World Energy Outlook (2000), fossil fuels will account for around 90 percent of the world primary energy supply mix by 2020. One major implication on reliance on fossil fuels, however, is the environmental consequences of their use. Use of fossil fuels may cause a number of environmental impacts, ranging from global climate change to regional and local impacts on air, land and water. Although the specific issues vary these impacts are concerns throughout the world. Hence, even with environmental policies in place, increasing demand for energy will be accompanied by an increase in emissions world wide. According to the

Intergovernmental Panel on Climate Change (IPCC) Special Report on Emission Scenarios (SRES), the future emissions of CO_2 are projected on the basis of six illustrative scenarios in which global CO_2 emissions range from 29 to 44 $GtCO_2$ (8–12 GtC) per year in 2020, and from 23 to 84 $GtCO_2$ (6–23 GtC) per year in 2050. It is also projected that the number of CO_2 emission sources from the electric power and industrial sectors will increase significantly until 2050, mainly in South and East Asia. As seen in Table 1-1, global CO_2 levels under the reference scenario will increase across the world by 60 %, or 13,697 Mt, between 1997 and 2020. Emissions will be specifically influenced by power generation which alone will account for 43 % of the increase in global CO_2 emissions over the next twenty years.

Table 1-1: Total carbon dioxide emissions (Mt) from fossil fuels in 1997, added by 2020 (Source: World Energy Outlook 2000)

Region	CO_2 Emissions (1997)	Added by 2020
OECD		
Coal	3952	331
Oil	5195	1221
Gas	2320	1280
Developing countries		
Coal	4012	3656
Oil	3537	3833
Gas	980	1972
Transition Economies		
Coal	792	336
Oil	652	383
Gas	1119	529
World		
Coal	8758	4324
Oil	9806	5592
Gas	4419	3781

Because climate change will have world-wide implications various courses of action are being considered internationally to reduce greenhouse gas emissions, the root

cause of the climate change problem (Freund, 1997). Four broad options are typically considered for reducing anthropogenic emissions of greenhouse gases and CO_2 in particular (carbon management): (a) improvement in energy efficiency in power generation or in end-use; (b) switching to fuels containing less carbon (e.g. natural gas); (c) substitution of electricity from carbon-free sources (e.g. renewable or nuclear); (d) Carbon dioxide capture and secure storage (CCS). The capture and secure storage of carbon dioxide that would otherwise be emitted to the atmosphere is defined as CO_2 sequestration (IPCC, 2005).

In practice it is unlikely that any single approach would be used alone. Most likely, a combination of these four options will be adopted to meet particular needs. According to the IPCC report on climate change, CCS will play an important role among mitigation strategies for global warming (IPCC, 2005). This report provides a detailed assessment of the current state of knowledge regarding the technical, scientific, environmental, economic and societal dimensions of CCS. The projected potential of CO_2 capture associated with the emission ranges explained above has been estimated at an annual 2.6 to 4.9 $GtCO_2$ by 2020 (0.7–1.3 GtC) and 4.7 to 37.5 $GtCO_2$ by 2050 (1.3–10 GtC). These numbers correspond to 9–12%, and 21–45% of global CO_2 emissions in 2020 and 2050, respectively (IPCC, 2005). The advantage of removing carbon dioxide from flue gases is that it will enable society to continue using fossil fuels and enjoy the standard of living that was attained over the years while minimizing the impact on the environment.

There are three broad based methods for carbon dioxide sequestration: (a) biological which exploits the natural process through which biomass accumulates CO_2

directly from the atmosphere i.e. biofixation-forestry, biofixation-microalgae; (b) geological which involves capture of CO_2 from large scale industrial processes e.g. power generation and its subsequent transport and storage to a suitable geological formation; and (c) ocean which mainly involves direct dissolution of captured CO_2 or injection at depths greater than 1 km.

There are two general approaches to capture CO_2: either carbon can be removed before the fuel is burned (*pre-combustion capture*) or CO_2 can be removed from the flue gas (*post-combustion capture*). Post-combustion capture deals with CO_2 from conventional power plants. On the other hand Integrated Gasification Combined Cycle (IGCC) plants offer one of the most promising routes to CO_2 capture by converting the gas from the gasifier into a stream of H_2 and CO_2 via a shift reaction (Barchas and Davis, 1992). CO_2 can then be removed for disposal and the resultant H_2 could be used in fuel cells or in gas turbines.

Separation of CO_2 from natural gas mixtures has been practiced in the past in order to recover CO_2 and meet gas specifications and also use it in enhanced oil recovery projects. A variety of processes have been developed for removing or isolating a particular gaseous component from a multi-component gaseous stream. These processes include absorption, adsorption, membrane separation etc. (Aaron and Tsouris, 2005; Barchas and Davis, 1992; Kikkinides et al., 1993). Commercial CO_2 separation plants employ chemical absorption with a solvent like monoethanolamine that selectively absorbs CO_2. This process requires a significant amount of energy, a key energy requirement for this process is the regenerator reboiler duty which accounts for 32-53% of the energy in the coal (Herzog et al., 1991). Also, some of the key operational

concerns for amine based separation process are corrosion, foaming, and solvent degradation (Herzog et al., 1991). In order to employ chemical absorption for CO_2 capture formulation of new solvents and reduction of equipment size are required in order to reduce energy costs (Herzog et al., 1997). The thorough review of the processes for post and pre combustion capture of CO_2 by Aaron and Tsouris (2005) concluded that absorption using amines is considered to be the most promising current method while some others are promising but too new for comparison. There is continued interest in the development of less energy intensive processes such as adsorption using materials like zeolites and pressure swing adsorption (PSA) which is employed in the natural gas industry for the separation of CO_2. Use of polymeric membranes for separating CO_2 from flue gases has also been reported (Ho et al., 2006a,b; Shingo et al., 2004).

One of the new promising methods for separating CO_2 from flue gas or fuel gas (mixture of CO_2 and H_2) is through clathrate or gas hydrate formation (Englezos and Lee, 2005; Han et al., 2007; Kang and Lee, 2000; Klara and Srivastava, 2002). Clathrate or gas hydrates are crystals formed by water molecules and a number of substances such as CO_2, N_2, O_2, H_2, and natural gas components (Davidson, 1973; Englezos, 1993; Ripmeester, 2000; Sloan, 1998). When gas hydrate crystals are formed from a mixture of gases, the concentration of these gases in the hydrate crystals is different than that in the original gas mixture. This is the basis for the utilization of clathrate hydrate formation/decomposition as a separation process.

Once CO_2 has been captured, it can be stored or utilized in order to prevent emissions from reaching the atmosphere. CO_2 can be used in enhanced oil recovery (EOR) and to make solid carbonate minerals. Large quantities of CO_2 could be stored in

the deep oceans or geological locations or sequestered in terrestrial ecosystems. Preliminary estimates of these capacities have been made but as represented in Table 1-2 there is a large range. Efforts are underway throughout the world to establish more accurate worldwide and national estimates and eventually establish standards for site selections.

Table 1-2: Worldwide capacity of potential CO_2 storage sites (Herzog, 2001).

Sequestration Option	**Worldwide Capacity ($GtCO_2$)**
Ocean	1000^2 to uncertain
Deep Saline Formations	1000 – uncertain, but possibly 10^4
Depleted Oil and Gas Reservoirs	675 – 900
Coal Seams (ECBM)	3 – 200

A major effort was devoted towards the development of technology for Ocean Disposal. This is not surprising since the ocean has a capacity of storing 10,000 Gigatons of Carbon (GtC) compared to a 1000 GtC capacity of depleted oil and gas reservoirs and 20 GtC of unminable coal seams. While these estimates vary, the deep ocean has by far the largest storage potential. It is noted that the annual global CO_2 emissions amount to an equivalent of 22 GtC (Herzog et al., 1997). The majority of work on CO_2 sequestration in the ocean concerned laboratory and modeling studies. However, these are insufficient to evaluate such a complex system and ocean CO_2 injection trials should be attempted to assess the viability of the technology (Sloan, 2000). One such trial concerned injection of liquid CO_2 into the Norwegian Sea but was cancelled by Norway's environment ministry

because the "*the use of deep sea areas as potential places for CO_2 must first be thoroughly discussed at the international level and clarified legally*". This trial would have been the world's first attempt to demonstrate sequestration of CO_2 in oceans by injecting liquid CO_2. A similar trial off the coast of Hawaii has also been cancelled. Therefore, there are serious concerns regarding ocean disposal of liquid CO_2 and alternative storage techniques such as dry ice and carbon dioxide hydrate and sites e.g. deep ocean aquifers are explored (Takahashi et al., 2000; Yamasaki, 2000).

Since there is a serious concern about ocean disposal as a mitigation option research work on geological storage (in depleted oil gas reservoirs, deep saline aquifers, deep unminable coal beds and mineralization) is underway in Canada, European Union, U.S., Australia and Japan (McKee, 2002). Figure 1-1 shows the various technological options for storing CO_2 in deep underground geological formations. Depending on the formation, CO_2 can be sequestered by a combination of three mechanisms: (a) hydrodynamic trapping (it is trapped as gas or supercritical fluid under a low-permeability cap rock similar to the way that natural gas is trapped in gas reservoirs or stored in aquifer gas storage); (b) solubility trapping (the CO_2 dissolves into the fluids); and (c) mineral trapping (the CO_2 reacts directly or indirectly with the minerals and organic matter in the formation to become part of a solid matrix (McKee, 2002).

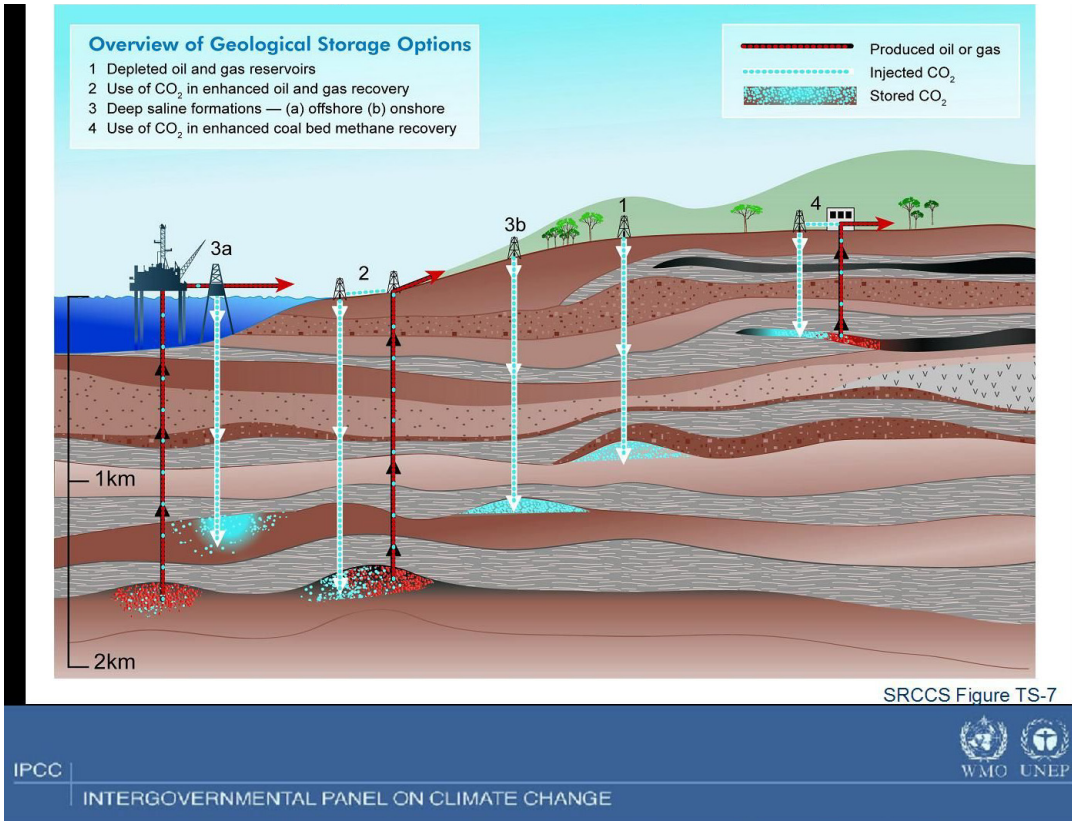

Figure 1-1: Methods for storing CO_2 in deep underground geological formations, Courtesy of Intergovernmental Panel on Climate Change, Special report on CO_2 Capture and Storage (IPCC, 2005).

Geological storage is actually being demonstrated in Norway where CO_2 from gas fields is stored in an undersea aquifer in the North Sea (Herzog et al., 1997; McKee, 2002). Because CO_2 and water forms solid gas hydrate under suitable temperature and pressure conditions hydrate formation may prevent the pumping of liquid CO_2 into deep saline aquifers. However, according to Takahashi et al. (2000) the temperature conditions due to geothermal heat fluxes raise the minimum pressure for hydrate formation above the hydrostatic pressure at the aquifer. However storage of CO_2 in oil reservoirs where CO_2 can enhance oil recovery enables the oil and gas industry to practice CO_2 capture and storage within the Kyoto time frame (2008-2012).

According to the IPCC (2005) special report on CO_2 capture and storage, the cost of capture of CO_2 from coal or gas fired power plants would be in the range of 15-75 US$/t$CO_2$ net captured. The cost of pipeline transport for a nominal distance of 250 km would be typically in the range of 1-8 US$/t$CO_2$ transported. The representative estimates of the costs for storage in saline formations and depleted oil and gas fields would be typically between 0.5-8 US$/t$CO_2$ injected while the costs of monitoring are 0.1-0.3 US$/t$CO_2$ additional. When storage is combined with EOR or ECBM or potentially Enhanced gas recovery (EGR), the economic value of CO_2 can reduce the total cost of CCS. Based on data and oil prices prior to 2003, it is reported that enhanced oil production for onshore EOR with CO_2 storage could yield net benefits of 10-16 US$/t$CO_2$ (including the costs of geological storage). All the above estimates were reported based on the cost for large-scale, new installations, with natural gas prices assumed to be 2.8-4.4 US$ GJ^{-1} and coal prices 1-1.5 US$ GJ^{-1} (IGCC, 2005).

Thus, technologies exist and are being developed that can prevent emissions from the production and use of fossil fuels from reaching the atmosphere. They are discussed in detail in a Technology Status Report from the International Energy Agency (McKee, 2002). The report concludes that a number of these technologies have not been optimized. Thus, it is recommended that *R&D* of the science and technology underlying each capture and storage option is continued in order to improve existing technologies and enable development of critical new components that can optimize capture and storage systems. Furthermore, the focus should be directed towards reducing costs and developing effective, safe and environmentally sound storage options. Recently in July 2008 at a summit in Hokkaido (Japan), the G8 (Britain, Canada, France, Germany, Italy,

Japan, Russia and United States) countries agreed in principle to the recommendations given by carbon sequestration leadership forum (CSLF) to diversify a portfolio of at least 20 fully integrated industrial scale installations (larger than 1 Mt per year). The expectation is that supporting technology learning and cost reduction will enable the broad deployment of CCS by 2020 (CSLF, 2008). The report also highlights the need for well-resourced research and development to drive the capture costs down to the levels needed for widespread deployment in the power sector. In addition to technology development optimization strategies have been proposed to tackle large single source emissions. For example, Elkamel and his group have focused on the Canadian oil sands industry, the petroleum refining industry and power generation (Ba-Shammakh et al., 2007; Elkamel et al., 2008; Ordorica-Garcia et al., 2008).

This thesis focuses on gas or clathrate hydrate crystallization for CO_2 separation from flue gas mixtures. Interestingly, gas hydrate formation also plays a role during ocean or geological sequestration and deep saline aquifers (Takahashi et al., 2000; Yamasaki, 2000). *The goal of this thesis is to examine the formation of hydrates from flue gas mixtures in order to obtain thermodynamic and kinetic data relevant to the hydrate-based process for CO_2 mitigation*. *Moreover, the thesis will propose relevant conceptual process flowsheets and assess their economic potential and scale up.*

Next the thesis presents essential background information on gas hydrates. This background information provides the framework and foundation to present and discuss the specific research objectives of the thesis (Section 1.3).

1.2. Background on gas hydrates

Clathrates are non-stoichiometric crystalline compounds (Davidson, 1973; Englezos, 1993; Makogon, 1981; Ripmeester, 2000; Sloan, 1998). They consist of two molecular species, one physically entrapping the other by making up a cage-like structure containing cavities. There are two categories of clathrates; those where the cage or lattice like structure is made up of water molecules bonded together, and those built up by molecules other than water. The first group mentioned is known as clathrate hydrates or gas hydrates.

In a hydrate, the species forming the lattice is commonly called the host, while the caged component is called the guest. In clathrate hydrates, the host-lattice is created by water molecules connected together through hydrogen bonding. The host-lattice is thermodynamically unstable without the presence of a guest molecule in the cavity. The guest molecule is held in place inside cavities of the hydrogen-bonded water molecules. The lattice is stabilized by van der Waals forces between host and guest molecules. It is important to note that there is no chemical bonding between the host-lattice and guest molecule, and that only one guest molecule is contained in each cavity. Recently, it was found that under certain T and P condition, more than one H_2 molecules can be trapped in a cavity (Florusse et al., 2004; Mao et al., 2002; Sluiter et al., 2004).

There are three known gas hydrate structures: Structure I; Structure II; Structure H (Ripmeester et al., 1987). Structure I consist of two different types of cavities. The first cavity is formed when water molecules hydrogen bond in such a way that they form a structure with 12 faces and 5 sides to each face called a pentagonal dodecahedron (5^{12}). This cavity or cage is present in all three gas hydrate structures.

When the pentagonal dodecahedral cages link together by their vertices a second type of cavity is created, a polyhedron with 12 pentagonal and 2 hexagonal faces ($5^{12}6^2$) called a tetrakaidecahedron, which is larger than the dodecahedron. A unit cell of this structure consists of six large $5^{12}6^2$ cavities, and two small 5^{12} cavities created by 46 water molecules. Only small molecules with a diameter between 4.2-6.0 Å, can form structure I hydrates. Common structure I forming gases are methane, ethane and carbon dioxide. When the pentagonal dodecahedral cages link together through face sharing, not by the vertices as in structure I, then the structure is known as structure II. By linking together through face sharing, they create a hexakaidecahedron, a polyhedron with 12 pentagonal and 4 hexagonal faces. Structure II hydrate consists of 16 small and 8 large cavities made up by 136 water molecules. Molecules forming structure II have a diameter less than 4.2 $\overset{o}{A}$ and between the range of 6-7 $\overset{o}{A}$. Some examples of structure II forming substances are nitrogen, propane, tetrahydrofuran and iso-butane.

Structure H was discovered in 1987 by Ripmeester et al (1987). It consists of three different kinds of crystal cavities, two which are small and of comparable sizes, and one large non-spherical cavity. It is unique compared to the two previous structures because it requires molecules of two different sizes to stabilize the crystal. Like structure I and structure II, structure H has the basic 5^{12} cage. The two other cavities are: a $4^3 5^6 6^3$ cage which has three fairly strained square faces, six pentagonal and three hexagonal faces and a large $5^{12}6^8$ cage made up of twelve pentagonal and eight hexagonal faces. The latter cavity is the largest hydrate cavity of any of the structures and is estimated to fit guests up to 9 $\overset{o}{A}$ in diameter. The shapes of all the cavities formed in structure I, Structure II and structure H are shown in Figure 1-2.

Small (S)	Medium (M)	Large (L)	Structure (Formula)
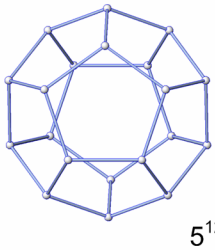 5^{12}		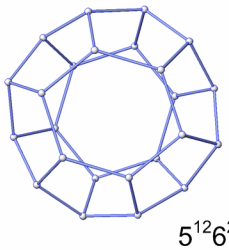 $5^{12}6^{2}$	Structure I (sI) $2S.6L.46H_2O$
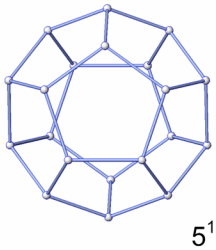 5^{12}		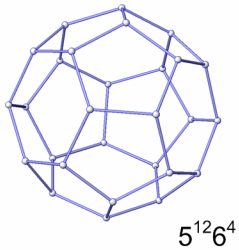 $5^{12}6^{4}$	Structure II (sII) $16S.8L.136H_2O$
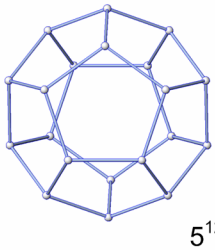 5^{12}	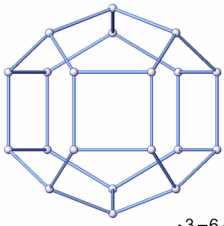 $4^{3}5^{6}6^{3}$	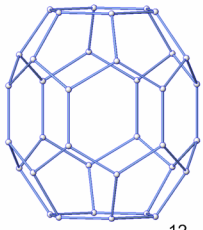 $5^{12}6^{8}$	Structure H (sH) $3S.2M.1L.34H_2O$

Figure 1-2: Gas hydrate cavity structures.

One unit cell of structure H can contain at most one large molecule, five small and 34 water molecules. Another feature of structure H hydrate that makes it unique compared to the two other structures is that it is not enough for the large molecule in structure H to have the right size as for structure I and structure II, the shape and efficient space filling is also important. Small molecules, known as help guests, such as methane, xenon or hydrogen sulfide, can occupy the two small cages in structure H, while intermediate sized hydrocarbons such as adamantane, cycloheptane or 2,2-dimetylbutane, also known as neohexane, can fill the large cavity of structure H.

Table 1-3 compares the structural properties of structures I, II and H. The structure of hydrate that is formed is primarily a function of the gas(es) used to form the hydrate. In certain cases, such as when hydrates are formed from mixtures of methane and ethane, there is a structural transition that is a function of the feed gas composition (Subramanian et al., 2000).

Table 1-3: Structural properties of hydrates.

	Structure I	Structure II	Structure H
Cavity types	5^{12}, $5^{12}6^2$	5^{12}, $5^{12}6^4$	5^{12}, $4^3 5^6 6^3$, $5^{12}6^8$
Radius (A)	3.91, 4.33	3.902, 4.683	3.91, 4.06, 5.71
Cages/unit cell	2, 6	16, 8	3, 2, 1
Co-ordination number	20, 24	20, 28	20, 20, 36
Crystal type	Cubic	Cubic	hexagonal

Sloan and Koh (2008) suggested that it would be instructive to consider the diameter ratio of guest molecules to each cavity for simple (single guest) hydrate formers to determine the upper and lower limits to guests size. In order to obtain a stable hydrate structure the ratio needs to be approximately in the range of 0.76-1.0. If the ratio is less than 0.76, the molecular attractive forces contribute less to cavity stability and if the ratio is above 1.0, the guest molecule cannot fit into a cavity without distortion (Sloan and Koh, 2008). The molecular diameters to cavity diameter ratios for nitrogen and carbon dioxide gases are shown in Table 1-4. CO_2 forms structure I (sI) hydrate and N_2 forms structure II (sII) hydrate (van Hinsberg et al., 1993) in its pure form. The structure of hydrate from the gas mixture of CO_2 and N_2 is either sI or sII depending upon the relative ratio of the

two gas molecules in the small and large cavities (Kang and Lee, 2000). A detailed description about the structure and stability of the CO_2/N_2 mixed hydrate is discussed in section 1.2.1.

Table 1-4: Size ratio for CO_2 and N_2.

		Struture I		Structure II	
	Cavity type	5^{12}	$5^{12}6^2$	5^{12}	$5^{12}6^4$
Molecule	Guest diameter (A)				
Carbon dioxide	5.12	1.0	0.834	1.02	0.769
Nitrogen	4.1	0.804	0.7	0.817	0.616

The thermodynamics of hydrate formation has been studied extensively over the years. Consequently, experimental data on the thermodynamics of gas hydrate formation has been obtained for many systems and the computational methods to predict gas hydrate formation conditions are well established. The first experimental observation of gas hydrates was made by Sir Humphry Davy (1811). Carson and Katz (1942) studied the four phase equilibria of gas-mixtures in the presence of gas hydrates and of hydrocarbon-rich liquids. Ng and Robinson (1976) investigated the conditions of hydrate formation in liquid hydrocarbon/water systems. Studies on hydrate equilibrium are focused on gathering incipient equilibrium hydrate formation data as well as developing predictive methods for the calculation of phase equilibria. Incipient hydrate formation conditions refer to the situation in which an infinitesimal amount of the hydrates are present in equilibrium with the fluid phases. A thorough account of the experimental work and the

computational methods on hydrate equilibria is available (Davidson, 1973; Englezos, 1993; Holder et al., 1987; Makogon, 1981; Ripmeester, 2000; Sloan, 1998).

Several models have been proposed over the years to predict the equilibrium hydrate formation conditions (Parrish and Prausnitz, 1972; Holder and John, 1983). They are all based on the statistical thermodynamics model of van der Waals and Platteeuw (1959) that described the hydrate phase. Bishnoi et al. (1989) developed a computational procedure to perform multi-phase flash calculations for systems that contain hydrates. Methods to account for the effect of electrolytes on hydrates from hydrocarbons and CO_2 have also been proposed (Englezos and Bishnoi, 1988; Englezos,1992) Clarke et al. (1999) modeled the conditions for hydrate formation in porous media. It is noted that in the above calculations the fugacity or a chemical component in the fluid phases is calculated by using a suitable equation of state such as the Trebble – Bishnoi equation of state (Trebble and Bishnoi, 1987),the Peng – Robinson equation of state (Peng and Robinson, 1978) or the Statistical Associating Fluid Theory (Li et al. 2006).

There are two fundamental questions that must be addressed when time is a consideration with respect to hydrates. The first is the amount of time required in order for a hydrate to reach a critical size nucleus. The second is how fast the hydrate grows after the critical size nucleus has been achieved.

Hydrate nucleation refers to the process where hydrate nuclei, grow and disperse until they attain a critical size for continued growth. If the size of the nuclei is less than the critical size, the nuclei are unstable and may continue to grow or break in the aqueous solution (Natarajan et al., 1994). If the growing nuclei reach the critical size it then becomes stable, which leads to the formation of hydrate crystals. This period when the

hydrate nuclei are forming and dissolving in a supersaturated solution to the time when the nuclei reach the critical size is called the induction time.

Gas hydrate formation is a crystallization process from a fluid/water system with "limited observability" because the number of variables that can be monitored is a small sub set of those needed to fully describe a hydrate forming system under time-dependent conditions. Traditionally, when a gas hydrate former (e.g. CO_2) is used, the measurements consisted of monitoring the rate of "gas consumption" or "gas uptake". In other words they focused on the gas phase. Recently, the focus shifted to the solid phase by using Raman techniques, optical microscopy and particle size analysis to alleviate the observability problem (Moudrakovski et al., 2004; Sloan, 2003). For example, Susilo et al. (2006) monitored the kinetics of structure I and H methane hydrate growth by employing Nuclear Magnetic Resonance (NMR) spectroscopy and imaging (MRI) and found out that the results agree with the results from gas uptake measurements obtained by Lee et al. (2005). Recently, Kumar et al. (2008) reported the kinetics and structure of gas hydrates from methane/ethane/propane mixtures relevant to the design of natural gas hydrate storage and transport facilities. The results obtained from kinetics at macroscopic level (gas uptake) were found to agree with the results obtained at molecular level (powder x-ray diffraction, NMR, and Raman spectroscopy). The composition of the gas phase and the hydrate phase was found to evolve over time, suggesting that kinetic and transport factors contribute in addition to thermodynamics (Kumar et al., 2008).

1.2.1. CO_2, N_2 and CO_2/N_2 mixed hydrates

CO_2 is known to form structure I hydrate. The CO_2 molecules occupy primarily the large cavities and some small ones (Ripmeester and Ratcliffe, 1998; Udachin et al., 2001). CO_2

can also serve as help gas for structure H hydrate (Ripmeester and Ratcliffe, 1998). Since CO_2 can be sequestered by mineral trapping and in depleted oil and gas reservoirs there could be implications for the use of CO_2 in secondary oil recovery if structure H hydrate forms in these systems. Hence, it is essential to know the equilibrium hydrate formation conditions in carbon dioxide containing systems. The equilibrium hydrate formation conditions for carbon dioxide have been extensively investigated and are available in the literature (Deaton and Frost, 1946; Falabella, 1975; Larson, 1955; Miller and Smythe, 1970; Ng and Robinson, 1985; Robinson and Mehta, 1971; Song and Kobayashi, 1987; Unruh and Katz, 1949). Deaton and Frost (1946) were first to report equilibrium hydrate formation conditions for carbon dioxide. Larson (1955) investigated equilibrium hydrate formation conditions of carbon dioxide at temperatures below the freezing point of water. Equilibrium hydrate formation conditions for carbon dioxide in ice were also reported by Miller and Smythe (1970). The equilibrium hydrate formation conditions for carbon dioxide in liquid water are shown in Figure 1-3. As it can be seen in the figure, for example at 274.15 K, the equilibrium pressure is 1.414 MPa. Hydrate is stable above this pressure while they do not exist below this pressure at 274.15 K. The CO_2 saturation curve (vapor pressure curve) is also shown.

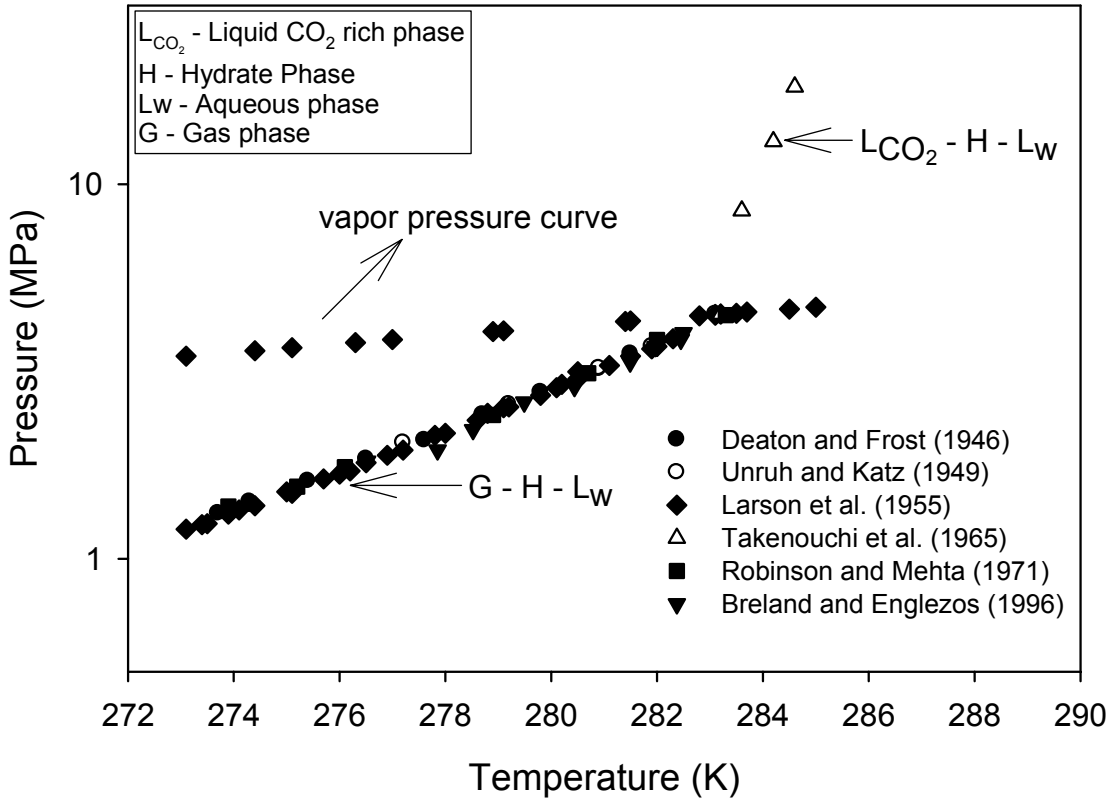

Figure 1-3: Equilibrium hydrate formation conditions for pure carbon dioxide hydrate.

The equilibrium hydrate formation conditions for nitrogen were first observed by van Cleef and Diepen (1960). Recently, Sugahara et al (2002) observed the equilibrium hydrate conditions of nitrogen for higher temperatures. Figure 1-4 shows the three phase equilibrium hydrate formation conditions (G – Lw – H) for nitrogen in water. As it can be seen in the figure, for example at 274.15 K the minimum pressure for N_2 to form hydrates is 17.807 MPa.

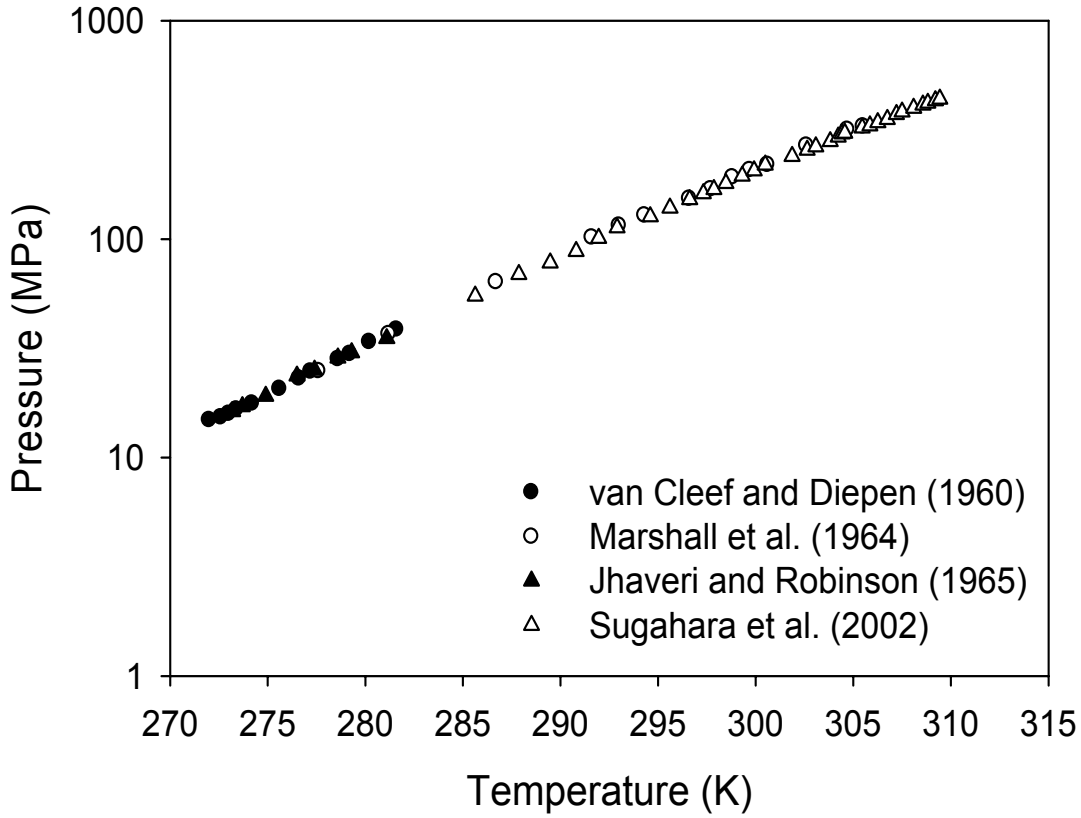

Figure 1-4: Equilibrium hydrate formation conditions for pure nitrogen hydrates.

Dholabhai et al. (1993) measured the formation conditions of CO_2 hydrates in aqueous electrolyte solutions. Englezos and Hall (1994) investigated the equilibrium hydrate formation conditions of carbon dioxide in the presence of aqueous electrolyte solutions, water soluble polymers and montmorillonite. Breland and Englezos (1996) investigated the equilibrium hydrate formation conditions of carbon dioxide in the presence of glycerol. Fan et al. (2000) studied the hydrate formation conditions for carbon dioxide and carbon dioxide rich gas mixtures in the presence of ethylene glycol. Olsen et al (1999) studied the equilibrium hydrate formation conditions of carbon the dioxide-nitrogen mixture. Mooijer-van-der Heuvel et al. (2001) investigated the effect of additives on carbon dioxide hydrate formation conditions. The additives used were

organic substances like tetrahydropyran, cyclobutanone, cyclohexane and methylcycohexane.

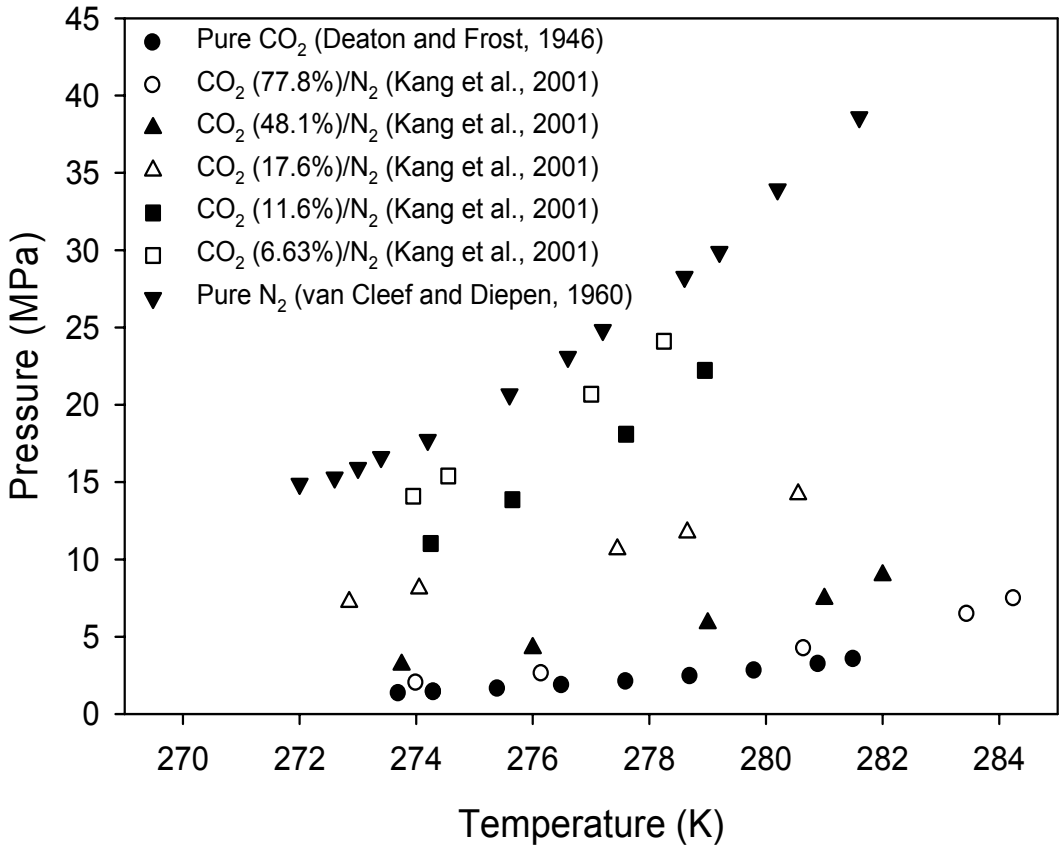

Figure 1-5: Equilibrium hydrate formation conditions for CO_2 – N_2 mixtures.

Kang et al. (2001) reported equilibrium hydrate formation data for a mixture of carbon dioxide and nitrogen with varying ratios of each. The equilibrium hydrate formation conditions for the mixture of carbon dioxide and nitrogen are shown in Figure 1-5. Kang et al. (2001) also reported thermodynamic data on the effect of tetrahydrofuran (THF) on the hydrate formation conditions for CO_2/N_2 mixtures.

Recently, Duc et al. (2007) studied the effect of tetra-*n*-butyl ammonium bromide (TBAB) on the hydrate formation conditions of CO_2, N_2 and CO_2/N_2 mixed hydrates.

Seo and Lee (2004) studied the structure and guest distribution of mixed (CO_2+N_2) hydrates of carbon dioxide and nitrogen using X – ray diffraction and C NMR spectroscopy. X–ray diffraction results showed that for mixed (CO_2+N_2) hydrates with 3 – 20 mol% CO_2, the unit cell parameter was ~11.8 À and the structure formed is structure I. For 1 mol% CO_2, the unit cell parameter was found to be 17.26 À and the structure formed was identified as Structure II. NMR spectra results revealed that carbon dioxide molecules mainly occupied the large $5^{12}6^2$ cages of structure I when the mixed hydrate (CO_2+N_2) was formed at a vapor phase composition range of 10 – 20 mol% CO_2. Seo and Lee (2004) also reported that CO_2 molecules may occupy both large and small cavities of structure I when the CO_2 content in the gas phase exceeds 33 %. Seo et al. (2005) studied CO_2-N_2 hydrate formation in porous silica gels and presented phase diagrams illustrating phase compositions. They also reported that C cross-polarization NMR spectral analysis and direct measurement of CO_2 content in the hydrate phase suggested that the mixed hydrate formed of more than 10 mol % of CO_2 gas is structure I and the CO_2 molecules occupy mainly the more abundant $5^{12}6^2$ cages.

1.3. Research objectives

Given that gas hydrate crystal formation offers the possibility for developing a novel technology for CO_2 separation from flue gases (post-combustion capture) and from fuel gas mixtures ("pre-combustion capture") in Integrated Gasification Combined Cycle (IGCC) power plants our scope is to provide fundamental data for the conceptual design of the hydrate-based CO_2 capture process. Our work is primarily concerned with CO_2/N_2 separation ("post-combustion capture"). However, the knowledge obtained from this work is sufficiently general and is expected to be useful in the other applications. In order for the hydrate-based process for CO_2/N_2 separation to be successful, we need to provide further basic thermodynamic and kinetic data relevant to the separation process. Moreover, gas/water contact modes should be studied in order to identify operating conditions that favor fast conversion of water to hydrate. One of the key elements for successful development of hydrate technology is the improvement of gas/liquid contact to improve hydrate growth (Mori, 2003). More specifically the objectives and the anticipated outcomes are as follows

1. Determination of the incipient equilibrium hydrate formation conditions whenever not available for (a) CO_2/N_2 hydrate; and (b) CO_2/N_2 hydrate in the presence of additives that lower the formation conditions. The outcome is to establish the most favorable process operating conditions (Temperatures and Pressures).

2. Determination of the kinetics of CO_2/N_2 hydrate formation. This will provide information about the extent of hydrate growth and the degree of separation achieved. Appropriate metrics will be introduced to assess the separation efficiency.

3. Elucidation of the effect of additives to nucleation and hydrate crystal growth. This would provide the basis to establish the role of additives as performance enhancers.

4. To set up a new apparatus to test the separation process at a larger scale. The outcome would be significant in terms of designing the most efficient gas/liquid hydrate formation vessel (“reactor) and scaling it up.

5. To test an alternative to gas/liquid water contact mode by dispersing water in a bed of silica sand particles. The kinetics of hydrate formation will be determined

1.4. Thesis organization

The basic information about gas hydrates is given in Chapter 1. This chapter also discusses the significance of gas hydrates towards human welfare and a variety of prospective applications involving gas hydrates. The current knowledge on hydrate research relevant to CO_2 capture is also discussed.

Chapter 2 presents the thermodynamic and kinetic data on hydrate formation for a flue gas mixture of CO_2 (16.9%) and rest N_2. While thermodynamic data are universally valid, the kinetic data after a certain time depend on the mass transfer limitations. The material for this chapter is published.

- Linga, P., Kumar, R., and Englezos, P., 2007. Gas hydrate formation from hydrogen/carbon dioxide and nitrogen/carbon dioxide gas mixtures. Chemical Engineering Science 62(16), 4268-4276.

Based on the results of chapter 2, chapter 3 presents on the clathrate hydrate process for the separation of CO_2 from flue gas mixture in three stages coupled with a membrane process to treat the lean CO_2 stream. The 99.0% CO_2 stream can be obtained in three stages. Two metrics defining CO_2 recovery or split fraction and Separation factor

were presented to assess the separation process. The high operating pressure of the process results in significant compression costs for the flue gases. In the next chapter an additive will be evaluated to reduce the operating pressure. The material for this chapter is published.

- Linga, P., Kumar, R., and Englezos, P., 2007. The clathrate hydrate process for post and pre-combustion capture of carbon dioxide. Journal of Hazardous Materials 149(3), 625-629.

Chapter 4 reports thermodynamic and kinetic data on the effect of tetrahydrofuran (THF) on separation of CO_2 from the flue gas mixture. 1.0 mol% THF was found to be the optimum for the separation process. It was found that 94-96% CO_2 can be obtained in three stages by adding 1.0 mol% THF without compromising the CO_2 recovery and separation factor significantly. Addition of a small amount of THF (1.0 mol %) significantly reduces the operating pressure for hydrate formation from 10.0 MPa to 2.5 MPa for the first hydrate stage and form 5.0 MPa to 2.5 MPa for the second hydrate stage.. The material for this chapter is published.

- Linga, P., Adeyemo, A., and Englezos, P., 2008. Medium-pressure clathrate hydrate/membrane hybrid process for postcombustion capture of carbon dioxide. Environmental Science & Technology 42(1), 315-320.

Chapter 5 presents a new large scale apparatus specifically designed and set up for demonstrating the separation process involving CO_2 capture. The specific objective of this apparatus is to test the medium pressure separation process presented in chapter 4 at a larger scale with improved gas-water contact. It was successfully demonstrated that it is possible to separate CO_2 from a flue gas mixture on a larger scale without

compromising on the separation efficiency and the CO_2 recovery. Even though the compression costs are low due to the addition of THF as an additive, there is a need for mechanical agitation which makes the hydrate process energy intensive. An alternative gas/water contact arrangement that does not involve agitation is evaluated in the next chapter. The material for this chapter is in preparation to be submitted for publication.

Chapter 6 presents a detailed study on the effect of silica sand on the kinetics of hydrate formation for different gas hydrate applications relevant to the storage and transportation of natural gas and also the separation processes involving post and pre combustion capture of CO_2. It was found dispersing water in silica sand significantly enhanced the gas uptake for hydrate formation for the systems involving water whereas for the systems involving 1.0 mol% THF relevant to post combustion capture of CO_2, the effect was minimal. The material for this chapter is in preparation to be submitted for publication.

Finally, in Chapter 7 the conclusions are highlighted and recommendations for future work are proposed.

1.5. References

Aaron, D., and Tsouris, C., 2005. Separation of CO_2 from flue gas: A review. Separation Science and Technology 40(1-3), 321-348.

Ba-Shammakh, M., Elkamel, A., Douglas, P., and Croiset, E., 2007. A mixed-integer non-linear programming model for CO_2 emission reduction in the power generation sector. International Journal of Environment and Pollution 29(1-3), 254-273.

Barchas, R., and Davis, R., 1992. The Kerr-Mcgee Abb Lummus Crest Technology for the Recovery of CO_2 from Stack Gases. Energy Conversion and Management 33(5-8), 333-340.

Bishnoi, P. R., Gupta, A. K., Englezos, P., and Kalogerakis, N., 1989. Multiphase Equilibrium Flash Calculations for Systems Containing Gas Hydrates. Fluid Phase Equilibria 53, 97.

Breland, E., and Englezos, P., 1996. Equilibrium Hydrate Formation Data for Carbon Dioxide in Aqueous Glycerol Solutions. Journal of Chemical and Engineering Data 41(1), 11-13.

Carson, D. B., and Katz, D. L., 1942. Natural Gas Hydrates. Trans. A.I.M.E. 146, 150-158.

Clarke, M. A., Pooladi-Darvish, M., and Bishnoi, P. R., 1999. A Method To Predict Equilibrium Conditions of Gas Hydrate Formation in Porous Media. Industrial & Engineering Chemistry Research 38(6), 2485-2490.

CSLF. (2008). "Results from G8-IEA Calgary Workshop on Near-Term Opportunities for Carbon Capture and Storage." Carbon Sequestration Leadership Forum, Calgary.

Davidson, D. W., 1973. Gas Hydrates. In Water: A Comprehensive Treatise, Plenum Press;, New York.

Davy, H., 1811. The Bakerian Lecture. On Some of the Combinations of Oxymuriatic Gasand Oxygene, and on the Chemical Relations of these Principles to Infl. Phil Trans Roy Soc (London) 101, 1-35.

Deaton, W. M., and Frost, E. M., 1946. Gas Hydrates and Their Relation to the Operation of Natural-Gas Pipe Lines. U.S. Dept. of the Interior, 1-101.

Dholabhai, P. D., Kalogerakis, N., and Bishnoi, P. R., 1993. Equilibrium Conditions for Carbon Dioxide Hydrate Formation in Aqueous Electrolyte Solutions. J. Chem. Eng. Data 38, 650.

Duc, N. H., Chauvy, F., and Herri, J. M., 2007. CO_2 capture by hydrate crystallization - A potential solution for gas emission of steelmaking industry. Energy Conversion and Management 48(4), 1313-1322.

Elkamel, A., Ba-Shammakh, M., Douglas, P., and Croiset, E., 2008. An optimization approach for integrating planning and CO_2 emission reduction in the petroleum refining industry. Industrial & Engineering Chemistry Research 47(3), 760-776.

Englezos, P., 1992. Computation of the Incipient Equilibrium Carbon Dioxide Hydrate Formation Conditions in Aqueous Electrolyte Solutions. Ind. Eng. Chem. Res. 31, 2232.

Englezos, P., 1993. Clathrate Hydrates. Industrial & Engineering Chemistry Research 32(7), 1251-1274.

Englezos, P., and Bishnoi, P. R., 1988. Prediction of Gas Hydrate Formation Conditions in Aqueous Electrolyte Solutions. AIChE Journal 34(10), 1718.

Englezos, P., and Hall, S., 1994. Phase Equilibrium Data on Carbon Dioxide Hydrates in the Presence of Electrolytes, Water Soluble Polymers and Montmorillonite. Can. Jrnl of Chem Eng. 72, 887 - 893.

Englezos, P., and Lee, J. D., 2005. Gas hydrates: A cleaner source of energy and opportunity for innovative technologies. Korean Journal of Chemical Engineering 22(5), 671-681.

Falabella, B. J., 1975. A Study of Natural Gas Hydrates.

Fan, S. S., Chen, G. J., Ma, Q. L., and Guo, T. M., 2000. Experimental and modeling studies on the hydrate formation of CO_2 and CO_2-rich gas mixtures. Chemical Engineering Journal 78(2-3), 173-178.

Florusse, L. J., Peters, C. J., Schoonman, J., Hester, K. C., Koh, C. A., Dec, S. F., Marsh, K. N., and Sloan, E. D., 2004. Stable low-pressure hydrogen clusters stored in a binary clathrate hydrate. Science 306(5695), 469-471.

Freund, P., 1997. Waste Management. The International Symposium on Ocean Disposal of Carbon Dioxide, 343-352.

Han, F. X. X., Lindner, J. S., and Wang, C. J., 2007. Making carbon sequestration a paying proposition. Naturwissenschaften 94(3), 170-182.

Herzog, H., 2001. What future for carbon capture and sequestration? Environmental Science & Technology 35(7), 148A-153A.

Herzog, H. J., Drake, E., and Adams, E. (1997). " CO_2 Capture, Reuse, and Storage Technologies for Mitigating Global Climate Change." DOE.

Herzog, H., Golomb, D., and Zemba, S., 1991. Feasibility, Modeling and Economics of Sequestering Power-Plant CO_2 Emissions in the Deep Ocean. Environmental Progress 10(1), 64-74.

Ho, M. T., Allinson, G., and Wiley, D. E., 2006a. Comparison of CO_2 separation options for geo-sequestration: are membranes competitive? Desalination 192(1-3), 288-295.

Ho, M. T., Leamon, G., Allinson, G. W., and Wiley, D. E., 2006b. Economics of CO_2 and mixed gas geo-sequestration of flue gas using gas separation membranes. Industrial & Engineering Chemistry Research 45(8), 2546-2552.

Holder, G. D., Zetts, S. P., and Pradhan, N., 1987. Phase Behavior in Systems Containing Clathrate Hydrates - A Review. Chem. Eng. Reviews.

IPCC. (2005). "Carbon dioxide capture and storage, IPCC Special report." Intergovernmental Panel on Climate Change.

Jhaveri, J., and Robinson, D. B., 1965. Hydrates in the Methane-Nitrogen System. The Canadian Journal of Chemical Engineering 43, 75-78.

Kang, S. P., and Lee, H., 2000. Recovery of CO_2 from flue gas using gas hydrate: Thermodynamic verification through phase equilibrium measurements. Environmental Science & Technology 34(20), 4397-4400.

Kang, S. P., Lee, H., Lee, C. S., and Sung, W. M., 2001. Hydrate phase equilibria of the guest mixtures containing CO_2, N_2 and tetrahydrofuran. Fluid Phase Equilibria 185(1-2), 101-109.

Kikkinides, E. S., Yang, R. T., and Cho, S. H., 1993. Concentration and Recovery of CO_2 from Flue-Gas by Pressure Swing Adsorption. Industrial & Engineering Chemistry Research 32(11), 2714-2720.

Klara, S. M., and Srivastava, R. D., 2002. US DOE integrated collaborative technology development program for CO_2 separation and capture. Environmental Progress 21(4), 247-253.

Kumar, R., Linga, P., Moudrakovski, I., Ripmeester, J. A., and Englezos, P., 2008. Structure and kinetics of gas hydrates from methane/ethane/propane mixtures relevant to the design of natural gas hydrate storage and transport facilities. AIChE Journal 54(8), 2132-2144.

Larson, S. D., 1955. Phase Studies of the Two-component Carbon Dioxide - Water System, Involving the Carbon Dioxide Hydrate, University of Illinois.

Lee, J. D., Susilo, R., and Englezos, P., 2005. Kinetics of structure H gas hydrate. Energy & Fuels 19(3), 1008-1015.

Li, X. S., Wu, H. J., and Englezos, P., 2006. Prediction of gas hydrate formation conditions in the presence of methanol, glycerol, ethylene glycol, and triethylene glycol with the statistical associating fluid theory equation of state. Industrial & Engineering Chemistry Research 45(6), 2131-2137.

Makogon, Y. F., 1981. Hydrates of Natural Gas. Pennwell books, Tulsa, Okla, 176.

Mao, W. L., Mao, H. K., Goncharov, A. F., Struzhkin, V. V., Guo, Q. Z., Hu, J. Z., Shu, J. F., Hemley, R. J., Somayazulu, M., and Zhao, Y. S., 2002. Hydrogen clusters in clathrate hydrate. Science 297(5590), 2247-2249.

Marshall, D. R., Saito, S., and Kobayashi, R., 1964. Hydrates at High Pressures: Part I. Methane-Water, Argon-Water, and Nitrogen-Water Systems. A.I.Ch.E. Journal 10, No. 2, 202-205.

McKee, B. (2002). "Zero Emissions Technologies – Technology status Report." OECD/IEA, Paris.

Miller, S. L., and Smythe, W. D., 1970. Carbon Dioxide Clathrate in the Martian Ice Cap. Science 170, 591-594.

Mooijer-van den Heuvel, M. M., Witteman, R., and Peters, C. J., 2001. Phase behavior of gas hydrates of carbon dioxide in the presence of tetrahydropyran, cyclobutanone, cyclohexane and methylcyclohexane. Fluid Phase Equilibria 182(1-2), 97-110.

Mori, Y. H., 2003. Recent Advances in Hydrate-based Technologies for Natural gas Storage-A Review. Journal of Chemical Industry and Engineering 54, 1-17.

Moudrakovski, I. L., McLaurin, G. E., Ratcliffe, C. I., and Ripmeester, J. A., 2004. Methane and carbon dioxide hydrate formation in water droplets: Spatially resolved measurements from magnetic resonance microimaging. Journal of Physical Chemistry B 108(45), 17591-17595.

Natarajan, V., Bishnoi, P. R., and Kalogerakis, N., 1994. Induction Phenomena in Gas Hydrate Nucleation. Chemical Engineering Science 49(13), 2075-2087.

Ng, H., and Robinson, D. B., 1976. The Measurement and Prediction of Hydrate Formation in Liquid Hydrocarbon-Water Systems. Ind. Eng. Chem., Fundam. 15, No. 4, 293-298.

Ng, H. J., and Robinson, D. B., 1985. Hydrate Formation in Systems Containing Methane, Ethane, Propane, Carbon Dioxide or Hydrogen Sulfide in Presence of Methanol. Fluid Phase Equilib. 21, 145-55.

Olsen, M., Majumdar, A., and Bishnoi, P., 1999. Experimental studies on hydrate equilibrium-carbon dioxide and its systems. International Journal of the Society of Materials Engineering for 7, 17.

Ordorica-Garcia, G., Elkamel, A., Douglas, P. L., Croiset, E., and Gupta, M., 2008. Energy optimization model with CO_2-emission constraints for the Canadian oil sands industry. Energy & Fuels 22(4), 2660-2670.

Peng, D. Y., and Robinson, D. B., 1978. Calculation of 3-Phase Solid-Liquid-Vapor Equilibrium Using an Equation of State. Abstracts of Papers of the American Chemical Society 176(Sep), 36-36.

Ripmeester, J., 2000. Hydrate Research - from correlations to a knowledge-based discipline The importance of structure. 3rd International Hydrate Conference SLCity, Holder, Bishnoi Eds. NYAS 912, 1.

Ripmeester, J. A., and Ratcliffe, C. I., 1998. The diverse nature of dodecahedral cages in clathrate hydrates as revealed by Xe-129 and C-13 NMR spectroscopy: CO_2 as a small-cage guest. Energy & Fuels 12(2), 197-200.

Ripmeester, J. A., Ratcliffe, C. I., Klug, D. D., and Tse, J. S., 1994. Molecular Perspectives on Structure and Dynamics in Clathrate Hydrates. International Conference on Natural Gas Hydrates 715, 161-176.

Ripmeester, J. A., Tse, J. S., Ratcliffe, C. I., and Powell, B. M., 1987. A New Clathrate Hydrate Structure. Nature 325, 135-136.

Robinson, D. B., and Mehta, B. R., 1971. Hydrates in the Propane-Carbon Dioxide-Water System. J. Can. Petrol. Tech 10, 33.

Seo, Y. T., and Lee, H., 2004. Structure and guest distribution of the mixed carbon dioxide and nitrogen hydrates as revealed by X-ray diffraction and C-13 NMR spectroscopy. Journal of Physical Chemistry B 108(2), 530-534.

Seo, Y. T., Moudrakovski, I. L., Ripmeester, J. A., Lee, J. W., and Lee, H., 2005. Efficient recovery of CO_2 from flue gas by clathrate hydrate formation in porous silica gels. Environmental Science & Technology 39(7), 2315-2319.

Shindo, Y., and Komiyama, H., 1994. The expanding world of chemical Engineering. Gordon and Breach Science Publishers.

Shingo, K., Shinichiro, M., Shigetoshi, T., Hiroshi, M., Tatsuaki, Y., Koichi, Y., and Kenji, H., 2004. Carbon Polyimide Membranes for CO_2 Capture from Flue Gases. 7th Conference on Greenhouse Gas Control Technologies, Vancouver.

Sloan, E., D.,. 2000. Evaluation of CO_2 sequestration in Ocean Hydrates. International Symposium on Deep Sea Sequestration of CO_2, Tokyo, Japan.

Sloan, E. D., 2003. Clathrate hydrate measurements: microscopic, mesoscopic, and macroscopic. Journal of Chemical Thermodynamics 35(1), 41-53.

Sloan, E. D., Jr., 1998. Clathrate Hydrates of Natural Gases, Second Edition, Revised and Expanded, Marcel Dekker, NY.

Sloan, E. D., Jr.; and Koh, C. A. (2008) Clathrate Hydrates of the Natural Gases, Third Edition, CRC Press, Boca Raton, FL.

Sluiter, M. H. F., Adachi, H., Belosludov, R. V., Belosludov, V. R., and Kawazoe, Y., 2004. Ab initio study of hydrogen storage in hydrogen hydrate clathrates. Materials Transactions 45(5), 1452-1454.

Song, K. Y., and Kobayashi, R., 1987. Water Content of CO_2 in Equilibrium with Liquid Water and/or Hydrates. SPE Formation Evaluation, 500.

Subramanian, S., Kini, R. A., Dec, S. F., and Sloan, E. D., 2000. Evidence of structure II hydrate formation from methane plus ethane mixtures. Chemical Engineering Science 55(11), 1981-1999.

Sugahara, K., Tanaka, Y., Sugahara, T., and Ohgaki, K., 2002. Thermodynamic stability and structure of nitrogen hydrate crystal. Journal of Supramolecular Chemistry 2(4-5), 365-368.

Susilo, R., Moudrakovski, I. L., Ripmeester, J. A., and Englezos, P., 2006. Hydrate kinetics study in the presence of nonaqueous liquid by nuclear magnetic resonance spectroscopy and imaging. Journal of Physical Chemistry B 110(51), 25803-25809.

Takahashi, T., Goldberg, D., and Mutter, J. C., 2000. International Symposium on Deep Sea Sequestration of CO_2, Tokyo, Japan.

Takenouchi, S., and Kennedy, G., 1965. Dissociation pressures of the phase CO_2 5 3/4 H_2O. Geology 73, 383.

Trebble, M. A., and Bishnoi, P. R., 1987. Development of New Four-Parameter Cubic Equation of State. Fluid Phase Equilibria 35, 1.

Udachin, K. A., Ratcliffe, C. I., and Ripmeester, J. A., 2001. Structure, composition, and thermal expansion of CO_2 hydrate from single crystal X-ray diffraction measurements. Journal of Physical Chemistry B 105(19), 4200-4204.

Unruh, C. H., and Katz, D. L., 1949. Gas Hydrates of Carbon Dioxide - Methane Mixtures. Petroleum Transactions, AIME, 83-86.

van Cleeff, A., and Diepen, G. A. M., 1960. Gas Hydrates of Nitrogen and Oxygen. Rec. Trav. Chim 79, 582.

van der Waals, J. H., and Platteeuw, J. C., 1959. Validity of Clapeyron's Equation for Phase Equilibria involving Clathrates. Nature 183, 4659, 462.

van Hinsberg, M. G. E., Scheerboom, M. I. M., and Schouten, J. A., 1993. The Vibrational Spectra of N_2 in Clathrate-Hydrates: A New High-Pressure Phase Transition. J. Chem. Phys. 99(1), 752.

WEO. (2000). "World Energy Outlook." International Energy Agency.

Yamasaki, A., 2000. International Symposium on Deep Sea Sequestration of CO_2, Tokyo, Japan.

2. KINETICS OF HYDRATE FORMATION FROM A FLUE GAS MIXTURE[1]

2.1. Introduction

Gas hydrate formation being a crystallization process is characterized by nucleation followed by growth and agglomeration. Kinetics is concerned with the rate at which the phase transformation occurs and the identification of the factors affecting it. The rate of nucleation e.g. number of hydrate crystal nuclei formed per unit time per unit volume is an extremely difficult measurement and to date there is no data reported. On the other hand the induction time marking the onset of crystallization is easily obtained experimentally. Most gas hydrate kinetics studies have focused on the growth phase coupled sometimes with measurement of the particle size distribution (Bishnoi and Natarajan, 1996; Clarke and Bishnoi, 2005; Englezos, 1993, 1996; Koh, 2002; Sloan, 1998).

The rate of hydrate crystal growth is defined operationally. Thus, one may determine the gas uptake rate to describe kinetics or the rate at which a hydrate/solution interface advances. The question that arises is how an intrinsic rate can be distinguished from the relevant transport processes. It is noted that it is difficult to distinguish the intrinsic rate from the relevant transport processes. Consequently, kinetic studies focusing

[1] A version of this chapter has been published. Linga, P., Kumar, R., and Englezos, P., 2007. Gas hydrate formation from hydrogen/carbon dioxide and nitrogen/carbon dioxide gas mixtures. Chemical Engineering Science 62(16), 4268-4276.

on particular hydrate forming systems and hydrate vessel configurations continue to appear.

Treated flue gas from power plants contains CO_2, N_2, O_2 and one of the methods for the separation for subsequent storage or utilization of CO_2 is through gas hydrate formation (Aaron and Tsouris, 2005; Englezos and Lee, 2005; Kang and Lee, 2000; Seo et al., 2005). Since N_2 and O_2 form hydrate crystals at approximately the same conditions the treated flue gas is considered a CO_2/N_2 mixture. In order to facilitate the development of hydrate based separation process, thermodynamic and kinetic data are needed to define the operating conditions. While equilibrium data for the above mixtures are in general available, studies on the kinetics of hydrate growth coupled with compositional analysis of the gas phase are not available. Thus, the purpose of the present study is to obtain such kinetic information.

2.2. Experimental section

2.2.1. Materials

The gas mixtures used in the present study were UHP grade and were supplied by Praxair Technology Inc. The gas compositions were chosen so that they represent industrial compositions. For example, in post-combustion capture from power plants using hydrates the task is to separate CO_2 from a CO_2/N_2 mixture in which the CO_2 molar content is approximately 15-20 %. The dry molar (%) gas compositions of the binary gas mixtures were determined by gas chromatography and are as follows: CO_2 (16.9)/N_2 (83.1) and CO_2 (39.2)/H_2 (60.8).

2.2.2. Apparatus and procedure

The apparatus is shown in Figure 2-1. It consists of a crystallizer (CR) immersed in a temperature-controlled bath. The crystallizer is a vessel made of 316 stainless steel. It has a volume of 323 cm^3. The crystallizer has two circular viewing windows made of Plexiglas on the front and back. Mixing of the crystallizer contents is accomplished using a magnetic stir bar. A baffle arrangement is used in the crystallizer in order to prevent vortex formation and to enhance mixing of the crystallizer contents. Two Rosemount smart pressure transducers, model 3051 (Norpac controls, Vancouver, BC) are employed for pressure measurement with a maximum uncertainty of 25 kPa. The temperature of the liquid phase in the crystallizer is measured using an Omega copper-constantan thermocouple with an uncertainty of 0.1 K.

The kinetics of hydrate formation were studied through gas uptake measurements following a technique pioneered at Bishnoi's laboratory (Englezos et al., 1987a; 1987b; Vysniauskas and Bishnoi, 1983). The procedure followed in this work is described in detail elsewhere (Lee et al., 2005). Essentially, one measures the amount of hydrate forming gas consumed in the crystallizer under constant temperature and pressure. The key to obtaining meaningful results is an accurate measurement of the amount of gas consumed and the control of the mixing conditions in the crystallizer. The first requirement is satisfied through accurate pressure measurements, a pressure control system and a reference gas reservoir. Use of mass flow meters is expected to be significantly less accurate and that it is discouraged. The second requirement is satisfied through the baffle arrangement described in detail by Lee et al. (2005).

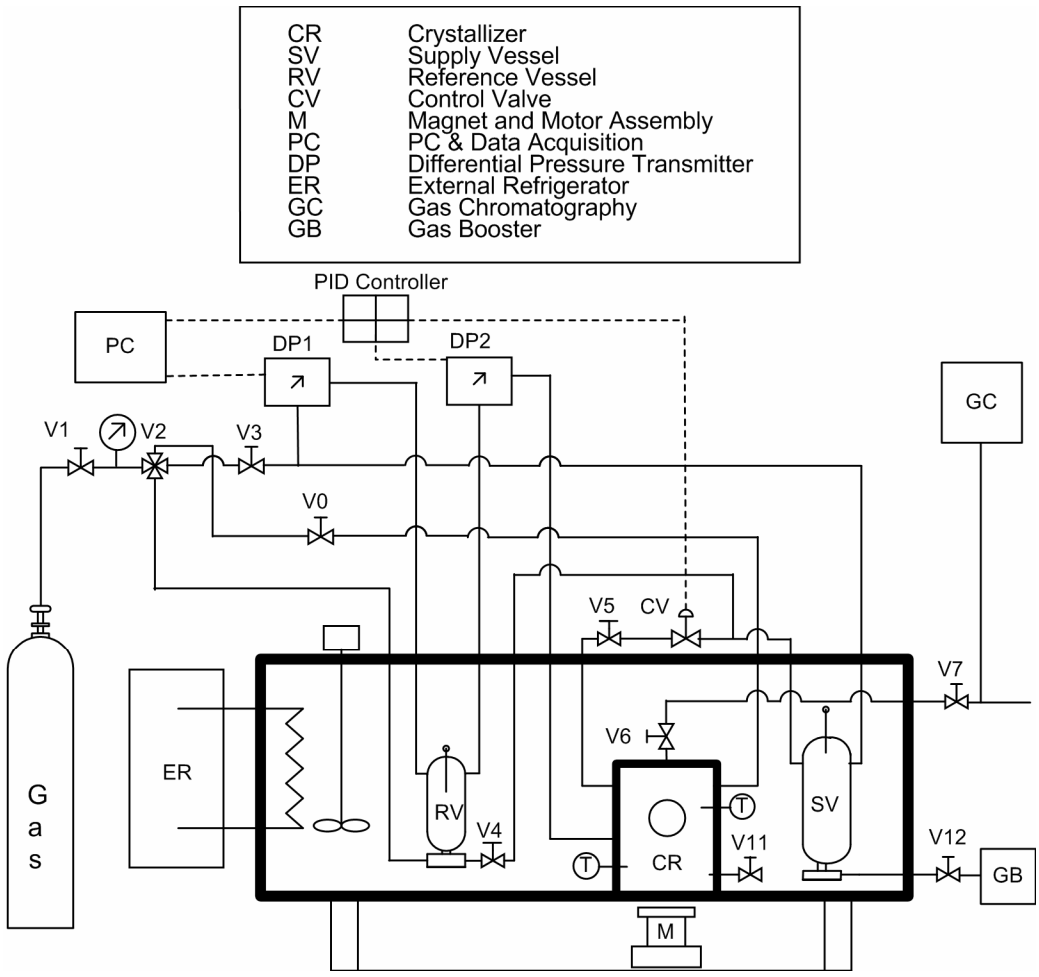

Figure 2-1: Apparatus.

The crystallizer was filled with 140 cm^3 of water. Any air present was flushed out by repeating three pressurizations with the gas mixture and depressurizations to atmospheric pressure. Subsequently, the crystallizer was filled with hydrate forming gas until the desired pressure is reached. Once the temperature was stabilized (typically within 2 min) the stirrer in the crystallizer was started. This is time zero. It is assumed that the amount of gas dissolved in water up to this point is negligible because the time is very small for mass transfer due to diffusion into the quiescent liquid water to be

significant. As the gas in the crystallizer was consumed for hydrate formation, additional gas was supplied and the pressure was maintained constant with a PID controller.

All kinetics experiments were carried out at pressures above the equilibrium so that a finite rate of crystallization is obtained. The deviation of the experimental pressure from the equilibrium pressure is frequently called *driving force*.

2.2.3. Calculation of the amount of gas consumed

At any given time, the total number of moles ($n_{T,t}$) in the system remains constant and is equal to that at time zero ($n_{T,0}$). The system includes the crystallizer (CR), the supply vessel (SV) and the connecting tubing. The total number of moles at any given time is the sum of the number of moles (n_{SV}) in the supply vessel, the number of moles (n_G) in gas phase (G) of the crystallizer and the number of moles (n_H) consumed to form hydrate (H) or dissolved in water.

$$n_{G,0} + n_{SV,0} + n_{H,0} = n_{G,t} + n_{SV,t} + n_{H,t} \tag{2.1}$$

The number of moles that have either gone into the water or have been consumed for hydrate formation can then be calculated as follows.

$$n_{H,t} - n_{H,0} = n_{G,0} - n_{G,t} + n_{SV,0} - n_{SV,t} \tag{2.2}$$

or

$$\Delta n_H = n_{H,t} - n_{H,0} = \left(\frac{PV}{zRT}\right)_{G,0} - \left(\frac{PV}{zRT}\right)_{G,t} + \left(\frac{PV}{zRT}\right)_{SV,0} - \left(\frac{PV}{zRT}\right)_{SV,t} \tag{2.3}$$

Where z is the compressibility factor calculated by Pitzer's correlation (Smith et al., 2001).

During the kinetic experiment, the composition of the gas phase is determined by gas chromatography. At any given time by knowing the composition of the gas mixture in the crystallizer, the number of moles of the individual gas component consumed for hydrate formation can be calculated by the component mass balance

$$\Delta n_H^i = n_{H,t}^i - n_{H,0}^i = \left(y^i \frac{PV}{zRT} \right)_{G,0} - \left(y^i \frac{PV}{zRT} \right)_{G,t} + \left(y^i \frac{PV}{zRT} \right)_{SV,0} - \left(y^i \frac{PV}{zRT} \right)_{SV,t}$$

$$= V_G \left[\left(y^i \frac{P}{zRT} \right)_{G,0} - \left(y^i \frac{P}{zRT} \right)_{G,t} \right] + y_{SV}^i V_{SV} \left[\left(\frac{P}{zRT} \right)_{SV,0} - \left(\frac{P}{zRT} \right)_{SV,t} \right] \qquad (2.4)$$

where, the superscript i refers to component of the gas mixture.

Conversion of water to hydrates is determined from the information obtained from gas uptake and the experimental conditions using the following equation

$$\text{Connversion of water to hydrates}\,(\text{mol}\%) = \frac{\Delta n_{H,\downarrow} \times \text{Hydration Number}}{n_{H_2O}} \times 100 \qquad (2.5)$$

where $\Delta n_{H,\downarrow}$ is the number of moles of gas consumed for hydrate formation at the end of the experiment determined from the gas uptake measurement and n_{H_2O} is the total number of moles of water in the system. The hydration number is defined as the number of water molecules per guest molecule. It can be determined experimentally using tools like NMR spectroscopy combined with statistical thermodynamics (Davidson et al., 1983; Ripmeester and Ratcliffe, 1988), Raman spectroscopy (Sum et al., 1997; Uchida et al., 1999) and single crystal and powder x-ray and neutron diffraction (Kumar et al. 2008; Rawn et al., 2003; Susilo et al. 2007; Udachin et al., 2002).

The uncertainties in the mole numbers due to the uncertainties in the measurement of pressure, temperature and composition were calculated. For example for the CO_2/N_2 system (Experiment 3, Table 2-1) the uncertainty was found to be 9.1 % at the induction time, 4.3 % at 20 minutes after the induction time and 1.9 % after 200 minutes. Thus, the uncertainty at the induction time and during the first 10-20 min is believed to be about 10 % and it decreases as the number of moles consumed increases.

2.2.4. Gas phase analysis

A Varian CX-3400 gas chromatograph (GC) with a Thermal conductivity detector and flame ionization detector along with a CP-PoraPLOT U capillary column were used. Ultra high purity He was used as carrier gas. The gas sample was transferred from the crystallizer to a 1/8" stainless steel sampling tube. The volume of the sampling tube is 300 μL, considering that the volume of crystallizer is 323 mL it is reasonable to assume that the amount in the sample does not affect the mass balance calculations. The sampling tube was flushed out three times with He before collecting a sample for analysis. The gas from the sampling tube was injected into the GC through a 6-port valve which had 100 μL of sampling loop.

2.3. Results and discussion

Incipient equilibrium hydrate formation conditions for a 16.9% CO_2 and the rest N_2 was determined using the isothermal pressure search method (Englezos and Ngan, 1994). The equilibrium pressure for three temperatures of 273.7, 274.8 and 275.9 K, respectively was determined and found to be 7.7, 8.4 & 9.2 MPa respectively. Figure 2-2 shows the comparison of the experimental data with data available in the literature and as it can be

seen, the data agrees well with the literature. The incipient equilibrium hydrate formation pressure at 273.7 K is 7.7 MPa. It is noted that at 273.7 K, the minimum pressure required to form pure CO_2 and pure N_2 hydrates is 1.32 and 17.13 MPa respectively (Deaton and Frost, 1946; van Cleeff and Diepen, 1960). CO_2 forms structure I (sI) and N_2 forms structure II (sII) hydrate. The structure of hydrate from the gas mixture is either sI or sII depending upon the relative ratio of the two gas molecules in the small and large cavities (Kang and Lee, 2000). For a gas mixture of more than 10% CO_2 and rest N_2, the hydrate structure formed is structure I (Seo et al., 2005).

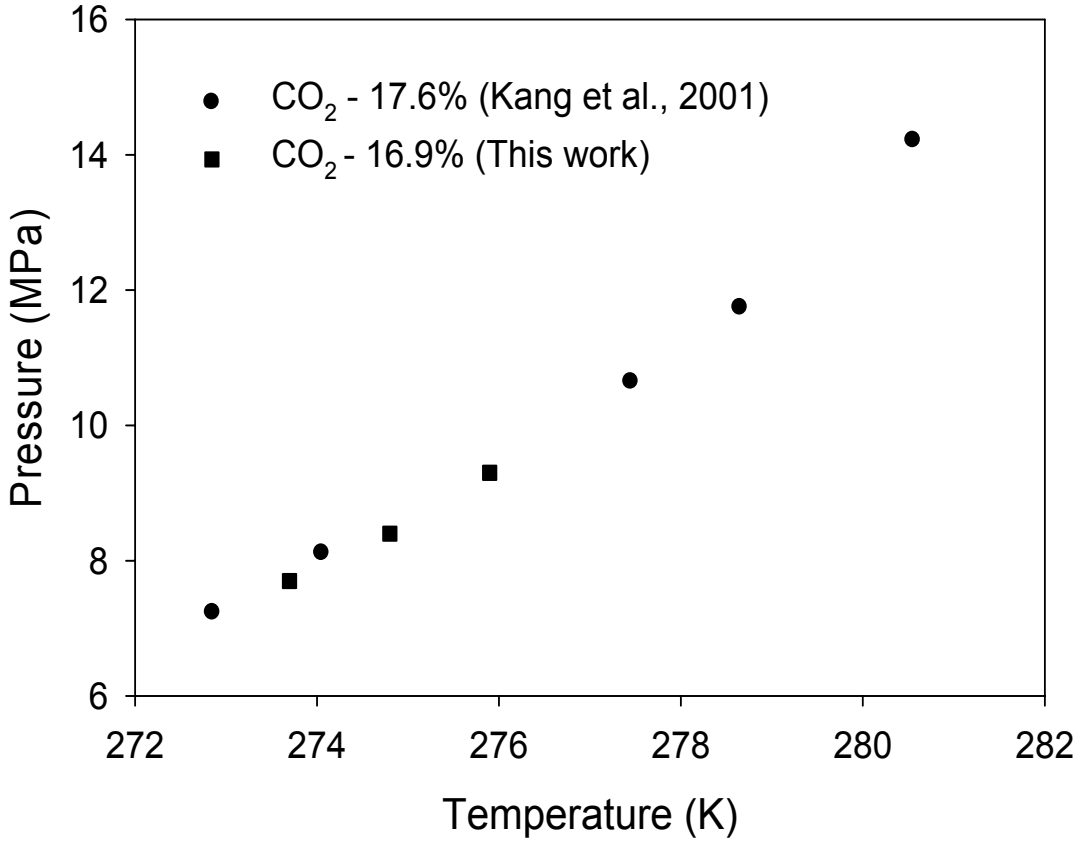

Figure 2-2: Incipient equilibrium hydrate formation conditions for CO_2/N_2 gas mixture.

Gas uptake measurements were carried out at 273.7 K and at 9.0, 10 and 11.0 MPa which correspond to 1.3, 2.3 and 3.3 MPa above the hydrate equilibrium pressure. Table 2-1 summarizes the results. Experiments with fresh water as well as with memory water were conducted. Memory refers to the situation where water that is used in the experiment has experienced hydrate formation. The water obtained is used three hours after hydrate decomposition.

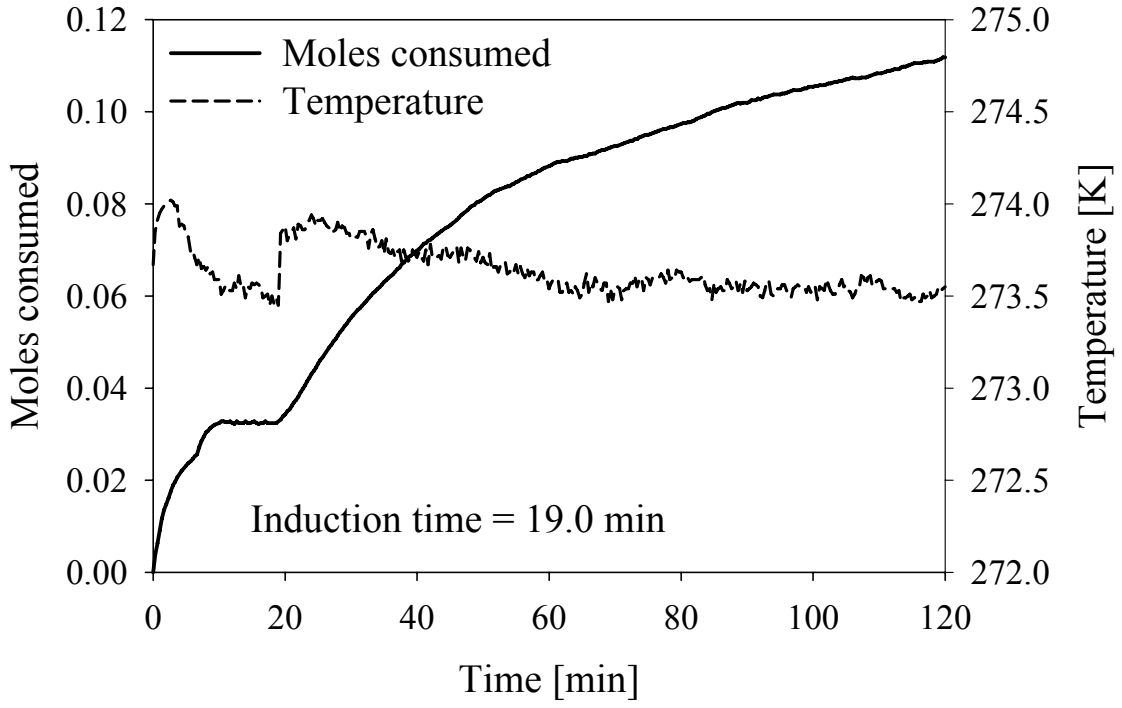

Figure 2-3: A typical gas uptake measurement curve together with the temperature profile in the aqueous phase (experiment 3, table 3-1).

A typical gas consumption or gas uptake curve for a period of two hours is shown in Figure 2-3. The general shape of this curve agrees with the behavior of the curve described in detail by Bishnoi and Natarajan (1996). As seen, nucleation takes place in 19 min and the number of moles of gas (CO_2/N_2) consumed up to that time (induction time) is 0.033. The rate of hydrate growth (R_f) is defined as the slope of the gas uptake curve

during the first 20 min after the induction time. The rates of hydrate growth along with other information are given in Table 2-1. The justification for this choice is the visual observation that the hydrate particles are well-dispersed in the water phase (Lee et al. 2005). Visual observations of the crystallizer contents allow the experimenter to approximately identify when the state of extensive hydrate crystal agglomeration commences and results in accumulation of crystals as stagnant pockets at the gas/water interface. This prevents more gas from coming into contact with the water. The agglomeration behavior of hydrate crystals has not received any considerable attention and thus it is difficult to correlate its behavior. However, this is changing. Fidel-Dufour et al. (2006) has studied the rheology of methane hydrates in water/dodecane emulsion system.

The temperature in the water phase is also shown in figure 2-3. Gas hydrate formation is an exothermic process. As seen, the temperature rises immediately after nucleation, reaches a higher level and then gradually is brought down because the temperature controller brings back the temperature to the set point value. The gas uptake curves for all of the experiments along with the temperature profile are given in Appendix A.

Table 2-1: Experimental conditions along with measured induction times and hydrate formation rates for $CO_2/N_2/H_2O$ system at 273.7 K.

Exp. No.	Sample State	Driving force[a] [MPa]	P_{exp} [MPa]	Induction Time [min]	R_f[b] [mol/min]	Final moles consumed [mol of gas/mol of H_2O]	Water conversion to hydrate[d] [%]
1	Fresh	3.30	11.0	14.0	0.0020	0.018	11.2
2	Memory	3.30	11.0	6.3	0.0020	0.013	8.4
3	Fresh	3.30	11.0	19.0	0.0018	0.014	9.0
4	Memory	3.30	11.0	9.7	0.0021	0.017	10.8
5	Fresh	2.30	10.0	10.3	0.0017	0.014	9.0
6	Memory	2.30	10.0	7.0	0.0021	0.017	10.6
7	Fresh	2.30	10.0	16.3	0.0014	0.013	8.1
8	Memory	2.30	10.0	9.3	0.0015	0.013	8.2
9	Fresh	1.30	9.0	1063.3	0.0005	0.008	5.3
10	Memory	1.30	9.0	154.0	0.0003	0.007	4.3
11	Fresh	1.30	9.0	No hydrate[c]	N/A	N/A	N/A
12	Memory	1.30	9.0	N/A	N/A	N/A	N/A

[a] Driving force = P_{exp} - P_{eq} (P_{exp} = experimental pressure, P_{eq} = equilibrium pressure)

[b] Rate of hydrate growth (gas consumption rate for the first 20 min after nucleation)

[c] Did not nucleate for two days.

[d] Hydration number of 6.28 (Kang et al., 2001) was used for the calculation.

It is generally accepted that the induction time required in a system with memory is shorter (Lee et al., 2005; Uchida et al., 2000). This is what was also found in this work. For example, as it can be seen in Figure 2-4, the induction time was shortened from 1063.3 min (experiment 9) to 154.0 min (experiment 10) for a driving force of 1.3 MPa. There is a weak correlation between induction time and driving force (Bishnoi and Natarajan, 1996). In general, the induction time is shorter as the driving force increases. This is seen in experiments 1 to 8. It is noted that the observed memory-related phenomena have not been explained yet. Buchanan et al. (2005) concluded that there is no significant difference between the structure of water before hydrate formation and the structure of water after hydrate decomposition nor is there any significant change to the methane hydration shell. It is noted that nucleation is heterogeneous under almost all circumstances encountered. This means that memory effects also are determined by impurities rather than structure (which is an intrinsic property).

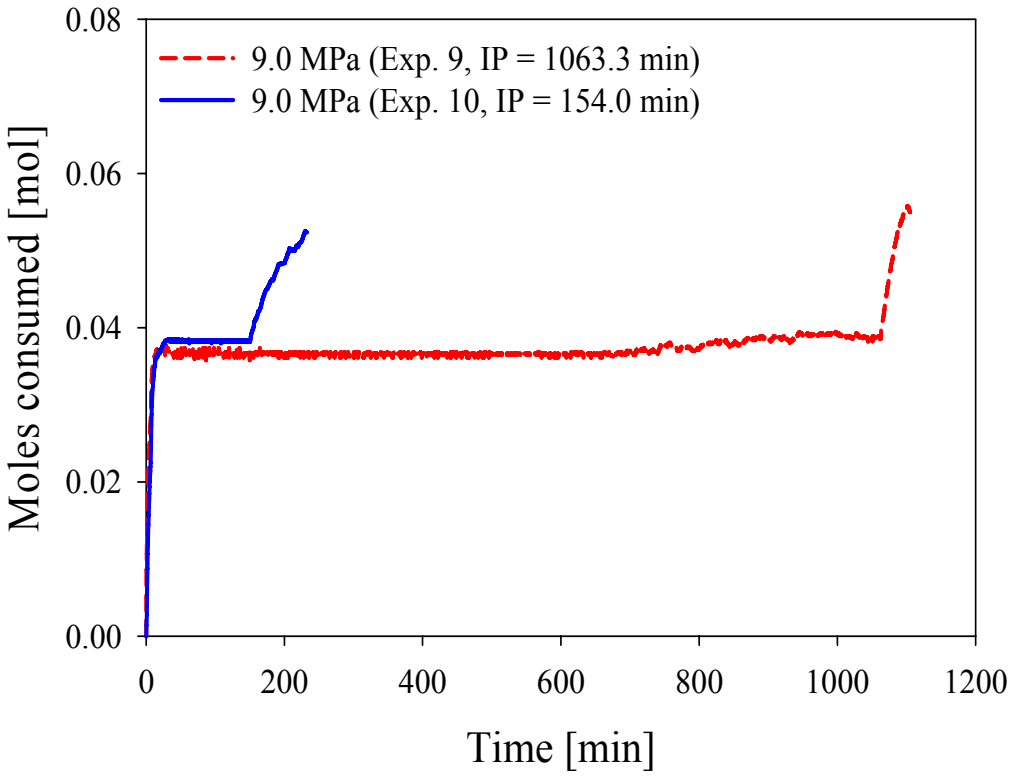

Figure 2-4: Memory effect on hydrate formation for experiment carried out at 9.0 MPa and 273.7 K.

The calculated rates (Table 2-1), R_f, indicate that in general the rate decreases with decreasing driving force. While one should be careful not to generalize these observations the observed rates indicate the relative speed of phase change of the different hydrate forming systems. It should be pointed out that kinetics through gas uptake measurements and macroscopic techniques in general are in reality "average kinetics" over the whole sample because the conversion to hydrate is quite an inhomogeneous process and that the observation of gradual conversion in bulk samples only arises as a result of averaging over many local environments (Moudrakovski et al., 2004). Susilo et al. (2006) employed Nuclear Magnetic Resonance (NMR) spectroscopy and imaging (MRI) to monitor the kinetics of structure I and H methane hydrate growth and found that the results agree with the results from gas uptake measurements obtained

by Lee et al. (2005). Figure 2-5 shows the calculated rates of hydrate formation plotted against the experimental pressure for all the experiments reported in Table 2-1. As it can be seen in the figure, in general the rate of hydrate formation increases with the increase in driving force. The standard errors and R^2 values for the calculated rates are given in Appendix A (Table A-1).

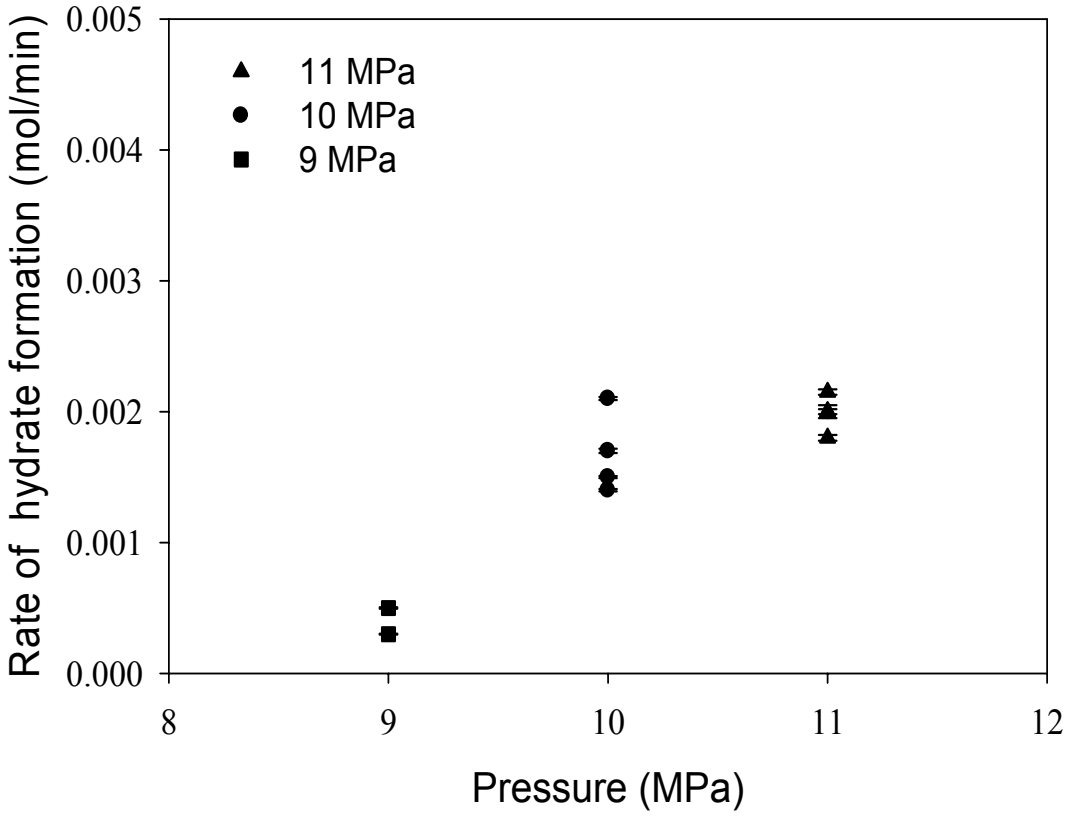

Figure 2-5: Rate of hydrate formation vs experimental pressure for the kinetic experiments given in Table 2-1.

The conversion of water to hydrate for all the kinetic experiments is given in Table 2-1. The conversions of water to hydrate for 1.3, 2.3 and 3.3 MPa driving force are in average 4.8, 9.0, and 9.9, respectively. There is certainly an increasing trend in the conversion with the increase in the driving force for hydrate formation. Overall, the conversion of water to hydrate is low because of the mass transfer resistance in the

existing lab scale apparatus which employs mixing the liquid contents using a magnetic stirrer bar coupled with a electric motor. Recall that, visual observations of the crystallizer contents allow the experimenter to identify the state of extensive hydrate crystal agglomeration which results in accumulation of crystals as stagnant pockets at the gas/water interface. This prevents more gas from coming into contact with the water. Eventually, the gas uptake slows down with time due to the formation of bulk hydrates at the water/gas interface which hinders further growth of hydrate formation (Figure 2-3).

Table 2-2: Vapor phase composition during hydrate formation from CO_2/N_2 mixture.

$CO_2/N_2/H_2O$ at 10.0 MPa (Experiment 7, table 3-1)		$CO_2/N_2/H_2O$ at 11.0 MPa (Experiment 3, table 3-1)	
Sampling time (min)	CO_2 mole fraction in CR (y_{CO_2})	Sampling time (min)	CO_2 mole fraction in CR (y_{CO_2})
0.0	0.169	0.0	0.169
15.0	0.132	16.0	0.127
52.0	0.108	30.0	0.118
82.0	0.096	52.0	0.108
260.0	0.097	128.0	0.109

The gas phase was analyzed for a typical hydrate formation experiment at 273.7 K and pressures 10.0 MPa and 11.0 MPa respectively. Table 2-2 shows the gas composition in the gas phase of the crystallizer at various times during experiments 3 and 7. As seen, the CO_2 content in the gas phase of the crystallizer decreases as the experiment progresses which indicates enrichment of the hydrate phase with this gas. It is interesting to recall that the crystallizer operates in a semi-batch mode and constant pressure. The

fate of the gases in the crystallizer is tracked through equation 2.4 and the results are plotted in Figure 2-6 and Figure 2-7 which show the CO_2 and N_2 moles consumed to form hydrate. The CO_2/N_2 molar ratio is also shown. As seen, more gas is consumed at 11 MPa (experiment 3) compared to experiment 7 at 10 MPa. Since the number of moles of CO_2 consumed is almost same it means that more N_2 went into hydrate at 11 MPa. This is intuitively correct since the equilibrium formation pressure for N_2 is much higher than that of CO_2. As seen, the formation of hydrates from the CO_2/N_2 mixture resembles a fractionation process whereby the composition of the hydrate is different than that in the gas phase. This is desirable and provides the basis for a hydrate based CO_2/N_2 separation process.

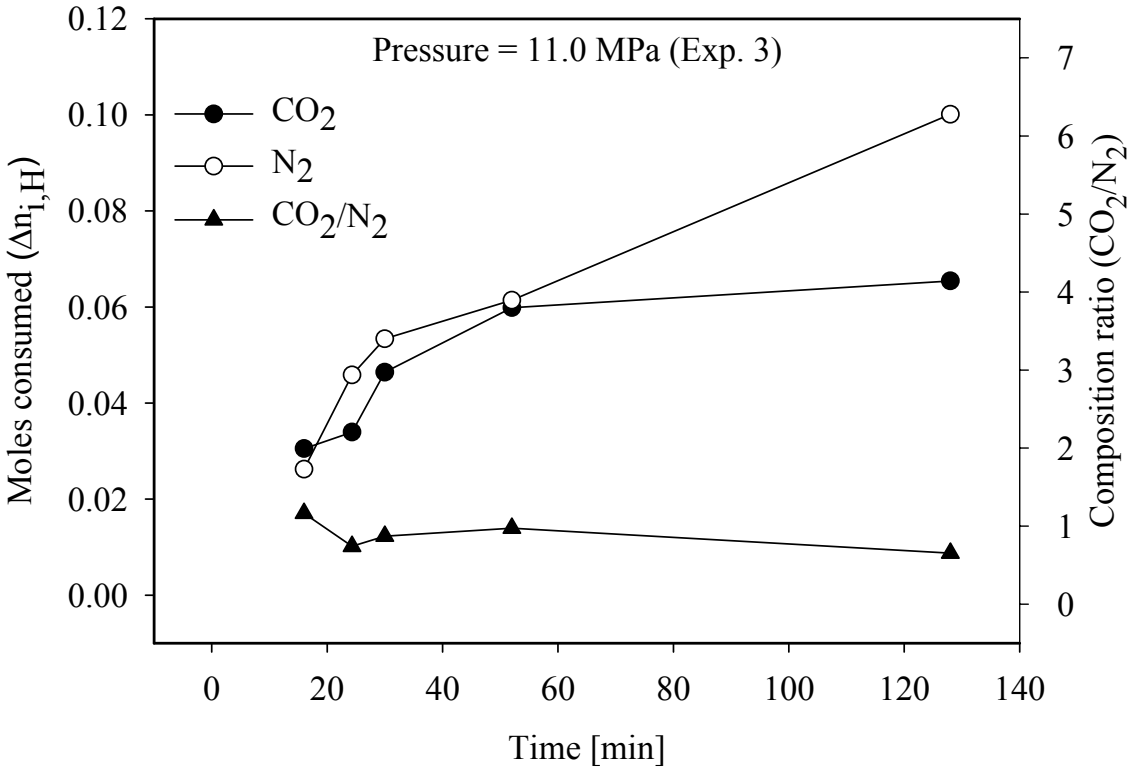

Figure 2-6: Mole consumption and molar ratio for the $CO_2/N_2/H_2O$ system at 11 MPa.

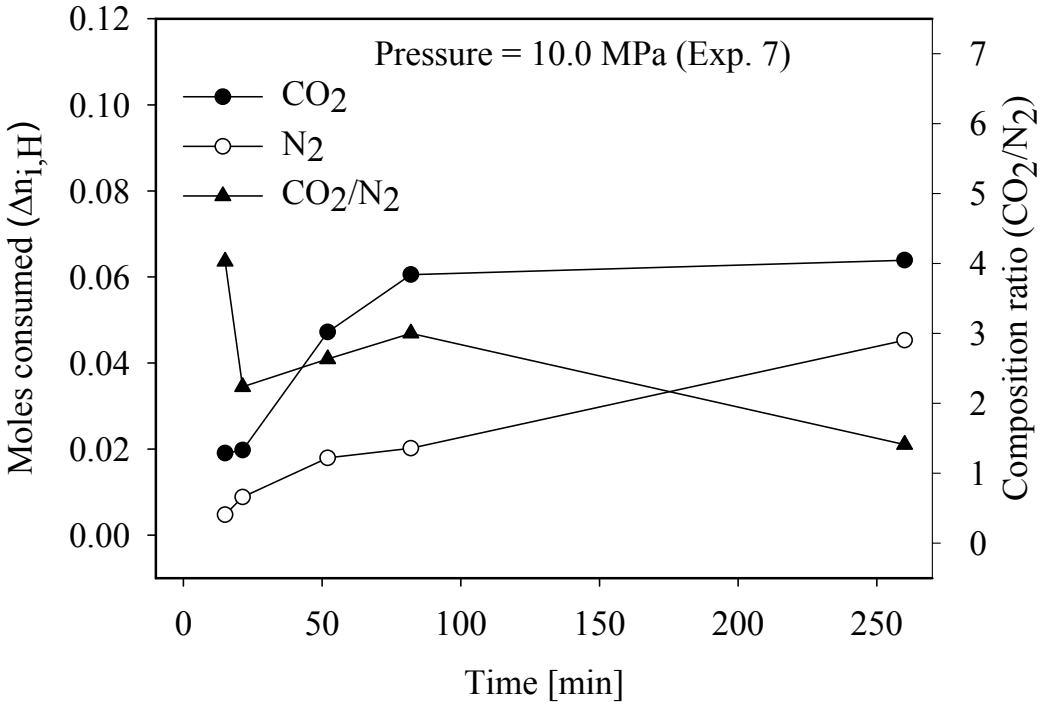

Figure 2-7: Mole consumption and molar ratio for the $CO_2/N_2/H_2O$ system at 10 MPa.

2.4. Conclusions

Incipient equilibrium hydrate formation data were presented for three temperatures for a 16.9% CO_2 rest N_2 gas mixture. The equilibrium pressure at 273.7, 274.8 and 275.9 K, was found to be 7.7, 8.4 & 9.2 MPa respectively. Gas hydrate formation kinetic experiments were carried out in a crystallizer operating in a semi-batch mode with a fixed amount of water and a continuous supply of gas at 273.7 K and constant pressure. Hydrates formed from memory water reduced the induction time significantly for experiment carried out at a lower driving force and the rate of hydrate formation decreases with decreasing driving force. CO_2 is preferentially incorporated into the hydrate crystal offering the possibility for separation from the binary CO_2/N_2 flue gas mixture. The water conversion achieved ranged from 4.3 to 11.2 %.

2.5. References

Aaron, D., and Tsouris, C., 2005. Separation of CO_2 from flue gas: A review. Separation Science and Technology 40(1-3), 321-348.

Bishnoi, P. R., and Natarajan, V., 1996. Formation and decomposition of gas hydrates. Fluid Phase Equilibria 117(1-2), 168-177.

Buchanan, P., Soper, A. K., Thompson, H., Westacott, R. E., Creek, J. L., Hobson, G., and Koh, C. A., 2005. Search for memory effects in methane hydrate: Structure of water before hydrate formation and after hydrate decomposition. Journal of Chemical Physics 123(16), -.

Clarke, M. A., and Bishnoi, P. R., 2005. Determination of the intrinsic kinetics of CO_2 gas hydrate formation using in situ particle size analysis. Chemical Engineering Science 60(3), 695-709.

Davidson, D. W., Leaist, D. G., and Hesse, R., 1983. Oxygen-18 Enrichment in the Water of A Clathrate Hydrate. Geochimical et Cosmochimica Acta 47, 2293.

Deaton, W. M., and Frost, E. M., 1946. Gas Hydrates and Their Relation to the Operation of Natural-Gas PipeLines. U.S. Dept. of the Interior, 1-101.

Englezos, P., 1993. Clathrate Hydrates. Industrial & Engineering Chemistry Research 32(7), 1251-1274.

Englezos, P., 1996. Nucleation and Growth of Gas Hydrate Crystals in Relation to "Kinetic Inhibition". Rev. IFP 51`(6), 789.

Englezos, P., Kalogerakis, N., Dholabhai, P. D., and Bishnoi, P. R., 1987a. Kinetics of Formation of Methane and Ethane Gas Hydrates. Chemical Engineering Science 42(11), 2647-2658.

Englezos, P., Kalogerakis, N., Dholabhai, P. D., and Bishnoi, P. R., 1987b. Kinetics of Gas Hydrate Formation from Mixtures of Methane and Ethane. Chemical Engineering Science 42(11), 2659-2666.

Englezos, P., and Lee, J. D., 2005. Gas hydrates: A cleaner source of energy and opportunity for innovative technologies. Korean Journal of Chemical Engineering 22(5), 671-681.

Fidel-Dufour, A., Gruy, F., and Herri, J. M., 2006. Rheology of methane hydrate slurries during their crystallization in a water in dodecane emulsion under flowing. Chemical Engineering Science 61(2), 505-515.

Kang, S. P., and Lee, H., 2000. Recovery of CO_2 from flue gas using gas hydrate: Thermodynamic verification through phase equilibrium measurements. Environmental Science & Technology 34(20), 4397-4400.

Kang, S. P., Lee, H., and Ryu, B. J., 2001. Enthalpies of dissociation of clathrate hydrates of carbon dioxide, nitrogen, (carbon dioxide plus nitrogen), and (carbon dioxide plus nitrogen plus tetrahydrofuran). Journal of Chemical Thermodynamics 33(5), 513-521.

Koh, C. A., 2002. Towards a fundamental understanding of natural gas hydrates. Chemical Society Reviews 31(3), 157-167.

Kumar, R., Linga, P., Moudrakovski, I., Ripmeester, J. A., and Englezos, P., 2008. Structure and kinetics of gas hydrates from methane/ethane/propane mixtures relevant to the design of natural gas hydrate storage and transport facilities. AIChE Journal 54(8), 2132-2144.

Lee, J. D., Susilo, R., and Englezos, P., 2005. Kinetics of structure H gas hydrate. Energy & Fuels 19(3), 1008-1015.

Linga, P., Kumar, R., and Englezos, P., 2006. Capture of Carbon dioxide from conventional power plants or from integrated gasification plants through gas hydrate formation/ dissociation. Journal of Energy & Climate Change 1(2), 75-82.

Moudrakovski, I. L., McLaurin, G. E., Ratcliffe, C. I., and Ripmeester, J. A., 2004. Methane and carbon dioxide hydrate formation in water droplets: Spatially resolved measurements from magnetic resonance microimaging. Journal of Physical Chemistry B 108(45), 17591-17595.

Rawn, C. J., Rondinone, A. J., Chakoumakos, B. C., Circone, S., Stern, L. A., Kirby, S. H., and Ishii, Y., 2003. Neutron powder diffraction studies as a function of temperature of structure II hydrate formed from propane. Canadian Journal of Physics 81(1-2), 431-438.

Ripmeester, J. A., and Ratcliffe, C. I., 1988. Low-temperature cross-polarization/magic angle spinning carbon-13 NMR of solid methane hydrates: structure, cage occupancy, and hydration number. J. Phys. Chem. 92(2), 337-9.

Seo, Y. T., Moudrakovski, I. L., Ripmeester, J. A., Lee, J. W., and Lee, H., 2005. Efficient recovery of CO_2 from flue gas by clathrate hydrate formation in porous silica gels. Environmental Science & Technology 39(7), 2315-2319.

Sloan, E. D., Jr., 1998. Clathrate Hydrates of Natural Gases, Second Edition, Revised and Expanded, Marcel Dekker, NY.

Smith, J. M., Van Ness, H. C., and Abbott, M. M., 2001. Introduction to Chemical Engineering Thermodynamics, McGraw-Hill, Inc., New York.

Sum, A. K., Burruss, R. C., and Sloan, E. D., 1997. Measurement of clathrate hydrates via Raman spectroscopy. Journal of Physical Chemistry B 101(38), 7371-7377.

Susilo, R., Moudrakovski, I. L., Ripmeester, J. A., and Englezos, P., 2006. Hydrate kinetics study in the presence of nonaqueous liquid by nuclear magnetic resonance spectroscopy and imaging. Journal of Physical Chemistry B 110(51), 25803-25809.

Susilo, R., Ripmeester, J. A., and Englezos, P., 2007. Characterization of gas hydrates with PXRD, DSC, NMR, and Raman spectroscopy. Chemical Engineering Science 62(15), 3930-3939.

Uchida, T., Ebinuma, T., and Narita, H., 2000. Observations of CO_2-hydrate decomposition and reformation processes. Journal of Crystal Growth 217(1/2), 189-200.

Uchida, T., Hirano, T., Ebinuma, T., Narita, H., Gohara, K., and Mae, S., 1999. Raman spectroscopic determination of hydration number of methane hydrates. AIChE Journal 45(12), 2641-2645.

Udachin, K. A., Ratcliffe, C. I., and Ripmeester, J. A., 2001. Structure, composition, and thermal expansion of CO2 hydrate from single crystal X-ray diffraction measurements. Journal of Physical Chemistry B 105(19), 4200-4204.

van Cleeff, A., and Diepen, G. A. M., 1960. Gas Hydrates of Nitrogen and Oxygen. Rec. Trav. Chim 79, 582.

Vysniauskas, A., and Bishnoi, P. R., 1983. A Kinetic-Study of Methane Hydrate Formation. Chemical Engineering Science 38(7), 1061-1072.

3. THE CLATHRATE HYDRATE PROCESS FOR POST COMBUSTION CAPTURE OF CO_2[2]

3.1. Introduction

There are two general approaches to CO_2 capture: either carbon can be removed before the fuel is burned (*pre-combustion capture*) or CO_2 can be removed from the flue gas (*post-combustion capture*) (Klara and Srivastava, 2002). Post combustion capture deals with CO_2 from conventional power plants. On the other hand Integrated Coal Gasification Cycle (IGCC) plants offer one of the most promising routes to CO_2 capture by converting the gas from the gasifier into a stream of H_2 and CO_2 via a shift reaction (Barchas and Davis, 1992). CO_2 can then be removed for disposal and the resultant H_2 could be used in fuel cells or in gas turbines. Further work is needed to improve efficiency and reduce operation cost of an IGCC plant, particularly with CO_2 capture (Audus, 1998; Davison, 2004).

A variety of processes have been developed for removing or isolating a particular gaseous component from a multi-component gaseous stream. These processes include absorption, adsorption, membrane separation etc. (Barchas and Davis, 1992; Kikkinides et al., 1993). It has been estimated that, the cost of separation and disposal of CO_2 from existing coal fired, air blown boilers would increase the cost of electricity by about 75 % (Hendriks, 1990). The cost of separation of CO_2 alone reduces the power generation efficiency from 38 to 26 % (Chakma et al., 1995). A thorough review on the processes

[2]A version of this chapter has been published. Linga, P., Kumar, R., and Englezos, P., 2007. The clathrate hydrate process for post and pre-combustion capture of carbon dioxide. Journal of Hazardous Materials 149(3), 625-629.

for CO_2 separation is available in the literature (Aaron and Tsouris, 2005). Liquid absorption using amines was considered the most promising current method while some other methods are promising but too new for comparison. There is continued interest in the development of less energy intensive processes.

3.2. The clathrate hydrate process

One of the new methods for separating CO_2 from flue gas or fuel gas (mixture of CO_2-H_2) is through clathrate or gas hydrate formation. As it was found in the previous chapter when gas hydrate crystals are formed from a CO_2/N_2 mixture the concentration of these gases in the hydrate crystals is different than that in the original gas mixture. This is the basis for the utilization of clathrate hydrate formation/decomposition as a separation process.

Treated flue gas contains CO_2, N_2, O_2. Since N_2 and O_2 form hydrate crystals at approximately the same conditions the treated flue gas is considered a CO_2/N_2 mixture. Thus, in post-combustion capture from power plants using hydrates, the task is to separate CO_2 from a CO_2/N_2 mixture in which the CO_2 molar content is approximately 15-20 %. Figure 3-1 illustrates the basic idea behind the gas separation using gas hydrate technology. A CO_2/N_2 mixture is fed in to the process where it comes into contact with water at suitable temperature and pressure conditions and forms hydrate crystals. The crystals are separated and subsequently decomposed to create the CO_2-rich stream while the rest constitute the CO_2-lean one.

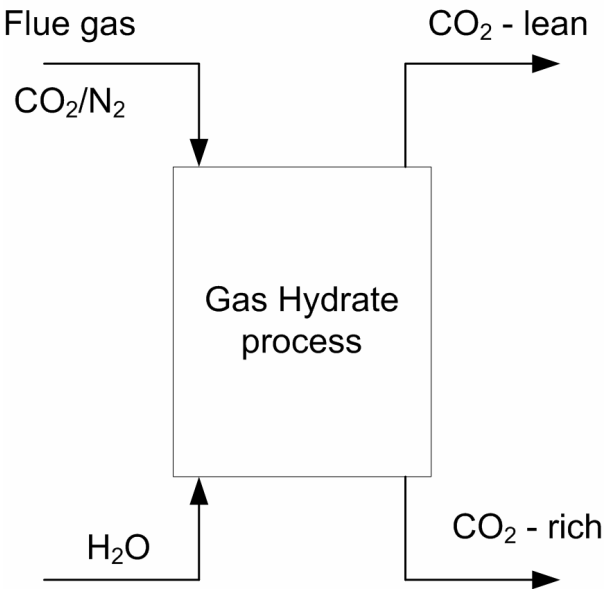

Figure 3-1: Hydrate based gas separation.

The first task towards process development is to determine the operating temperature and the minimum hydrate formation pressure at the operating temperature for the flue gas mixture. A conventional power plant emits flue gas of composition 15-20 % CO_2, 5- 9 % O_2 and rest N_2. Pretreatment involves removal of acid gases (H_2S, SO_2) and particulates. The pretreated flue gas is to be used in the clathrate hydrate process for CO_2 separation. A CO_2/N_2 gas mixture containing 16.9 % CO_2 was used in our work. A temperature of 273.7 K was chosen as the operating temperature since it was decided to form hydrate crystals from liquid water instead of ice. The hydrate formation pressure increases with temperature and in order to minimize compression costs the smallest possible pressure is desired. The minimum pressure to form hydrate crystals from this flue gas at 273.7 K was found to be 7.7 MPa. It is noted that at 273.7K, the minimum pressure required to form pure CO_2 and pure N_2 hydrates is 1.32 (Deaton and Frost, 1946) and 17.13 MPa (van Cleeff and Diepen, 1960) respectively.

The second task is to establish the rate of hydrate formation and separation efficiency. For that purpose hydrate formation/decomposition experiments were carried out at 273.7 K in a semi-batch mode. The hydrate formation experiments are described in detail in Chapter 2.

The rate of phase change from a water-gas mixture to hydrate is dependent on the magnitude of the deviation of the experimental conditions from those at equilibrium (Englezos, 1993; Lee et al., 2005). Thus, hydrate formation experiments were carried out at 10.0 and 11.0 MPa. These conditions are significantly above the minimum pressure (7.7 MPa) required for hydrate formation.

Following hydrate formation for about 120 minutes hydrate crystal/gas separation was carried out. The pressure in the crystallizer was quickly brought down to atmospheric pressure and the hydrates were allowed to completely dissociate. The gas which evolved from the decomposed hydrate and that released from the liquid water phase (dissolved amount at the higher pressure) was collected and analyzed by gas chromatography. The procedures for the hydrate formation and separation experiments are given as a flow diagram in Figure 3-2.

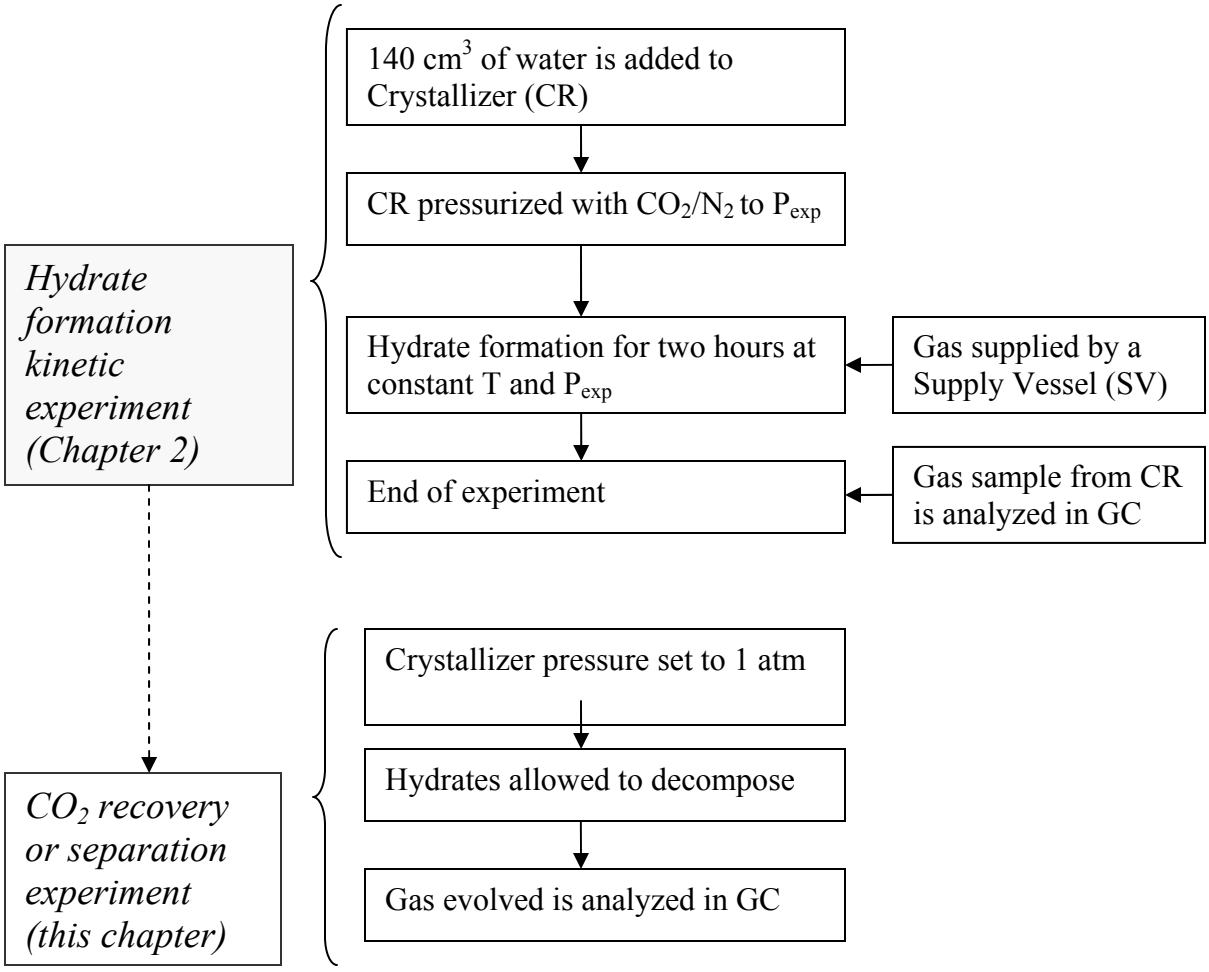

Figure 3-2: Block diagram of the experimental methods for the hydrate formation kinetic and separation experiments.

3.3. CO_2 recovery and separation factor

The following quantities are introduced in order to provide appropriate metrics for the separation. Their values are calculated based on the kinetic and separation experiments. The CO_2 *recovery* or *split fraction* (S.Fr.) of carbon dioxide in gaseous and hydrate phase is calculated as follows

$$S.Fr. = \frac{n_{CO_2}^{H}}{n_{CO_2}^{Feed}} \tag{3.1}$$

where $n_{CO_2}^{Feed}$ is the as number of moles of CO_2 in feed gas and $n_{CO_2}^{H}$ is the number of moles of CO_2 in hydrate phase at the end of the experiment. In addition, the *separation factor* (S.F) is given by

$$S.F. = \frac{n_{CO_2}^{H} \times n_{N_2}^{gas}}{n_{N_2}^{H} \times n_{CO_2}^{gas}} \tag{3.2}$$

where $n_{CO_2}^{gas}$ is the number of moles of CO_2 in the gas phase at the end of the kinetic experiment, $n_{N_2}^{gas}$ is the number of moles of N_2 in the gas phase at the end of the kinetic experiment and $n_{N_2}^{H}$ is the number of moles of N_2 in the hydrate phase.

3.4. Results and discussion

Figure 3-3 shows the CO_2 content in the flue gas mixture (initial composition), the hydrate formed and the residual gas phase (final composition). As seen, flue gas (17% CO_2) forms hydrate which contains about 55 to 57 % CO_2. The split fraction or CO_2 recovery was calculated and was found to be 36.7 % for the experiment carried out at 11.0 MPa and 273.7 K. The separation factor for the above experiment calculated from equation 2 is 5.3. For the experiment at 10.0 MPa and 273.7 K the values obtained for CO_2 recovery and separation factor are 42.1 % and 13.2 respectively (see Table 3-1). As the pressure increases the CO_2 recovery decreases. This is due to the fact that at higher pressure more number of N_2 gas will occupy its corresponding cages in the hydrate structure. This is also seen in the decrease in the separation factor.

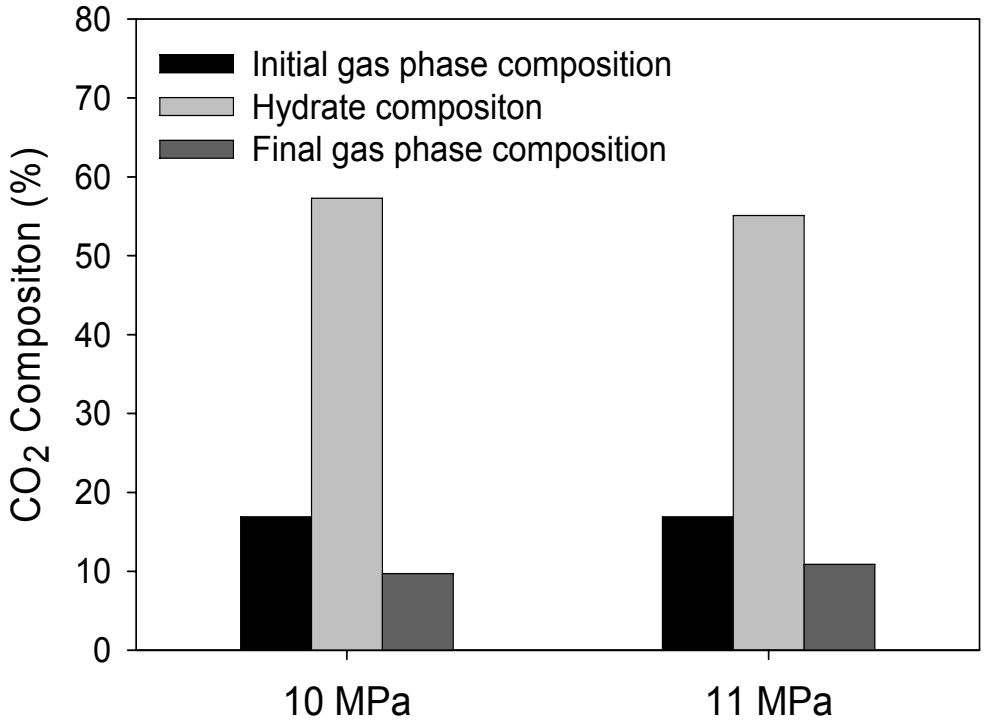

Figure 3-3: Hydrate based separation for CO_2 (16.9 mol %) – N_2 (83.1 mol %) gas mixture (Temperature = 273.7 K, 120 Minutes growth).

The above results indicate that following a one-stage hydrate formation/decomposition process for the CO_2/N_2 mixture, a CO_2-rich gas is obtained which contains 57.3 % CO_2 at 10 MPa. Given that the equilibrium hydrate formation pressure of this gas mixture is about 2.4 MPa, a second stage is advocated to obtain a more concentrated CO_2 mixture. The second hydrate formation vessel would operate at a lower pressure compared to the first one since the equilibrium pressure is lower by about 5.3 MPa. The hydrate formation/separation experiment was carried out for a gas mixture consisting of 57.0% CO_2 and rest N_2 at 5.0 MPa and 273.7 K. Figure 3-4 shows the gas uptake curve for the above experiment. The composition of this hydrate after decomposition had 83.2% CO_2 and the rest N_2. Hence a third stage of hydrate formation/separation is carried out using this gas mixture. Hydrate formed from the

83.0%/17.0% (CO_2/N_2) gas mixture at 2.5 MPa and 273.7 K gave a hydrate with a composition of 99.1% CO_2. This CO_2 can be readily disposed for sequestration. Figure 3-5 shows the gas uptake curve for the experiment conducted. The uptake curves in figure 3-4 and figure 3-5 display the expected characteristics of the gas uptake curve.

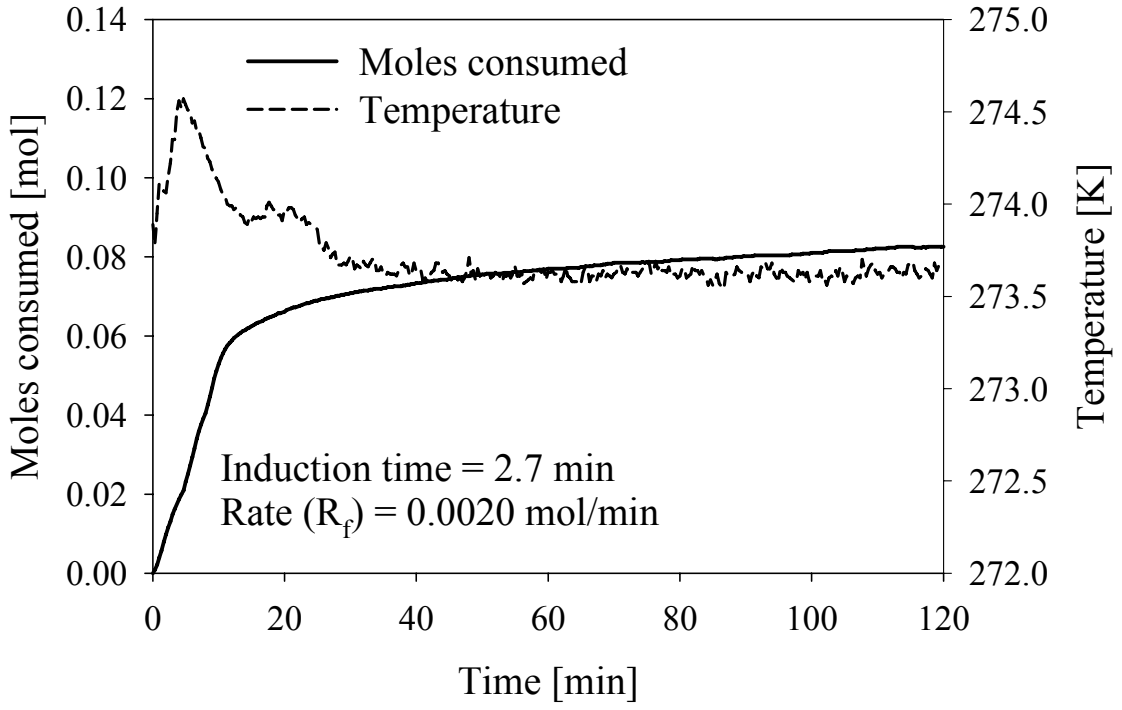

Figure 3-4: Gas uptake measurement curve for the second stage (Pressure = 5.0 MPa & Temperature = 273.7K).

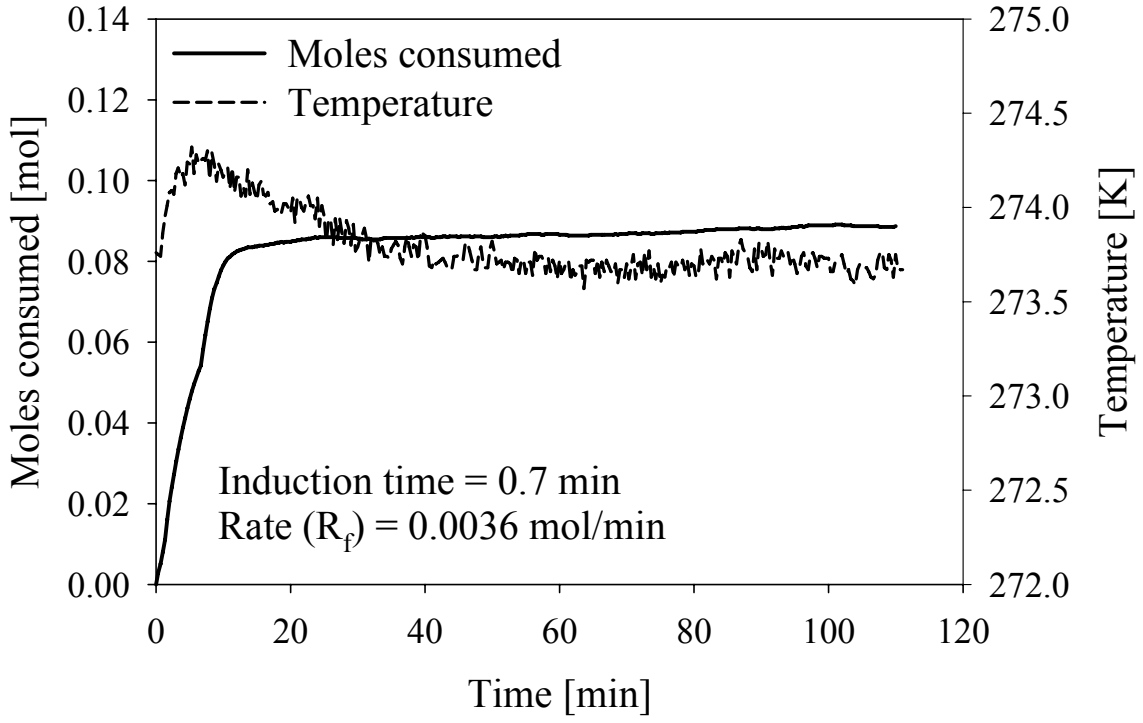

Figure 3-5: Gas uptake measurement curve for the third stage (Pressure = 2.5 MPa & Temperature = 273.7K).

Figure 3-6 shows the CO_2 content in the flue gas mixture (initial composition), the hydrate formed and the residual gas phase (final composition) for the three stages. Hence, in three stages of hydrate formation/decomposition it is possible to obtain a CO_2 rich stream consisting of 99.0% CO_2. Moreover, we envision a hybrid process whereby hydrate formation in three stages is combined with a membrane process. This concept is illustrated in Figure 3-7.

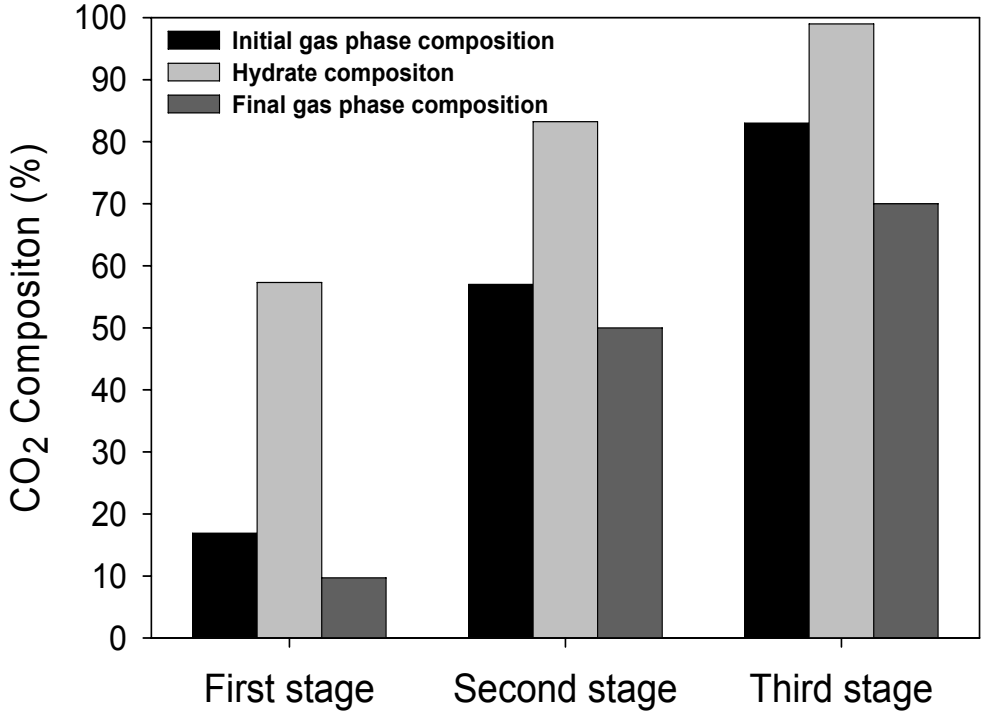

Figure 3-6: Composition changes due to stage-wise hydrate formation from CO_2/N_2 mixtures.

Table 3-1 shows the calculated split fraction and separation factors for the three stages for CO_2/N_2 separation. The major disadvantage of the process shown in Figure 3-7 is the high pressure required specially in the first stage. The above-illustrated process shows the feasibility of the concept but not the economic viability. Compression costs were calculated for a 500 MW conventional power plant, in order to pressurize the flue gas from 0.1 MPa and 70^{o}C to 10 MPa and 1^{o}C. It was found that four compression stages with inter-cooling are required. The power penalty was found to be 385 MW, which is 75% of the power output (The calculations are given in Appendix B). Clearly, from an economic viewpoint lower pressures are required. This can be achieved by adding a proper chemical to reduce the hydrate formation pressure at any given temperature without compromising the CO_2 recovery and separation efficiency. Clearly,

this demonstrates the need for additives to render the hydrate process economically attractive. Tetrahydrofuran (THF) is one such additive (Kang and Lee, 2000). Its evaluation is presented in the next chapter.

Table 3-1: Split fraction and separation factors for the three stages for CO_2/N_2 separation.

System	Experimental conditions		Split fraction or CO_2 recovery	Separation factor
	Pexp (MPa)	Peq (MPa)		
CO_2 (16.9%)/N_2	10.0	7.7	0.42	13.2
CO_2 (57.0%)/N_2	5.0	2.4	0.32	7.3
CO2 (83.0%)/N_2	2.5	1.6	0.38	36.7

Pexp: Experimental pressure; Peq: Equilibrium pressure

3.5. Conclusions

New kinetic and thermodynamic data on the separating of carbon dioxide from flue gas (post combustion capture) using gas hydrate formation are presented. Hydrate crystal formation/decomposition from CO_2/N_2 mixtures showed that CO_2 prefers the hydrate phase compared to N_2. Two metrics split fraction or CO_2 recovery and separation factor were introduced to quantify the separation achieved by the hydrate process. CO_2 recovery was found to be 36.7 to 42.1 % in one stage at 11.0 and 10.0 MPa respectively. A hybrid hydrate-membrane process was proposed for the post combustion capture of carbon dioxide involving three hydrate formation/decomposition stages. The process is able to produce a 99.0% CO_2 stream. Compression calculations revealed that additives must be used in order to reduce the operating pressure and thus improve the economics of the process.

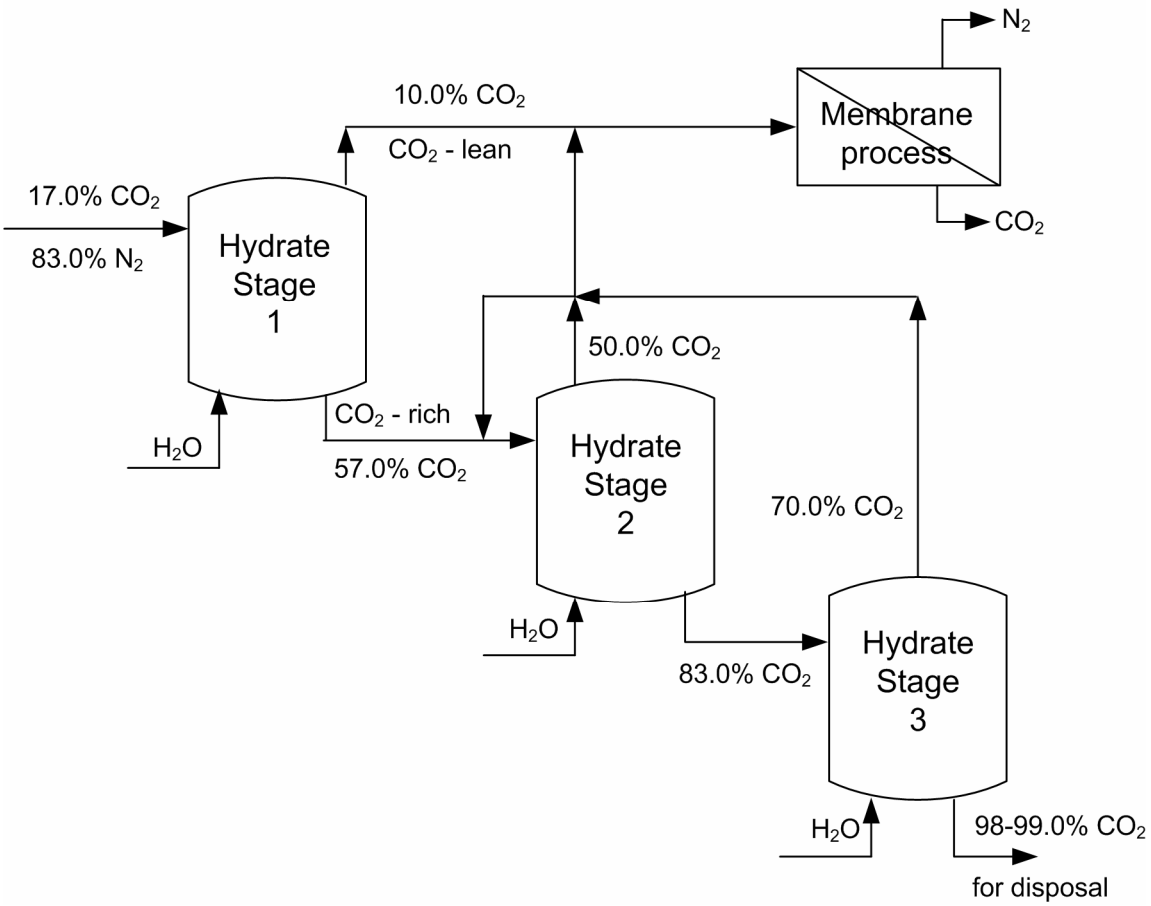

Figure 3-7: A hybrid hydrate-membrane process for CO_2 recovery from flue gas.

3.6. References

Aaron, D., and Tsouris, C., 2005. Separation of CO_2 from flue gas: A review. Separation Science and Technology 40(1-3), 321-348.

Audus, H., Olav, K. and Geoff, S., 1998. International Conference on Greenhouse Gas Control Technologies, Interlaken, Switz., 557-562.

Barchas, R., and Davis, R., 1992. The Kerr-Mcgee Abb Lummus Crest Technology for the Recovery of CO_2 from Stack Gases. Energy Conversion and Management 33(5-8), 333-340.

Chakma, A., Mehrotra, A. K., and Nielsen, B., 1995. Comparison of Chemical Solvents for Mitigating CO_2 Emissions from Coal-Fired Power-Plants. Heat Recovery Systems & Chp 15(2), 231-240.

Davison, J., Bressan, L. and Domenichini, R., 2004. CO_2 Capture in Coal-Based IGCC Power Plants. 7th International Conference on Greenhouse Gas Control Technologies, Vancouver, 167.

Deaton, W. M., and Frost, E. M., 1946. Gas Hydrates and Their Relation to the Operation of Natural-Gas Pipe Lines. U.S. Dept. of the Interior, 1-101.

Englezos, P., 1993. Clathrate Hydrates. Industrial & Engineering Chemistry Research 32(7), 1251-1274.

Hendriks, C. B., K.; Turkenburg, W., 1990. Climate and Energy. Dordrec, The Netherlands, 125-188.

Kang, S. P., and Lee, H., 2000. Recovery of CO_2 from flue gas using gas hydrate: Thermodynamic verification through phase equilibrium measurements. Environmental Science & Technology 34(20), 4397-4400.

Kikkinides, E. S., Yang, R. T., and Cho, S. H., 1993. Concentration and Recovery of CO_2 from Flue-Gas by Pressure Swing Adsorption. Industrial & Engineering Chemistry Research 32(11), 2714-2720.

Klara, S. M., and Srivastava, R. D., 2002. US DOE integrated collaborative technology development program for CO_2 separation and capture. Environmental Progress 21(4), 247-253.

Lee, J. D., Susilo, R., and Englezos, P., 2005. Kinetics of structure H gas hydrate. Energy & Fuels 19(3), 1008-1015.

Linga, P., Kumar, R., and Englezos, P., 2007. Gas hydrate formation from hydrogen/carbon dioxide and nitrogen/carbon dioxide gas mixtures. Chemical Engineering Science 62(16), 4268-4276.

van Cleeff, A., and Diepen, G. A. M., 1960. Gas Hydrates of Nitrogen and Oxygen. Rec. Trav. Chim 79, 582.

4. THE MEDIUM-PRESSURE CLATHRATE HYDRATE/MEMBRANE HYBRID PROCESS FOR POST COMBUSTION CAPTURE OF CO_2[3]

4.1. Introduction

A conceptual process flow sheet was presented in Chapter 3 for the recovery of carbon dioxide from a flue gas mixture in three stages. The first stage requires a pressure of 10 MPa. In order to compress the flue gas from a 500 MW conventional power plant 75 % of the power output would be required. Consequently, the need for a lower pressure process was recognized. It is known that the addition of tetrahydrofuran (THF) even in small quantities considerably reduces the equilibrium pressure (Kang and Lee, 2000). While the THF reduces the equilibrium pressure it is not known how the kinetics of the phase change is influenced. Therefore, it is of interest to assess how the addition of THF also affects the kinetics of hydrate formation and separation efficiency and CO_2 recovery.

Thus, the objective is to provide a conceptual process based on the use of THF along with the relevant thermodynamic data and kinetic information as well as data on the CO_2 recovery and separation efficiency of the process.

4.2. Experimental section

A CO_2/N_2 gas mixture containing 16.9 % CO_2 was used in our experimental work to simulate a pre-treated flue gas mixture. THF used in the experimental work was supplied

[3]A version of this chapter has been published. Linga, P., Adeyemo, A., and Englezos, P., 2008. Medium-pressure clathrate hydrate/membrane hybrid process for post combustion capture of carbon dioxide. Environmental Science & Technology 42(1), 315-320.

by Fisher Scientific with 99% purity. The water used was distilled and deionised. The apparatus and procedures to carry out hydrate phase equilibrium measurements, hydrate kinetic experiments and CO_2 recovery determination (separation experiment) are all described in chapter 2 & chapter 3. Therefore, only a brief description will be given along with relevant references.

The isothermal pressure search method to determine the incipient phase equilibrium hydrate formation pressure at a given temperature and a given THF concentration in the water was followed. Gas hydrate formation kinetic experiments were conducted in a high pressure vessel operating like a chemical reactor in a semi-batch manner at constant temperature and pressure. The apparatus is properly instrumented with pressure and temperature sensors to allow calculation of the mass of gas being consumed in the crystallizer (gas uptake) versus time. In addition, gas phase composition in the hydrate vessel was also measured with a Varian CX-3400 gas chromatograph (GC) with a thermal conductivity detector.

After the end of a kinetic (gas uptake measurement) experiment, the pressure in the crystallizer was quickly brought down to the atmospheric pressure and the hydrates were allowed to completely dissociate. The gas which evolved from the decomposed hydrate and that released from the liquid water phase (dissolved amount at the higher pressure) was collected in the crystallizer (CR).

A temperature of 273.7 K was chosen as the operating temperature. It is noted that the minimum pressure to form hydrate crystals from this flue gas in pure water at 273.7 K was found to be 7.7 MPa. Hydrate kinetic measurements in which the gas uptake in the hydrate crystallizer is measured were carried out at 273.7 K and at different pressures for

0.5, 1.0 and 1.5 mol% THF solutions. All kinetics experiments were carried out at pressures above the equilibrium so that a finite rate of crystallization is obtained. The rate of phase change from a water-gas mixture to hydrate depends on the magnitude of the deviation of the experimental conditions from those at equilibrium (Lee et al., 2005; Uchida et al., 2000). The deviation of the experimental pressure from the equilibrium pressure (overpressure) is called *driving force*. Experiments with fresh water as well as with memory water were conducted.

Conversion of water to hydrates is determined from the information obtained from gas uptake and the experimental conditions using the following equation

$$\text{Connversion of water to hydrates}\,(\text{mol}\%) = \frac{(\Delta n_{H,\downarrow} + \Delta n_{THF}) \times \text{Hydration Number}}{n_{H_2O}} \times 100 \quad (4.1)$$

where $\Delta n_{H,\downarrow}$ is the number of moles of gas consumed for hydrate formation at the end of the experiment determined from the gas uptake measurement, n_{H_2O} is the total number of moles of water in the system and Δn_{THF} is the number of moles of THF consumed for hydrate formation at the end of the kinetic experiment. Δn_{THF} is calculated based on the occupancy ratio for sII (16S:8L), i.e. 1 mole of gas consumed in small cages would require ½ mole of THF in the large cage.

4.3. Results and discussion

4.3.1. Phase equilibrium measurements

Table 4-1 presents the incipient hydrate formation conditions for the flue gas mixture in the presence of varying amounts of THF at 273.7, 274.8 and 275.9 K. The CO_2 composition in the gas phase at the equilibrium condition was determined by gas

chromatography and is also given in the table. As seen, the gas phase is slightly leaner in CO_2 compared to that of the original gas mixture as expected due to the differential solubility of CO_2 and N_2 in water.

Phase equilibrium measurements were carried out for three molar concentrations of THF which are 0.5, 1.0 and 1.5 mol% respectively. For all the three molar concentrations of THF and 17% CO_2/N_2 gas mixture, the hydrates structure formed is sII (Kang and Lee, 2000; Kang et al., 2001a). It is noted that 17.0% CO_2 and rest N_2 gas mixture in pure water forms structure I (Seo and Lee, 2004).

Table 4-1: Incipient equilibrium hydrate formation conditions for CO_2/N_2/THF/water system.

THF Concentration	0.5 mol %		1.0 mol %		1.5 mol %	
Temperature (K)	Pressure (kPa)	% CO_2 in gas phase at equilibrium	Pressure (kPa)	% CO_2 in gas phase at equilibrium	Pressure (kPa)	% CO_2 in gas phase at equilibrium
273.7	920	16.8	345	16.8	130*	16.8
274.8	1090	15.8	500	15.9	200	15.6
275.9	1350	15.2	690	15.6	410	15.2

* Obtained at 274.2 K

Figure 4-1 shows the incipient equilibrium hydrate formation conditions obtained in the presence of THF compared to that of pure water for the same flue gas mixture. Incipient refers to the situation that an infinitesimal amount of hydrate crystals coexist in equilibrium with the gas and aqueous phases (Englezos and Ngan, 1994). As seen, there is a considerable reduction in the equilibrium formation pressures in the presence of THF

compared to hydrate formation in pure water. The results also agree well with the literature (Kang and Lee, 2000; Kang et al., 2001a). Interestingly, the system with 1.5 mol% THF formed hydrates at ambient pressure at 273.7K.

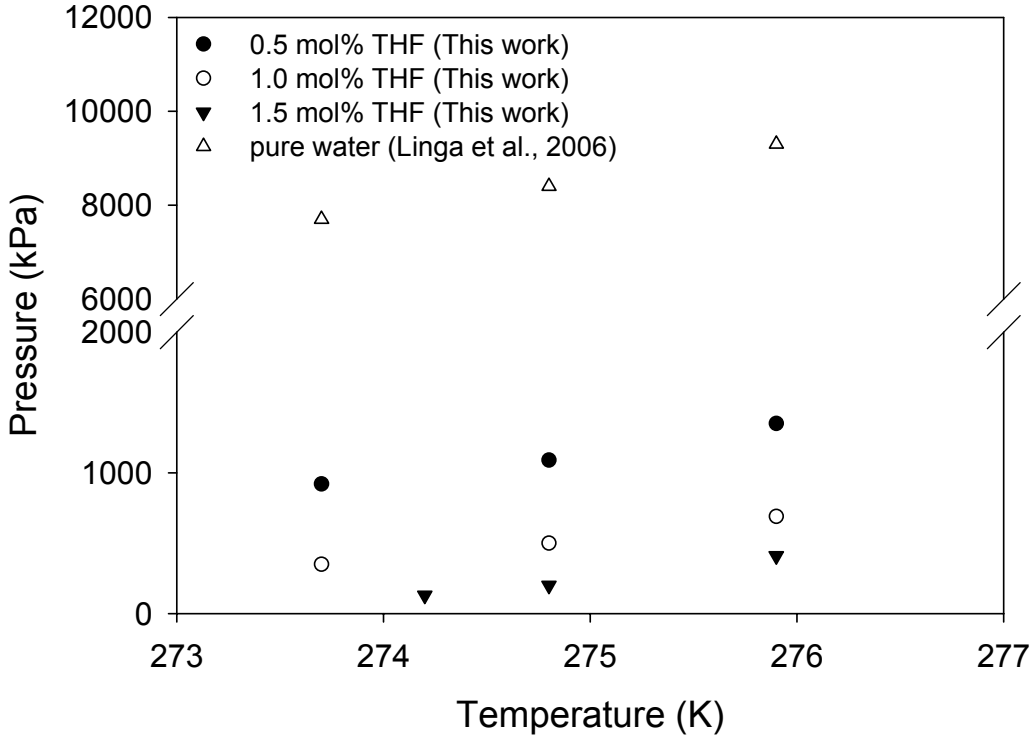

Figure 4-1: Incipient equilibrium hydrate formation conditions for 16.9 % CO_2 and rest N_2 gas mixture.

The incipient equilibrium measurements indicate that it is preferable from a process design point of view to select the highest THF concentration and thus achieve the greater reduction in pressure. For instance, the flue gas mixture that required a minimum pressure of 7.7 MPa at 273.7 K, now requires only 0.345 MPa to form crystals with the addition of 1 mol% THF.

Makino et al. (2005) reported phase equilibria for the tetrahydrofuran + water system below atmospheric pressure in the temperature range from 272 to 278 K. The temperature-composition diagram of THF + water system (not isobaric conditions) is

given in Figure 4-2. Makino et al. (2005) reported that a 1.13 mol% THF solution can form crystals at 272.27 K & 1.2 kPa while a 2.44 mol% THF solution can form crystals at 275.73 K & 2.6 kPa. This explains why the 1.5 mol % THF solution formed hydrates at ambient pressure and 273.7 K.

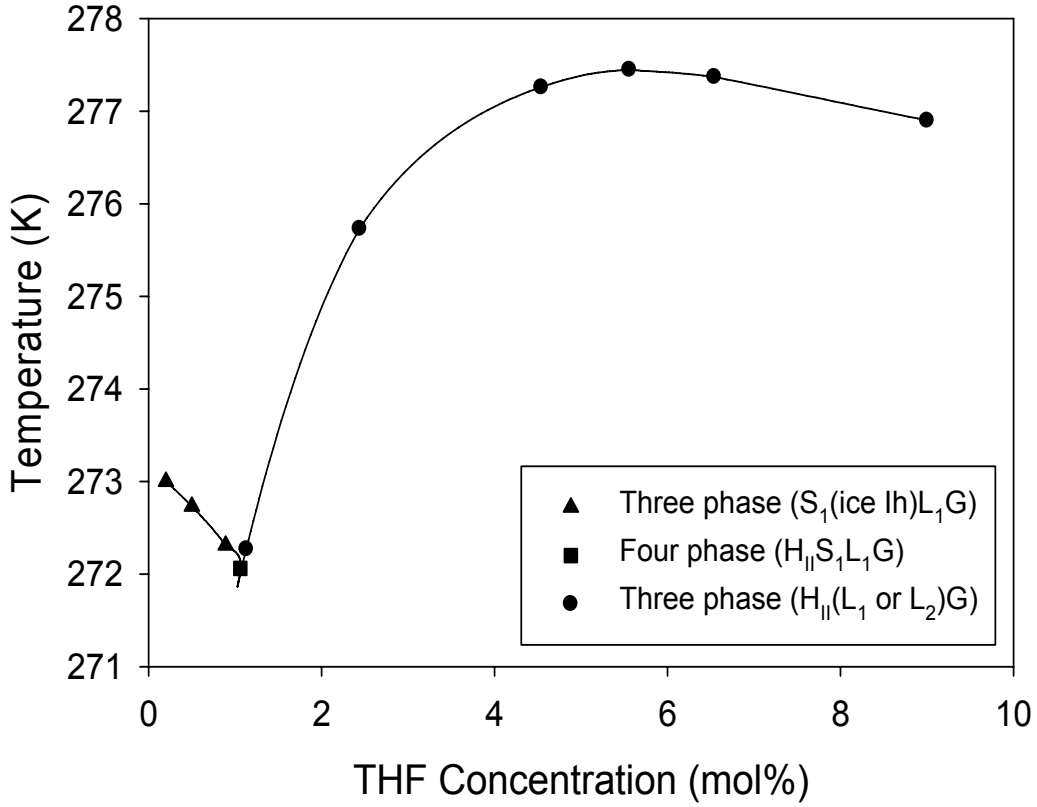

Figure 4-2: Temperature-Composition equilibrium data for THF + water system (not isobaric condition). The symbols H_{II}, S, L, and G stand for s-II THF hydrate, solid (ice Ih), aqueous solution, and gas phases, respectively. The subscript 1 means that the THF composition is lower than the stoichiometric ratio of s-II THF hydrate, and 2 means a composition greater than the stoichiometric ratio (stoichiometric ratio of s-II THF hydrate is 5.56 mol%). Reprinted ("Adapted") with permission from Makino et al. (2005). Copyright 2005 American Chemical Society.

4.3.2. Gas uptake measurements

Table 4-2 summarizes the results from the kinetic experiments at 273.75 K. As seen, the induction times at the pressures chosen to conduct the experiments are very

short (less than 7 minutes). Short induction times are definitely desirable from a practical stand point to speed up the process but the drawback of increasing the pressure is the higher compression costs. Finally, the induction times with memory water are either smaller or practically the same with those in fresh water. Thus, the memory effect is either very small or negligible because the induction times with fresh water are very short.

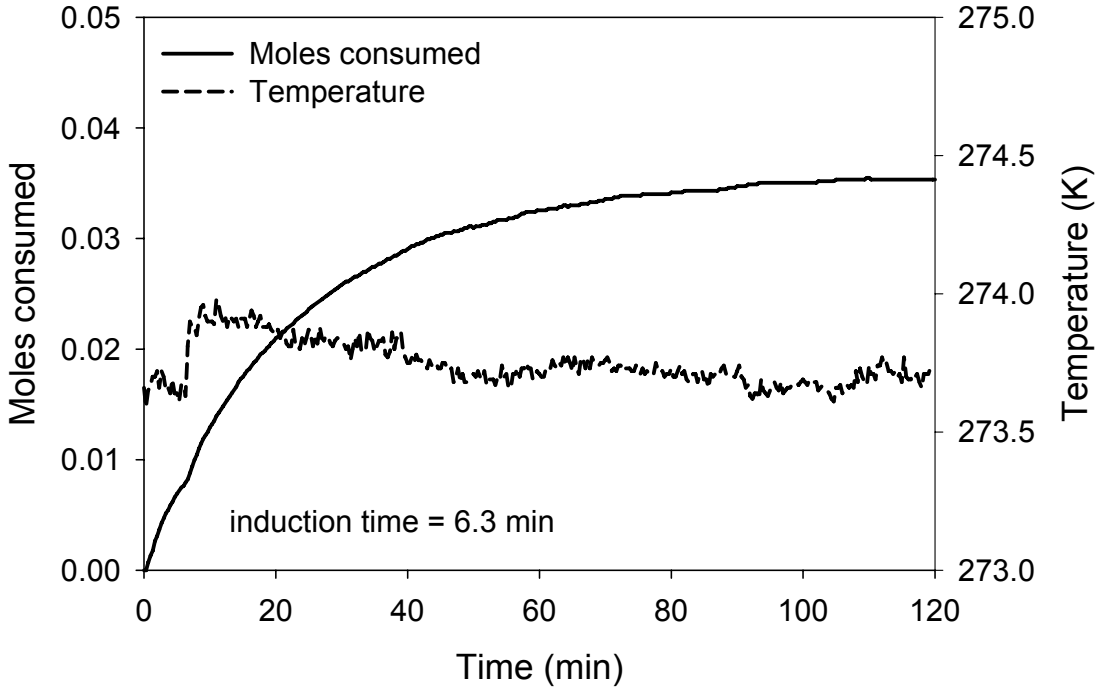

Figure 4-3: Gas uptake measurement for the CO_2/N_2/THF hydrate at 273.7 K and 2.2 MPa in the presence of 0.5 mol% THF (experiment 1).

Figure 4-3 shows a typical gas uptake curve for a period of two hours. This curve represents the kinetics of hydrate growth and agglomeration for the indicated time. The general shape of this curve agrees with the gas uptake curve described in detail by Bishnoi and Natarajan (1996) and Lee et al. (2005). The temperature in the aqueous water phase was also measured and shown in the figure. As seen in the figure, the temperature rises immediately after nucleation because hydrate formation is an exothermic process. The temperature reaches a higher level and then gradually is brought down because the

temperature controller brings back the temperature to the set point value. The number of moles of gas (CO_2/N_2) consumed up to the induction time of 6.3 min is 0.0079. The gas uptake curves for all the other experiments reported in the Table 4-2 are given in Appendix C.

The rate of hydrate growth, R_f, is defined operationally as the slope of the gas uptake curve during the first 20 min after the nucleation point (Lee et al., 2005; Linga et al., 2007b). The standard errors and R^2 values for the calculated rates (given in Table 4-2) are given in Appendix C (Table C-1). As seen in Table 4-2, the rates increase with increasing driving force at the same THF concentration as expected. However, the effect of THF concentration is interesting because the observed rates are maximum at 1 mol % THF. The total number of moles consumed at the end of the experiment was also found to be higher in the case of 1.0 mol% THF. Figure 4-4 shows the gas uptake measurements at a constant driving force of 1.2 MPa and different THF concentrations. It is interesting to note that this concentration dependency was also observed for the memory experiments at the same corresponding driving force. The same was observed for experiments carried out at the higher driving force of 2.2 MPa. Figure 4-5 shows the gas uptake curves obtained from three experiments carried out at a 2.2 MPa driving force with memory water. It is not known why the addition of more THF would decrease the rate of gas uptake. From a practical standpoint the 1.0 mol % THF concentration is considered optimum at 273.7 K. It has to be noted that for the same temperature the minimum pressure required for hydrate formation is 7.7 MPa for the CO_2/N_2 system in the absence of THF.

Table 4-2: Experimental conditions along with measured induction times and hydrate formation rates for $CO_2/N_2/THF/H_2O$ system at 273.7 K. The CO_2/N_2 composition of the mixture was 16.9 mol % CO_2 and balance N_2.

THF concentration (mol%)	Exp. No.	Sample State	Driving force[a] (MPa)	Pexp (MPa)	Induction Time (min)	R_f[b] (mol/min)	Final moles consumed (mol of gas/mol of H_2O)	Water conversion to hydrate[d] (%)
0.5	1	Fresh	1.25	2.15	6.3	0.0008	0.0046	4.0
	2	Memory	1.25	2.15	2.7	0.0009	0.0042	3.6
	3	Fresh	2.25	3.15	4.3	0.0013	0.0061	5.2
	4	Memory	2.25	3.15	2.7	0.0014	0.0062	5.3
1.0	5	Fresh	0.70	1.05	1.3	0.0005	0.0031	2.6
	6	Memory	0.70	1.05	1.3	0.0006	0.0024	2.1
	7	Fresh	1.20	1.55	1.0	0.0010	0.0057	4.8
	8	Memory	1.20	1.55	1.0	0.0010	0.0052	4.5
	9	Fresh	2.20	2.55	0.7	0.0012	0.0083	7.1
	10	Memory	2.20	2.55	0.3	0.0016	0.0083	7.1
1.5[c]	11	Fresh	1.20	1.35	0.3	0.0008	0.0046	3.9
	12	Memory	1.20	1.35	0.3	0.0008	0.0043	3.7
	13	Fresh	2.20	2.35	0.3	0.0007	0.0069	5.9
	14	Memory	2.20	2.35	0.3	0.0007	0.0055	4.7
	15	Fresh	1.20	1.35	0.3	0.0007	0.0053	4.5
	16	Memory	1.20	1.35	0.3	0.0008	0.0034	2.9
	17	Fresh	2.20	2.35	0.3	0.0009	0.0075	6.4
	18	Memory	2.20	2.35	0.3	0.0009	0.0048	4.1

[a] Driving force = P_{exp} - P_{eq} (P_{exp} = experimental pressure, P_{eq} = equilibrium pressure)

[b] Rate of hydrate growth (gas consumption rate for the first 20 min after nucleation)

[c] Experiments carried out at 274.2 K

[d] Hydration number of 5.71 (Kang et al., 2001b) was used for the calculation.

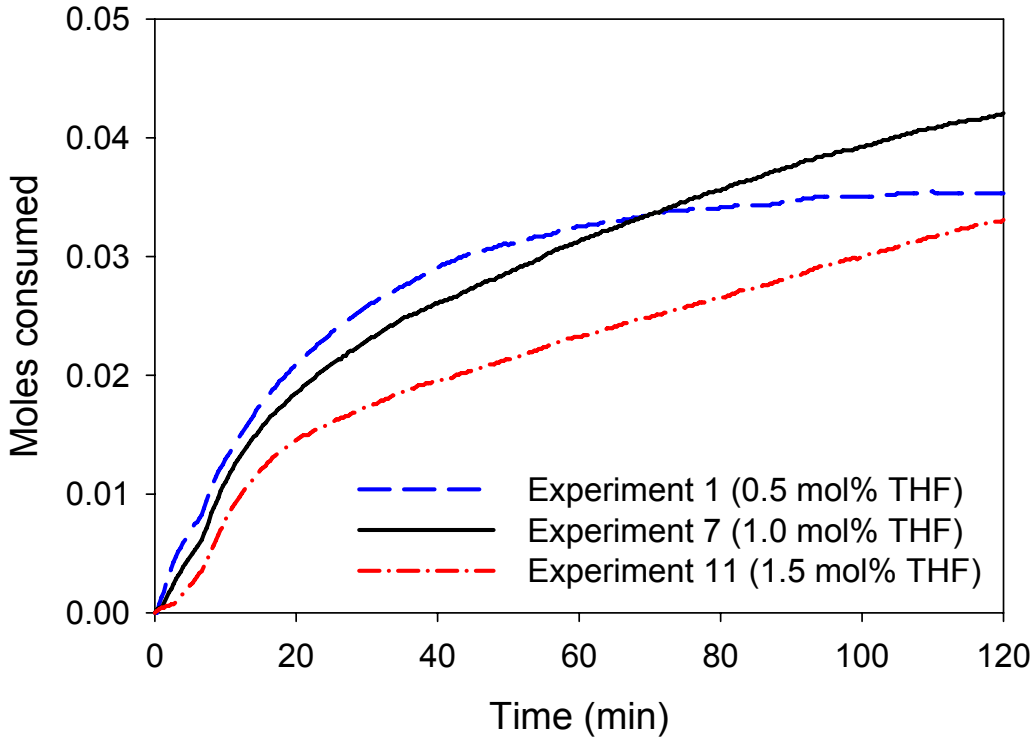

Figure 4-4: Gas uptake measurement curves for 0.5, 1.0 and 1.5 mol% THF fresh solutions carried out at a driving force of 1.2 MPa or at a pressure of 2.15, 1.55 and 1.4 MPa, respectively.

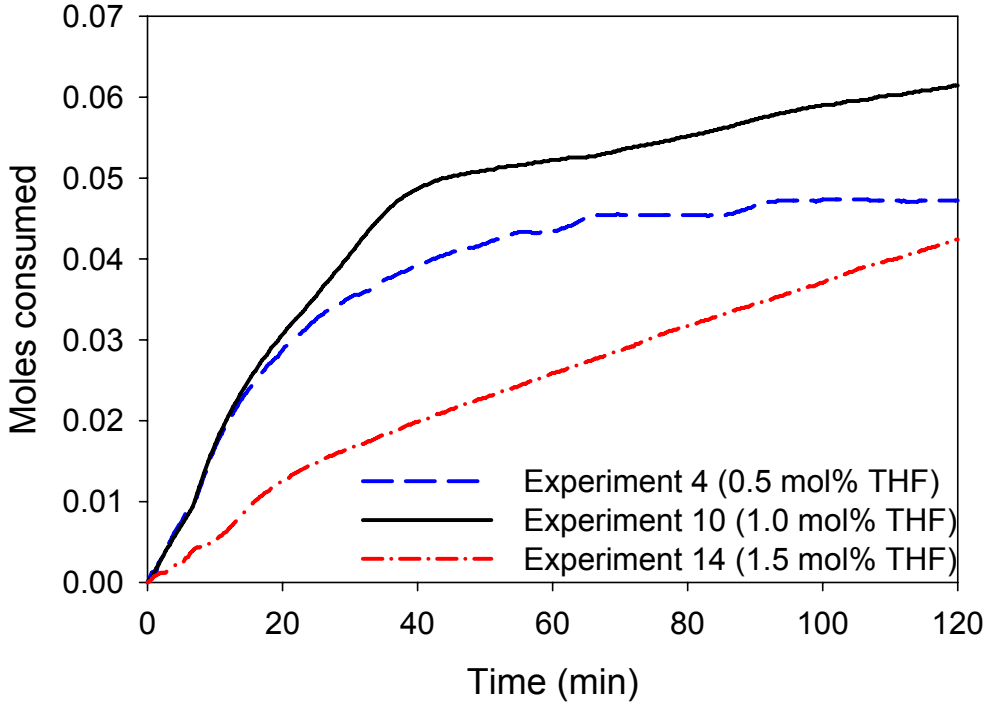

Figure 4-5: Gas uptake measurement curves for 0.5, 1.0 and 1.5 mol% THF memory solutions carried out at a driving force of 2.2 MPa or at a pressure of 3.15, 2.55 and 2.35 MPa, respectively.

The conversion of water to hydrate for the kinetic experiments performed for different THF concentrations and at different driving force is also given in Table 4.2. The increase in the driving force gave better yields for the experiments for any given THF concentration. The same trend was observed for the other THF concentrations. It is noted that the water conversion to hydrates for 0.5, 1.0 and 1.5 mol% THF solutions are 5.25%, 7.10% and 5.28%, respectively for the experiments conducted at a driving force of 2.2 MPa. This is due to the fact that higher gas consumption was achieved for 1.0mol% THF experiments compared to 0.5 and 1.5mol% THF experiments. Similar trend can be seen for the experiments conducted at the lower driving force (1.2MPa).

Table 4-3: Vapor phase composition during hydrate formation from CO_2/N_2/THF system.

CO_2/N_2/1.0 mol% THF/H_2O at 1.0 MPa (Experiment 5)		CO_2/N_2/1.5mol%THF/H_2O at 1.4 MPa (Experiment 16)	
Sampling time (min)	CO_2 mole fraction in CR (y_{CO_2})	Sampling time (min)	CO_2 mole fraction in CR (y_{CO_2})
0.0	0.169	0.0	0.169
5.0	0.149	10.0	0.157
10.0	0.131	20.0	0.131
20.0	0.120	40.0	0.111
40.0	0.109	60.0	0.103
60.0	0.101	120.0	0.099
120.0	0.098		

The composition of the gas phase was analyzed using a GC during the kinetic experiment. Table 4-3 shows the gas composition in the gas phase of the crystallizer at various times during experiments 5 and 16. As seen, the CO_2 content in the gas phase of

the crystallizer decreases as the experiment progresses which indicates enrichment of the hydrate phase with this gas. The compositional changes during the experiment resemble the experiments carried out without the presence of THF reported in chapter 2. Recall that a CO_2 composition of 9.7% and 10.9% for experiments carried out at 10.0 and 11.0 MPa, respectively after two hours of hydrate formation with the absence of THF was found.

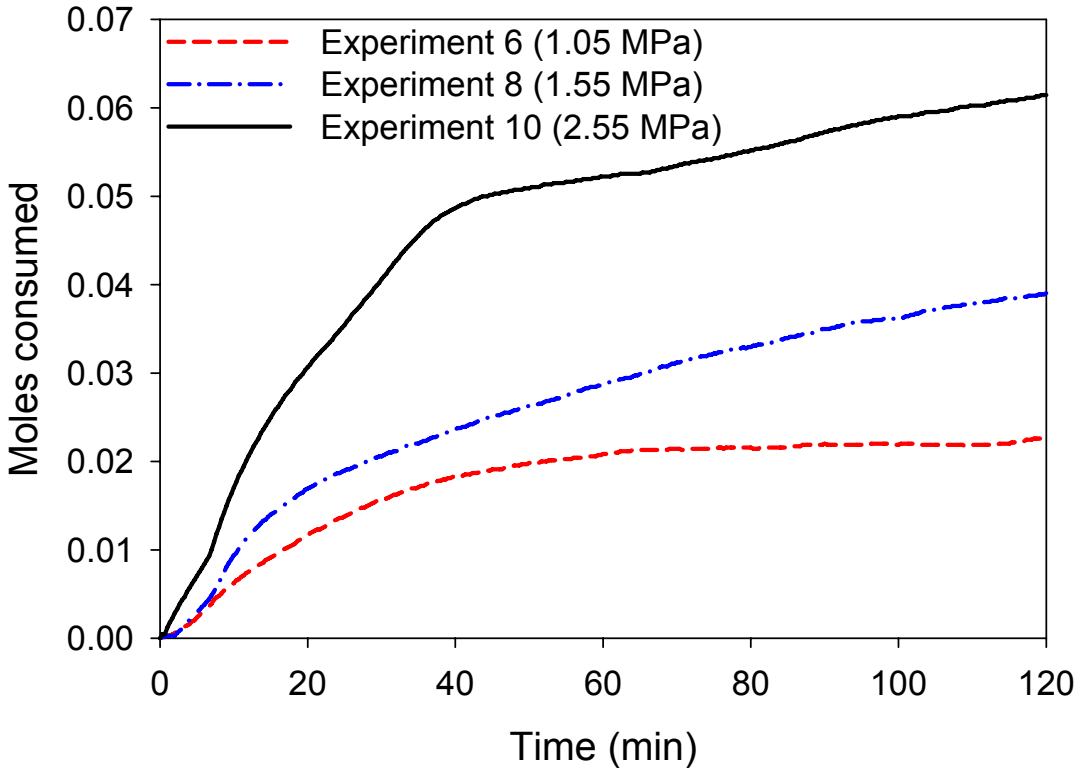

Figure 4-6: Gas uptake curves for 1.0 mol% THF concentration solutions with memory at 273.7 K and different pressures.

Figure 4-6 shows the effect of driving force on the rate of hydrate formation for 1.0 mol % THF solution. As can be seen, the total number of moles consumed increases with the increase in driving force. Thus a driving force of 2.2 MPa is preferable. A separation experiment was conducted after the end of a kinetic experiment at 273.7 K and

2.55 MPa with 1.0 mol % THF. The released gas was analyzed by gas chromatography and the composition was found to be 36.9 % CO_2 and the balance N_2.

The above results indicate that following a one-stage hydrate formation/decomposition process for the CO_2/N_2 gas mixture with a 1.0 mol% THF aqueous solution, a CO_2-rich gas is obtained which contains approximately 37 % CO_2 at 2.5 MPa. This gas mixture obtained from the first stage will form hydrate at a pressure of at least 3.60 MPa in pure water. Hence, a second stage with 1.0 mol% is advocated to obtain a more concentrated CO_2 mixture as well as to achieve it at a lower experimental pressure. The equilibrium hydrate formation pressure of CO_2/N_2 gas mixture with 38% CO_2 and the rest nitrogen in the presence of 1.0 mol% THF is 0.30 MPa at 273.7 K. A hydrate formation experiment at 2.5 MPa and 273.7 K was carried out to form hydrate with a 38% CO_2/62% N_2 mixture in 1.0 mol% THF, the new CO_2-rich mixture contained 71.2% CO_2 in the hydrate phase. The equilibrium hydrate formation pressure of CO_2/N_2 gas mixture with 70% CO_2 and rest nitrogen in the presence of 1.0 mol% THF is 0.28 MPa at 273.7 K. A kinetic hydrate formation/dissociation experiment was performed for 70.0% CO_2 and the rest N_2 at 2.5 MPa and 273.7 K. The hydrate consisted of 94% CO_2 on a water free basis.

Figure 4-7 shows the CO_2 content in the gas phase (initial composition), the hydrate formed and the residual gas phase (final composition) for a typical kinetic experiment. Figure 4-8 shows the gas uptake measurement curves for the experiments conducted for the three stages. As seen, the rate correlates with the CO_2 content and is fastest at the third stage which contains the most CO_2. Split fraction or CO_2 recovery for the above experiments were determined from equations 3.1 and 3.2 and the calculated

values are reported in Table 4-4. The split factors for the first two stages indicate that nearly half of the CO_2 contained in the flue gas is converted into hydrate and feeds the third stage where 37 % is recovered and thus separated.

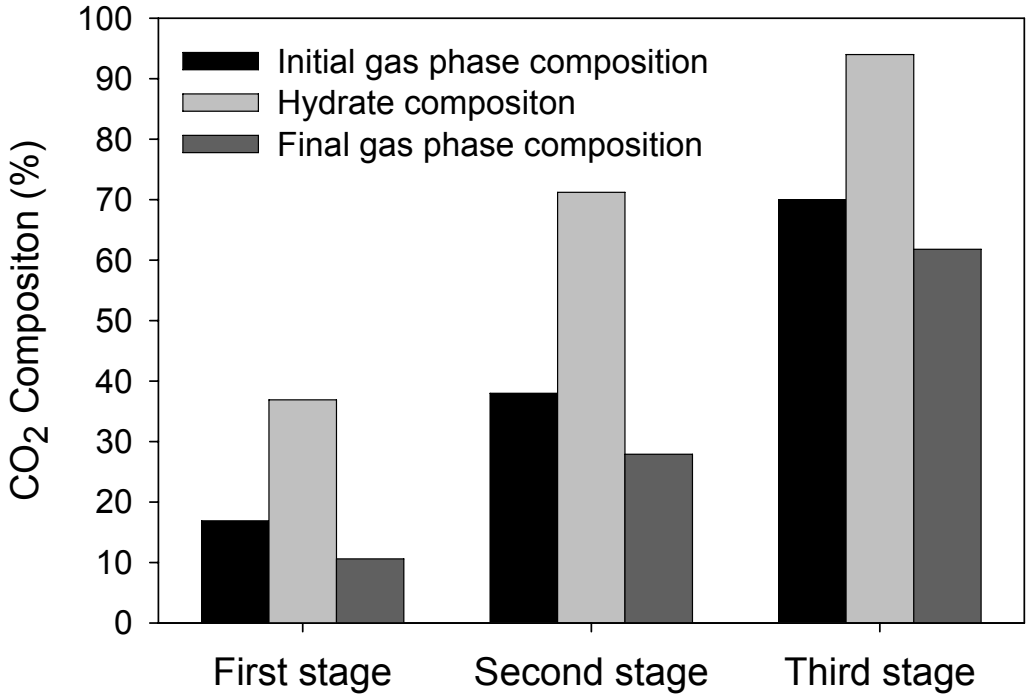

Figure 4-7: CO_2 content in the gas phase (initial composition), hydrate phase and residual gas phase (final composition) for the three process stages all operating at 2.5MPa and 273.7 K.

Table 4-4: Experimental conditions along with measured induction times and hydrate formation rates for hydrate formation from CO_2/N_2 mixtures corresponding to the initial gas phase composition for the three process stages at 273.7 K.

System	Pexp (MPa)	Induction Time (min)	R_f[a] (mol/min)	Split fraction or CO_2 recovery	Separation factor
(16.9%CO_2/N_2/ 1.0 mol% THF)-stage 1	2.5	0.7	0.0013	0.46	7.6
(38.0%CO_2/N_2/ 1.0 mol% THF)-stage 2	2.5	0.7	0.0016	0.47	6.8
(70.0%CO_2/N_2/ 1.0 mol% THF)-stage 3	2.5	0.3	0.0026	0.37	7.7

[a]Rate of hydrate growth (gas consumption rate for the first 20 min after nucleation)

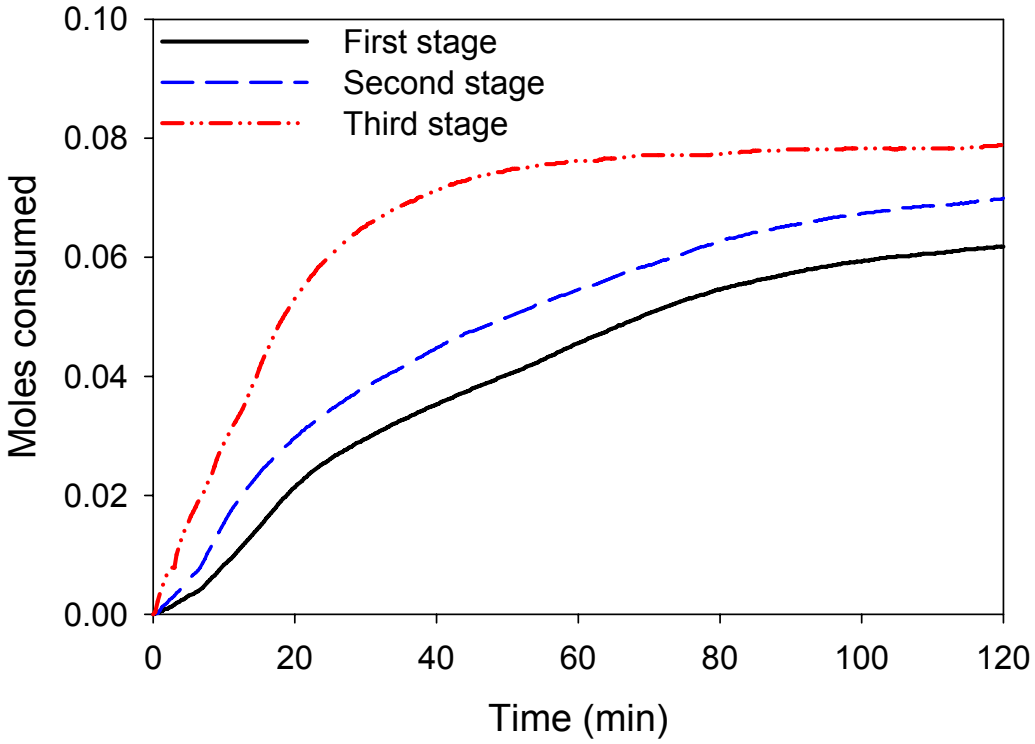

Figure 4-8. Gas uptake curves for hydrate formation with flue gas mixtures corresponding to the initial gas phase composition of the three process stages at 2.5 MPa and 273.7 K (the initial gas phase compositions are shown in Figure 4-7).

4.3.3. Proposed medium pressure hybrid process

The medium pressure conceptual process with the use of THF (1.0 mol %) operates at 2.5 MPa and 273.75 K as seen in Figure 4-9. Similar to the high pressure process we envision a hydrate process coupled most likely with a membrane-based separation to deal with the lean CO_2 stream. There is still a need for three compression stages to bring the flue gas pressure up to 2.5 MPa in the first crystallizer. If the operating pressure was 1.6 MPa then only two stages would be required. However, the rate of gas consumption as seen in Figure 4-6 is 37 % smaller. *Hence, there is a need for a more efficient gas/water contacting that would enhance the rate of hydrate crystallization that would yield better gas consumption for hydrate formation*.

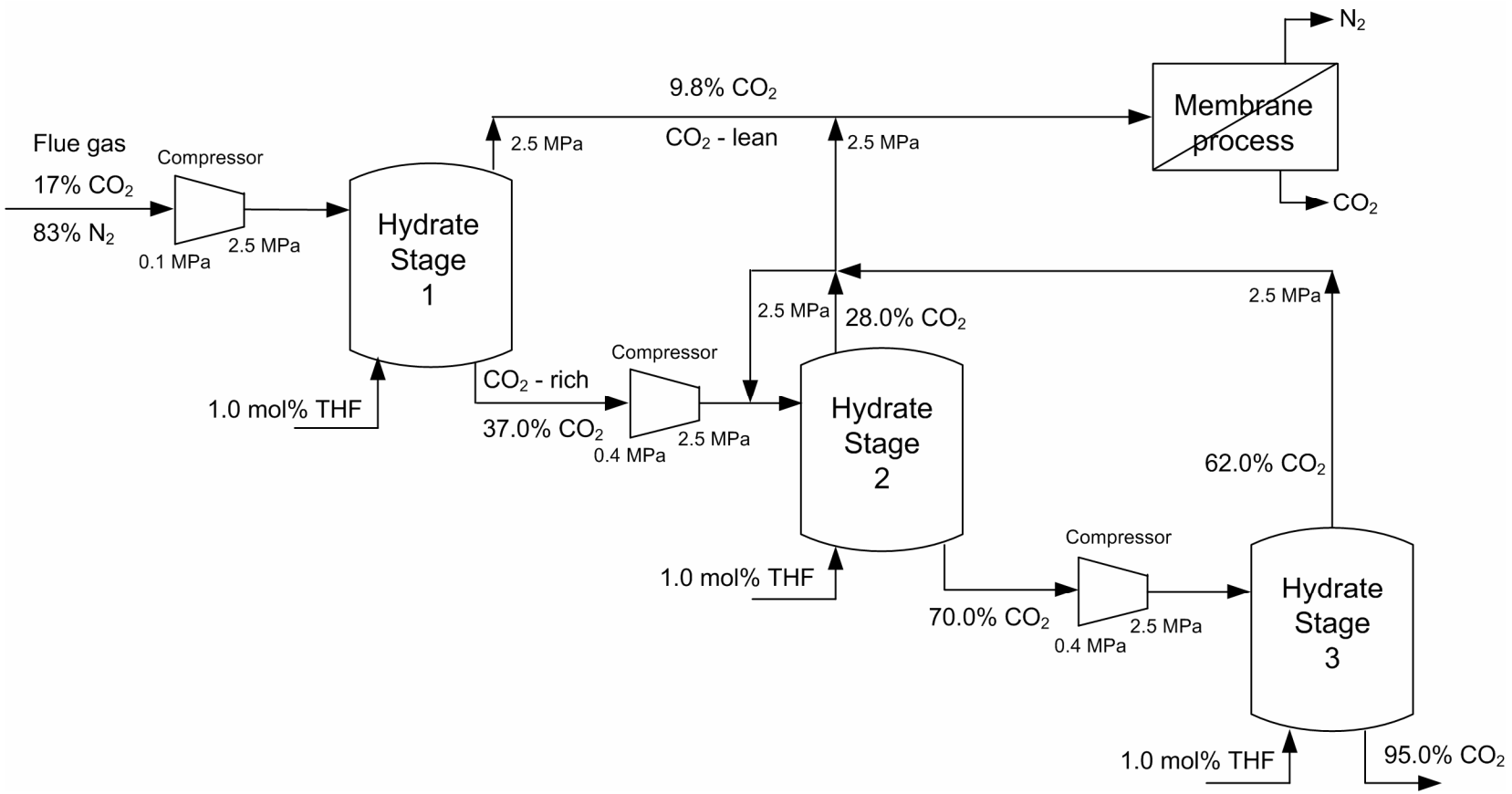

Figure 4-9: A hybrid hydrate-membrane process for CO_2 recovery from flue gas in the presence of THF as additive. Hydrate formation is carried out at 273.75 K and 2.5 MPa in the three stages.

It would be of interest to compare hydrate process with a membrane or other processes. Herzog et al. (1991) evaluated the performance of the membrane separation process for the capture of CO_2 from conventional power plants and compared it with cryogenic separation and amine absorption. Therefore, we will attempt to compare the proposed medium pressure hybrid process with the membrane process.

4.3.4. Membrane unit for CO_2/N_2 separation

Membrane separation is believed to be one of the promising methods to separate CO_2/N_2 gas mixtures (Ho et al., 2006a,b; Herzog et al., 1991; Shingo et al, 2004). The performance of gas separation via membranes relies on the fact that different components in a gas mixture interact differently with the membrane material. One component may dissolve or diffuse preferentially into the membrane and will enrich the permeate or product stream. The other component will enrich the waste or retentate stream. Membranes can be classified into organic, inorganic and hybrids of organic/inorganic systems. Selectivity and permeation rate are the most important properties of a membrane with respect to gas separation. However, a membrane's durability and mechanical integrity under the operating conditions must be balanced against cost issues. Gas separation using polymeric membranes was first reported over 180 years ago by Mitchell (Mitchell, 1831). Polymeric membranes are economical compared to inorganic ceramic/metal membrane (Feron and Jansen, 2002; Paul and Yampolskii, 1994).

A two stage membrane separation process for CO_2 capture from a flue gas mixture was presented by Herzog et al. (1991). The flowsheet is shown in Figure 4-10.

As can be seen in the figure, a two stage membrane process would produce a CO_2 rich stream consisting of 90% CO_2. The feed for the first membrane stage would have a recycle stream coming out of the second membrane stage with a composition of 36% CO_2. Essentially, 25.5% CO_2 feed stream would produce a permeate stream (CO_2 rich stream) having 55.0% CO_2.

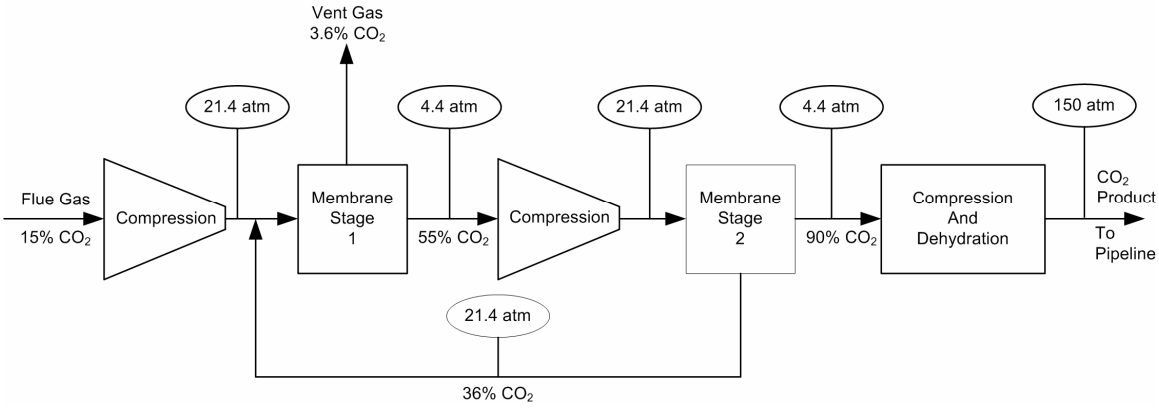

Figure 4-10: Membrane separation process for flue gas separation, Reprinted from Herzog et al. (1991) with permission of John Wiley & Sons, Inc., Copyright 1991.

Herzog et al. (1991) also presented a comparison of the energy requirements to capture a certain percentage of CO_2 and to compress it to 150 bars for transport as a supercritical fluid. They compared four methods namely, air separation/FG recycling, an amine scrubbing process, cryogenic fractionation and a membrane separation process. For a 500MW, CO_2 capture by Air separation/FG recycling would require an energy requirement of 26-31% of the energy of coal, Amine scrubbing requires 47-79% of the energy of coal, Cryogenic fractionation would require 55-95% of the energy of coal and the membrane separation process would require 50-75% of the energy of the coal. Moreover, only amine scrubbing and cryogenic fractionation would produce a CO_2 rich

stream consisting of >95% CO_2. The other two processes only produce a 90% CO_2 stream. In order to further enrich the CO_2 concentration, a third stage would be required for the membrane separation process. Overall, in a membrane separation process, the dominant cost is the cost associated with the compression of the flue gas to induce the pressure differences between the feed side and the permeate side of the membrane (Herzog et al., 1991; Ho et al., 2006a; Shingo et al., 2004).

Table 4-5: Comparison of energy penalty between membrane separation process and hydrate process.

	Membrane separation (Ho et al., 2006a)			Hydrate process (Tajima et al., 2004)
	PPO	PEO	PI	
Power plant (MW)	500	500	500	1000
CO_2 in feed (%)	14	14	14	10
Total power loss	267	243	254	158.4
Energy penalty (% power plant output)	53.4	48.6	50.8	15.8

4.3.5. Comparison of hydrate process with membrane separation

Ho et al. (2006a) presented a detailed comparison for the performance of the three membranes (Poly phenylene oxide (PPO), Poly ethlene oxide (PEO) and Polyimide (PI)), for CO_2 capture from a flue gas mixture. Tajima et al. (2004) estimated the energy consumption required for a hydrate based separation process for CO_2 capture from a flue gas mixture. It was found that for a 1000MW power plant the total energy consumption for the hydrate based separation process would be 158.4 MW. Tajima et al. (2004) reported the energy consumption for a single stage hydrate formation/decomposition operating at 274.0 K and 140 bars. Tajima et al. (2004) also reported that some of the compression work on the feed gas can be recovered by the expansion of the off gas

stream in a turbine. The results from Ho et al. (2006a) and Tajima et al. (2004) are summarized in Table 4-5. It can be seen in the table that the membrane separation process for the available gas separation membranes are more costly for CO_2 capture compared to the hydrate process. Several studies have been reported on the energy penalty for the amine process for flue gas separation (Halmann and Steinberg, 1999; Ho et al., 2006a; IEA GHG, 2004; NETL, 2002; Parsons, 2002; Rubin et al., 2005; Simbeck, 2002). Energy penalties for CO_2 capture utilizing amine process from the above mentioned studies vary between 7.0 - 28.8% of the power output. Based on these reports it can be concluded that among the novel (new) methods for capturing CO_2 from flue gas mixtures emitted from conventional power plants, the energy penalty is clearly less for the hydrate process (15.8%) compared to the membrane separation process (48 – 54%). Moreover, the energy penalty for the hydrate process is comparable to the more mature amine based process (7.0 - 28.8%).

Recently, Duc et al. (2007) reported that capturing CO_2 from the steelmaking industry via hydrate crystallization would be profitable compared to technologies like the amine process and the membrane separation process. The authors' reported the cost for hydrate based separation process to be in the range of 14.5 to 29.6 €/ton of CO_2 captured for a CO_2 feed composition in the range of 23-36% (Duc et al., 2007). The costs for membranes and amine process is reported to be in the range of 20-30 €/ton of CO_2 captured for steelmaking industry (Duc et al., 2007).

4.3.6. Justification of the hybrid process

In the conceptual process flowsheet presented in Figure 4-9, the CO_2 (9.8%) lean gas exiting the first stage of hydrate process would be at a pressure of 2.5 MPa. In the current

conceptual process (Figure 4-9), when membrane separation is used in conjunction with hydrate separation process, the membrane separation unit only takes the load of the residual gas phase from stage one (9.8% CO_2 and the purge streams from stage 2 and 3).

Another worthwhile alternative would be to have a membrane separation unit before the first hydrate separation unit. There is no experimental data available in the literature to evaluate a membrane separation process for such a scenario. The membrane separation process shown in Figure 4-10 would require an operating pressure of 2.14 MPa. Since the hydrate process and the membrane process would require similar operating pressures the compression costs to either the first membrane stage or the 1st hydrate stage are the same. The compression ratio required after the 1st stage is also the same for the two processes. However, the gas flow rates are not the same. Here is where information about the membrane process is lacking whereas for the hydrate process the flow rates can be determined. The flue gas mixture from a first stage membrane process would yield a permeate stream (after the first stage) consisting 45% CO_2 assuming a 90% CO_2 recovery (Ho et al., 2006a). Experimental results obtained for the first stage of the hydrate process (46% CO_2 recovery) produced a CO_2 rich stream of ~37% CO_2. However, if we also assume 90% CO_2 recovery for the first hydrate stage, then the CO_2 rich stream would have a composition of 96% CO_2.

Hence, in our opinion there is no advantage in using a membrane separation as a first stage replacing the hydrate formation stage. Thus, we envision a hybrid gas separation process, combining the advantage of high selectivity (hydrate crystallization) and small size (membranes) as illustrated in Figure 4-9. This hybrid process will produce

a CO_2 rich stream of >95% CO_2 and also the residual flue gas exiting the membrane separation unit will have less than 1% CO_2 which can be released to the atmosphere.

4.4. Conclusions

Thermodynamic, kinetic and separation efficiency data were presented for a process to capture and separate CO_2 from a flue gas from a conventional power plant in the presence of THF. The data enabled the creation of a conceptual process for post combustion capture of CO_2 which consists of three hydrate formation/decomposition stages operating at 273.75 K and 2.5 MPa coupled with a membrane separation stage to tackle a CO_2-lean stream. Nearly 50 % of CO_2 is recovered in the first two hydrate stages and 37 % in the third one. The presence of a small amount of THF (1.0 mol %) reduces the operation pressure for hydrate formation considerably compared to a system without THF. There is some room for the operating pressure to be reduced further but better gas/water contacting is needed in order to enhance the rate of hydrate formation that would lead to higher gas consumption and eventually better CO_2 recovery. The energy penalty of the hydrate process appears to be comparable to that of the mature amine process and less than that of a membrane-based process.

4.5. References

Aaron, D., and Tsouris, C., 2005. Separation of CO_2 from flue gas: A review. Separation Science and Technology 40(1-3), 321-348.

Bacher, P., 2002. Meeting the energy challenges of the 21st century. International Journal of Energy Technology and Policy 1(1-2), 1-26.

Bishnoi, P. R., and Natarajan, V., 1996. Formation and decomposition of gas hydrates. Fluid Phase Equilibria 117(1-2), 168-177.

Chakma, A., Mehrotra, A. K., and Nielsen, B., 1995. Comparison of Chemical Solvents for Mitigating CO_2 Emissions from Coal-Fired Power-Plants. Heat Recovery Systems & Chp 15(2), 231-240.

Davidson, D. W., 1973. Gas Hydrates. In Water: A Comprehensive Treatise, Plenum Press;, New York.

Davison, J., and Thambimuthu, K., 2004. Technologies for Capture of Carbon Dioxide. 7th International Conference on Greenhouse Gas Control Technologies (GHGT-7), Vancouver.

Duc, N. H., Chauvy, F., and Herri, J. M., 2007. CO_2 capture by hydrate crystallization - A potential solution for gas emission of steelmaking industry. Energy Conversion and Management 48(4), 1313-1322.

Englezos, P., 1993. Clathrate Hydrates. Industrial & Engineering Chemistry Research 32(7), 1251-1274.

Englezos, P., Kalogerakis, N., Dholabhai, P. D., and Bishnoi, P. R., 1987. Kinetics of Formation of Methane and Ethane Gas Hydrates. Chemical Engineering Science 42(11), 2647-2658.

Englezos, P., and Ngan, Y. T., 1994. Effect of Polyethylene Oxide on Gas Hydrate Phase Equilibria. Fluid Phase Equilibria 92, 271.

Feron, P. H. M., and Jansen, A. E., 2002. CO_2 separation with polyolefin membrane contactors and dedicated absorption liquids: performances and prospects. Separation and Purification Technology 27(3), 231-242.

Halmann, M. M., and Steinberg, M., 1999. Greenhouse gas carbon dioxide mitigation: science and technology, Lewis Publishers, Boca Raton.

Herzog, H. J., Drake, E., and Adams, E. (1997). " CO_2 Capture, Reuse, and Storage Technologies for Mitigating Global Climate Change." DOE.

Herzog, H., Golomb, D., and Zemba, S., 1991. Feasibility, Modeling and Economics of Sequestering Power-Plant CO_2 Emissions in the Deep Ocean. Environmental Progress 10(1), 64-74.

Ho, M. T., Allinson, G., and Wiley, D. E., 2006a. Comparison of CO_2 separation options for geo-sequestration: are membranes competitive? Desalination 192(1-3), 288-295.

Ho, M. T., Leamon, G., Allinson, G. W., and Wiley, D. E., 2006b. Economics of CO_2 and mixed gas geo-sequestration of flue gas using gas separation membranes. Industrial & Engineering Chemistry Research 45(8), 2546-2552.

IEA GHG. (2004). "Improvements in power generation with postcombustion capture of CO_2." report PH4/33, IEA Greenhouse Gas R&D Programme, Cheltenham, UK.

Kang, S. P., and Lee, H., 2000. Recovery of CO_2 from flue gas using gas hydrate: Thermodynamic verification through phase equilibrium measurements. Environmental Science & Technology 34(20), 4397-4400.

Kang, S. P., Lee, H., Lee, C. S., and Sung, W. M., 2001a. Hydrate phase equilibria of the guest mixtures containing CO_2, N_2 and tetrahydrofuran. Fluid Phase Equilibria 185(1-2), 101-109.

Kang, S. P., Lee, H., and Ryu, B. J., 2001b. Enthalpies of dissociation of clathrate hydrates of carbon dioxide, nitrogen, (carbon dioxide plus nitrogen), and (carbon dioxide plus nitrogen plus tetrahydrofuran). Journal of Chemical Thermodynamics 33(5), 513-521.

Lee, J. D., Susilo, R., and Englezos, P., 2005. Kinetics of structure H gas hydrate. Energy & Fuels 19(3), 1008-1015.

Linga, P., Kumar, R., and Englezos, P., 2006. Capture of Carbon dioxide from conventional power plants or from integrated gasification plants through gas hydrate formation/ dissociation. Journal of Energy & Climate Change 1(2), 75-82.

Linga, P., Kumar, R., and Englezos, P., 2007a. The clathrate hydrate process for post and pre-combustion capture of carbon dioxide. Journal of Hazardous Materials 149(3), 625-629.

Linga, P., Kumar, R., and Englezos, P., 2007b. Gas hydrate formation from hydrogen/carbon dioxide and nitrogen/carbon dioxide gas mixtures. Chemical Engineering Science 62(16), 4268-4276.

Makino, T., Sugahara, T., and Ohgaki, K., 2005. Stability boundaries of tetrahydrofuran plus water system. Journal of Chemical and Engineering Data 50(6), 2058-2060.

Mitchell, J. K., 1831. Polymeric gas separation membrane. J. Med. Sci. 9(36).

NETL. (2002). "Advanced fossil power systems comparison study." Final report prepared for NETL by E.L. Parsons (NETL), W.W. Shelton and J.L. Lyons (EG&G Technical Services, Inc.), Morgantown, WV.

Parsons. (2002). "Updated cost and performance estimates for fossil fuel power plants with CO_2 removal." Report under Contract No. DE-AM26-99FT40465 to U.S.DOE/NETL,, Parsons Infrastructure & Technology Group, Inc., Pittsburgh, PA, and EPRI, Palo Alto, CA.

Paul, D. R., and Yampolskii, Y. P., 1994. Polymeric gas separation membranes, CRC press, Boca Raton, Florida.

Rubin, E. S., A.B. Rao, and Chen, C., 2005. Comparative Assessments of Fossil Fuel Power Plants with CO_2 Capture and Storage. 7th International Conference on Greenhouse Gas Control Technologies.

Seo, Y. T., and Lee, H., 2004. Structure and guest distribution of the mixed carbon dioxide and nitrogen hydrates as revealed by X-ray diffraction and C-13 NMR spectroscopy. Journal of Physical Chemistry B 108(2), 530-534.

Shingo, K., Shinichiro, M., Shigetoshi, T., Hiroshi, M., Tatsuaki, Y., Koichi, Y., and Kenji, H., 2004. Carbon Polyimide Membranes for CO_2 Capture from Flue Gases. 7th Conference on Greenhouse Gas Control Technologies, Vancouver.

Simbeck. (2002). "New power plant CO_2 mitigation costs." SFA Pacific, Inc., Mountain View, California.

Sloan, E. D., Jr., 1998. Clathrate Hydrates of Natural Gases, Second Edition, Revised and Expanded, Marcel Dekker, NY.

Tajima, H., Yamasaki, A., and Kiyono, F., 2004. Energy consumption estimation for greenhouse gas separation processes by clathrate hydrate formation. Energy 29(11), 1713-1729.

Uchida, T., Ebinuma, T., and Narita, H., 2000. Observations of CO_2-hydrate decomposition and reformation processes. Journal of Crystal Growth 217(1/2), 189-200.

Vysniauskas, A., and Bishnoi, P. R., 1983. A Kinetic-Study of Methane Hydrate Formation. Chemical Engineering Science 38(7), 1061-1072.

White, C. M., Strazisar, B. R., Granite, E. J., Hoffman, J. S., and Pennline, H. W., 2003. Separation and capture of CO_2 from large stationary sources and sequestration in geological formations – Coal beds and deep saline aquifers. Journal of the Air & Waste Management Association 53(6), 645-715.

5. A NEW LARGE SCALE APPARATUS TO TEST CO_2 CAPTURE PROCESS VIA HYDRATE CRYSTALLIZATION[4]

5.1. Introduction

In chapter 3 a conceptual process flow sheet was presented for the recovery of carbon dioxide from a flue gas mixture in three stages. However, the operating pressures required for the process is high. For the flue gas separation, the first stage requires 10 MPa. The addition of THF even in small quantities considerably reduces the operating pressure. For example, a gas mixture of 16.9% CO_2 and rest N_2 forms hydrate at 7.7 MPa at 273.7 K. With the addition of 1 mol% THF, the mixture readily forms hydrate at 0.345 MPa In chapter 4, thermodynamic and kinetic data obtained from a semi batch stirred tank reactor on the effect of THF on the hydrate formation from a CO_2/N_2 gas mixture was presented. Based on this experimental information, a medium pressure clathrate process for CO_2 capture operating at 273.7 K and 2.5 MPa was presented. Nearly 50% of CO_2 is recovered in the first two hydrate stages and 37% in the third one. The process uses 1 mol % THF. Even though, the operating pressure is reduced significantly, the rate of hydrate formation, the overall gas consumption for hydrate formation and the water conversion were less compared to the high pressure process without THF (Linga et al., 2008; Linga et al., 2007b). Thus, a major technological challenge for the hydrate based

[4]A version of this chapter will be submitted for publication. Linga, P., Kumar, R., Ripmeester, J. A., Englezos, P. Demonstration of hydrate process for pre and post combustion capture of CO_2 in a large scale apparatus. Manuscript in preparation.

separation process is to enhance the rate of hydrate formation that would lead to higher gas consumption.

Mori (2003) presented in detail the advantages and disadvantages of several reactor configuration aimed at enhancing the kinetics of hydrate formation. Mori (2003) also attempted to compare the rate of hydrate formation between different reactors available in the literature by defining a metric called rate of guest-gas fixation by hydrate formation per unit volume inside the reactor. It is noted that the above metric does not take into account the amount of water used in the hydrate formation experiment. Mori (2003) concluded that the rate of hydrate formation is not necessarily limited by the total rate of heat removal from the reactor but is limited by local rate processes inside the reactor such as kinetics of hydrate formation and heat transfer from the hydrate formation sites to the bulk of the water pool. Finally, Mori (2003) concluded that there is a need to focus on developing reactors and the operating schemes aimed at achieving higher hydrate forming efficiencies.

The objective of this work is to develop a new apparatus which will be at a larger scale compared to that presented in earlier chapters and at the same time utilize different gas/water contact modes so that the rate of hydrate formation is enhanced. The apparatus will then be used to test the hydrate based separation process of CO_2 capture from a flue gas mixture in order to determine the CO_2 recovery or separation efficiency of the process.

5.2. Experimental section

5.2.1. A new large scale hydrate apparatus

The schematic of the new apparatus is given in Figure 5-1. It consists of the crystallizer (CR) and a supply vessel (SV), which is used to supply gas during hydrate formation experiments. Both CR and SV are immersed in a water bath. The temperature of the water bath is controlled by an external refrigerator (VWR Scientific) in order to maintain a constant temperature. Two Rosemount smart pressure transmitters, model 3051 (Norpac controls, Vancouver, BC) are employed for pressure measurement with a maximum uncertainty of 0.075% of the span (0-15,000 kPa) i.e. 11 kPa. The temperatures of the hydrate phase and the gas phase of the crystallizer are measured using Omega copper-constantan thermocouples with an uncertainty of 0.1 K. A control valve (Fisher Bauman) coupled with a PID controller enables carrying out the formation experiment at constant pressure. The data acquisition system (National Instruments) is coupled with a computer to record the data as well as to communicate with the control valve during the experiment and the software used for this purpose is LabView 7.0 (National Instruments). The apparatus is also equipped with a safety pressure valve.

Figure 5-2 shows the top view and the side view of the designed crystallizer with the design specifications. Figure 5-3 shows the cross section A of the crystallizer as indicated in Figure 5-2. It is a modular type crystallizer with two removable sections connected together with top and bottom flanges. The total volume of the crystallizer is 1892.7 cm^3. The crystallizer is equipped with a stirrer. The shaft of the stirrer has a special arrangement with the propeller so that when the experiment is run under a pressure it allows the flow of gas through the shaft and then releases it in the liquid

through the propeller blades. Hence, it enables proper mixing as well as internal circulation of gas into the liquid. The crystallizer is also connected to a high pressure pump. The crystallizer can also be operated in continuous mode by circulating the liquid contents from the bottom of the crystallizer using the pump and spraying it through two nozzles connected at the top of the crystallizer as shown in figure 3 and 4.

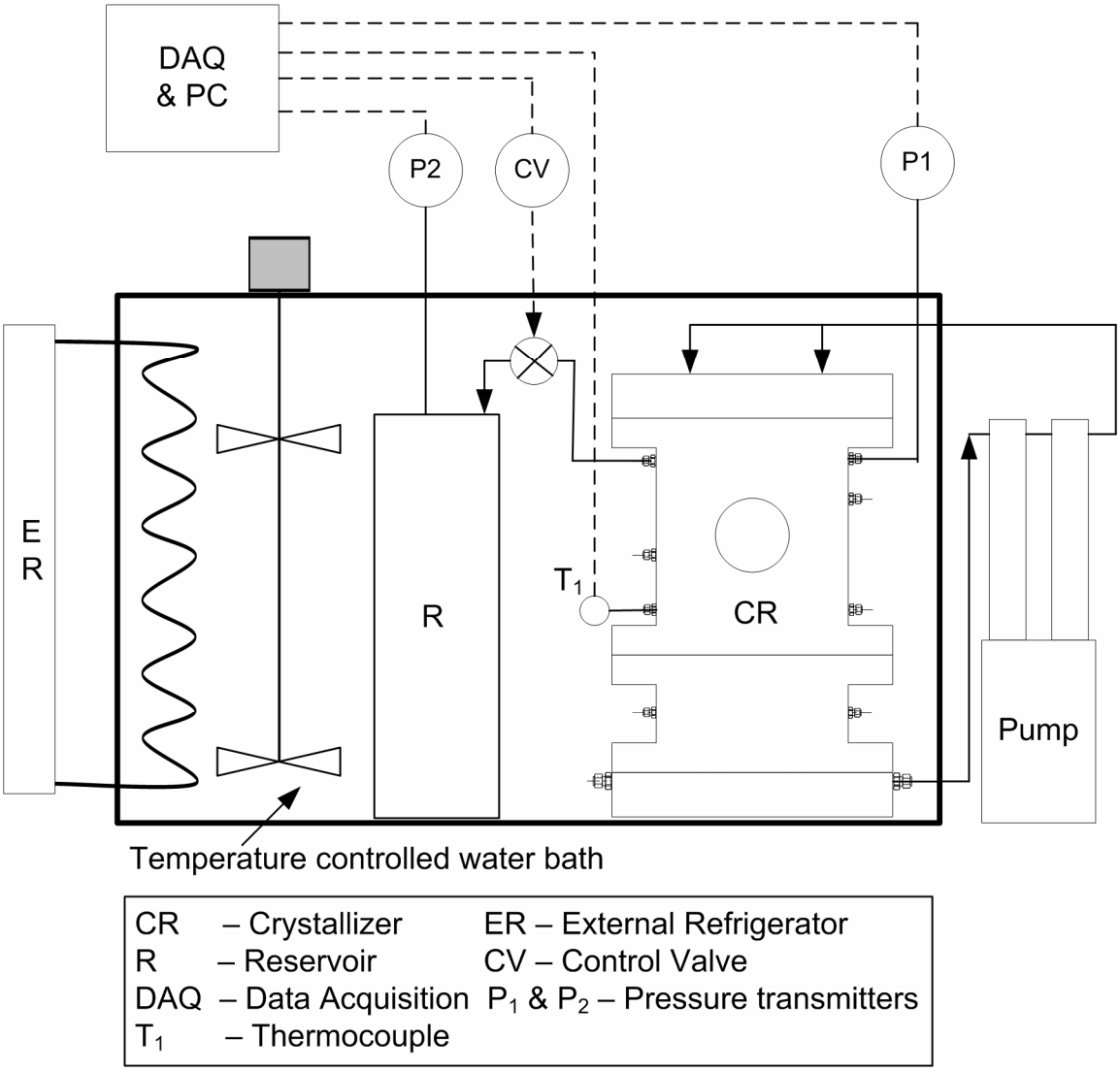

Figure 5-1: Schematic of the apparatus.

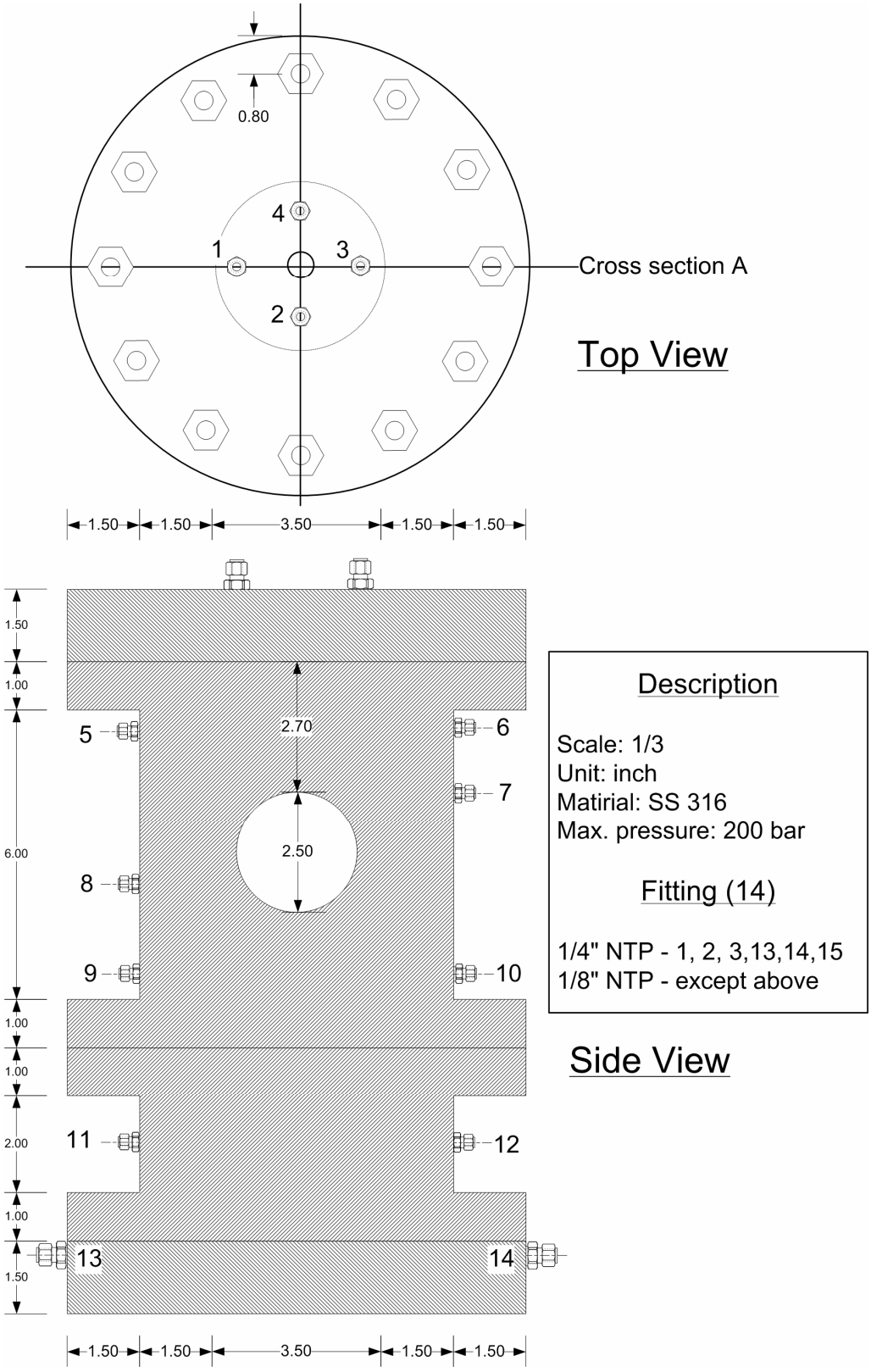

Figure 5-2: Top and side view of the crystallizer with dimensions.

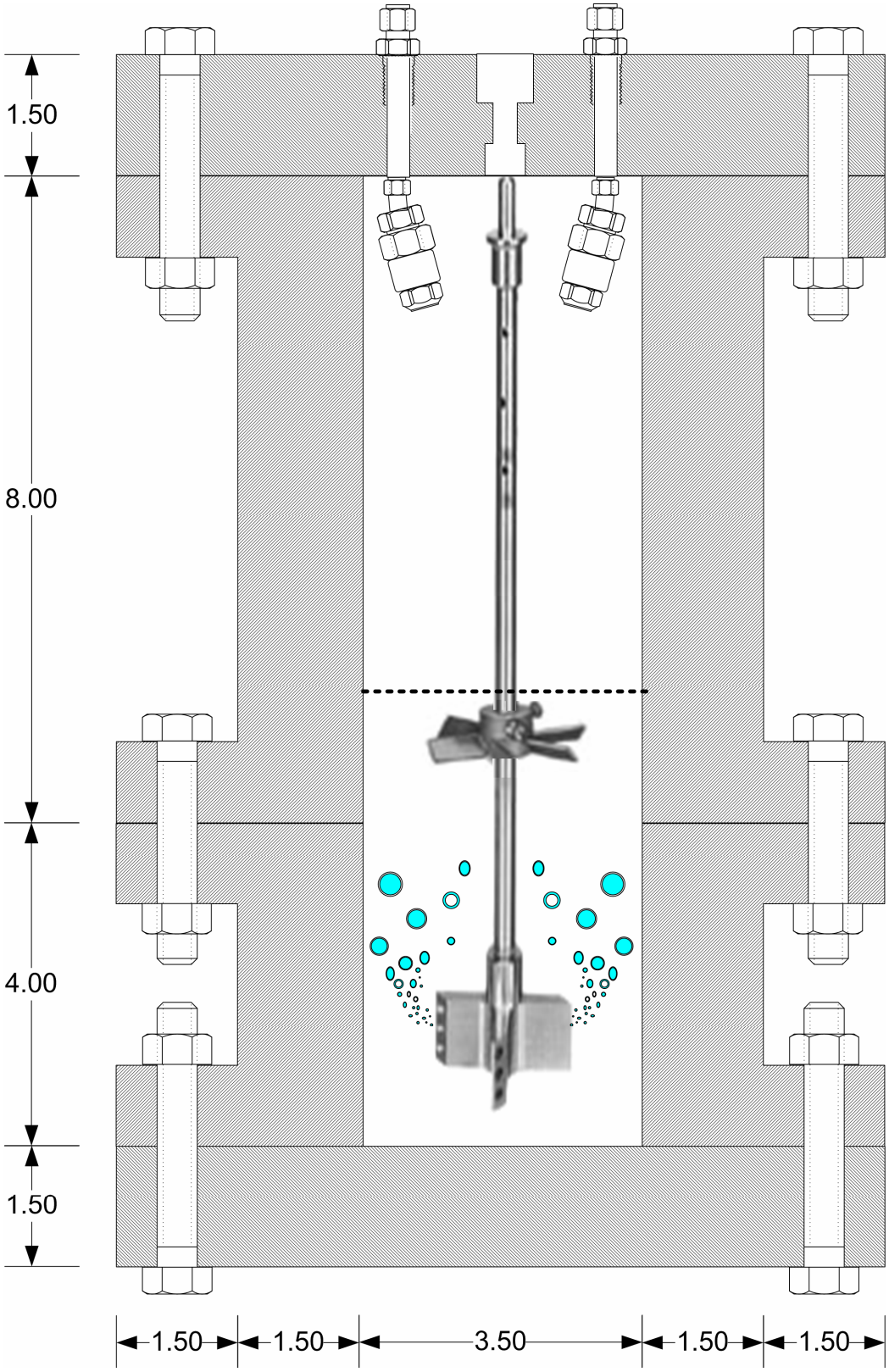

Figure 5-3: Cross section of the crystallizer with the stirrer and nozzle arrangement.

5.2.2. Hydrate formation procedure for "batch operation"

Hydrate formation experiments were carried out at various stirrer speeds in order to study the effect of stirring rate on the hydrate formation. A volume of 700 mL of 1.0 mol% aqueous THF solution is added into the crystallizer. The pressure is then set to the desired experimental value and the temperature is allowed to reach the desired value. The stirrer is set at the desired speed setting and is started. This is time zero for the formation experiment. Data is then logged in the computer for every 20 seconds. All hydrate formation experiments are carried out with a fixed amount of water and gas (closed system). The temperature in the crystallizer is maintained constant by an external refrigerator. When hydrate formation occurs, gas will be consumed and hence the pressure in the closed system drops. Pressure and temperature data are used to calculate the moles of gas consumed in the crystallizer (gas uptake) for hydrate formation.

5.2.3. Hydrate formation procedure for "semi-batch operation"

Experiments in this mode were carried out following procedures similar to those for kinetic experiments and CO_2 recovery determination (separation experiment) described in chapter 2 & chapter 3. The mass of gas being consumed in the crystallizer (gas uptake) versus time is easily calculated based on the temperature and pressure measurements as described in chapters 2 & 3. In addition, gas phase composition in the hydrate vessel was also measured with a Varian CX-3400 gas chromatograph (GC) equipped with a thermal conductivity detector.

After the end of a kinetic (gas uptake measurement) experiment, the pressure in the crystallizer was quickly brought down to the atmospheric pressure and the hydrates were allowed to completely dissociate. The gas which evolved from the decomposed

hydrate and that released from the liquid water phase (dissolved amount at the higher pressure) was collected in the crystallizer (CR).

Hydrate kinetic measurements in which the gas uptake in the hydrate crystallizer is measured were carried out for 1.0 and 1.5 mol% THF solutions. Experiments with fresh water as well as with memory water were conducted. Memory refers to the situation where water that is used in the experiment has experienced hydrate formation. In the experiments reported in this work memory water was obtained by decomposing hydrates and using it to form new hydrate three hours after the hydrate decomposition.

5.3. Results and discussion

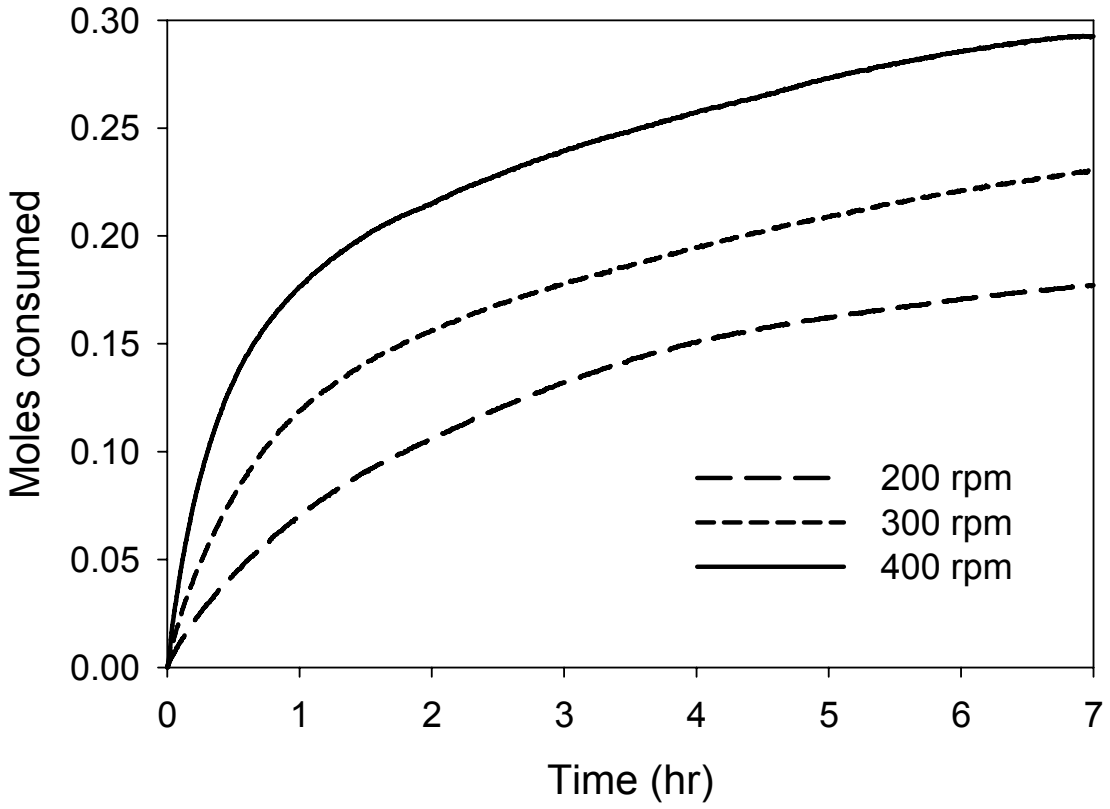

Figure 5-4: Effect of stirring rate on hydrate formation at 273.7 K and 2.5 MPa. The experiment was performed under a batch mode.

Figure 5-4 shows a comparison of the gas uptake measurement curves obtained for the three experiments conducted at different stirring rates. Clearly, the gas uptake was considerably higher for the experiment conducted at 400 rpm compared to the one conducted at 200 and 300 rpm. Experiments were not performed at stirring rates higher than 400 rpm due to the mechanical stability of the experimental set up. In the current experimental set up, the motor required to run the stirrer is mounted on the top of the crystallizer which causes slight vibration when the stirrer is operated at speeds higher than 400 rpm. Hence, for all the hydrate formation experiments that were conducted in a semi-batch operation the stirring speed was fixed as 400 rpm.

The separation process for capture of CO_2 from a flue gas mixture was also assessed in the new apparatus. Table 5-1 summarizes the experimental conditions and the results. Hydrate formation experiments were studied at 1.0 and 1.5 mol % THF concentrations. It is noted that for both these THF concentrations, the 17% CO_2/N_2 gas mixture forms structure II hydrate (Kang and Lee, 2000; Kang et al., 2001a). It is also noted that 17.0% CO_2 and rest N_2 gas mixture in pure water forms structure I (Seo and Lee, 2004). Experiments with 1.0 mol% were carried out for two driving forces of 2.2 and 1.2 MPa at 273.75 K. The equilibrium hydrate formation pressure for the 1.0 mol% THF for 16.9% CO_2/N_2 gas mixture at 273.75 K are 0.345 MPa (Linga et al., 2008).

It can also be seen in Table 5-1 that memory water experiments have less induction times compared to the fresh water experiments. The induction times for 1.0mol% THF and for the same gas composition reported in chapter 4 for similar driving forces were all less than 1 min when experiments were studied at a small scale (140 cm^3

of aqueous solution). However, for a larger amount of liquid contents in this study (700 cm^3) in a new apparatus, the induction times were significantly higher for the fresh water. However, for the memory water the induction times were less than 2 min and hence similar to the results for the small scale apparatus reported in chapter 4. Short induction times are definitely desirable from a practical stand point to speed up the process and hence the results demonstrate that it is desirable to use memory water for hydrate formation. The final gas consumption at the end of the experiment is approximately the same for both fresh and memory solutions.

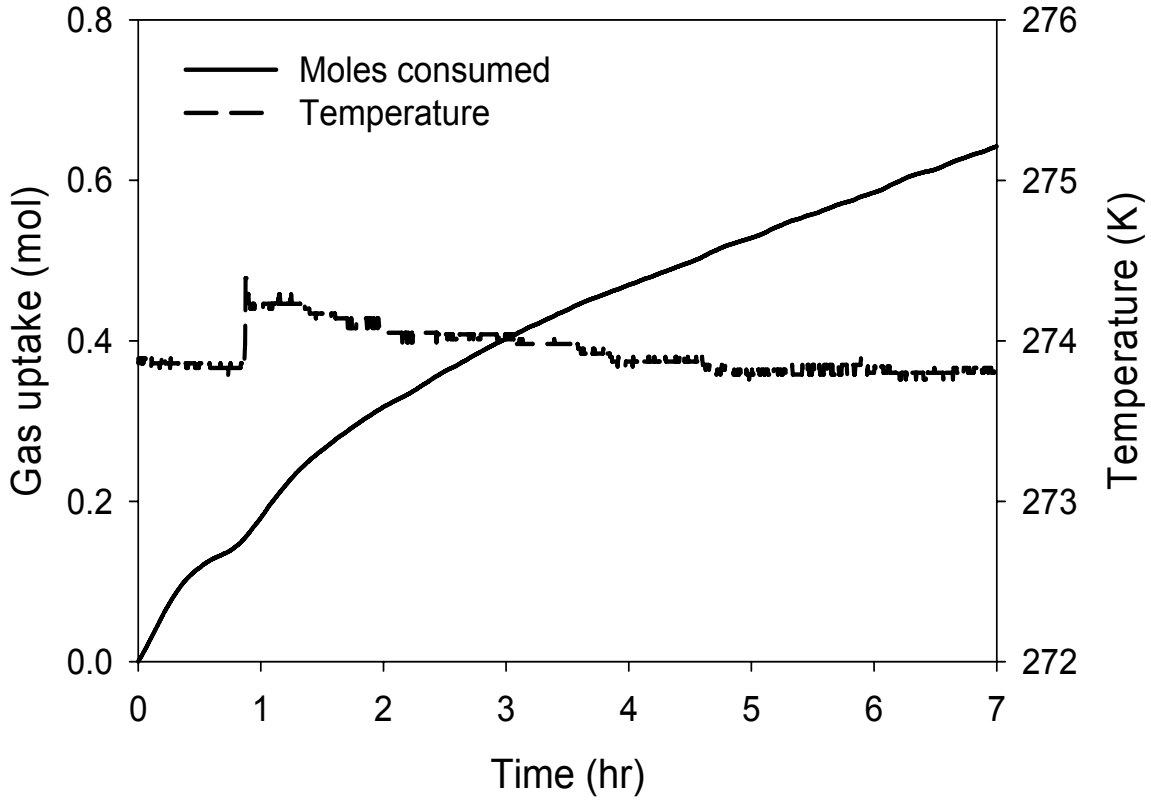

Figure 5-5: A typical gas uptake measurement curve carried out at 2.5 MPa and 273.7 K (experiment 3).

Figure 5-5 shows a typical gas uptake measurement with the temperature profile. This curve represents the kinetics of hydrate growth and agglomeration for the indicated

time. The induction time for this experiment (experiment 1) is 70.3 min. The general shape of this curve agrees with the behavior of the curve for hydrate formation in stirred vessels described in detail by Bishnoi and Natarajan (1996). Gas hydrate formation is an exothermic process and as seen in the figure the temperature rises immediately after nucleation, reaches a higher level and then gradually is brought down because the temperature controller brings back the temperature to the set point value. The gas uptake curves for the all the experiments along with the temperature profile are given in Appendix D.

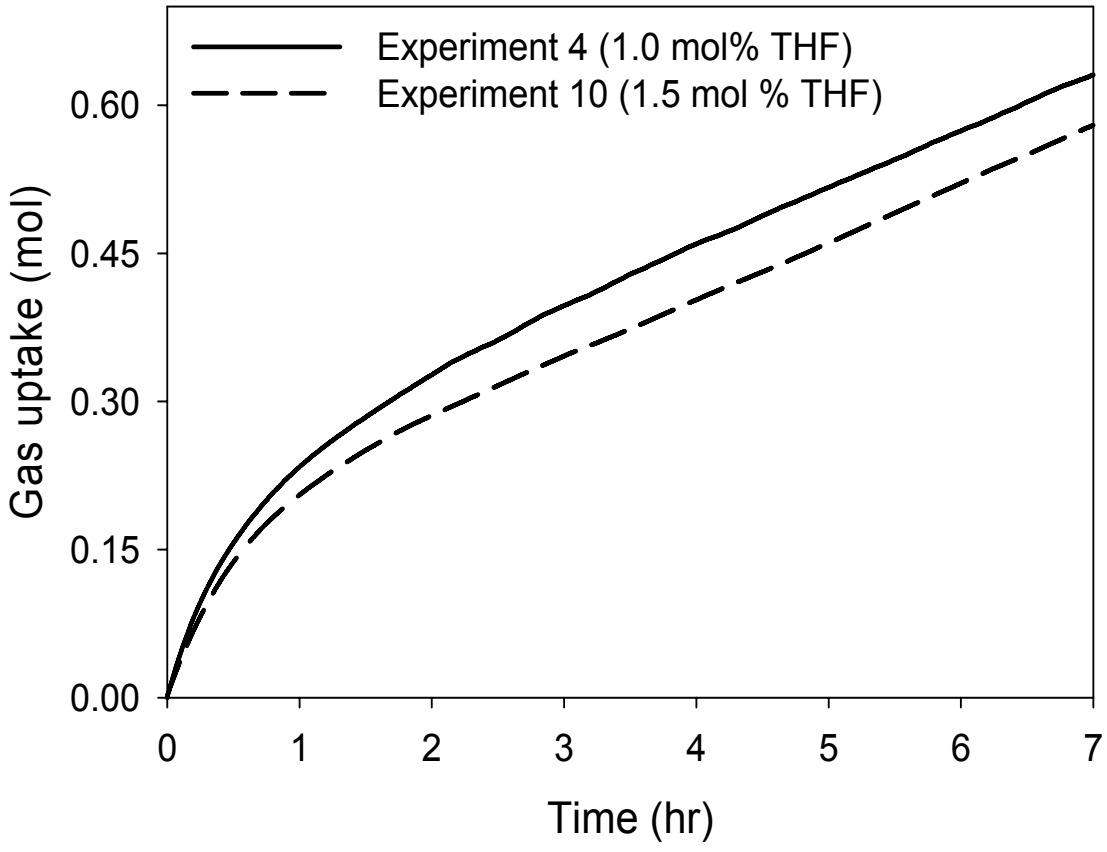

Figure 5-6: Gas uptake measurement curves for 1.0 and 1.5 mol% THF memory solutions carried out at a driving force of 2.2 MPa or at 2.5 and 2.3 MPa respectively.

Table 5-1: Experimental conditions along with measured induction times and hydrate formation rates for $CO_2/N_2/THF/H_2O$ system at 273.7 K. The CO_2/N_2 composition of the mixture was 16.9 mol % CO_2 and balance N_2.

System	Exp. No.	Sample State	Driving force[a] (MPa)	Pexp (MPa)	Induction Time (min)	Final gas consumed (mol of gas/mol of H_2O)	Water conversion to hydrate[c] (%)
($CO_2/N_2/THF/H_2O$) 1.0 mol% THF	1	Fresh	1.2	1.5	70.3	0.0098	8.4
	2	Memory	1.2	1.5	1.7	0.0089	7.6
	3	Fresh	2.2	2.5	52.0	0.0178	15.2
	4	Memory	2.2	2.5	0.7	0.0174	14.9
	5	Fresh	2.2	2.5	10.7	0.0181	15.4
	6	Memory	2.2	2.5	0.7	0.0180	15.3
	7	Fresh	1.2	1.5	60.3	0.0092	7.8
	8	Memory	1.2	1.5	2.7	0.0090	7.6
($CO_2/N_2/THF/H_2O$) 1.5 mol% THF[b]	9	Fresh	2.2	2.3	4.0	0.0163	13.9
	10	Memory	2.2	2.3	0.3	0.0164	14.1

[a] Driving force = $P_{exp} - P_{eq}$ (P_{exp} = experimental pressure, P_{eq} = equilibrium pressure)

[b] Experiments carried out at 274.2 K

[c] Hydration number of 5.71 (Kang et al., 2001b) was used for the calculation.

Figure 5-6 shows a comparison of the gas uptake measurements obtained at a constant driving force of 2.2 MPa and two different THF concentrations. It can be seen that the total number of moles consumed at the end of the experiment was found to be higher in the case of 1.0 mol% THF. This concentration dependency was also observed for the fresh experiments at the same corresponding driving force. Linga et al. (2008) (see chapter 4) observed and reported the same behavior for several experiments carried out at different driving forces for experiments carried out at 0.5, 1.0 and 1.5 mol% THF solutions at a smaller apparatus (see chapter 4). One of the possible reasons for this concentration dependency could be that, for the kinetic experiments conducted at higher THF concentration, THF readily occupies the large cage in structure II and stabilizes the hydrate leaving little time for the gas to occupy the small cages in the structure, hence resulting in lower gas consumption. This would lead to THF occupying the large cages which is enough to stabilize the structure leaving many small cages empty. A similar THF concentration dependency was observed by Lee at al. (2005) when experiments were performed with H_2 gas for hydrogen storage in clathrate hydrate. Lee et al. (2005) reported the storage potential of H_2 in a mixed hydrate of THF/H_2 by investigating hydrate formation with different THF concentrations and at high operating pressures (120 bars). They found that experiments conducted with THF concentrations of less than 1.0 mol% offered a higher storage potential for H_2 (Lee et al., 2005). A similar trend can be seen with the water conversion to hydrates between 1.0 and 1.5 mol% THF concentrations given in Table 5-1 which is due to the higher gas consumption obtained for 1.0 mol% THF experiments. Hence, based on experiments conducted in the lab-scale

and the new large apparatus, we believe that 1.0 mol% should be the optimum concentration which reduces the operating pressure of the hydrate vessel significantly.

Table 5-2: CO_2 composition at start and end of the experiment as analyzed by gas chromatography.

Description	Experiment 1	Experiment 3	Experiment 4	Experiment 9
THF concentration (mol%)	1.0	1.0	1.0	1.5
Feed gas composition (start)	0.169	0.169	0.169	0.169
Gas phase composition (end)	0.100	0.092	0.095	0.105
Hydrate phase composition	0.351	0.383	0.372	0.321

Figure 5-7 shows the effect of driving force on the rate of hydrate formation for 1.0 mol % THF solution. As seen in the figure, the total number of moles consumed increases with the increase in driving force. The same trend was also observed for the fresh water experiments. Water conversion to hydrates for all the experiments carried out is given in Table 5-1. As seen in the table, the conversion is significantly higher (twice) for the higher driving force experiments (15%) compared to the lower driving force experiments (8.0%). Thus, a driving force of 2.2 MPa is preferable.

The composition of gas phase was analyzed using a GC at the end of the kinetic experiment. The CO_2 composition in the gas phase of the crystallizer at the end of the kinetic experiment is given in Table 5-2. As seen the CO_2 content in the gas phase of the crystallizer decreases as the experiment progresses which indicates enrichment of the hydrate phase with this gas. The compositional changes during the experiment resemble to the experiments carried out with the presence of THF reported by Linga et al (2008). Linga et al. (2008) reported a CO_2 composition of 9.8% for the experiment carried out at

1.0 MPa (1.0 mol% THF) and 9.9% for the experiment carried out at 1.4 MPa (1.5 mol% THF). A separation experiment was conducted after the end of a kinetic experiment in order to determine the composition of the hydrate phase. The released gas was analyzed by gas chromatography and the CO_2 composition is also given in Table 5-2.

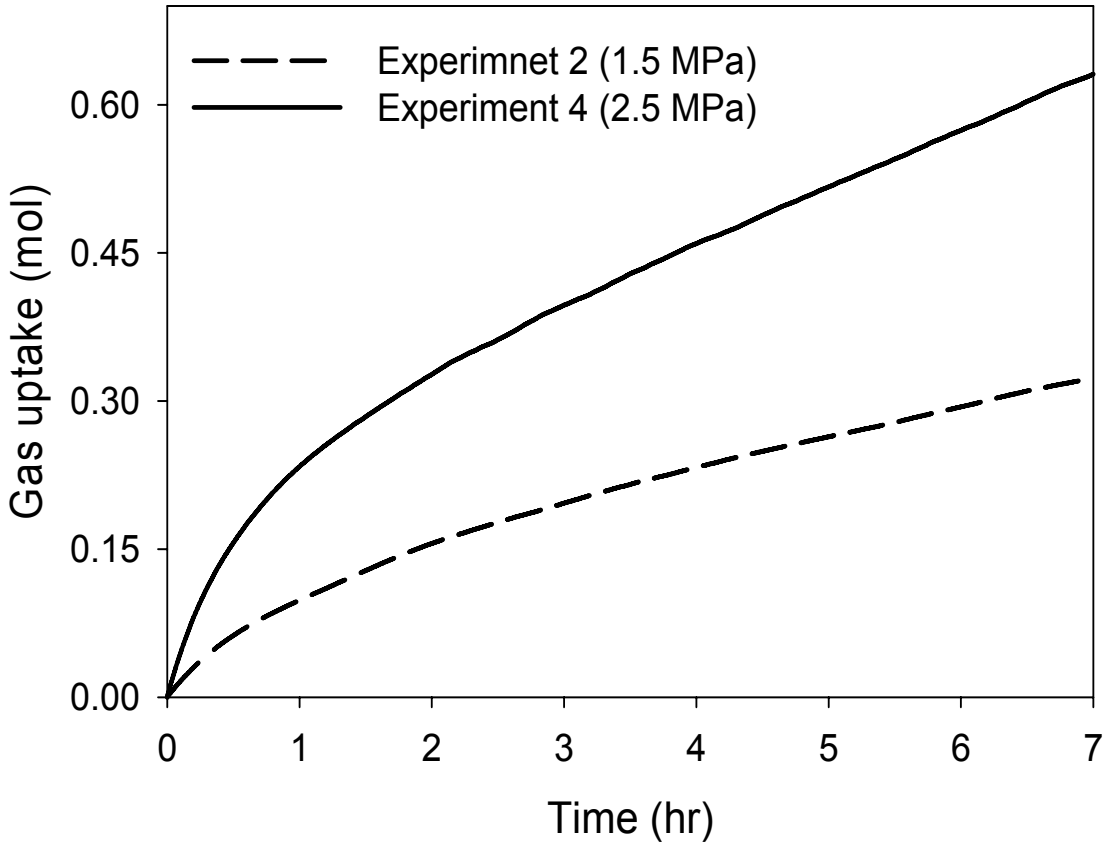

Figure 5-7: Gas uptake curves for 1.0 mol% THF concentration solutions with memory at 273.7 K and different pressures.

Split fraction or CO_2 recovery and the separation factor were determined from equations 3.1 and 3.2 and the calculated values are reported in Table 5-3. As it can be seen in the table the split fraction for all the experiments carried out with 1.0 mol% THF solutions was greater than 0.6 while that of 1.5 mol% THF solution was slightly less than

0.6 indicating that 60% of the CO_2 in the feed gas is separated in one stage of hydrate formation. One can see from the table and conclude that it would be wise to have the first stage of hydrate formation for CO_2 capture from a flue gas operating at 1.5 MPa since the CO_2 recovery is practically the same with that of the experiments studied at 2.5 MPa. However when we compare the CO_2 recovery (Table 5-3) and the gas uptake (Figure 5-7) in tandem, we can see that for the experiment at 2.5 MPa the final gas consumption is almost 2 times greater than the experiment at 1.5 MPa. It is desirable to have a good CO_2 recovery and also a better gas uptake for the separation process.

Table 5-3: Split fraction or CO_2 recovery and separation factor.

Description	Exp. 1	Exp. 3	Exp. 4	Exp. 9
THF concentration (mol%)	1.0	1.0	1.0	1.5
Pressure (MPa)	1.5	2.5	2.5	2.3
Gas consumption (end)	0.36	0.66	0.65	0.59
Split Fraction or CO_2 recovery	0.60	0.61	0.63	0.58
Separation factor	4.12	4.31	4.52	3.88

The rates of hydrate formation were calculated for all the kinetic experiments conducted using the forward difference method given below,

$$\left(\frac{dn}{dt}\right)_t = \frac{n_{t+\Delta t} - n_t}{\Delta t}, \quad \Delta t = 20 \text{ sec} \tag{5.1}$$

The average of theses rates are calculated for 20 min due to the very large number of data points and also to minimize the noise in the calculated rates using the following equation,

$$\text{Average rate of hydrate formation } (R_{av}) = \left[\frac{\left(\frac{dn}{dt}\right)_1 + \left(\frac{dn}{dt}\right)_2 + \ldots + \left(\frac{dn}{dt}\right)_m}{m} \right], \; m = 60 \qquad (5.2)$$

The calculated rate (equation 5.1) and the average rate (equation 5.2) along with the hydrate growth for a typical experiment are shown in Figure 5-8. Time zero in the graph corresponds to the induction time of the experiment given in Table 5-1. As seen, the rate during the first hour is greater than 0.15 mol/hr but it gradually slows down and remains more or less constant at about 0.06 mol/hr after two hours. It is noted that the maximum rate found with the small apparatus is 0.0016 mol/min or 0.096 mol/hr (see Table 4.2).

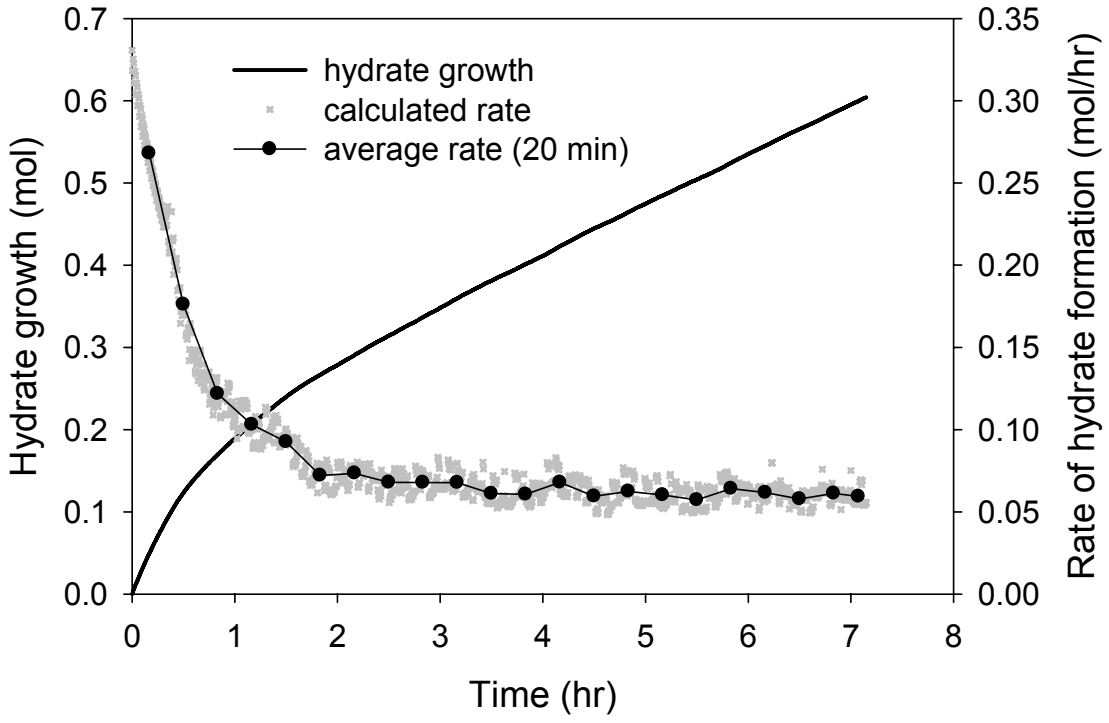

Figure 5-8: Hydrate growth for a typical hydrate formation experiment (experiment 5) along with the calculated average rates for 20 min.

Figure 5-9 shows a comparison of the calculated average rates for the experiments conducted at different driving force using memory solutions. As seen in the figure, there is a strong dependency of the rate on the driving force for the first two hours. The calculated rates are considerably higher for the experiments carried out at the higher driving force. Recall that a similar dependency was reported in chapter 4 for the experiments conducted at the lab-scale apparatus.

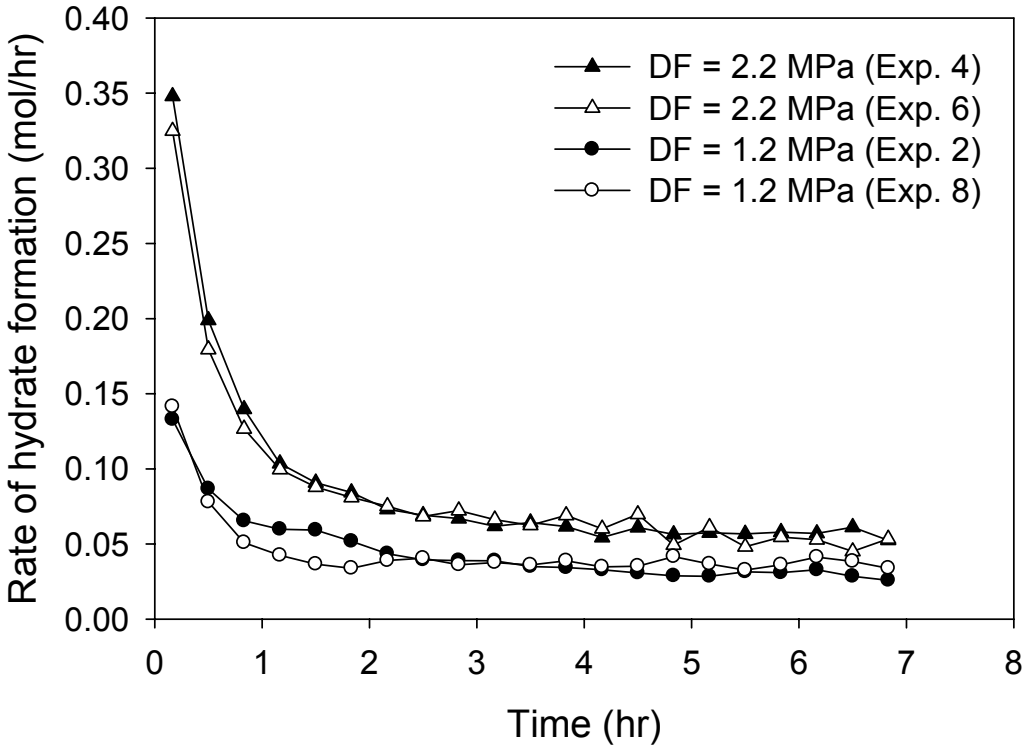

Figure 5-9: Rate of hydrate formation vs driving force for the kinetic experiments carried with 1.0mol% memory solutions.

One of the primary objectives of this work was to illustrate the separation process of CO_2 capture from a flue gas mixture in a large scale apparatus with a focus on improving the gas uptake and also improving the CO_2 recovery. Hence, a comparison can be made if the gas uptake is compared (on a water free basis) with the apparatus

described in chapter 2 and also reported by Linga et al. (2008). Figure 5-10 shows a comparison of gas uptake per mole of water to two such experiments performed under same pressure and temperature. As it can be seen in the figure, the gas uptake is substantially higher for the experimented conducted at a larger scale than that reported by Linga et al. (2008). During the first 2 hrs, the rates are similar with that in the new large apparatus somewhat higher. During this phase, the hydrate particles are well suspended in water and appear as shown in section C of Figure 5-11. After 2 hrs of hydrate growth, particle agglomeration and growth results in accumulation of gas hydrate crystals at the gas/liquid interface of the laboratory apparatus as shown in section D of Figure 5-11. On the other hand, hydrate continues to grow in the new large apparatus. This is due to better contacting of gas and liquid by mechanical agitation and due to the circulation of gas through the liquid phase by the special arrangement of the shaft and impeller. Additionally, the presence of the second impeller just below the gas/liquid interface (as shown in Figure 5-3) constantly renews the interface and also prevents any agglomeration of hydrate crystals at the gas/liquid interface. As a result, the gas uptake is 72.6% higher for the new apparatus. Similar results from other experiments as shown in Figure 5-12 demonstrate the improvement achieved in the gas uptake on a water free basis.

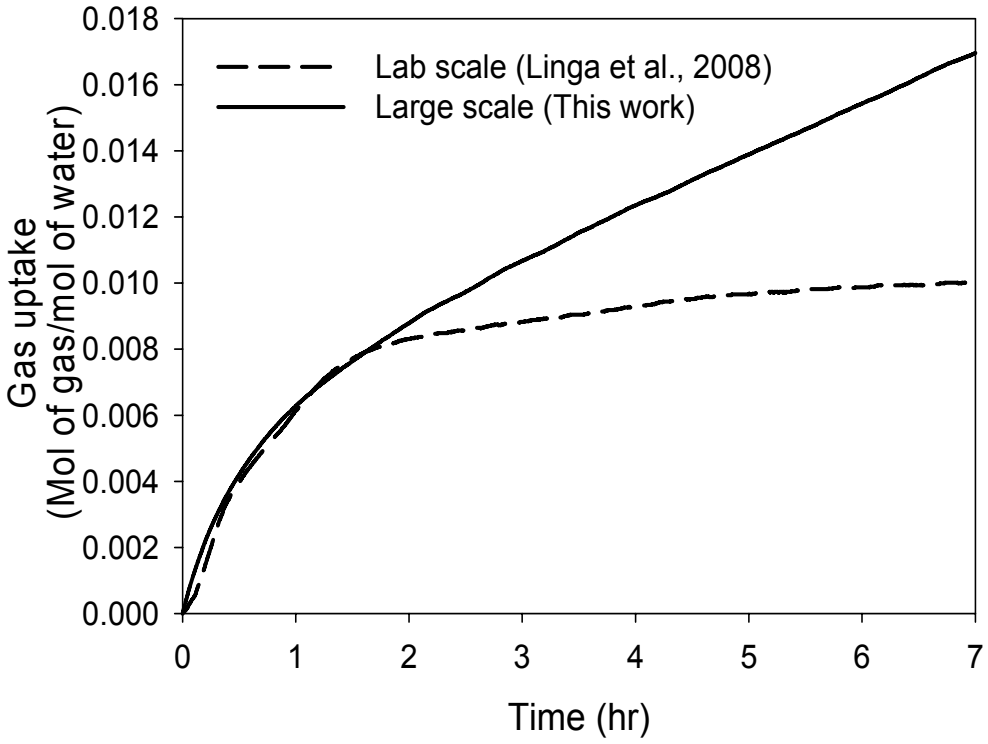

Figure 5-10: Comparison of gas uptake for hydrate formation for 1.0 mol% (Pressure = 2.5 MPa, Temperature = 273.7 K).

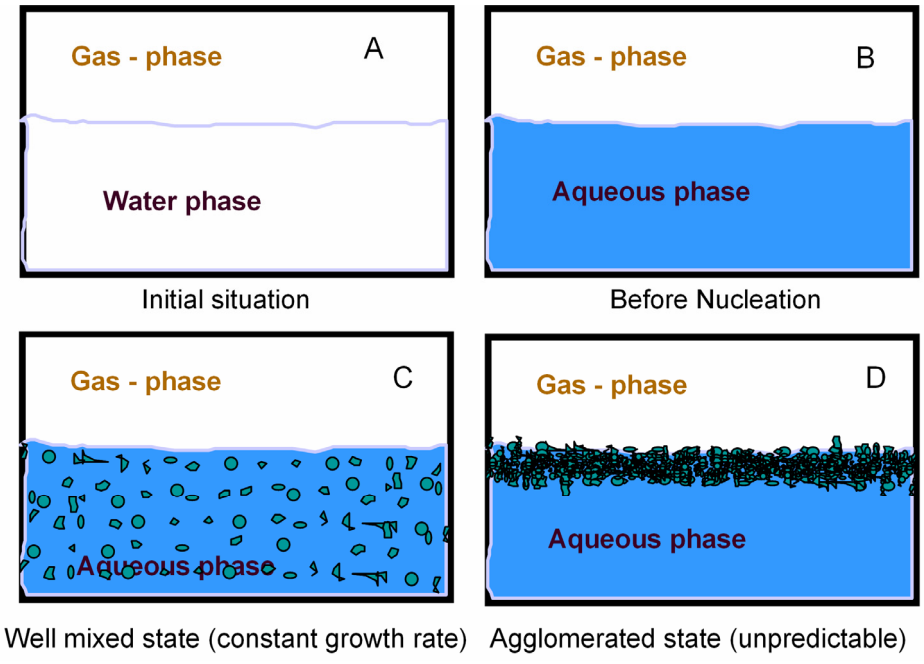

Figure 5-11: Schematic of the mass transfer resistance encountered in the lab scale apparatus described in Chapter 2.

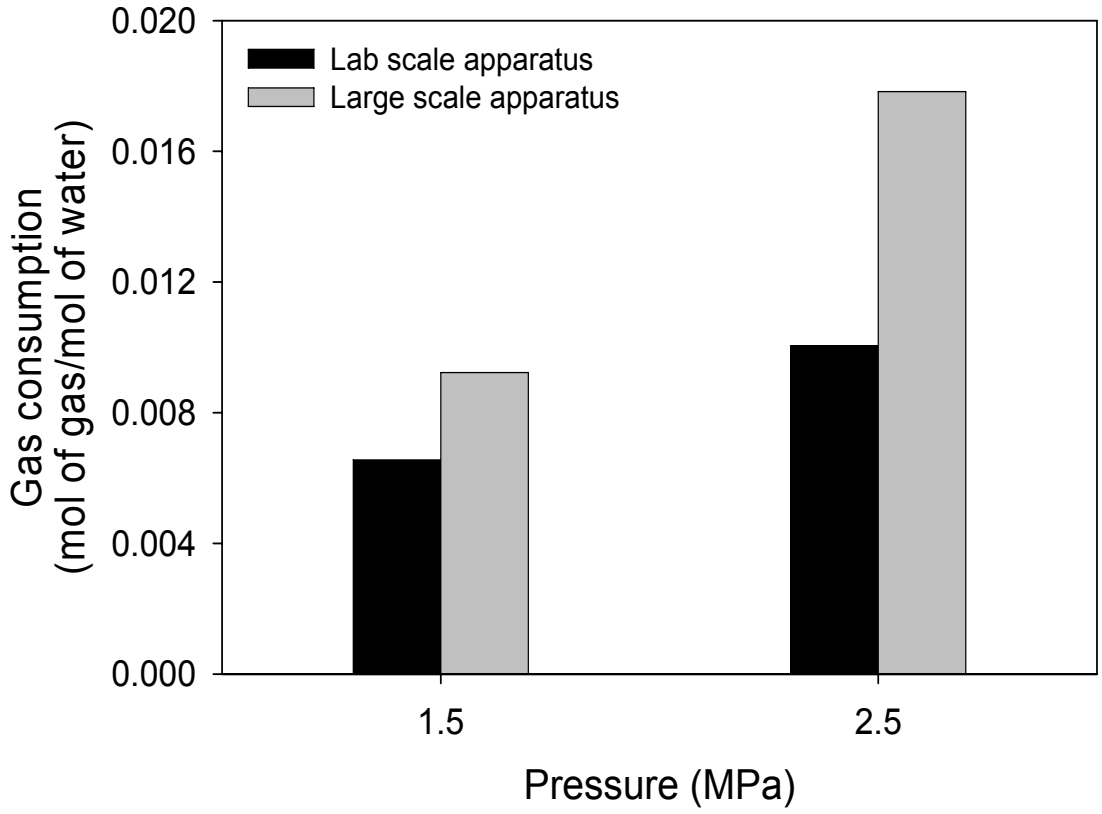

Figure 5-12: Comparison of the gas consumption for the lab scale apparatus and the new apparatus on a water free basis plotted against experimental pressure.

The second objective of this work was to compare the CO_2 recovery or split fraction obtained with the smaller scale apparatus of chapter 2 (Linga et al. 2008). The experimental conditions and the results for the two experiments shown in Figure 5-10 are given in Table 5-4. The CO_2 recovery is 36.9% higher for the new apparatus indicating a better capture of CO_2 in the crystals. Also, the conversion of water to hydrates was more than twice in the new apparatus compared to the lab scale apparatus.

Table 5-4: Comparison of CO_2 recovery or split fraction between small and the new large scale apparatus. Both experiments run for 7 hours.

Description	Exp. 4 (this work)	Linga et al. (2008)
THF concentration (mol%)	1.0	1.0
Volume of THF solution (ml)	700	140
Temperature (K)	273.7	273.7
Pressure (MPa)	2.50	2.55
Split Fraction or CO_2 recovery	0.63	0.46
Water conversion to hydrate (%)	14.9	7.1

Mori (2003) compared the rate of hydrate formation between different reactors available in the literature by defining a metric called rate of guest-gas fixation by hydrate formation per unit volume inside the reactor. It is noted that the above metric does not take into account the amount of water used in the hydrate formation experiment. We believe that the amount of water should also be taken into account in any meaningful comparison between the performances of the different reactors for a particular hydrate forming system. The normalized rate of gas supply taking into account the amount of water taken in the experiment is represented as follows,

$$\text{Normalized rate of gas supply, } \left(\frac{(mol/mol)}{(hr)}\right) = \left[\frac{(\Delta n_{H,\downarrow})_{end} / n_{H_2O}}{(\Delta t)_{end}}\right] \tag{5.3}$$

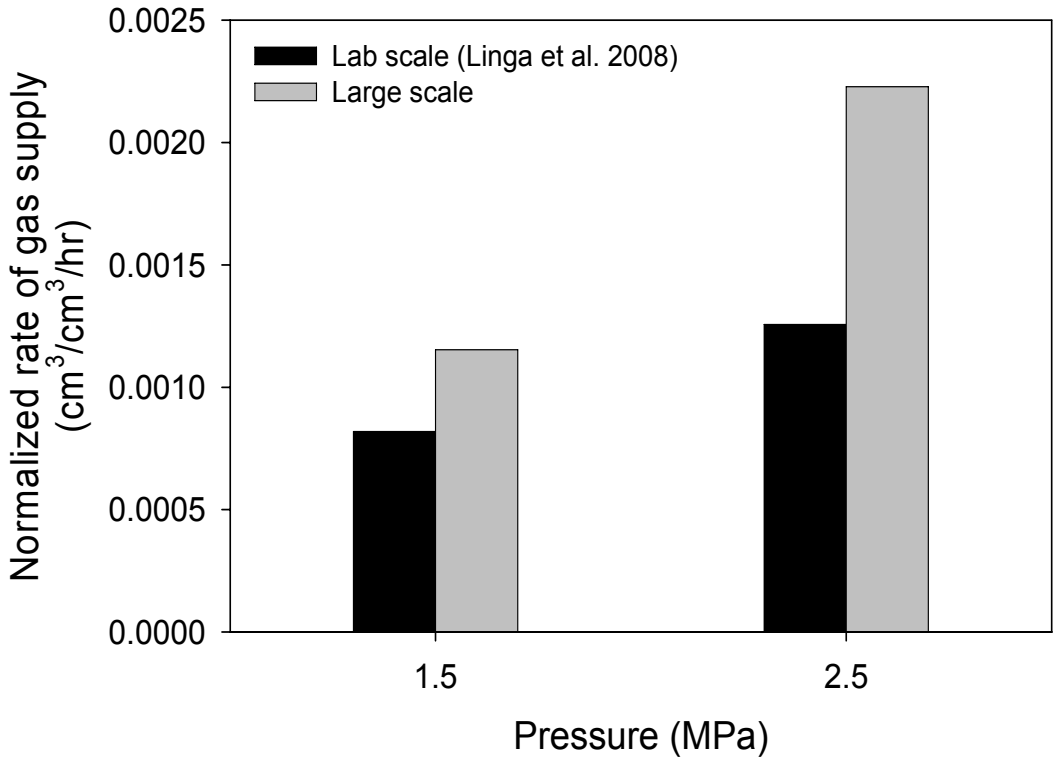

Figure 5-13: The normalized rate of gas supply calculated by taking into account of amount of water (equation 5.3) for the experiments conducted in the presence of 1.0 mol% THF in the lab-scale apparatus (Linga et al., 2008) and the new large scale apparatus plotted against the experimental pressure.

Figure 5-13 represents the calculated normalized rate of gas supply with respect to the amount of water for the lab-scale and the new large scale reactors. As seen in the figure, the calculated normalized rate of gas supply is on more than ~1.4 times higher for the new large scale apparatus compared to the lab-scale apparatus for the experiment carried out at a lower driving force and ~1.8 times higher at higher driving force.

For a comparison we also determined the normalized rate of gas supply with respect to the volume of the reactor (Mori, 2003). The equation is represented as,

$$\text{Normalised rate of gas supply,} \left(\frac{(cm^3/cm^3)}{(hr)} \right) = \left[\frac{(V_{gas,STP})_{end}/V_{reactor}}{(t)_{end}} \right] \quad (5.4)$$

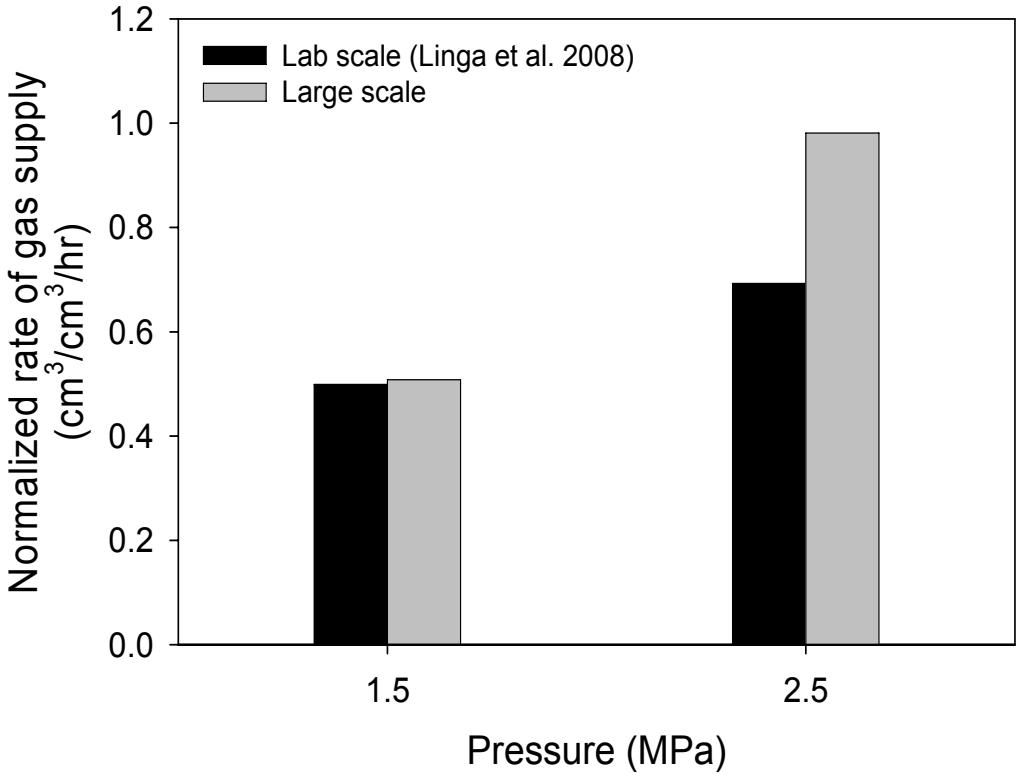

Figure 5-14: The normalized rate of gas supply calculated by taking into account of the volume of reactor (equation 5.4) for the experiments conducted in the presence of 1.0 mol% THF in the lab-scale apparatus (Linga et al., 2008) and the new large scale apparatus plotted against the experimental pressure.

Figure 5-14 shows the calculated normalized rate of gas supply with respect to the volume of the reactor for the lab-scale and the new large scale reactors. As seen in the figure, the normalized rate of gas supply for the new large scale apparatus is the same as that of the lab scale for the experiments conducted at lower driving force. While, at the higher driving force, the normalized rates are ~1.4 times higher for the new large scale reactor compared to lab-scale reactor. Hence overall, normalized rates calculated taking into account the amount of water or the volume of the reactor were higher in the new large scale reactor compared to the lab scale reactor. It is also noted that from the

calculated normalized rates it's also clearly evident that an operating pressure of 2.5 MPa is essential for the hydrate process.

Hence, we have successfully demonstrated the applicability of gas hydrate process for the separation of CO_2 from a flue gas mixture with the presence of 1.0 mol% THF using a new apparatus which operates at a larger scale compared to the laboratory apparatus presented in Chapter 2. It is envisioned that the results from this work will lead to a pilot plant testing and a possible demonstration plant implementation of the technology in the medium to long term. However it is noted that the fact that the apparatus relies on mechanical stirring will require additional energy in addition to that required for the compression of the flue gas. This energy is significant, thus the use of static mixer (Tajima et al., 2004) or an alternative contact mode should be investigated. One such way is to disperse water in silica gel and contact with water as a fixed bed column (Adebola, 2009; Seo et al., 2005). Another way is to use silica sand as a contact medium in a fixed bed column which is investigated in Chapter 6.

5.4. Conclusions

A new hydrate formation apparatus equipped with a modular-type crystallizer having a volume of 1,899.5 cm^3 is presented. The new apparatus improves the gas/water contact and as a result the gas uptake increases significantly (~77 % at 2.2MPa driving force) compared to the previously used laboratory apparatus. The rate of hydrate formation was calculated and found to correlate with the driving force (overpressure) as expected. Moreover, the normalized rates calculated by taking into account the volume of water and also the volume of reactor were found to be higher in the new apparatus. Moreover, the CO_2 recovery was found to be significantly higher (37%) indicating a better separation of

CO_2 from the feed gas. Hence, it is possible to scale up the separation process of CO_2 capture from a flue gas mixture. It is also possible that the new apparatus can be employed to form hydrates from natural gas for storage and transportation and also for CO_2 capture from fuel gas (pre-combustion capture).

5.5. References

Adeyemo, A., 2008. Post Combustion Capture of Carbon Dioxide through Hydrate Formation in Silica Gel Column, University of British Columbia, Vancouver.

Bishnoi, P. R., and Natarajan, V., 1996. Formation and decomposition of gas hydrates. Fluid Phase Equilibria 117(1-2), 168-177.

Kang, S. P., and Lee, H., 2000. Recovery of CO_2 from flue gas using gas hydrate: Thermodynamic verification through phase equilibrium measurements. Environmental Science & Technology 34(20), 4397-4400.

Kang, S. P., Lee, H., Lee, C. S., and Sung, W. M., 2001a. Hydrate phase equilibria of the guest mixtures containing CO_2, N_2 and tetrahydrofuran. Fluid Phase Equilibria 185(1-2), 101-109.

Kang, S. P., Lee, H., and Ryu, B. J., 2001b. Enthalpies of dissociation of clathrate hydrates of carbon dioxide, nitrogen, (carbon dioxide plus nitrogen), and (carbon dioxide plus nitrogen plus tetrahydrofuran). Journal of Chemical Thermodynamics 33(5), 513-521.

Lee, H., Lee, J. W., Kim, D. Y., Park, J., Seo, Y. T., Zeng, H., Moudrakovski, I. L., Ratcliffe, C. I., and Ripmeester, J. A., 2005. Tuning clathrate hydrates for hydrogen storage. Nature 434(7034), 743-746.

Linga, P., Adeyemo, A., and Englezos, P., 2008. Medium-pressure clathrate hydrate/membrane hybrid process for postcombustion capture of carbon dioxide. Environmental Science & Technology 42(1), 315-320.

Linga, P., Kumar, R., and Englezos, P., 2007a. The clathrate hydrate process for post and pre-combustion capture of carbon dioxide. Journal of Hazardous Materials 149(3), 625-629.

Linga, P., Kumar, R., and Englezos, P., 2007b. Gas hydrate formation from hydrogen/carbon dioxide and nitrogen/carbon dioxide gas mixtures. Chemical Engineering Science 62(16), 4268-4276.

Mori, Y. H., 2003. Recent Advances in Hydrate-based Technologies for Natural gas Storage-A Review. Journal of Chemical Industry and Engineering (China) 54, 1-17.

Seo, Y. T., and Lee, H., 2004. Structure and guest distribution of the mixed carbon dioxide and nitrogen hydrates as revealed by X-ray diffraction and C-13 NMR spectroscopy. Journal of Physical Chemistry B 108(2), 530-534.

Seo, Y. T., Moudrakovski, I. L., Ripmeester, J. A., Lee, J. W., and Lee, H., 2005. Efficient recovery of CO_2 from flue gas by clathrate hydrate formation in porous silica gels. Environmental Science & Technology 39(7), 2315-2319.

Tajima, H., Yamasaki, A., and Kiyono, F., 2004. Energy consumption estimation for greenhouse gas separation processes by clathrate hydrate formation. Energy 29(11), 1713-1729.

6. ENHANCED RATE OF GAS HYDRATE FORMATION IN A SILICA SAND MATRIX COMPARED TO A STIRRED VESSEL[5]

6.1. Introduction

Successful scale up of hydrate formation vessels for the industrial application of hydrate-based processes for CO_2 capture, other gas separations e.g. CO_2/CH_4 and natural gas storage and transport will depend significantly on the ability to have enhanced rates of crystal formation. Various designs of reactors can be seen in the literature, particularly in the patent documents. The majority of these designs use either the dispersion of gas in liquid water or the dispersion of liquid in gas in order to generate a large gas/water interfacial area per unit volume of the reactor. Mori (2003) presented in detail the advantages and disadvantages of the above mentioned configurations aimed at enhancing the kinetics of hydrate formation. Mori (2003) concluded that there is a need to focus on developing reactors and the operating schemes aimed at achieving higher hydrate forming efficiencies. McCallum et al. (2007) discussed the impact of the size of the hydrate formation vessel on induction time and hydrate formation/decomposition. Mesoscale experiments were conducted on a 72 liter seafloor process simulator (SPS) and were compared with a 450mL Parr vessel. They concluded that hydrates from the SPS consistently had less overpressures and shorter induction times than the equivalent experiments in the Parr vessel (McCallum et al 2007). McCallum et al. (2007) reported

[5]A version of this chapter will be submitted for publication. Linga, P., Haligva, C., Ripmeester, J. A., Englezos, P. Enhanced rate of gas hydrate formation in a silica sand matrix compared to a stirred vessel. Manuscript in preparation.

that the large volume of the SPS was a contributing variable which increased the likelihood of the initial hydrate nucleation clusters to grow and accumulate. However, McCallum et al. (2007) did not report any kinetic data (gas uptake or hydrate formation rate) or the conversion of water to hydrate.

One of the new approaches to enhance the kinetics of the hydrate formation is to disperse water in a porous media that could lead to the faster and higher conversion of water to hydrates (Lee et al., 2005; Seo et al., 2005). Seo et al. (2005) reported hydrate yields of about 85% in one hour of hydrate formation with water dispersed in silica gel pores when reacted with CO_2 based on ^1H NMR microimaging experiments. Linga et al. (2009) and Haligva (2008) reported hydrate conversion of more than 73% for all the hydrate formation experiments that were performed with methane/water system by dispersing water in silica sand conducted at 4.0 and 1.0 C starting with an experimental pressure of 8.0 MPa.

Therefore, a bed of silica sand particles offers an alternative way of carrying out hydrate formation. The objective of this work is to compare the kinetics of gas hydrate formation in a silica sand matrix and in a stirred vessel. Kinetics are correlated with the gas uptake during hydrate formation. The percent conversion of water to hydrate is also determined. In addition to CO_2 containing systems (CO_2/water, $CO_2/H_2/C_3H_8$/water and CO_2/N_2/THF) experiments with three hydrocarbon systems namely, CH_4/water, CH_4/C_3H_8/water and CH_4/C_2H_6/water were conducted in order to be able to generalize the conclusions.

6.2. Experimental section

6.2.1. Materials

The gas/mixtures that were used for this work were UHP grade supplied by Praxair Technology Inc., silica sand with an average diameter of 329 μm (diameter ranges from 150 to 630 μm) supplied by Sigma-Aldrich and distilled and deionised water was used.

6.2.2. Apparatus

Two experimental apparatus were used in this study. Figure 6-1 shows the schematic of one of the apparatus (Apparatus #1). The detailed description of this apparatus is available elsewhere (Haligva, 2008). It consists of a crystallizer (CR) which is immersed in a temperature controlled water bath. The temperature of the water bath is controlled by an external refrigerator (VWR Scientific). The temperatures of the hydrate phase and the gas phase of the crystallizer are measured using Omega copper-constantan thermocouples with an uncertainty of 0.1 K. The data acquisition system (National Instruments) is coupled with a computer to record the data as well as to communicate with the control valve during the experiment and the software used for this purpose is LabView 8.0 (National Instruments). The apparatus is also equipped with a safety pressure valve.

A detailed description of the other apparatus (Apparatus # 2) that was used for the experiments carried out in stirred tank reactor is given in chapter 2.

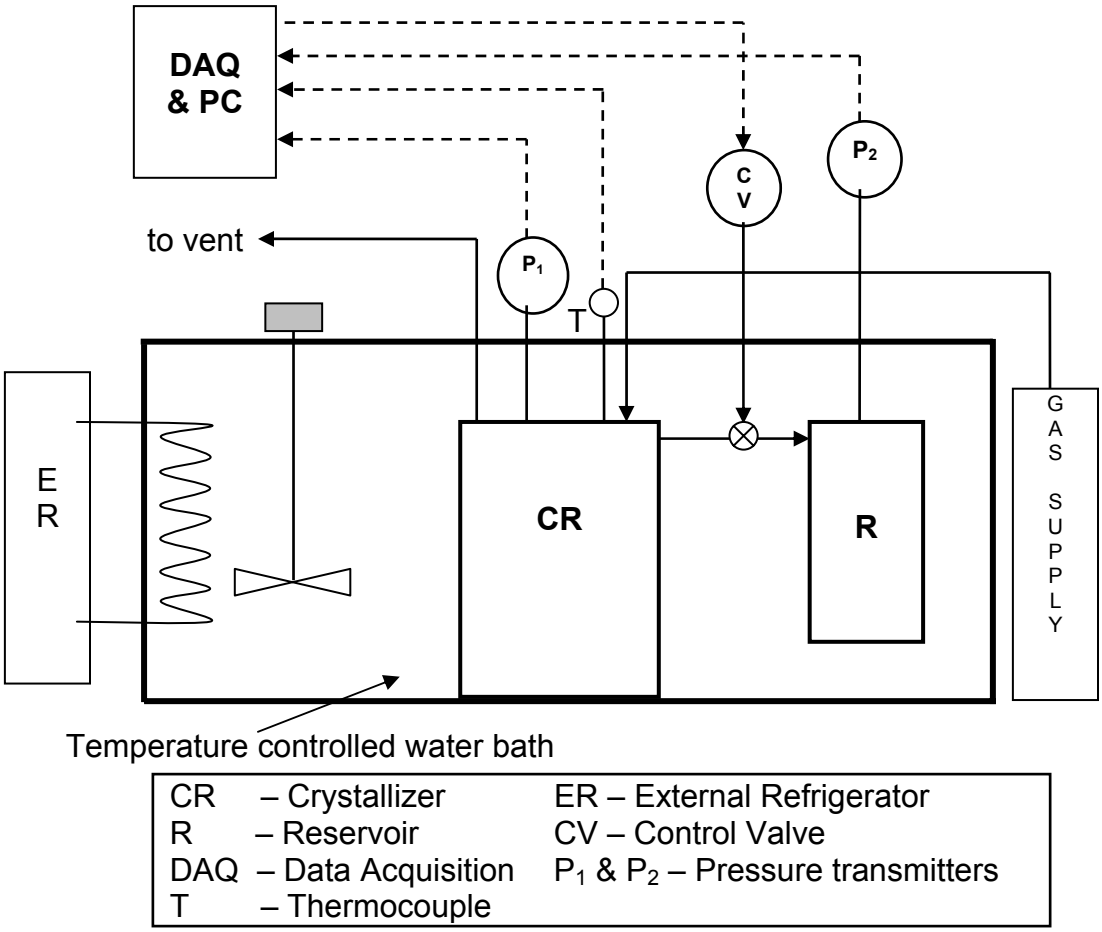

Figure 6-1: Schematic of the experimental apparatus.

6.2.3. Procedure for hydrate formation

6.2.3.1. Silica sand experiments

The amount of silica sand placed in the crystallizer for each experiment is 228.5 g. The volume of water required to fill the void space with water was found to be 35.0 ml for 161.0 g of sand. Accordingly, 49.7 ml of water is added into the sand. Once the crystallizer bed is setup with the required amount of sand and water, it is closed. The crystallizer is pressurized with the experimental gas mixture and depressurized at a pressure below the equilibrium hydrate formation pressure three times in order to

eliminate the presence of any air bubbles in the system. The pressure in the crystallizer is then set to the desired experimental value and the temperature is allowed to reach the target value (approximately 5 min). This is time zero for the formation experiment. Data is logged in the computer for every 20 seconds. All hydrate formation experiments for this work are carried out in a closed system (fixed amount of water and gas) at a constant temperature. When hydrate formation occurs, gas will be consumed and hence the pressure in the closed system drops. The pressure and temperature data are recorded and the data are used to calculate the moles of gas being consumed in the crystallizer (gas uptake).

6.2.3.2. Bulk water experiments with mixing

The experimental procedure for the experiments carried out with bulk water is as follows. The amount of water taken for the bulk water experiments is 49.7 ml (amount of water is the same as taken for the silica sand experiments). The crystallizer is pressurized with the experimental gas/mixture and depressurized at a pressure below the equilibrium hydrate formation pressure three times in order to eliminate the presence of any air bubbles in the system. The pressure in the crystallizer is then set to the desired experimental pressure and the temperature is allowed to reach the experimental temperature (approximately 5 min). The liquid contents in the crystallizer are now stirred using the magnetic stirrer at a constant speed of 300 rpm. This is time zero for the experiment. All hydrate formation experiments carried out for this case are also conducted in a closed system (fixed amount of water and gas) at a constant temperature. When hydrate formation occurs, gas will be consumed and hence the pressure in the closed system drops. The pressure and

temperature data are recorded and the data are used to calculate the moles of gas being consumed in the crystallizer (gas uptake).

6.2.4. Calculation of the amount of gas consumed during hydrate formation

At any given time, the total number of moles ($n_{T,t}$) in the system remains constant and equal to that at time zero ($n_{T,0}$). The system includes the crystallizer (CR) and the connecting tubing. The total number of moles at any given time is the sum of the number of moles (n_G) in the gas phase (G) of the crystallizer and the number of moles (n_H) consumed to form hydrate (H) or dissolved in water.

At any given time, the number of moles of the gas that has been consumed for hydrate formation is the difference between the number of moles of the gas at time t = 0 present in the gas phase of the crystallizer (CR) and the number of moles of the gas present in the gas phase of CR at time t = t and is given by the following equation,

$$n_{H,t} - n_{H,0} = n_{G,0} - n_{G,t} \tag{6.1}$$

or

$$\Delta n_{H,\downarrow} = n_{H,t} - n_{H,0} = \left(\frac{PV}{zRT}\right)_{G,0} - \left(\frac{PV}{zRT}\right)_{G,t} \tag{6.2}$$

where z is the compressibility factor calculated by Pitzer's correlation (Smith et al., 2001), V is the volume of gas phase of the crystallizer, P and T are the pressure and temperature of the crystallizer.

Percent conversion of water to hydrates is determined from the information obtained from gas uptake and the experimental conditions using the following equation

$$\text{Connversion of water to hydrates}\,(\text{mol}\%) = \frac{\Delta n_{H,\downarrow} \times \text{Hydration Number}}{n_{H_2O}} \times 100 \qquad (6.3)$$

where $\Delta n_{H,\downarrow}$ is the number of moles of gas consumed for hydrate formation at the end of the experiment determined from the gas uptake measurement and n_{H_2O} is the total number of moles of water in the system.

For the systems containing aqueous THF solutions, conversion of water to hydrates is determined from the following equation

$$\text{Connversion of water to hydrates}\,(\text{mol}\%) = \frac{(\Delta n_{H,\downarrow} + \Delta n_{THF}) \times \text{Hydration Number}}{n_{H_2O}} \times 100 \quad (6.4)$$

where $\Delta n_{H,\downarrow}$ is the number of moles of gas consumed for hydrate formation at the end of the experiment determined from the gas uptake measurement, n_{H_2O} is the total number of moles of water in the system and Δn_{THF} is the number of moles of THF consumed for hydrate formation at the end of the kinetic experiment. Δn_{THF} is calculated based on the occupancy ratio for sII (16S:8L), i.e. 1 mole of gas consumed in small cages would require ½ mole of THF in large cage.

6.3. Results and discussion

Table 6-1 summarizes the experimental conditions for the systems studied in this work. Hydrate formation is a crystallization process and an exothermic reaction. Induction point is the time when hydrate formation occurs and is determined from the experimental data and reported in Table 6-1. The experiment end times are also reported in the table.

6.3.1. CH_4/water system

Figure 6-2 shows a comparison of the methane uptake curves obtained for the experiment with water dispersed in silica sand and the stirred tank reactor. As seen, methane uptake is faster in the stirred tank reactor. We believe that nuclei formed are forced to circulate within the liquid phase and essentially "seed" the entire system with hydrates. On the other hand the extensive work on the CH_4/H_2O system in silica sand showed occurrence of localized nucleation (Haligva, 2008). It is noted that mixing the contents become impossible after 180 min (visual observation) because a significant mass of hydrate and occluded water prevents efficient gas/water contact. Thus, the gas uptake decreases and becomes less than that in the sand system. Overall, the methane uptake is considerably faster and higher for the experiment carried out with water dispersed in silica sand. For instance, at 10 hours the methane uptake for the experiment carried out in the presence of silica sand is more than two times that of the stirred tank reactor.

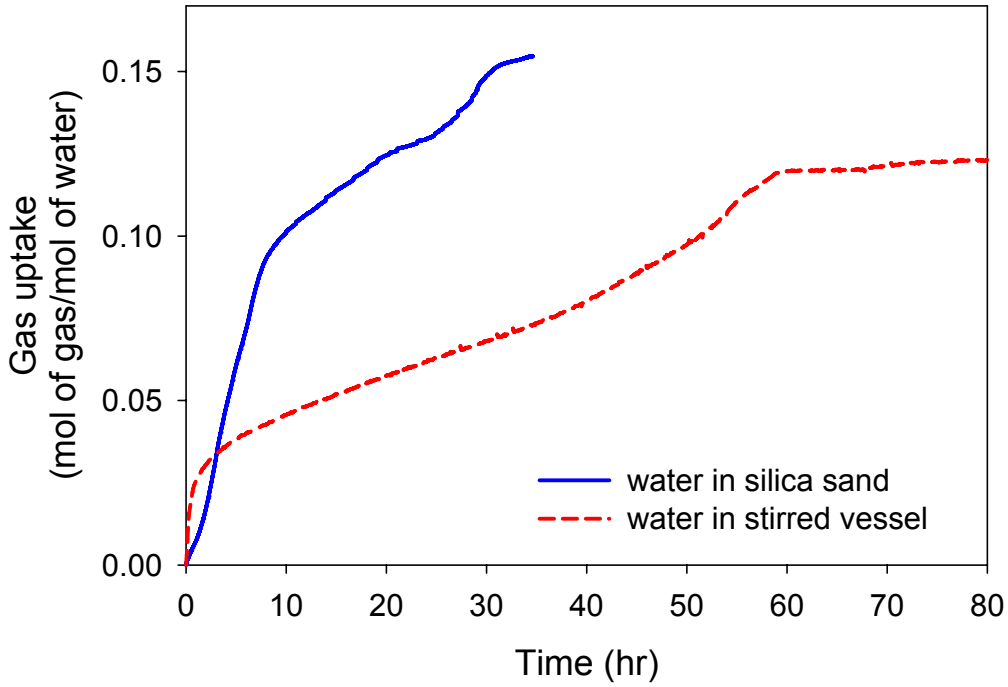

Figure 6-2: Comparison of gas uptake (hydrate growth) measurement curves for CH_4/water hydrate formation experiments. Time zero in the graph is induction time for the corresponding experiment (given in Table 6-1).

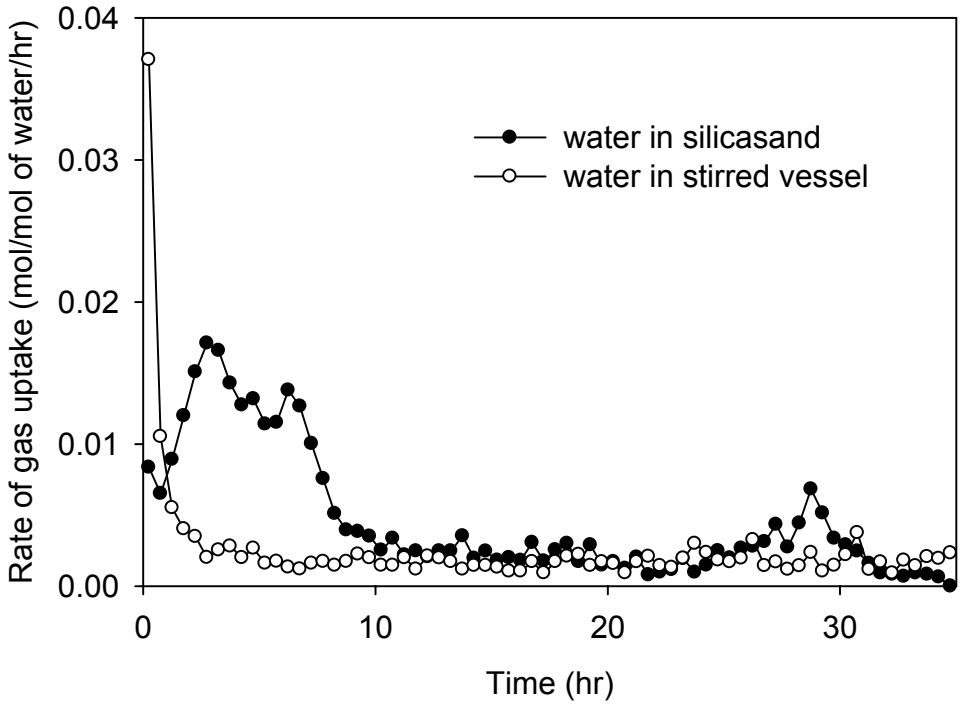

Figure 6-3: Comparison of the rate of methane uptake per mol of water for CH_4/water system.

The rate of hydrate formation was determined for every 5 min using forward difference method and the average of these rates for 30 min is determined and presented in Figure 6-3. As it can be seen in the figure, the rate is higher for the experiment conducted in stirred vessel by around by 4 times at the start but it gradually decreases due to extensive hydrate formation which leads to mass transfer limitations. However, in the case of the experiment in the presence of silica sand, hydrate formation continues to occur, however at varying rates. Kneafsey et al. (2007) reported a similar behavior of hydrate growth occurring at different rates, when hydrates were formed at 6.2 MPa and 1.1°C in the presence of silica sand with a particle size of 100 to 200 μm. They achieved a water to hydrate conversion of 65% using a hydration number of 5.75. Seo et al. (2005) reported that gas molecules can easily penetrate a bed of silica gel particles saturated with water and the dispersed water presents a huge surface for contacting gas molecules. It is noted that based on ^{1}H NMR microimaging experiments, Seo et al. (2005) reported hydrate yields of about 85% in one hour of hydrate formation with water dispersed in silica gel pores when reacted with CO_2.

Percent conversion of water to hydrate (hydrate saturation) was determined from equation 6.3 using a hydration number of 6.1 (Tulk et al., 2000) and is given in Table 6-1. Conversion of 94.7% was achieved for the experiment with the presence of silica sand in 34 hours while the hydrate saturation achieved for the experiment carried out in stirred vessel was 76.1% in 80 hours.

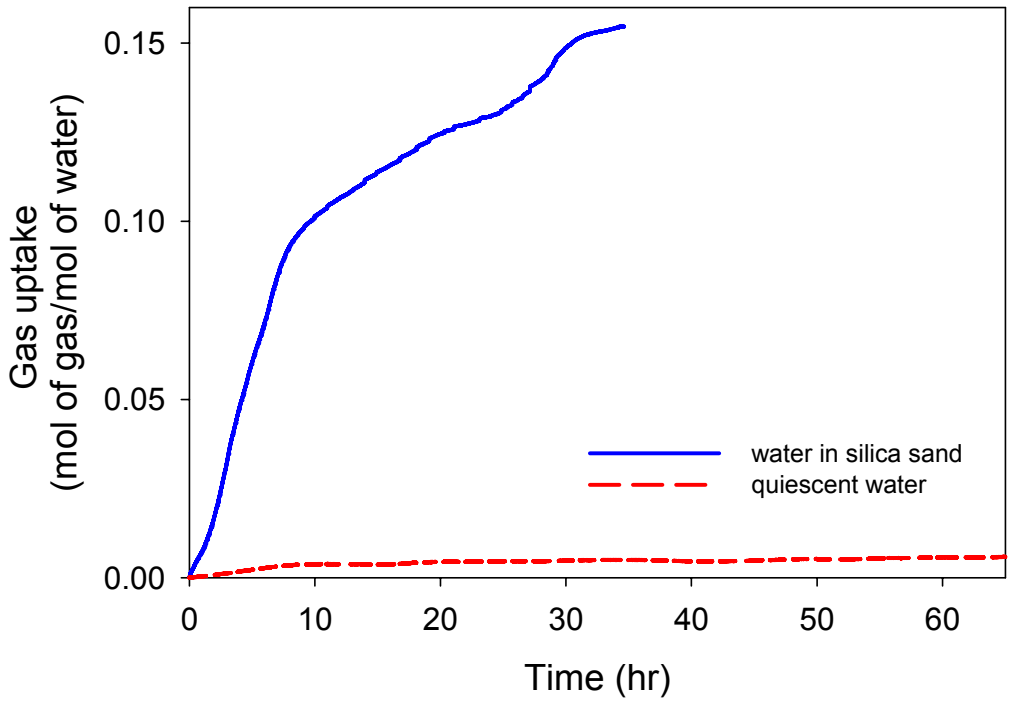

Figure 6-4: Comparison of gas uptake (hydrate growth) measurement curves for CH_4/water hydrate formation experiment conducted in the same apparatus with and without the presence of silica sand.

One hydrate formation experiment was performed in the apparatus shown in figure 1 with the absence of silica sand. 49.7 ml of water was placed in the crystallizer and the pressure and temperature was set to experimental conditions as shown in Table 6-1. Figure 6-4 shows the comparison of the kinetic experiments studied with and without the presence of silica sand conducted in the same apparatus. As one can see in the figure, hydrate formation in a quiescent liquid water/gas system is very slow compared to the experiment where the water is dispersed in the interstitial spaces of silica sand particles. As it can be seen from Figure 6-2 & 6-4 the system with the presence of silica sand resulted in achieving significantly higher methane consumption in a shorter time.

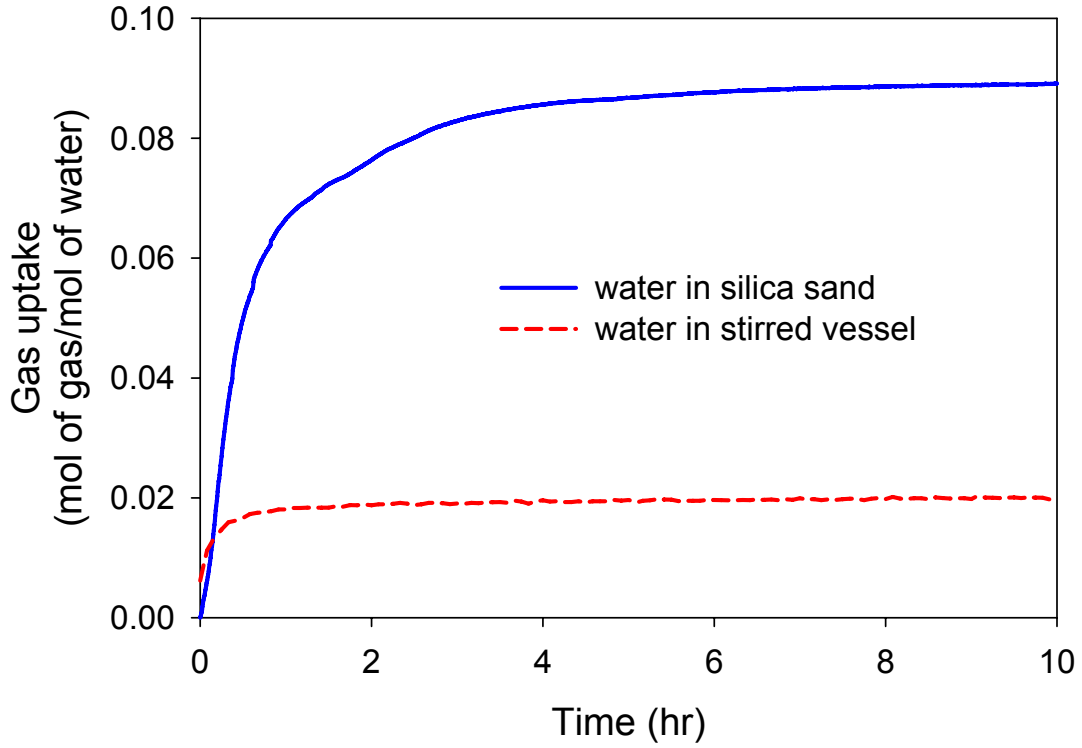

Figure 6-5: Comparison of gas uptake (hydrate growth) for CH_4 (90.5%)/C_3H_8 (9.5%)/water system. Time zero in the graph is induction time for the corresponding experiment (given in Table 6-1).

6.3.2. CH_4/C_3H_8/water system

Figure 6-5 shows a comparison of gas uptake obtained for the system with silica sand and the other system carried out in a stirred tank reactor. As it can be seen in the figure, the gas uptake for the experiment in the stirred vessel is faster initially (first 15 min) but soon decreases and reaches a steady state. On the other hand the uptake in the silica sand bed continues to increase indicating extensive hydrate formation. The final conversion of water to hydrates was 73.8 % for the experiment carried out with water in the presence of silica sand as compared to 18.1% for the experiment conducted in a stirred vessel. Percent conversion of water to hydrate was calculated assuming a hydration number of 8.0 for this system (CSMHYD: Sloan, 1998). Figure 6-6 shows the comparison of the rate of hydrate formation for both the experiments studied with and without the presence

of silica sand. As we can see in the figure, hydrate continues to form till about 4 hours for the experiment with the presence of silica sand even though the rate is decreasing along the time where as for the system with mixing the rate becomes near zero at 75 min.

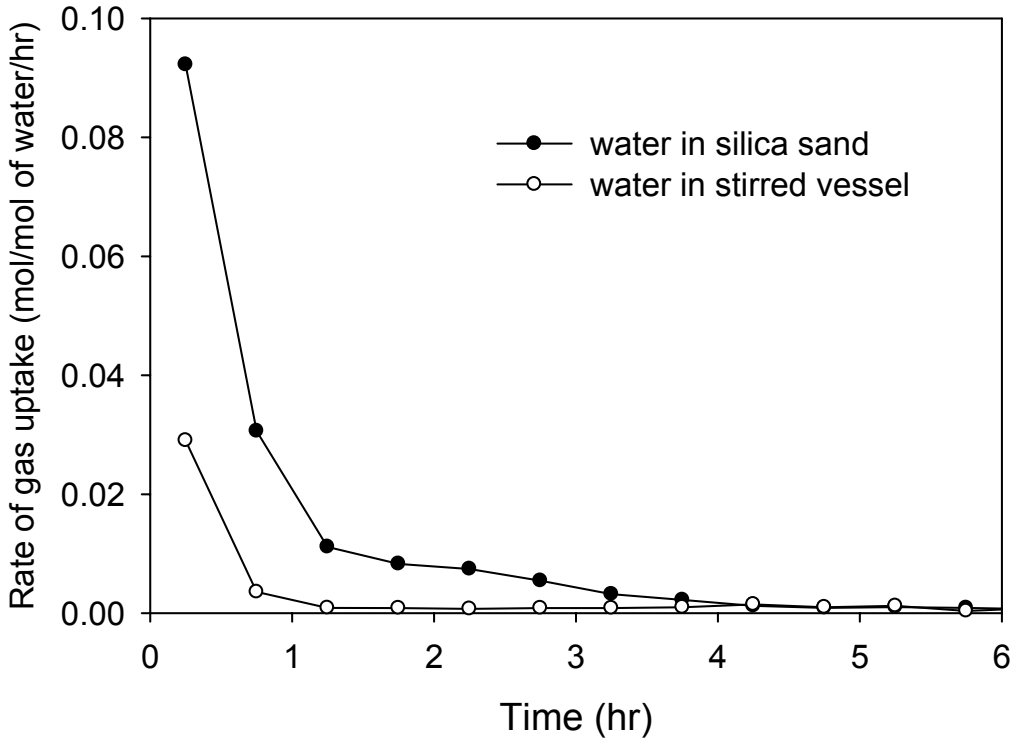

Figure 6-6: Comparison of the rate of gas uptake for CH_4 (90.5%)/C_3H_8 (9.5%)/water system.

6.3.3. CH_4/C_2H_6/water system

Figure 6-7 shows a comparison of gas uptake obtained for the system with silica sand and the uptake in the stirred tank reactor. As it can be seen in the figure, the gas uptake for the experiment with the presence of silica sand was greater and resulted in more hydrates. However, the behavior of the uptake curve in the stirred vessel is similar to that for the CH_4/water system (Figure 6-2). It is interesting to note that in this case stirrer stopped after 3 hours due to the presence of hydrate crystal but in spite of that hydrates continue

to grow for the next 15 hours. At the end of the experiment, 75.6% of water was converted to hydrate for the system with silica sand while 60.3% of water was converted for the experiment conducted in a stirred vessel. Percent conversion of water to hydrate was calculated assuming a hydration number of 6.2 for this system (CSMHYD: Sloan, 1998).

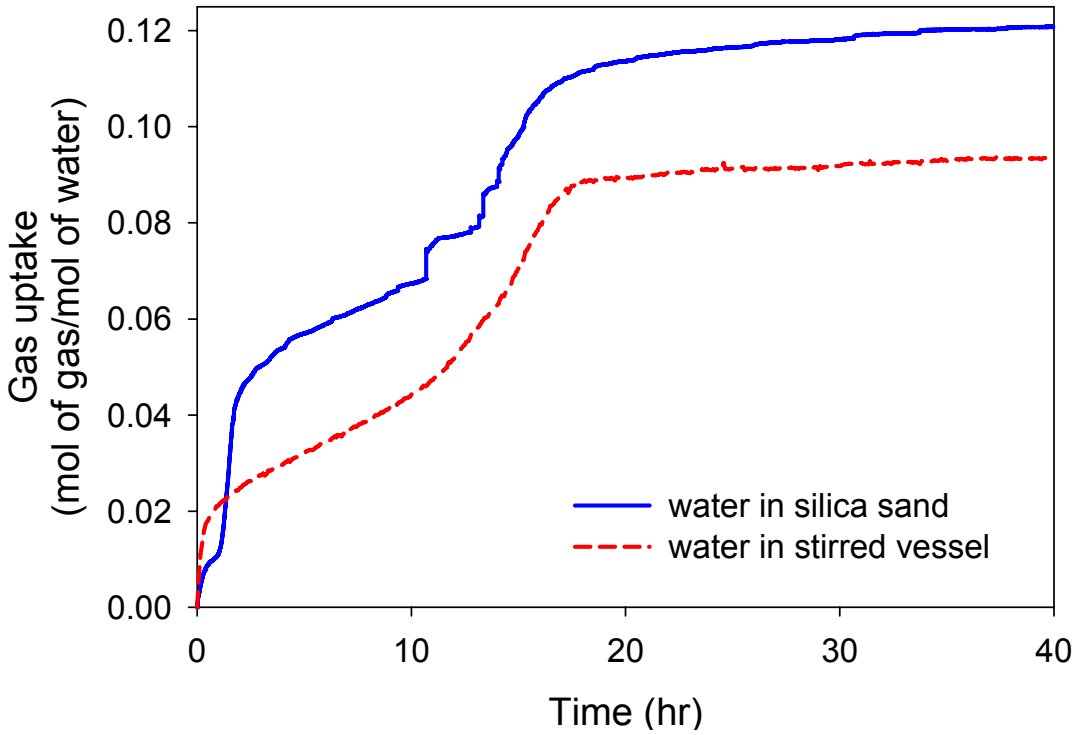

Figure 6-7: Comparison of gas uptake (hydrate growth) for CH_4 (91.0%)/C_2H_6 (9.0%)/water system. Time zero in the graph is induction time for the corresponding experiment (given in Table 6-1).

For all the hydrocarbon systems studied, the gas consumption was higher for the experiments carried out with the presence of silica sand. Figure 6-8 shows the comparison of gas consumption for the two experiments carried out for all the three systems. The comparison is made at the same experimental time (hydrate formation time was same). As can bee seen in the figure, the gas consumption is significantly higher for the experiments conducted in the presence of silica sand compared to the experiments

conducted in a stirred vessel. Also, higher percent conversion of water to hydrates was achieved for the experiments carried out with the presence of silica sand at the end of the experiment. For example, for CH_4 (90.5%)/C_3H_8 (9.5%)/water system the mole consumption is more than 4 times higher for the experiment conducted with the presence of silica sand compared to the experiment conducted in a stirred vessel even after running the experiment for ~97 hr.

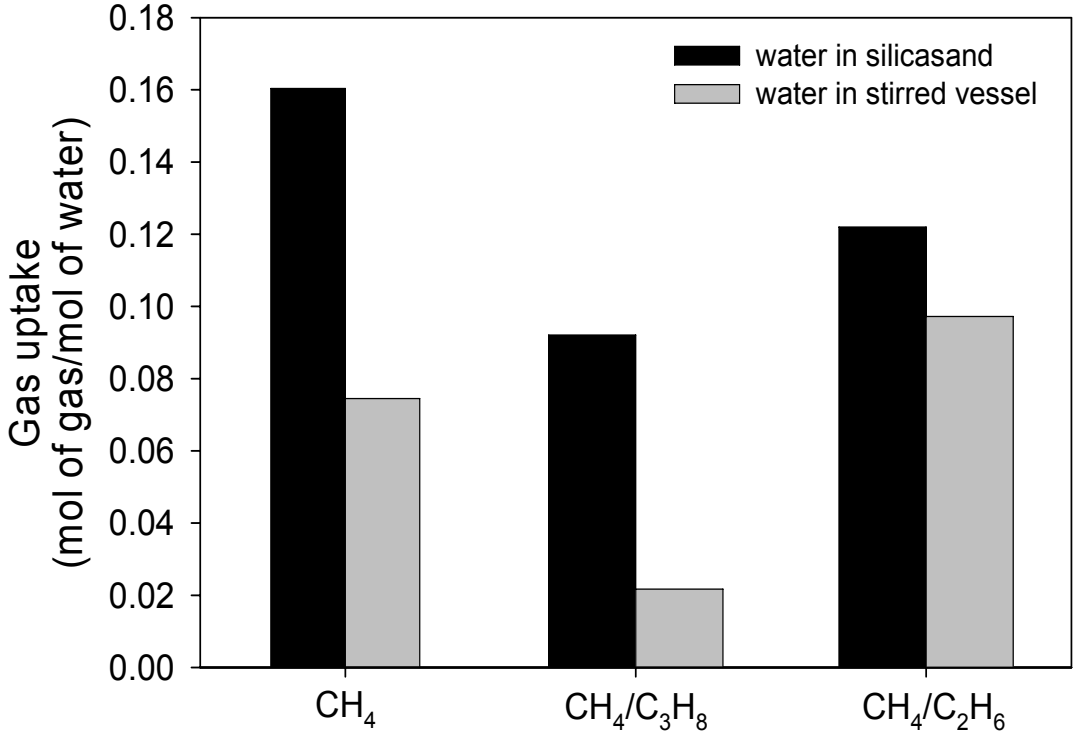

Figure 6-8: Comparison of gas consumption for all the three hydrocarbon containing systems. The experimental time is the same for both experiments carried for each system.

Figure 6-9 shows a comparison of the temperature profiles for the system mentioned above along with the gas uptake as a function of time. It is clearly evident from seeing the temperature profiles and the gas uptake in conjunction that the extent of heat released from the experiment performed in the presence of silica sand is due to the extensive formation of hydrates as opposed to the experiment performed in a stirred

vessel. Figure 6-10 shows a similar comparison of the temperature profiles along with the gas uptake as a function of time for the CH_4 (91%)/C_3H_8 (9.0%)/water system. As one can see for the experiment carried out with silica sand, there are three large temperature spikes occurring at ~ 3.3, 75.3 & 565.7 min, respectively and several small spikes occurring due to hydrate formation inside the bed which results in higher gas consumption and subsequently higher percent conversion of water to hydrates.

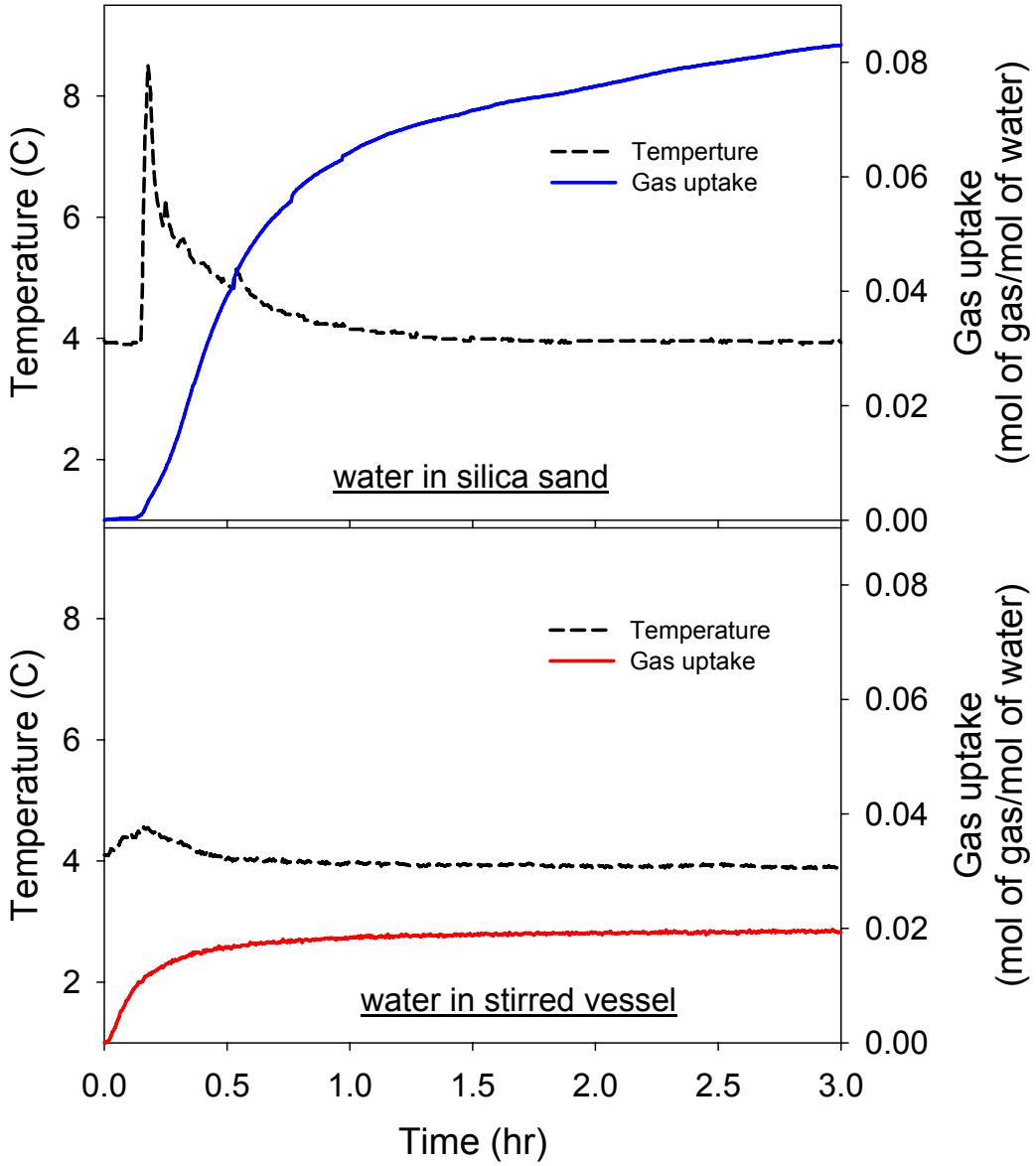

Figure 6-9: Comparison of temperature profiles and gas uptake for CH_4 (90.5%)/C_3H_8 (9.5%)/water system.

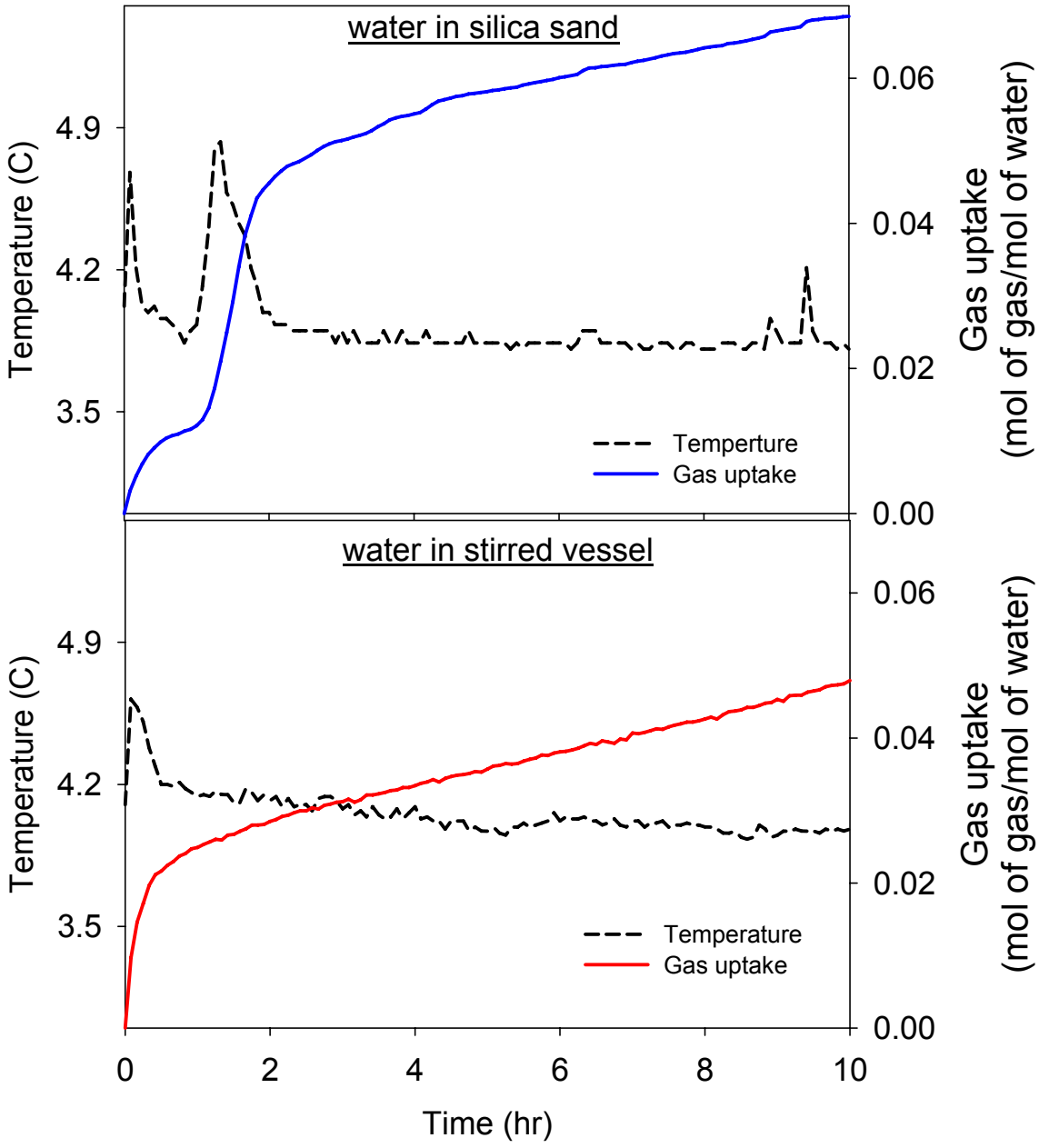

Figure 6-10: Comparison of temperature profiles and gas uptake for CH_4 (91.0%)/C_2H_6 (9.0%)/water system.

6.3.4. CO_2/water system

Figure 6-11 shows a comparison of gas uptake obtained for the system with silica sand and the other system carried out in a stirred tank reactor. As it can be seen in the figure, the gas uptake for the experiment with the presence of silica sand was greater and resulted in more hydrates. The gas uptake for the experiment conducted in stirred vessel reached a plateau at around 5 hr where as in the other case, hydrate growth continues till 47 hr and reaches a plateau thereafter. The gas consumed for the silica sand experiment at the end of the experiment is 2.4 times higher than that of the experiment conducted in a stirred vessel. Also, 59.8% of water was converted to hydrate for the system with silica sand while 25.3% of water was converted for the experiment conducted in a stirred vessel. Percent conversion of water to hydrate was calculated assuming a hydration number of 6.5 for this system (Udachin et al., 2001).

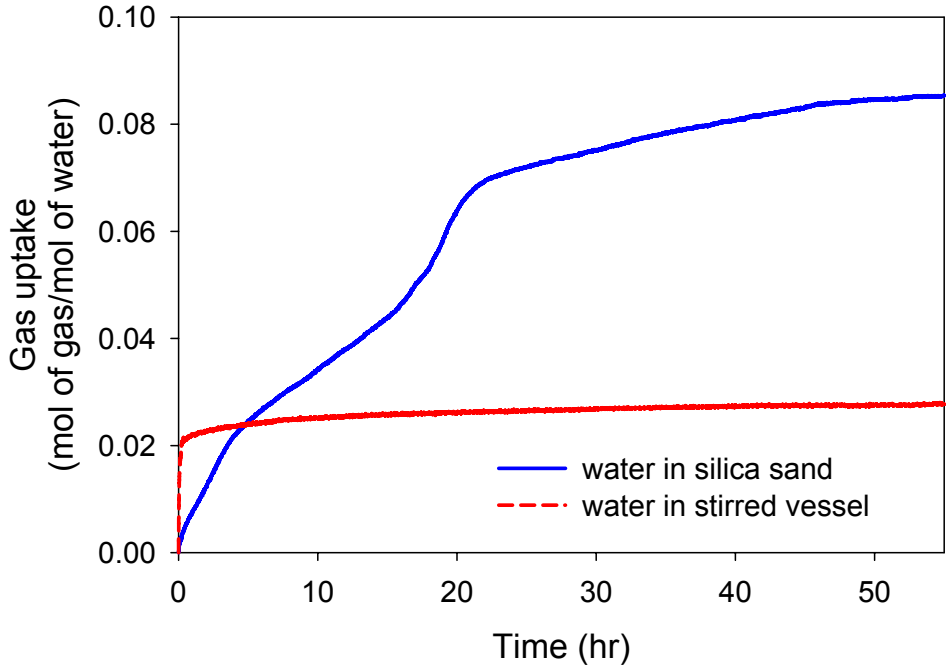

Figure 6-11: Comparison of gas uptake (hydrate growth) for CO_2/water system (Temperature = 1.0 C, Pstart = 3.1 MPa). Time zero in the graph is induction time for the corresponding experiment (given in Table 6-1).

6.3.5. $CO_2/H_2/C_3H_8$/water system

Formation experiment for CO_2 (38.1%)/H_2 (59.4%)/C_3H_8 (2.5%)/water system with and without silica sand was carried out at 1.0 °C and the experimental pressure at the start of the experiment for this system was 5.1 MPa. This gas mixture is of particular interest for the pre-combustion capture of carbon dioxide from a fuel gas mixture coming out of an IGCC plant. It has been demonstrated that with the presence of small amount of propane as an additive the equilibrium hydrate formation pressure is significantly lower for any given temperature compared to CO_2 (40%)/H_2 (60%)system (Kumar et al., 2006). It was found that 99% CO_2 stream can be obtained from the above mentioned gas mixture in two stages of hydrate formation/dissociation with or without the presence of propane as an additive (Kumar et al., 2008; Linga et al., 2007). The presence of propane significantly reduces the operating pressure at any given temperature without compromising the CO_2 recovery from the fuel gas mixture (Kumar et al., 2008).

Figure 6-12 shows a comparison of gas uptake obtained for the system with silica sand and the experiment conducted in stirred vessel. Gas uptake for the experiment with the presence of silica sand was more than 4 times higher than the experiment carried out in a stirred vessel at the end of the experiment. The final conversion of water to hydrates was 86.4% for the experiment carried out with water dispersed in silica sand compared to only 19.8% for the experiment conducted in a stirred vessel. The hydration number used for this system was 10.05 (Kumar et al., 2009).

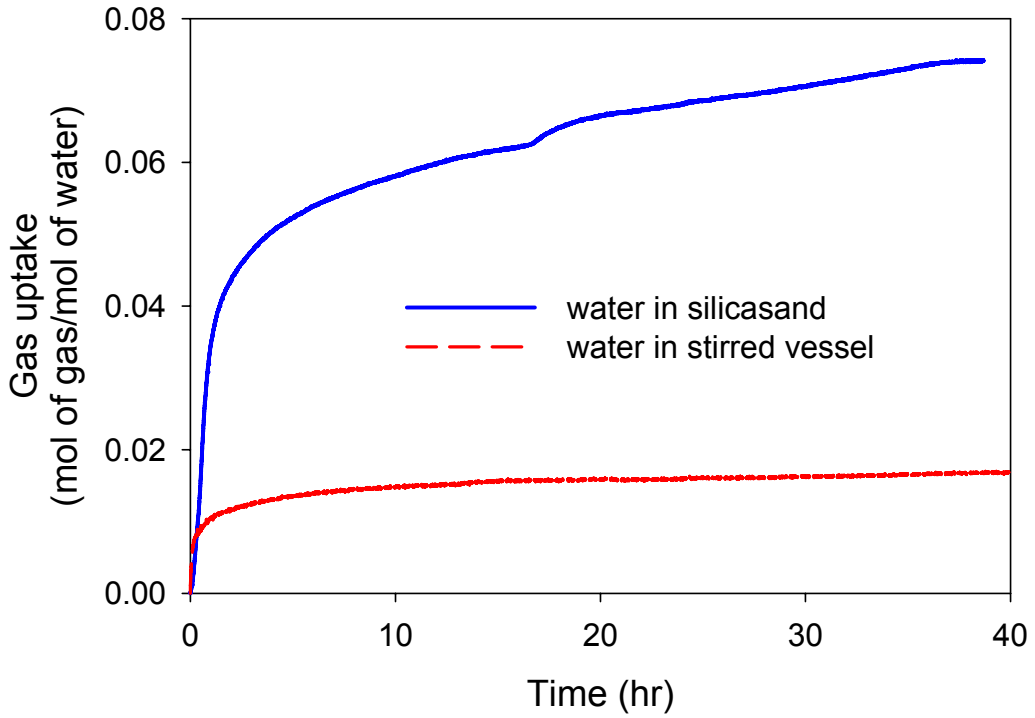

Figure 6-12: Comparison of gas uptake (hydrate growth) for CO_2 (38.1%)/H_2 (59.4%)/C_3H_8 (2.5%)/water system (Temperature = 1.0 C, Pstart = 5.1 MPa). Time zero in the graph is induction time for the corresponding experiment (given in Table 6-1).

6.3.6. CO_2/N_2/1.0 mol% THF system

Figure 6-13 shows a comparison of gas uptake obtained for the system with silica sand and the other system carried out in a stirred vessel. As seen in the figure, the gas uptake for both the experiments is the same. For all the systems shown above involving water and different gas or gas mixtures, the gas consumption was significantly higher for the experiments carried out with the presence of silica sand. However, with the presence of 1.0 mol% THF instead of water, the difference is not that much (Figure 6-13). Linga et al. (2008) found out that the optimum concentration of THF to be 1.0 mol% for experiments carried out in a stirred tank vessel for hydrate formation from a flue gas mixture (CO_2/N_2). May be, the optimum for the system with the presence of silica sand might be different. Hence, the effect of THF concentration should be further investigated. Moreover, the

interaction of silica with THF is not well understood. Similar observations were made by Adeyemo (2008) for experiments carried out in the presence of 1.0 mol% THF in the presence of silica gel pores at 5.0 MPa. In order to elucidate the effect of driving force, we decided to perform another experiment at a higher pressure of 5.0 MPa. Figure 6-14 shows a comparison of the gas uptake obtained for the system with silica sand and the other system carried out in a stirred vessel. As it can bee seen in the figure, the gas consumption was not significantly higher for the silica sand compared to the one carried out in a stirred vessel.

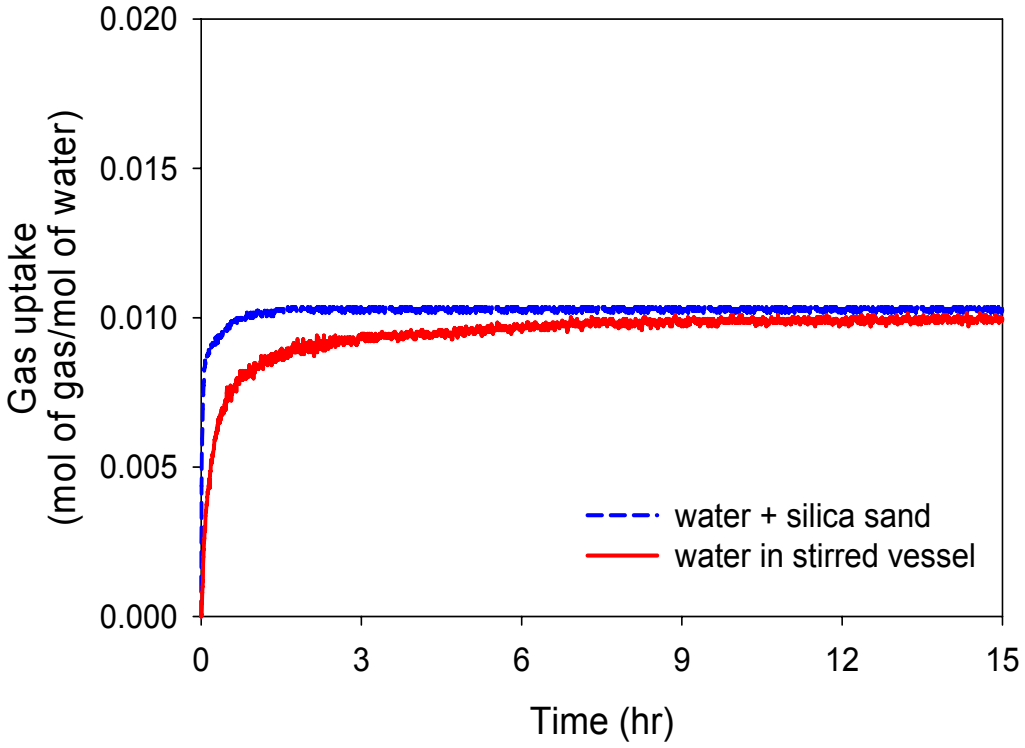

Figure 6-13: Comparison of gas uptake (hydrate growth) for CO_2 (16.9%)/N_2 (83.1%)/1.0 mol% THF system (Temperature = 1.9 C, Pstart = 2.5 MPa). Time zero in the graph is induction time for the corresponding experiment (given in Table 6-1).

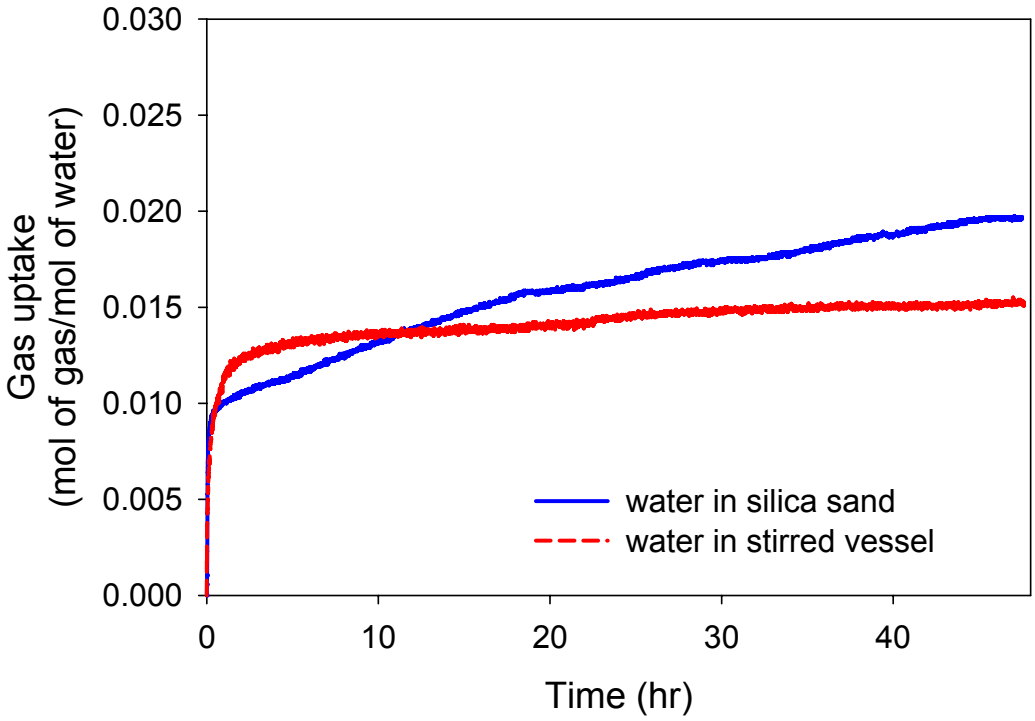

Figure 6-14: Comparison of gas uptake (hydrate growth) for CO_2 (16.9%)/N_2 (83.1%)/1.0 mol% THF system (Temperature = 1.9 C, Pstart = 5.0 MPa). Time zero in the graph is induction time for the corresponding experiment (given in Table 6-1).

Figure 6-15 shows the comparison of the gas consumption for all the CO_2 containing systems performed in a stirred vessel and by dispersing the liquid in silica sand. Overall, the gas consumption was significantly higher for the systems studied in water (CO_2, $CO_2/H_2/C_3H_8$ systems) while there was not much of a significant difference in the gas consumption for the system studied in aqueous 1.0mol% THF solutions (CO_2/N_2 system). For instance, the gas consumption was 4.5 times higher for the $CO_2/H_2/C_3H_8$ system carried out by dispersing water in silica sand compared to the experiment conducted in a stirred vessel. Moreover, as can bee seen in Figure 6-12, the hydrate growth was significantly faster for the system carried out by dispersing water in silica sand compared to the experiment conducted in a stirred vessel. Dispersing water in silica sand offers an

excellent possibility for employing hydrate based separation process for the capture of CO_2 from a fuel gas mixture ($CO_2/H_2/C_3H_8$ system).

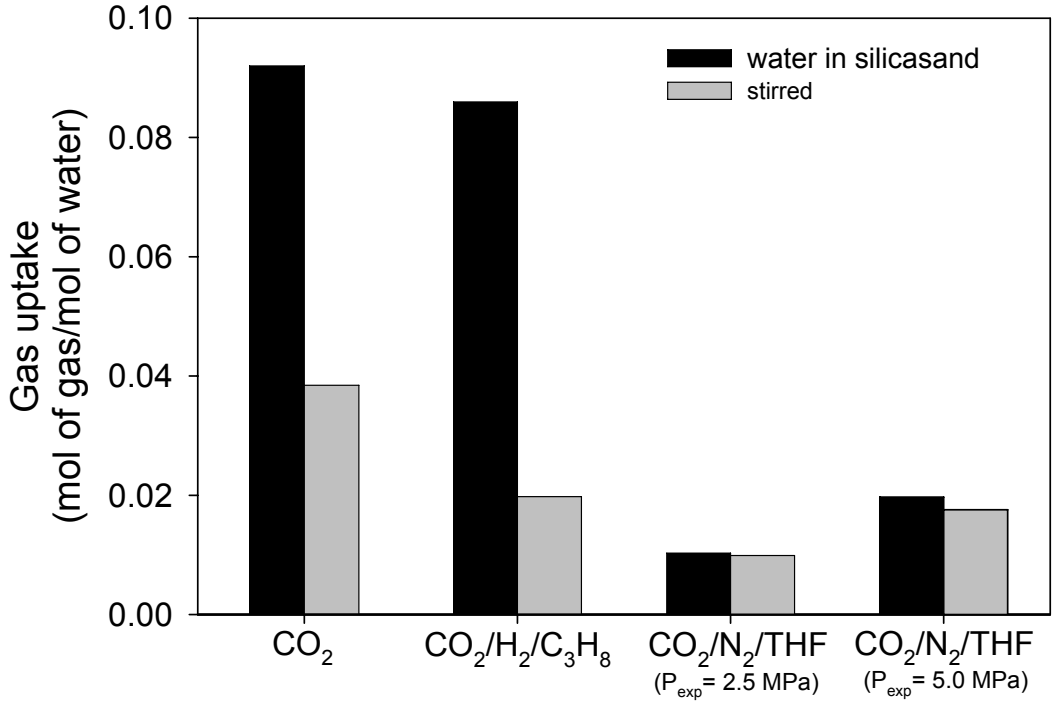

Figure 6-15: Comparison of gas consumption for all the three hydrocarbon containing systems. The experimental time is the same for both experiments carried for each system.

Dispersing liquid contents in a bed of silica sand particles offers a large contact area for gas/liquid and also the possibility of multiple nucleation sites occurring in the bed for hydrate formation that resulted in higher gas uptake and subsequently higher conversion of water to hydrates. In an actual industrial application, mode of contact of gas/water would depend on whether the process requires higher yields or better initial reaction rates. For all the experiments, the initial rate of hydrate formation was faster for the experiments carried out in a stirred tank system. However the final gas consumption and

hydrate yield was significantly higher for the experiments conducted by dispersing water in silica sand.

6.4. Conclusions

The gas uptake for hydrate formation in a bed of silica sand particles was compared with that in a stirred vessel where gas is contacted with bulk water. Hydrate formation experiments were carried out for three systems, CH_4/water, CH_4/C_3H_8/water and CH_4/C_2H_6/water, respectively that are of interest for natural gas transport and storage facilities. The gas uptake for all the three systems was found to be significantly higher for systems studied with water dispersed in silica sand. Subsequently it resulted in a higher percent conversion of water to hydrates. Similar experiments were studied for CO_2 and two CO_2 containing mixtures $CO_2/H_2/C_3H_8$, CO_2/N_2/1.0 mol% THF that are of interest for CO_2 capture via clathrate hydrate crystallization. The gas uptake was found to be significantly higher for the CO_2 and $CO_2/H_2/C_3H_8$ systems with water dispersed in silica sand. Dispersing liquid contents in a bed of silica sand particles offers a large contact area for gas/liquid and also the possibility of multiple nucleation sites occurring in the bed for hydrate formation. This results in higher gas uptake and subsequently higher conversion of water to hydrates.

Table 6-1: Summary of experimental conditions along with the induction time and percent conversion of water to hydrates achieved at the end of the experiment.

System	Experimental state	T [C]	Pexp [MPa]	Induction time [min]	End of experiment		Hydration Number	Water conversion to hydrate (mol %)
					Time [hr]	gas consumed [mol/mol of H_20]		
CH_4/water	Water + silica sand	4.0	8.0	7.3	34.7	0.1604	6.1	94.7
	Water	4.0	8.0	181.7	91.1	0.0197	6.1	12.0
	Water in stirred vessel	4.0	8.0	2.0	66.7	0.1249	6.1	74.1
CH_4/C_3H_8/water	Water + silica sand	4.0	4.6	8.7	43.0	0.0921	8.0	73.8
	Water in stirred vessel	4.0	4.6	1.0	96.6	0.0226	8.0	18.1
CH_4/C_2H_6/water	Water + silica sand	4.0	8.0	2.0	40.0	0.1220	6.2	75.6
	Water in stirred vessel	4.0	8.0	0.7	68.3	0.0972	6.2	60.3
CO_2/water	Water + silica sand	1.0	3.1	8.0	55.3	0.0920	6.5	59.8
	Water in stirred vessel	1.0	3.1	1.7	68.5	0.0389	6.5	25.3
$CO_2/H_2/C_3H_8$/water	Water + silica sand	1.0	5.1	244.7	42.8	0.0859	10.0	86.4
	Water in stirred vessel	1.0	5.1	1.7	42.8	0.0197	10.0	19.8
CO_2/N_2/THF (1.0mol %)	Water + silica sand	1.9	2.5	21.7	15.6	0.0103	5.7	8.8
	Water in stirred vessel	1.9	2.5	1.3	22.7	0.0102	5.7	8.7
	Water + silica sand	1.9	5.0	1.7	47.5	0.0197	5.7	16.9
	Water in stirred vessel	1.9	5.0	1.3	47.6	0.0176	5.7	15.0

* Pexp is the pressure at the start of the formation experiment.

6.5. References

Adeyemo, A., 2008. Post Combustion Capture of Carbon Dioxide through Hydrate Formation in Silica Gel Column, University of British Columbia, Vancouver.

Haligva, C., 2008. Natural Gas Recovery from Hydrates in a Silica Sand Matrix, University of British Columbia, Vancouver.

Kneafsey, T. J., Tomutsa, L., Moridis, G. J., Seol, Y., Freifeld, B. M., Taylor, C. E., and Gupta, A., 2007. Methane hydrate formation and dissociation in a partially saturated core-scale sand sample. J. Petrol. Sci. Eng. 56(1-3), 108-126.

Kumar, R., Linga, P., Ripmeester, J., A.;, and Englezos, P., 2008. A two-stage clathrate hydrate/membrane process for pre-combustion capture of carbon dioxide and hydrogen. Journal of Environmental Engineering, accepted September 2008.

Kumar, R., Moudrakovski, I., Ripmeester, J. A., and Englezos, P., 2009. Structural and compositional characterization of hydrates formed from CO_2/H_2 and $CO_2/H_2/C_3H_8$ gas mixtures in relation to simultaneous CO_2 capture and H_2 production. AIChE Journal, accepted for publication, January 13.

Kumar, R., Wu, H. J., and Englezos, P., 2006. Incipient hydrate phase equilibrium for gas mixtures containing hydrogen, carbon dioxide and propane. Fluid Phase Equilibria 244(2), 167-171.

Lee, H., Lee, J. W., Kim, D. Y., Park, J., Seo, Y. T., Zeng, H., Moudrakovski, I. L., Ratcliffe, C. I., and Ripmeester, J. A., 2005. Tuning clathrate hydrates for hydrogen storage. Nature 434(7034), 743-746.

Linga, P., Adeyemo, A., and Englezos, P., 2008. Medium-pressure clathrate hydrate/membrane hybrid process for postcombustion capture of carbon dioxide. Environmental Science & Technology 42(1), 315-320.

Linga, P., Haligva, C., Nam, S.-C., Ripmeester, J. A., and Englezos, P., 2009. Recovery of methane from hydrate formed in a variable volume bed of silica sand particles. AIChE Journal, In preparation.

Linga, P., Kumar, R., and Englezos, P., 2007. The clathrate hydrate process for post and pre-combustion capture of carbon dioxide. J. Haz. Mater. 149(3), 625-629.

McCallum, S. D., Riestenberg, D. E., Zatsepina, O. Y., and Phelps, T. J., 2007. Effect of vessel size on the formation of gas hydrates. J. Pet. Sci. Eng. 56(1-3), 54-64.

Mori, Y. H., 2003. Recent Advances in Hydrate-based Technologies for Natural gas Storage-A Review. Journal of Chemical Industry and Engineering 54, 1-17.

Seo, Y. T., Moudrakovski, I. L., Ripmeester, J. A., Lee, J. W., and Lee, H., 2005. Efficient recovery of CO_2 from flue gas by clathrate hydrate formation in porous silica gels. Environmental Science & Technology 39(7), 2315-2319.

Smith, J. M., Van Ness, H. C., and Abbott, M. M., 2001. Introduction to Chemical Engineering Thermodynamics, McGraw-Hill, Inc., New York.

Tulk, C. A., Ripmeester, J. A., and Klug, D. D., 2000. The application of Raman spectroscopy to the study of gas hydrates. Gas Hydrates: Challenges for the Future 912, 859-872.

Udachin, K. A., Ratcliffe, C. I., and Ripmeester, J. A., 2001. Structure, composition, and thermal expansion of CO_2 hydrate from single crystal X-ray diffraction measurements. Journal of Physical Chemistry B 105(19), 4200-4204.

7. CONCLUSIONS, CONTRIBUTION TO KNOWLEDGE AND RECOMMENDATIONS FOR FUTURE WORK

7.1. Conclusions

One of the new promising methods for separating CO_2 from flue gas or fuel gas is through clathrate or gas hydrate formation (Englezos and Lee, 2005; Han et al., 2007; Kang and Lee, 2000; Klara and Srivastava, 2002). Post combustion capture of CO_2 from a flue gas mixture via hydrate crystallization has been investigated for different operating conditions. Gas hydrate formation experiments were carried out in a crystallizer ($323cm^3$) operating in a semi-batch mode for a CO_2 (17%)/N_2 (83%) gas mixture (Linga et al., 2007a). Kinetics experiments coupled with compositional analysis using a GC revealed that CO_2 is preferentially incorporated into the hydrate crystal.

Two metrics, CO_2 recovery and separation factor were defined based on the hydrate separation experiments in order to asses the separation efficiency of the CO_2 capture process (Linga et al., 2007b). CO_2 recovery was found to be 36.7 to 42.1 % in one stage at 11.0 and 10.0 MPa respectively. Hybrid hydrate-membrane processes were proposed for the post combustion capture of carbon dioxide involving three stages of hydrate formation resulting in a 99.0% CO_2 stream (Linga et al., 2007b). Because the operating pressures are high the associated compression costs are significant. Tetrahydrofuran (THF) is known to form hydrates and can reduce the hydrate formation pressure for the flue gas mixture (Kang and Lee, 2000). The thesis also examined the impact of adding small amounts of THF on hydrate formation from the CO_2/N_2 mixture (Linga et al., 2008). It was found that, the presence of THF reduces the operating pressure and induction time

significantly without compromising the separation efficiency but also resulted in lower gas consumption and rate of hydrate growth. The new thermodynamic, kinetic and separation efficiency data enabled the creation of a conceptual process which consists of three hydrate formation/decomposition stages operating at 273.75 K and at a pressure of 2.5 MPa coupled with a membrane separation stage to tackle a CO_2-lean stream. Nearly 50 % of CO_2 is recovered in the first two hydrate stages and 37 % in the third one (Linga et al., 2008). The energy penalty of the hydrate process associated with the compression of the flue gas was estimated. However stirring power costs were not taken into account.

A new hydrate formation apparatus equipped with a modular-type crystallizer having a volume of 1,899.5 cm^3 was presented. The gas uptake and the CO_2 recovery were found to be significantly higher in the apparatus compared to the lab-scale apparatus. Thus, it is possible to scale up the separation process of CO_2 capture from a flue gas mixture. The new apparatus can be employed to test several other technological applications of gas hydrates like natural gas storage and transportation and pre-combustion capture of CO_2. Even though the new apparatus improves the mass transfer resistance, the energy costs associated with the stirring makes the process energy intensive.

Finally, the kinetics of hydrate formation for six different gas/mixtures that are of interest in several technological applications of gas hydrates were studied in a crystallizer where gas is contacted with water dispersed in a silica sand matrix. This arrangement is desirable as it does not require mechanical stirring. The gas uptake and water conversion to hydrate were found to be significantly higher compared to the results obtained in the same scale stirred vessel described in chapter 2.

7.2. Contribution to the knowledge

This thesis provides new insights on a new method for separation of carbon dioxide from a flue gas mixture via hydrate formation. The contributions to knowledge are as follows:

1. Our findings were the first to validate through kinetic gas uptake measurements the applicability of gas hydrates process to separate CO_2 from flue gas mixtures by providing information on the time dependant compositional changes during the kinetic experiment.
2. We proposed two metrics, the CO_2 recovery and the separation factor to determine the efficiency of the separation process.
3. Hybrid hydrate-membrane processes is proposed for post combustion capture of carbon dioxide involving three stages of hydrate formation resulting in a 99.0% CO_2 stream.
4. The presence of THF significantly reduces the operating pressures for hydrate formation and renders the separation process more attractive for an industrial scale. One mol % THF was determined to be the optimum concentration for the kinetic experiments conducted in a stirred tank crystallizer. Nearly 50 % of CO_2 is recovered in the first two hydrate stages and 37 % in the third one (all the three stages operating at 2.5 MPa & 273.7 K).
5. The addition of 1.0 mol% THF reduces the compression costs for the first stage of hydrate formation by 29.3% compared to the high pressure process with no additives.

6. A new hydrate formation apparatus was designed and set up to demonstrate the hydrate based separation process at a larger scale with better gas/liquid contacting. The results showed a significant increase in the gas uptake on a water free basis and also an increase in the CO_2 recovery.
7. When gas is contacted with water dispersed in a silica sand matrix the gas uptake and water conversion to hydrate were found to be significantly higher compared to the results obtained in the same scale stirred vessel described in chapter 2.

7.3. Recommendations for future work

Based on the forgoing conclusions, a number of recommendations can be made as to how this work may be improved and extended in future investigations.

1. Demonstrate the hydrate based separation process for post combustion capture in a pilot plant scale. Such a pilot plant study would enable to study the cost analysis of the hydrate based separation process for the separation of CO_2 from flue gas mixture which can be compared with more mature processes like amine based separation.
2. Establish how the hydrate process can operate in a continuous manner. Our experiments showed that the hydrate process can definitely be operated in a semi-batch manner. We believe, the hydrate process can also be operated in a continuous manner, if the hydrate slurry could be replaced with fresh THF solution.

3. Carry out molecular level studies like ^{1}H NMR micro imaging experiments in order to understand the mechanism of hydrate formation for systems involving water in the presence of silica sand.
4. Review and attempt alternative crystallizer designs such as fluidizing silica gel particles in the flue gas stream or circulating the liquid contents and spraying through nozzles.
5. Employ an alternative rotor arrangement in the new apparatus described in chapter 5 in order to be able to operate at stirrer speeds higher than 400 rpm.

7.4. References

Englezos, P., and Lee, J. D., 2005. Gas hydrates: A cleaner source of energy and opportunity for innovative technologies. Korean Journal of Chemical Engineering 22(5), 671-681.

Han, F. X. X., Lindner, J. S., and Wang, C. J., 2007. Making carbon sequestration a paying proposition. Naturwissenschaften 94(3), 170-182.

Kang, S. P., and Lee, H., 2000. Recovery of CO_2 from flue gas using gas hydrate: Thermodynamic verification through phase equilibrium measurements. Environmental Science & Technology 34(20), 4397-4400.

Klara, S. M., and Srivastava, R. D., 2002. US DOE integrated collaborative technology development program for CO2 separation and capture. Environmental Progress 21(4), 247-253.

Linga, P., Adeyemo, A., and Englezos, P., 2008. Medium-Pressure Clathrate Hydrate/Membrane Hybrid Process for Postcombustion Capture of Carbon Dioxide. Environmental Science & Technology 42(1), 315-320.

Linga, P., Kumar, R., and Englezos, P., 2007a. Gas hydrate formation from hydrogen/carbon dioxide and nitrogen/carbon dioxide gas mixtures. Chemical Engineering Science 62(16), 4268-4276.

Linga, P., Kumar, R., and Englezos, P., 2007b. The clathrate hydrate process for post and pre-combustion capture of carbon dioxide. Journal of Hazardous Materials 149(3), 625-629.

APPENDIX A

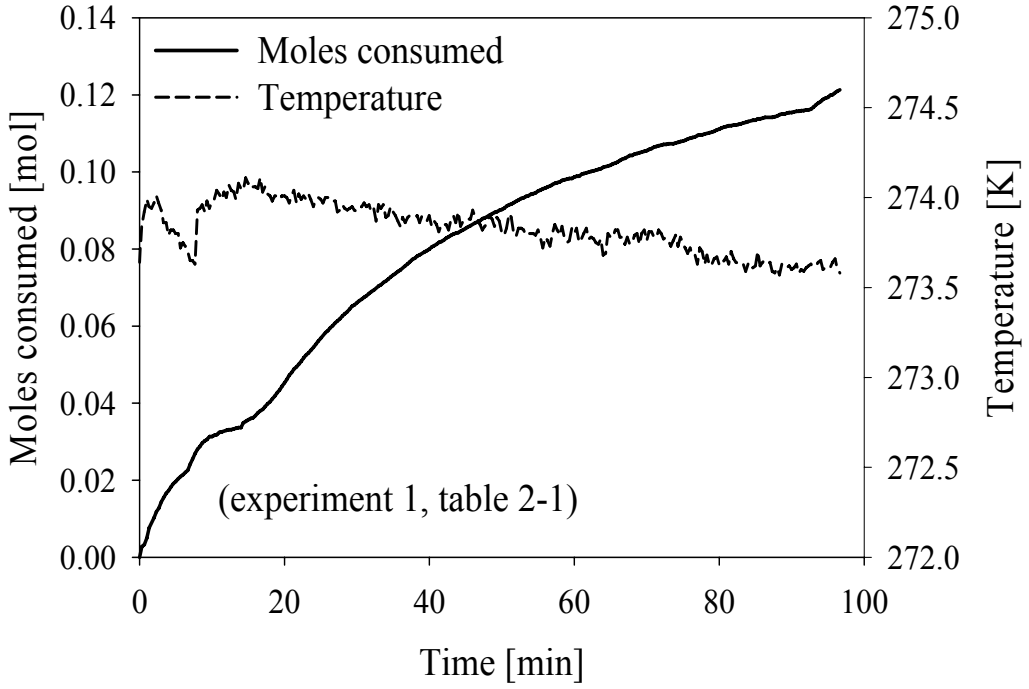

Figure A-1. Gas uptake measurement curve with temperature profile.

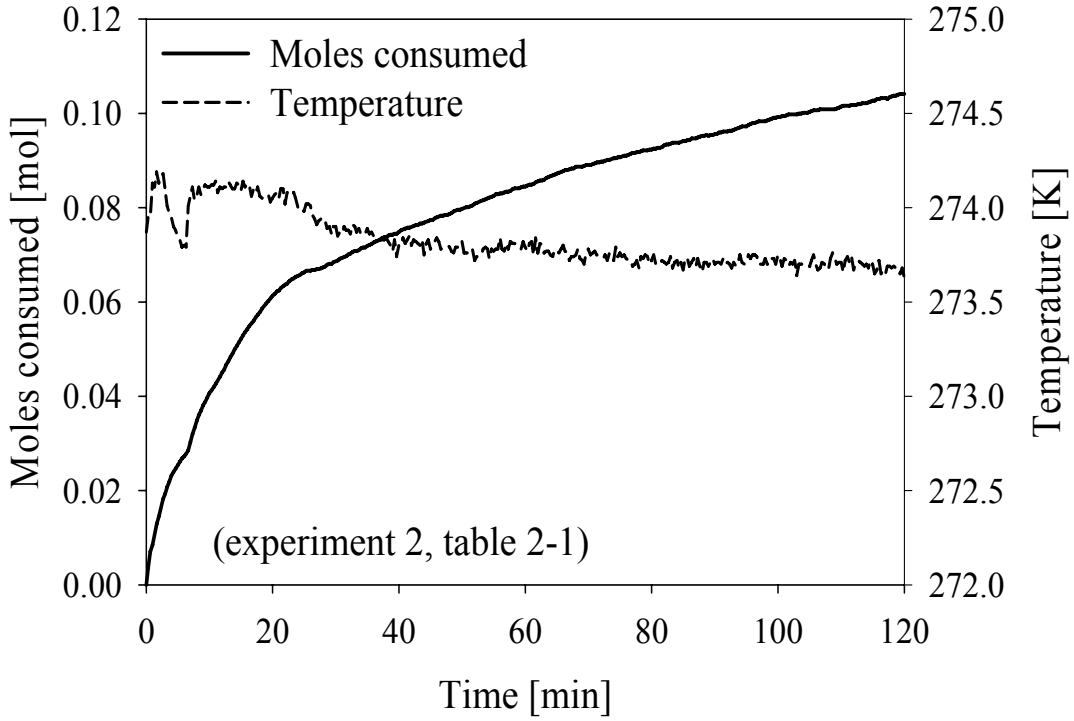

Figure A-2. Gas uptake measurement curve with temperature profile.

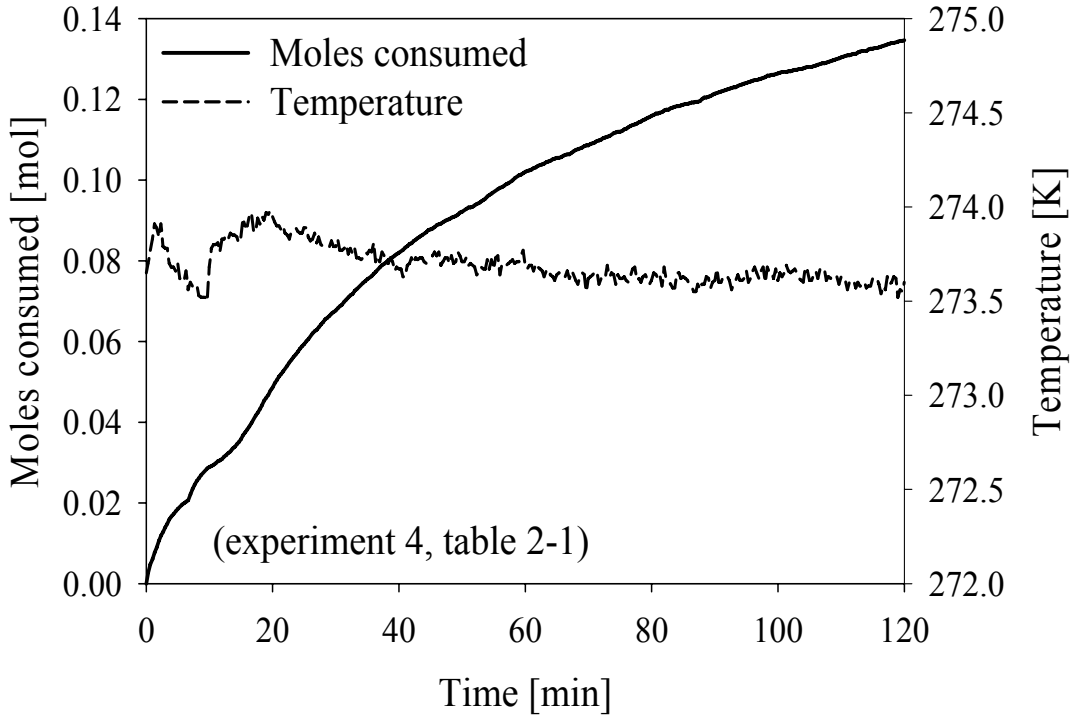

Figure A-3. Gas uptake measurement curve with temperature profile.

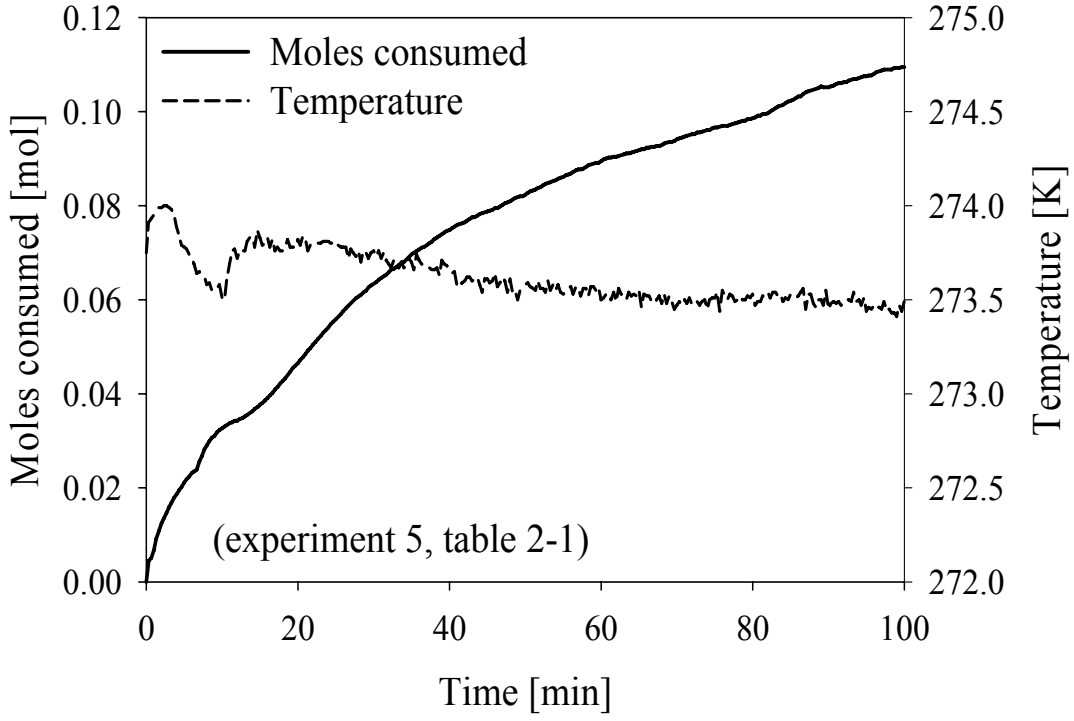

Figure A-4. Gas uptake measurement curve with temperature profile.

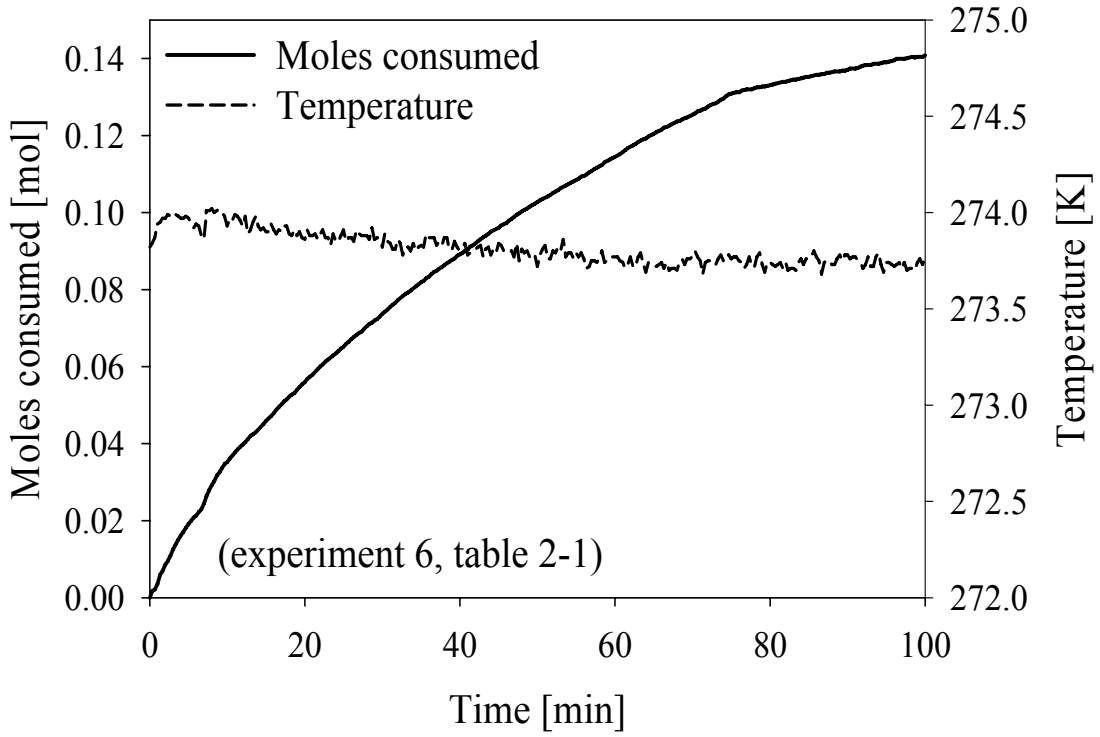

Figure A-5. Gas uptake measurement curve with temperature profile.

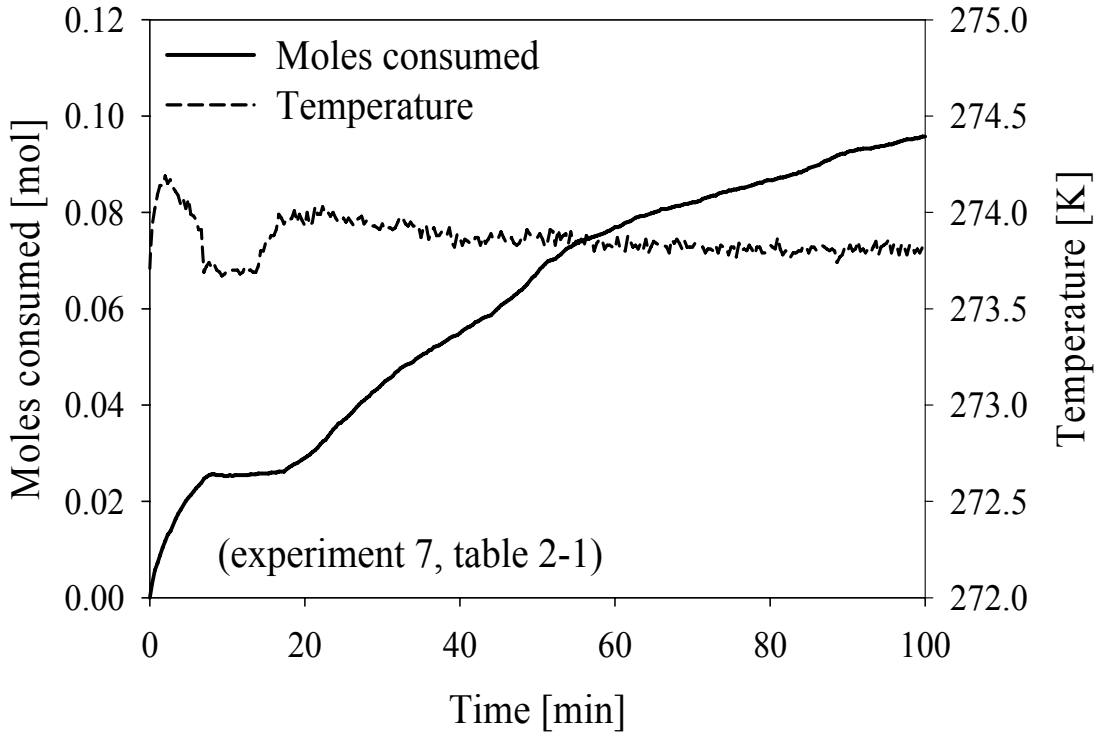

Figure A-6. Gas uptake measurement curve with temperature profile.

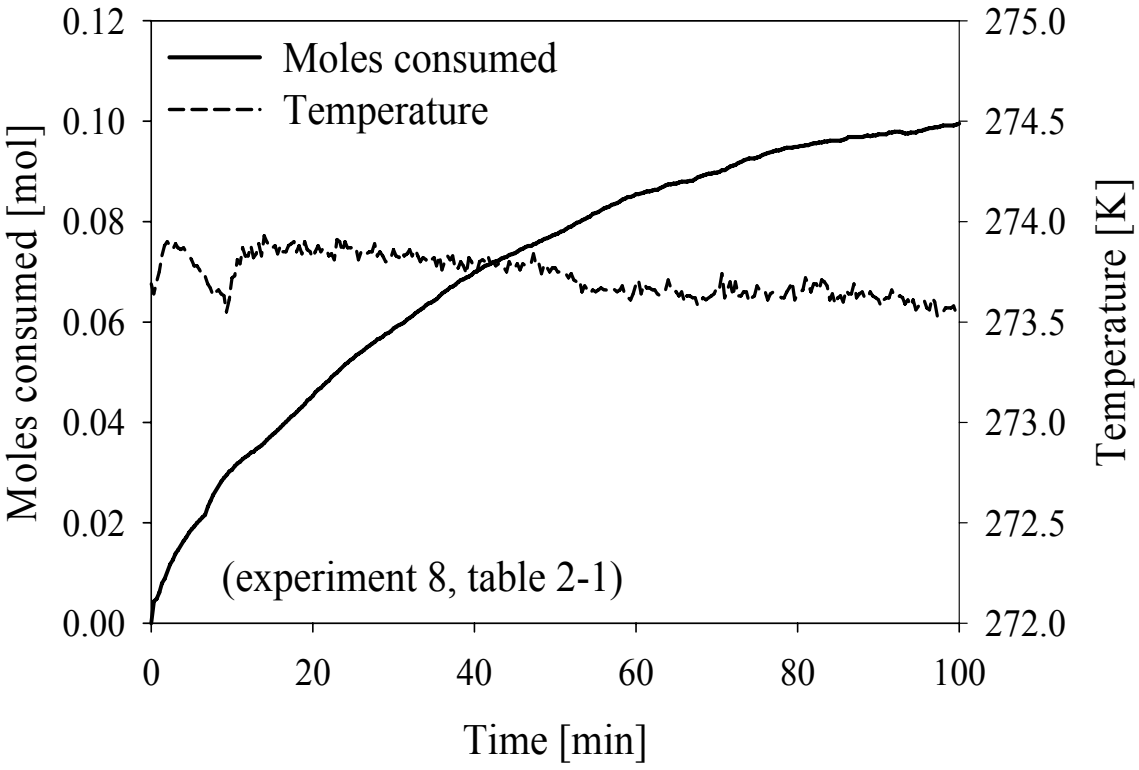

Figure A-7. Gas uptake measurement curve with temperature profile.

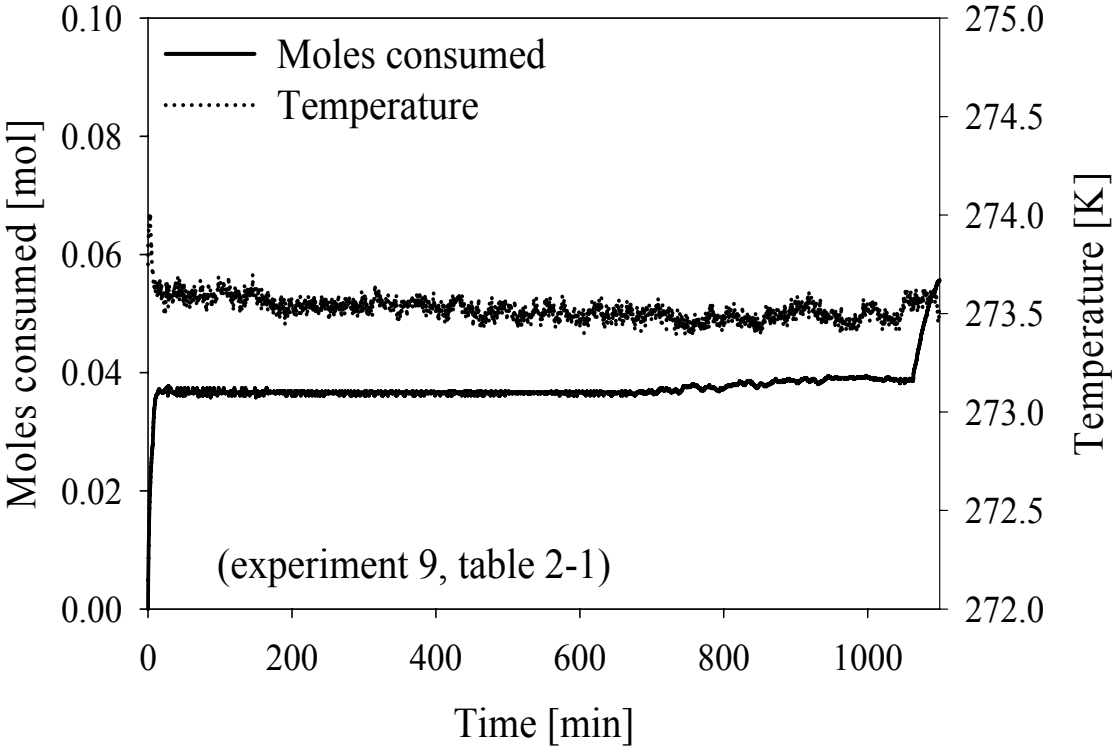

Figure A-8. Gas uptake measurement curve with temperature profile.

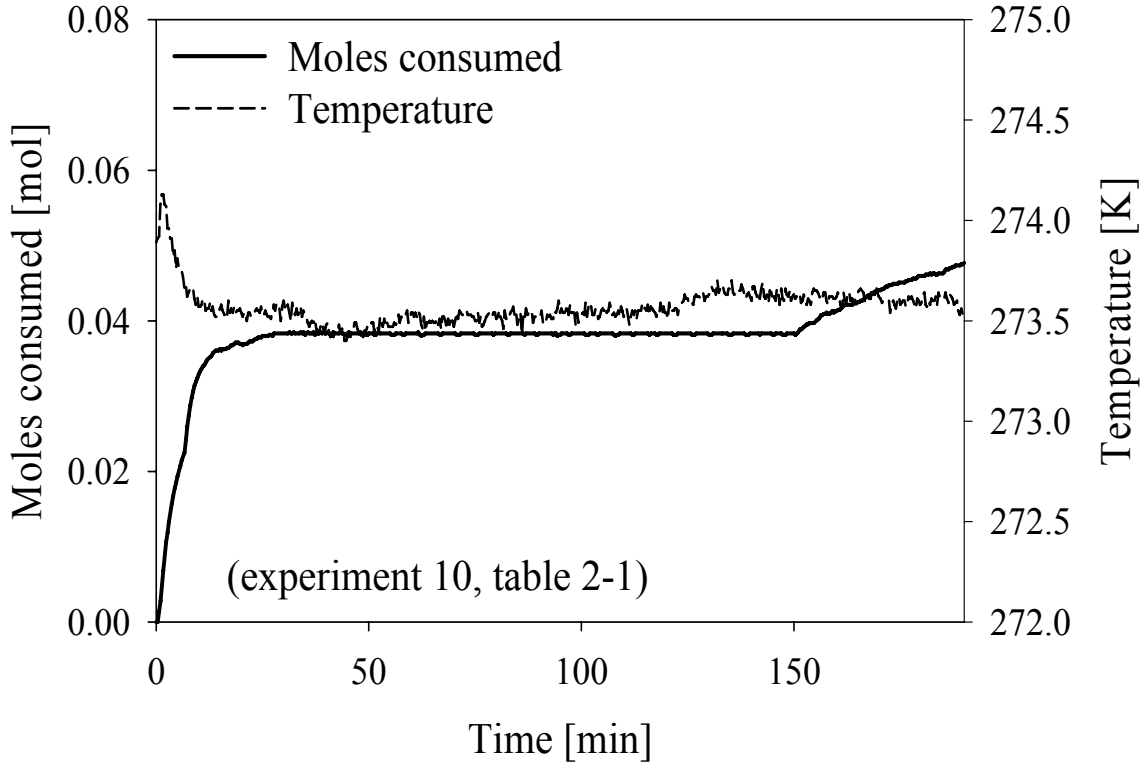

Figure A-9. Gas uptake measurement curve with temperature profile.

Table A-1. The standard errors and the R^2 values for the calculated rates reported in Table 2-1.

Exp No	Rate (mol/min)	Standard error for rate	R^2
1	0.002	0.000019	0.9977
2	0.002	0.000049	0.9614
3	0.0018	0.000022	0.9913
4	0.0021	0.000019	0.9977
5	0.0017	0.000016	0.9947
6	0.0021	0.000011	0.9980
7	0.0014	0.000009	0.9957
8	0.0015	0.000008	0.9981
9	0.0005	0.000005	0.9958
10	0.0003	0.000003	0.9898
11	N/A	N/A	N/A
12	N/A	N/A	N/A

APPENDIX B

Gas compression calculations for the separation of CO_2 from flue gas mixture from a power plant.

The mass flow rates used for the calculations were obtained from the MIT report, "the future of coal" available at http://web.mit.edu/coal/. Details of the power plant emissions are shown in the figure below,

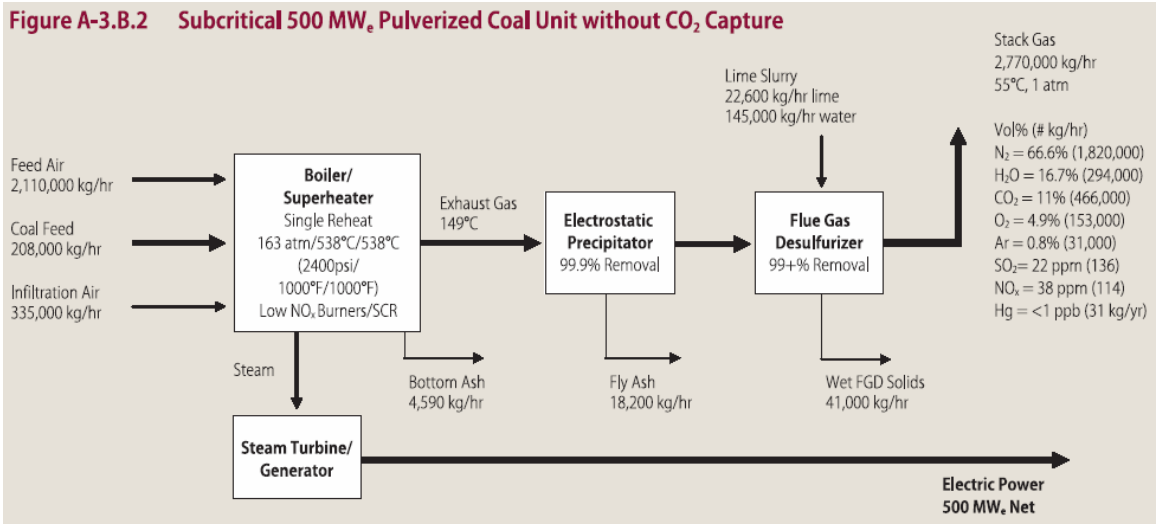

Figure B-1. A Subcritical 500 MW_e Pulverized Coal Unit without CO_2 capture, Courtesy of Massachusetts Institute of Technology's report on Future of Coal (MIT, 2007).

Assuming that H_2O can be removed by condensation, if we add up CO_2, N_2 and O_2, the flow rate is 2,439,000 kg/hr. The molar percent is 74.6% N_2, 19.0% CO_2 and 6.4 % O_2.

The operating pressure of the crystallizer is 10.0 MPa. Pout/Pin = 10.0/0.1 = 100, we need four compression stages, heuristic from Seider et al. (2004).

According to Biegler et al. (1997), the work required is given by,

$$W = \mu \times N \times \left(\frac{\gamma}{\gamma - 1} \right) \times R \times T_0 \times \left[\left(\frac{P_N}{P_0} \right)^{\frac{\gamma-1}{\gamma N}} - 1 \right] \quad \text{(B1)}$$

where,

μ = molar flow rate = 80,372 kmol/hr

N = 4 (Number of compression stages)

P_N = 10 MPa

P_0 = 0.1 MPa

γ = Cp/Cv = 1.4

R = 8.314 kJ/kmol K

T_0 = 274 K

The theoretical value of W was determined from equation B1 to be 277 MW. Assuming a compressor efficiency of 0.8 and motor efficiency of 0.9, the W_{real} was determined to be 385 MW.

References

Biegler, L. T., Grossmann, I. E., and Westerberg, A. W., 1997. Systematic Methods of Chemical Process Design, Prentice Hall PTR, New Jersey.

Seider, W. D., Seader, J. D., and Lewin, D. R., 2004. Product and Process Design Principles: Synthesis, Analysis, and Evaluation, Wiley.

MIT. (2007). "The Future of Coal." Available from: http://web.mit.edu/coal/.

APPENDIX C

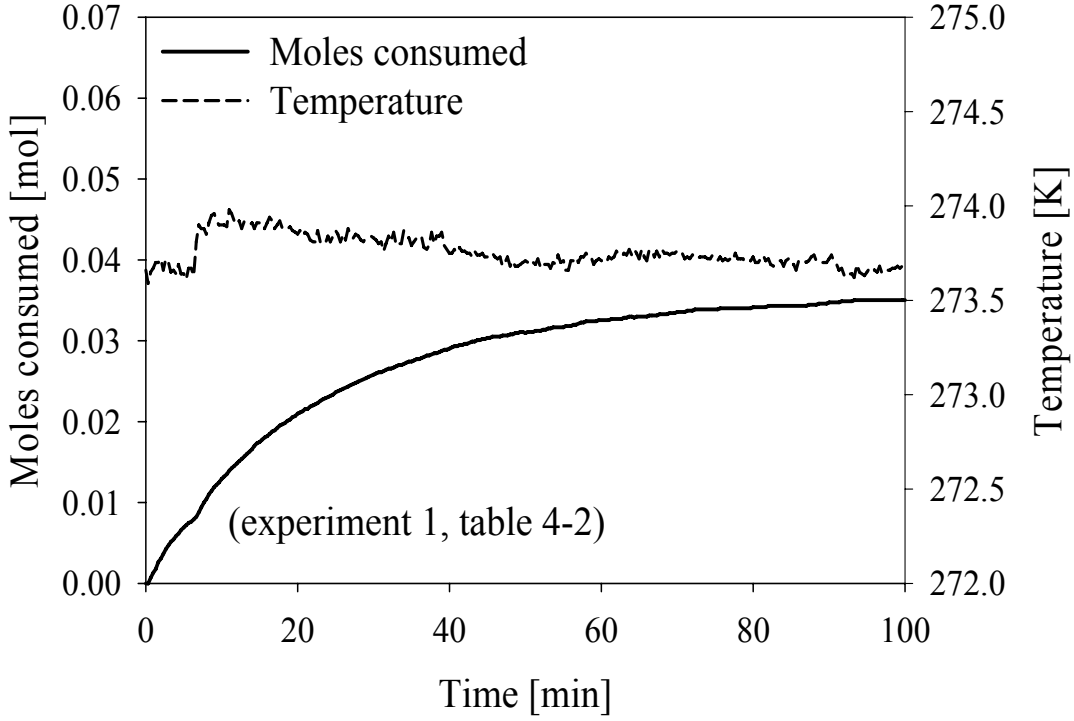

Figure C-1. Gas uptake measurement curve along with temperature profile**.**

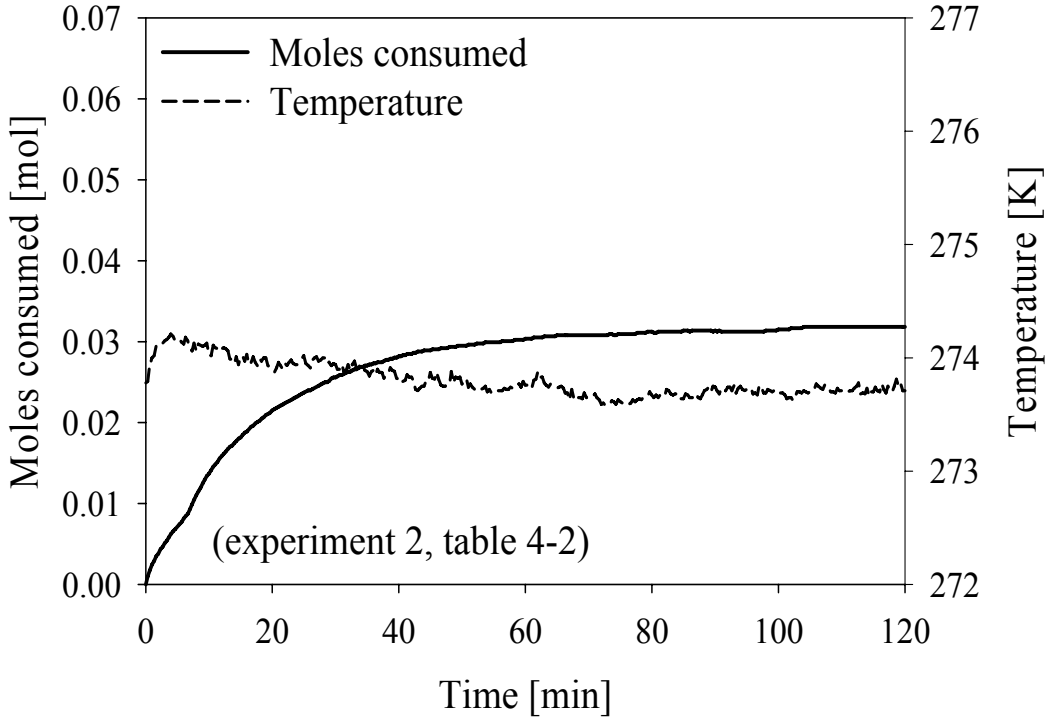

Figure C-2. Gas uptake measurement curve along with temperature profile.

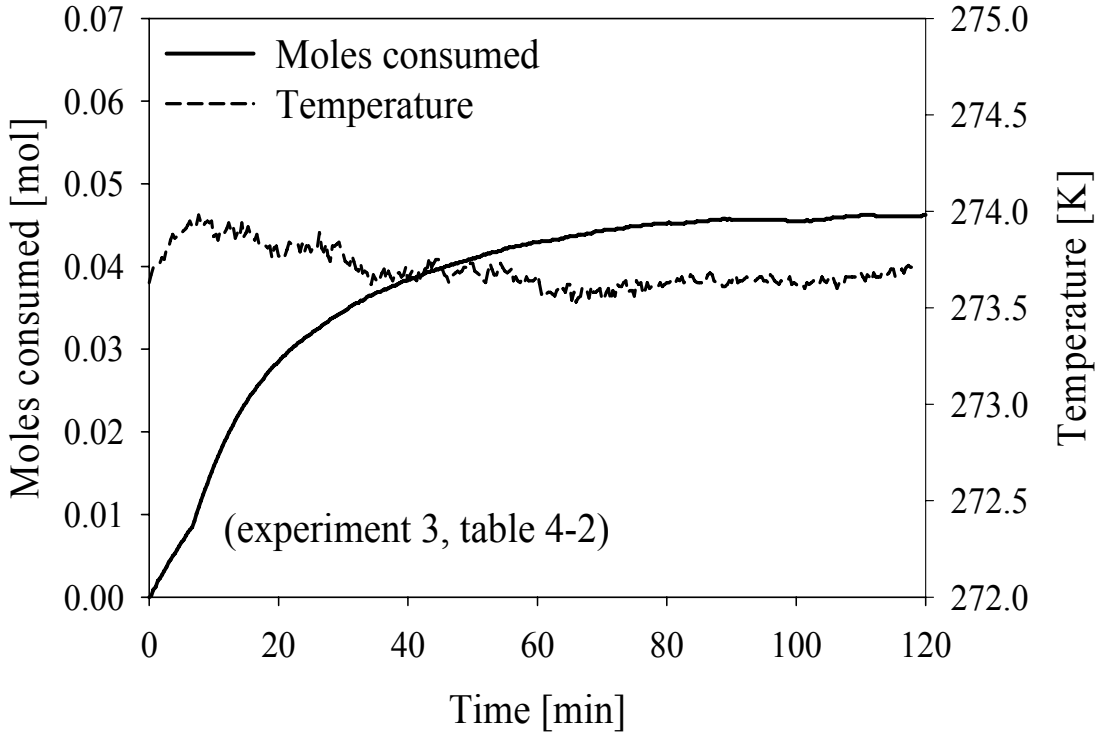

Figure C-3. Gas uptake measurement curve along with temperature profile.

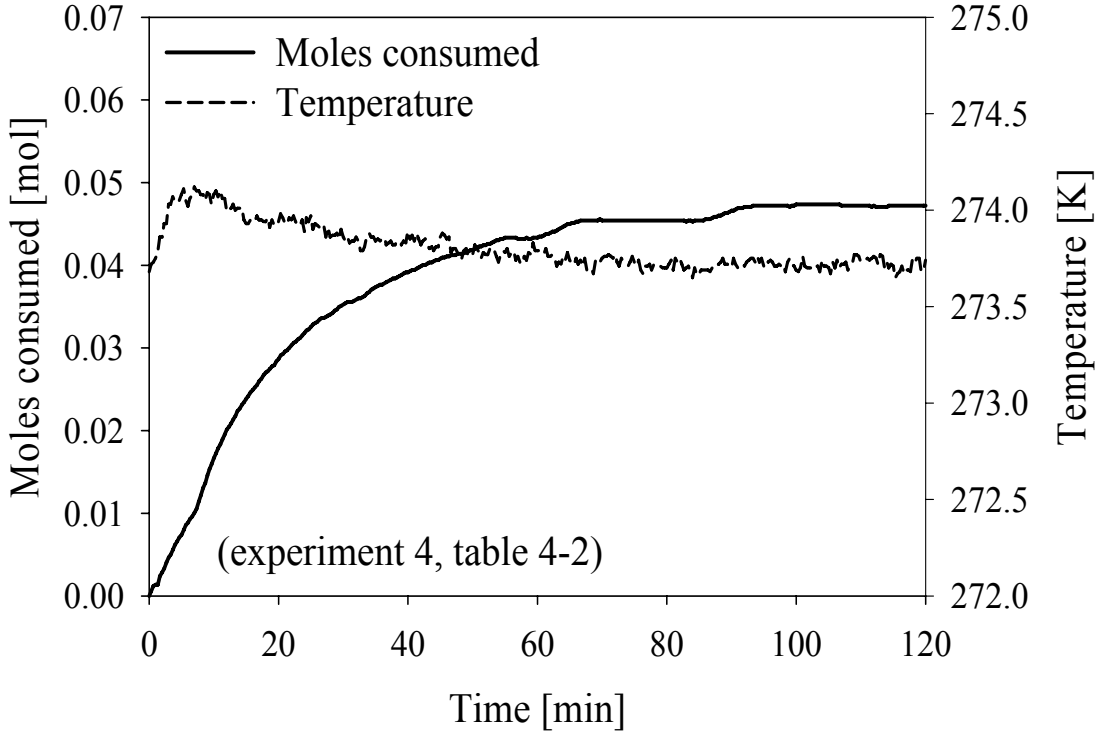

Figure C-4. Gas uptake measurement curve along with temperature profile.

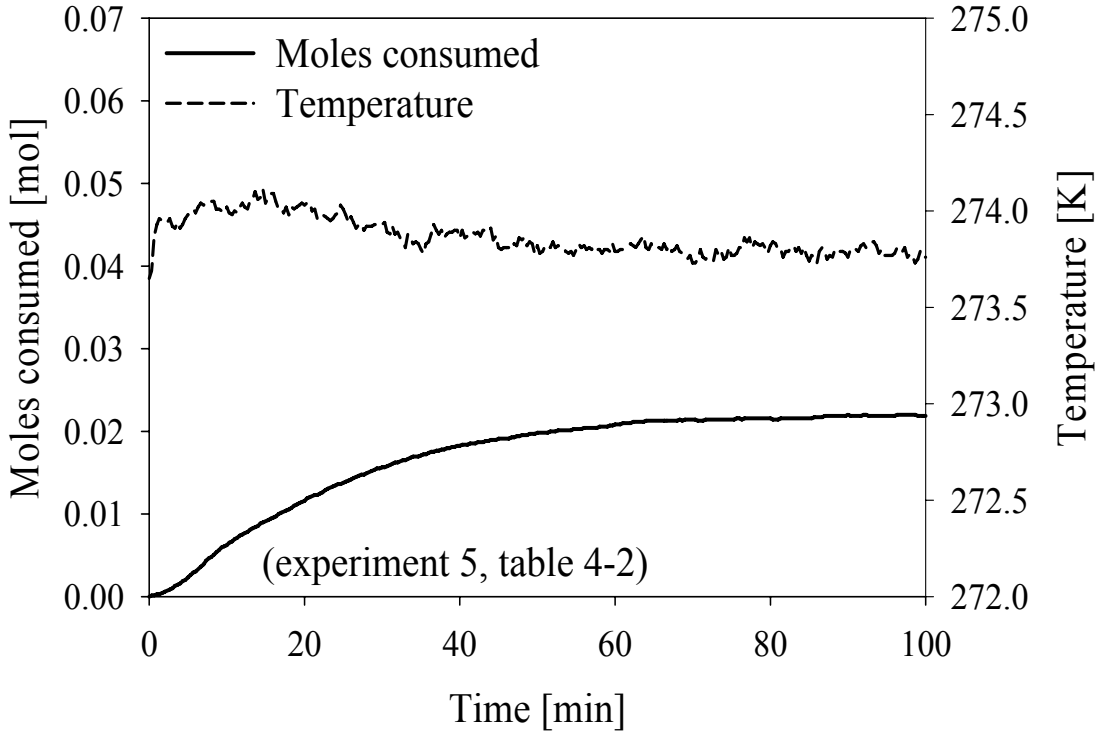

Figure C-5. Gas uptake measurement curve along with temperature profile.

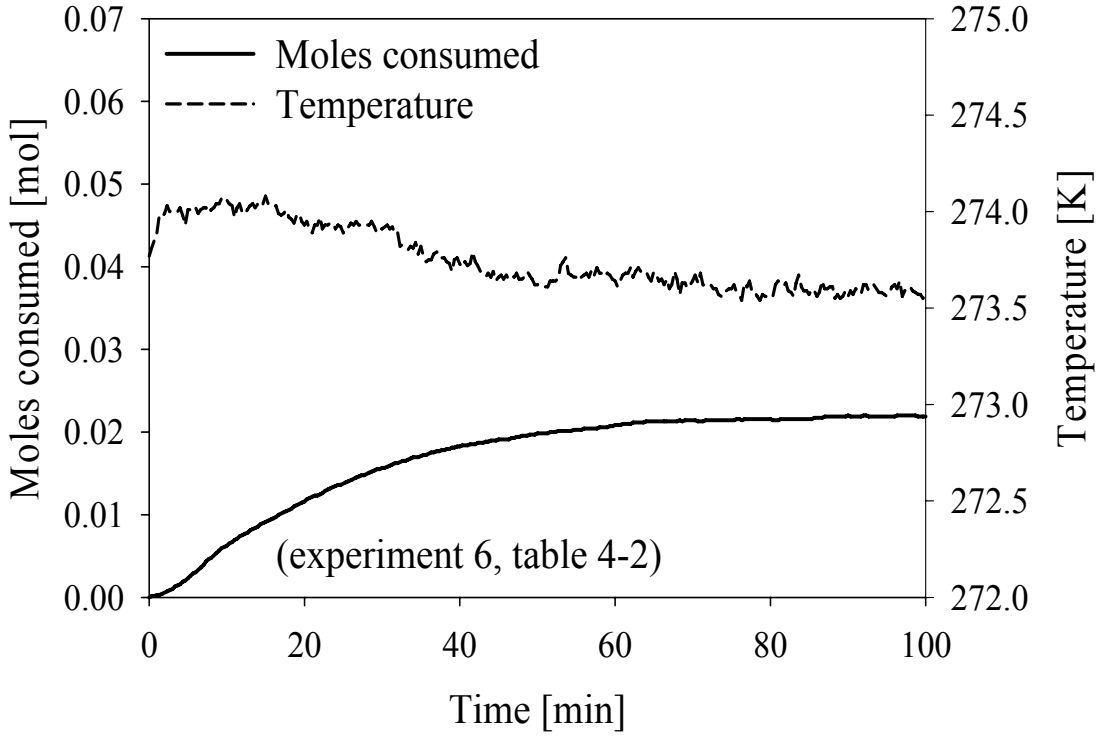

Figure C-6. Gas uptake measurement curve along with temperature profile.

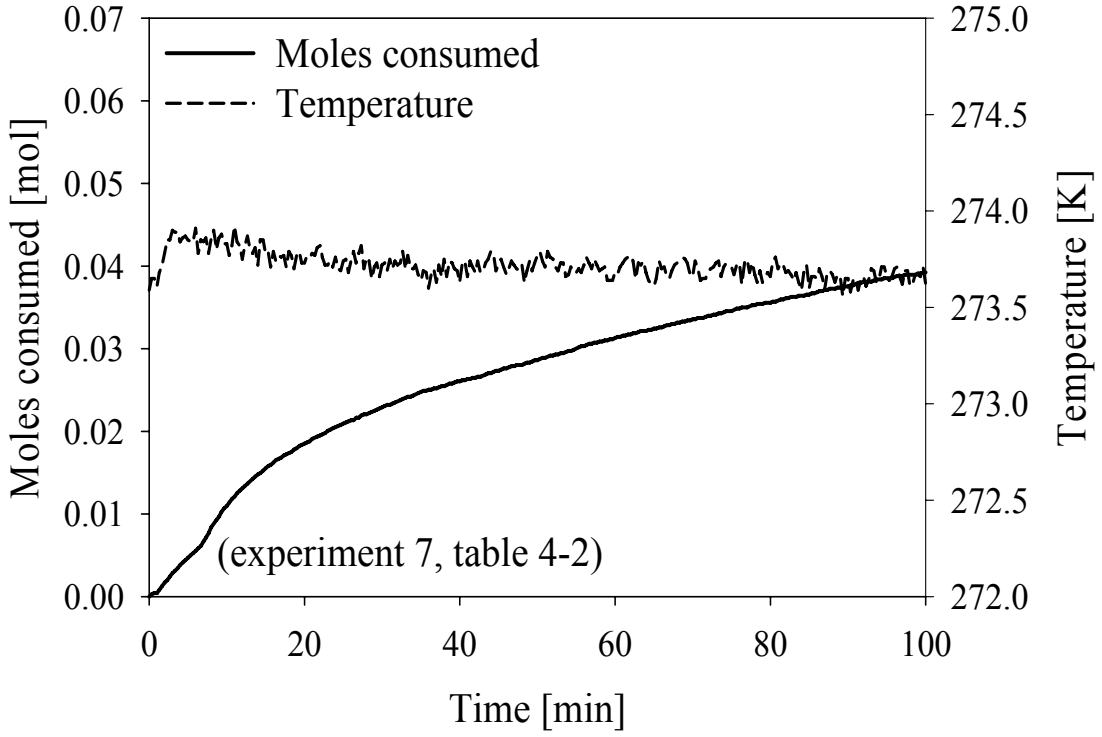

Figure C-7. Gas uptake measurement curve along with temperature profile.

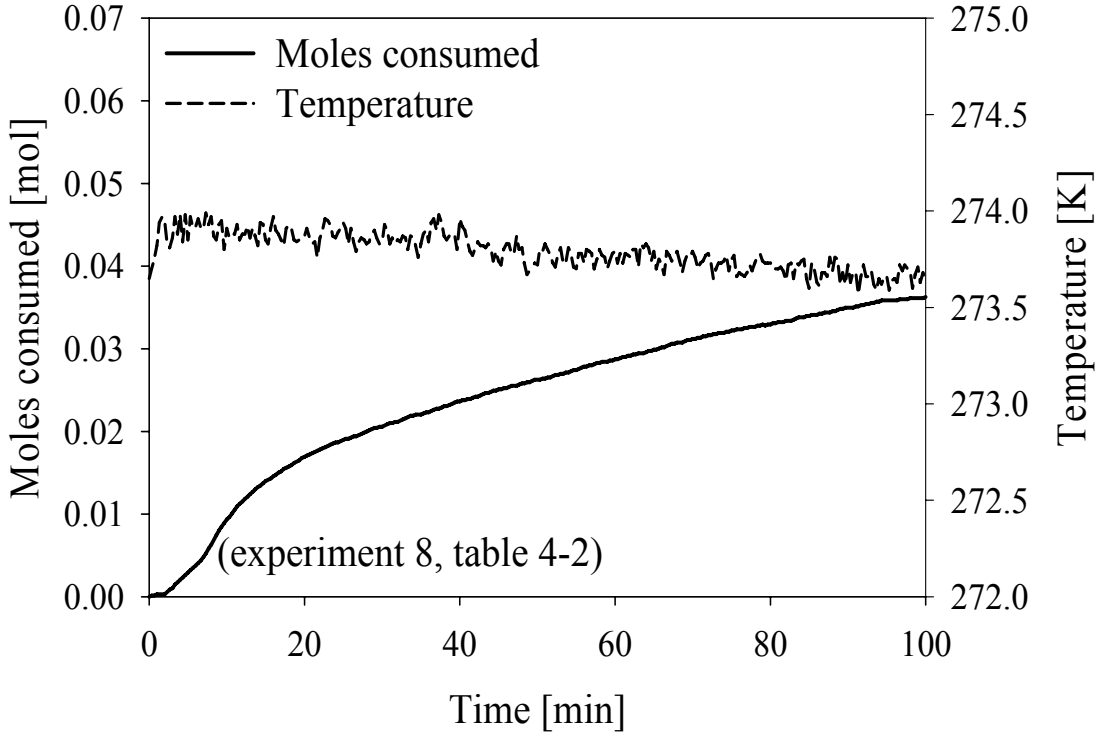

Figure C-8. Gas uptake measurement curve along with temperature profile.

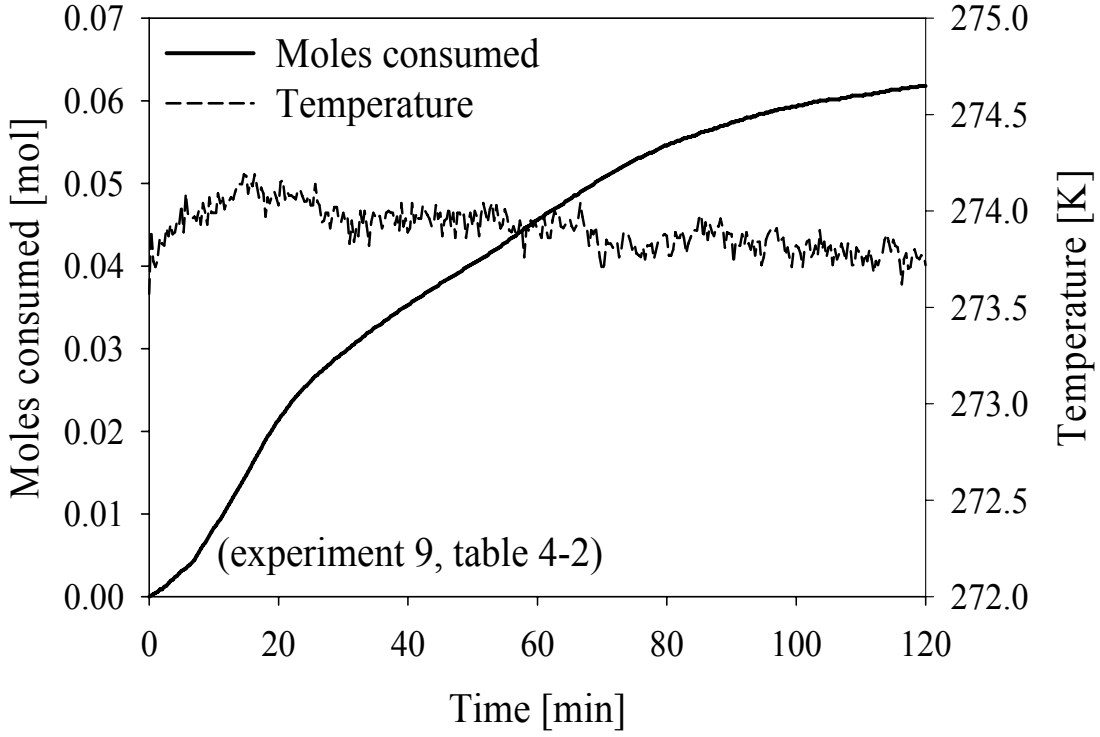

Figure C-9. Gas uptake measurement curve along with temperature profile.

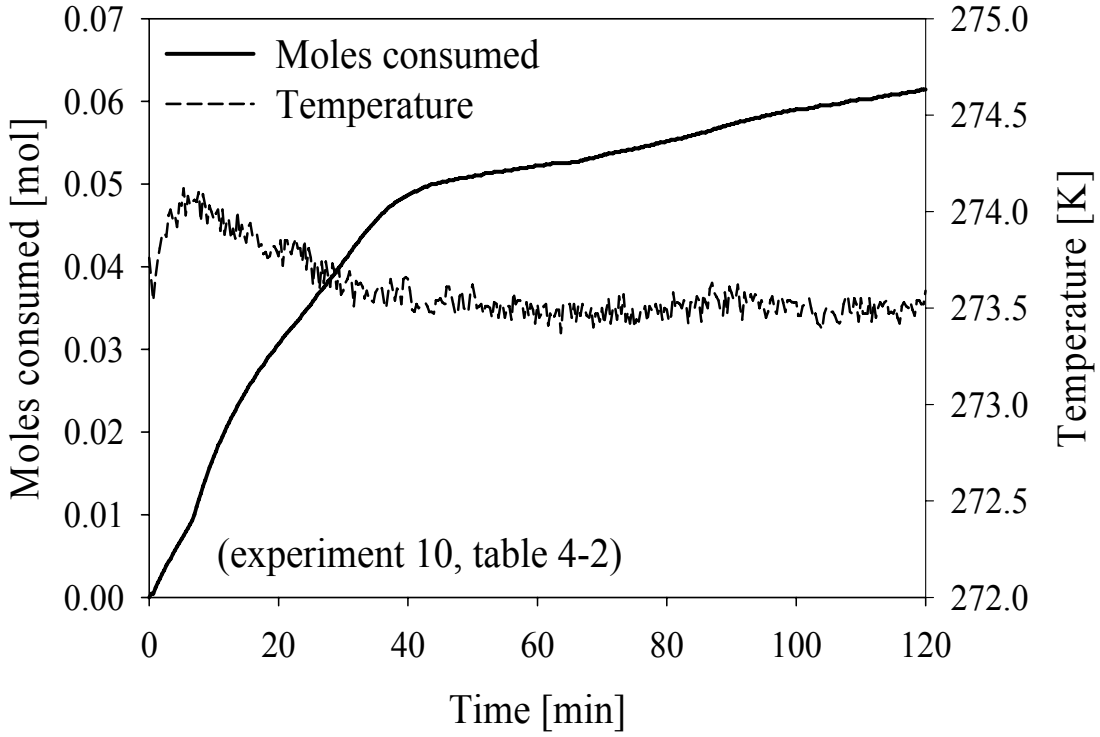

Figure C-10. Gas uptake measurement curve along with temperature profile.

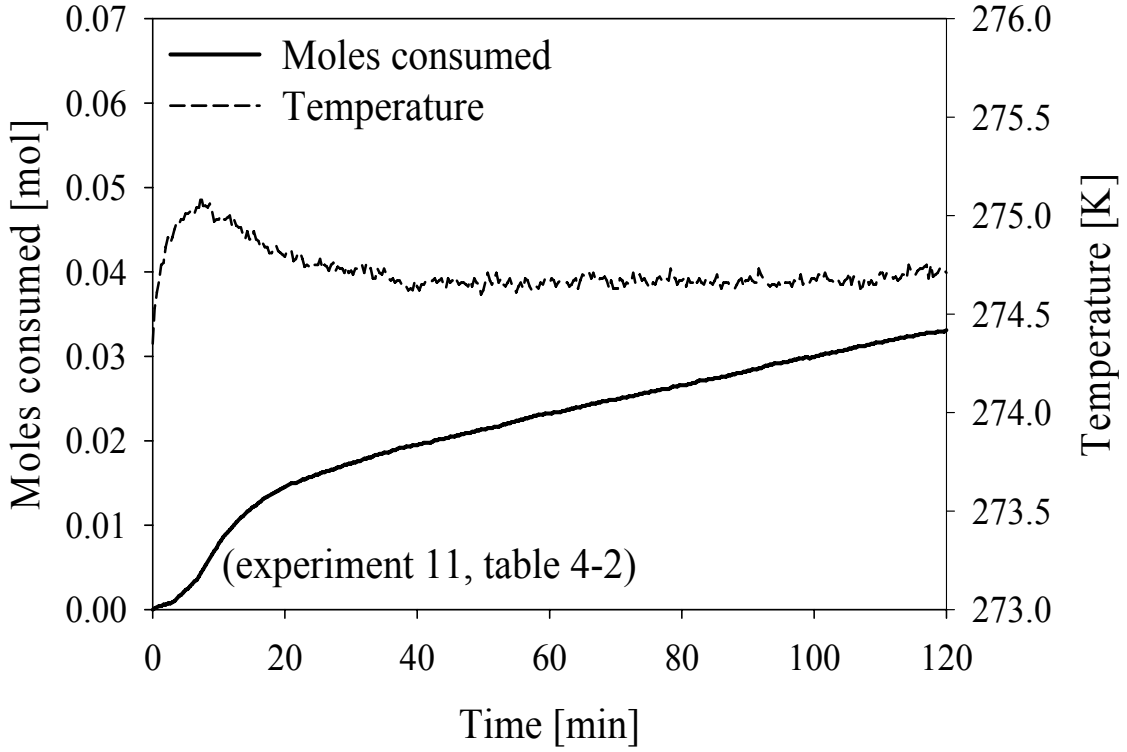

Figure C-11. Gas uptake measurement curve along with temperature profile.

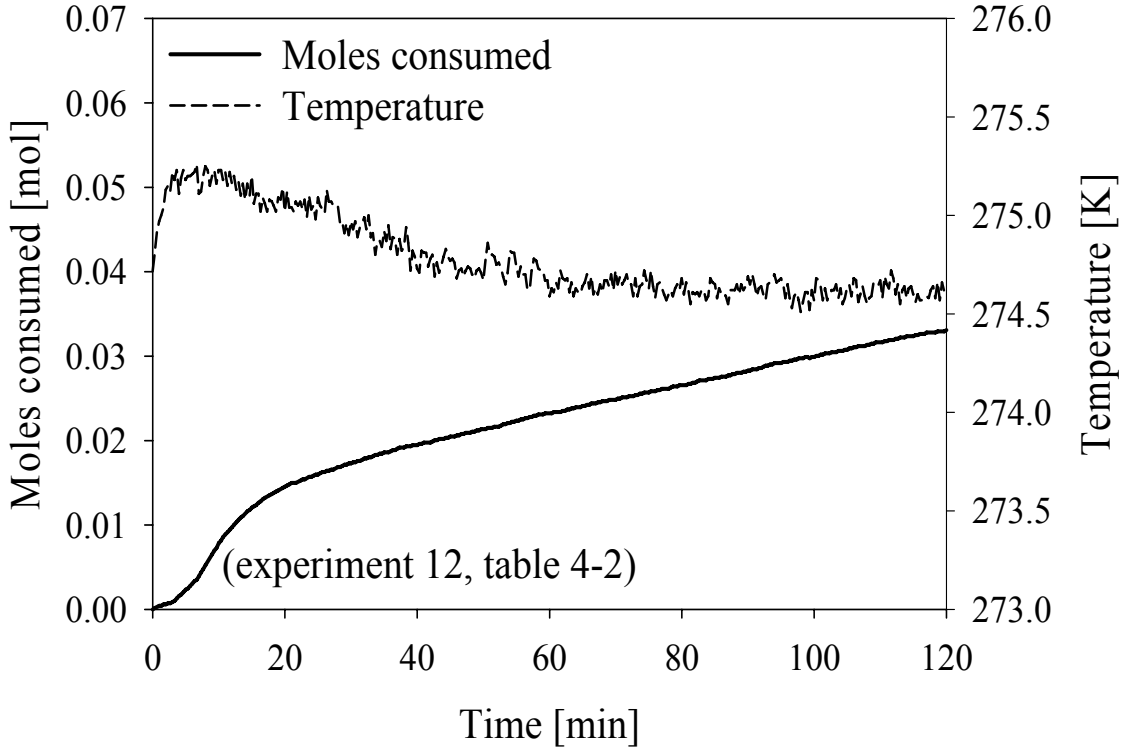

Figure C-12. Gas uptake measurement curve along with temperature profile.

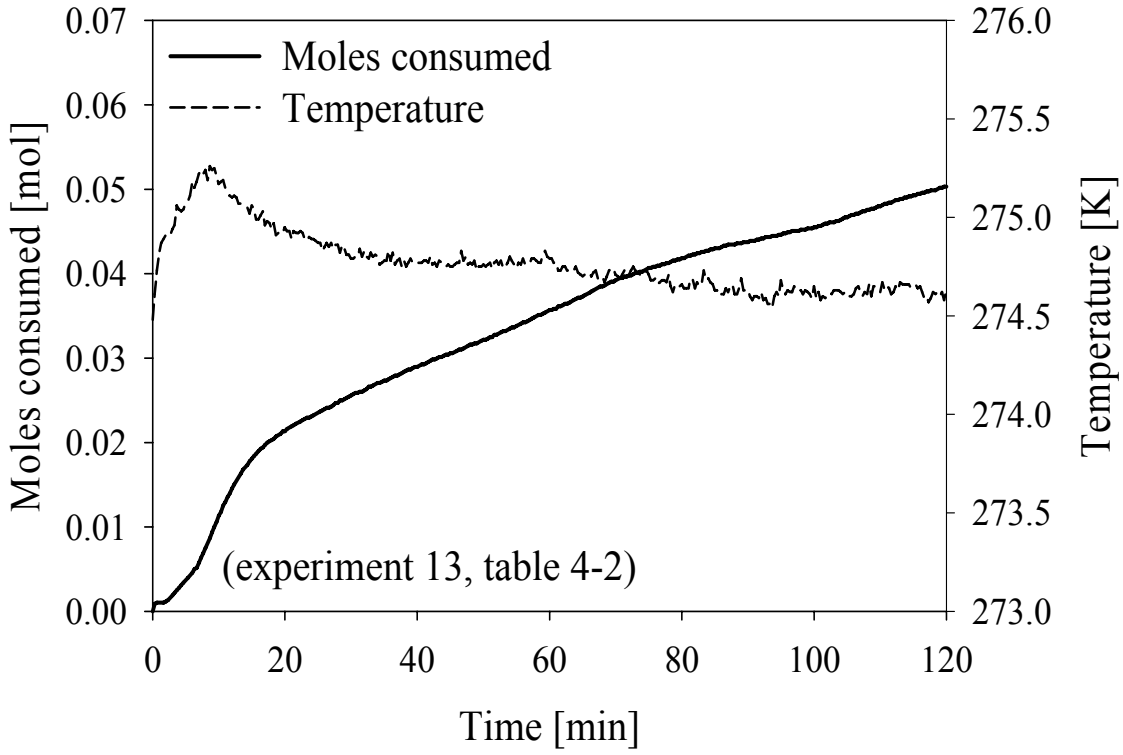

Figure C-13. Gas uptake measurement curve along with temperature profile.

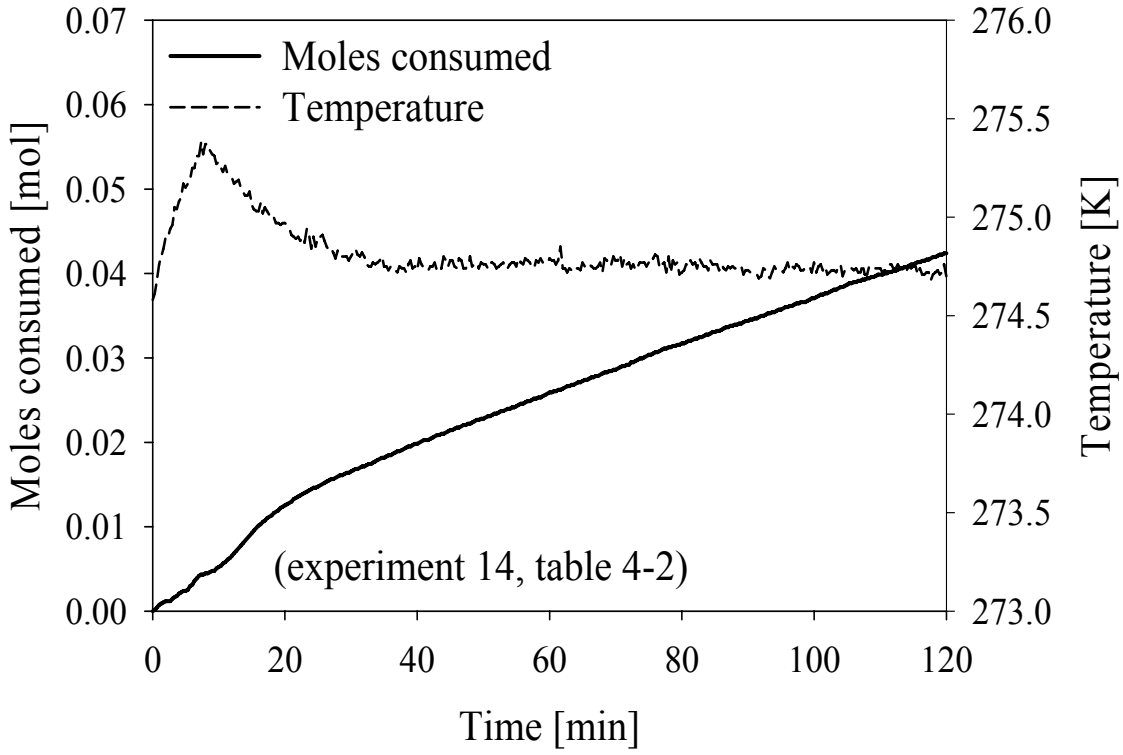

Figure C-14. Gas uptake measurement curve along with temperature profile.

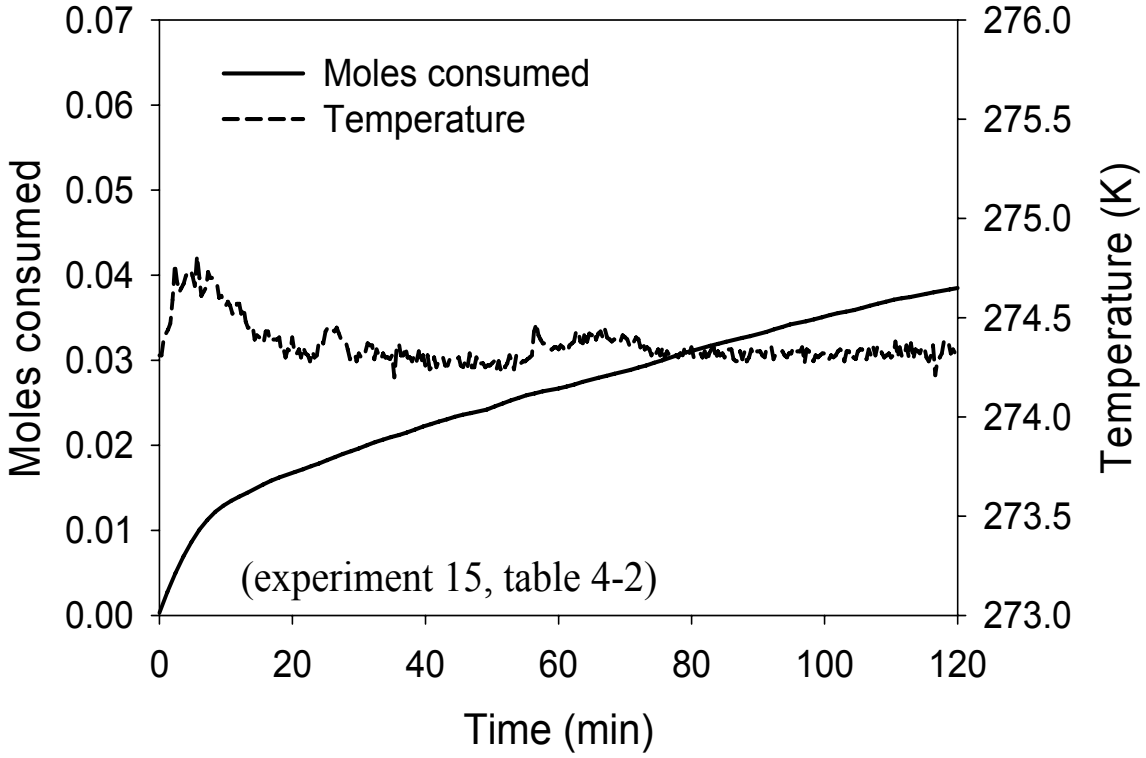

Figure C-15. Gas uptake measurement curve along with temperature profile.

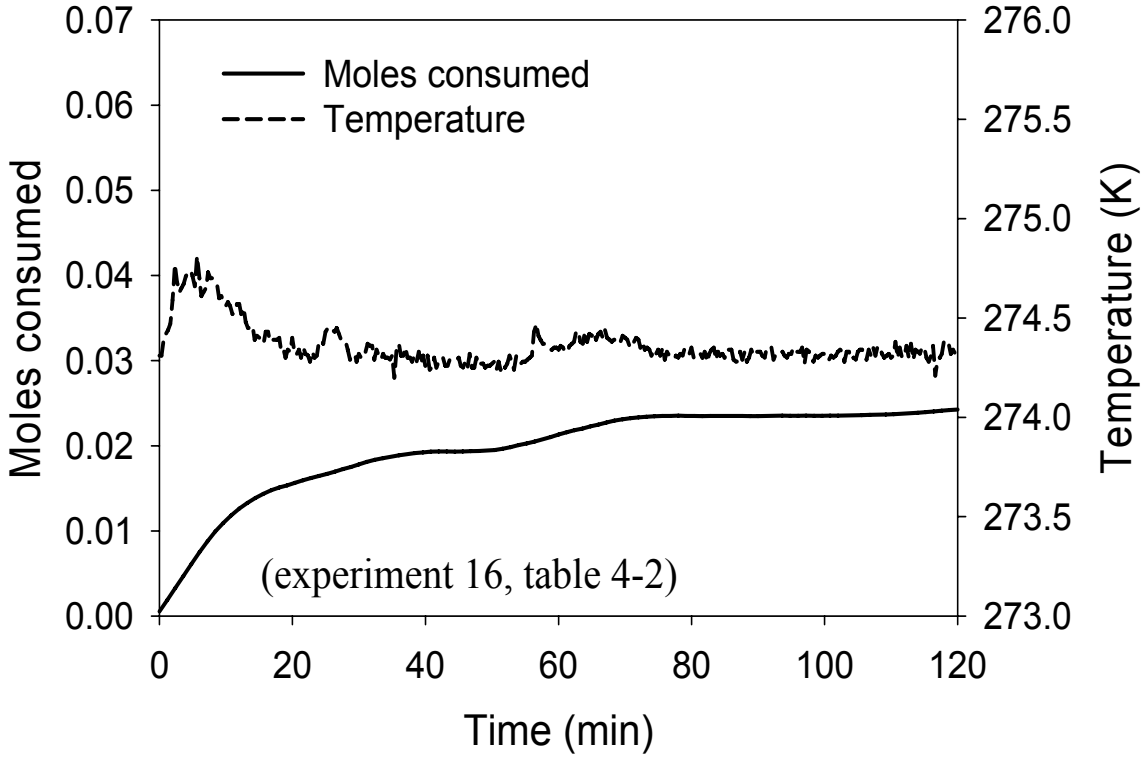

Figure C-16. Gas uptake measurement curve along with temperature profile.

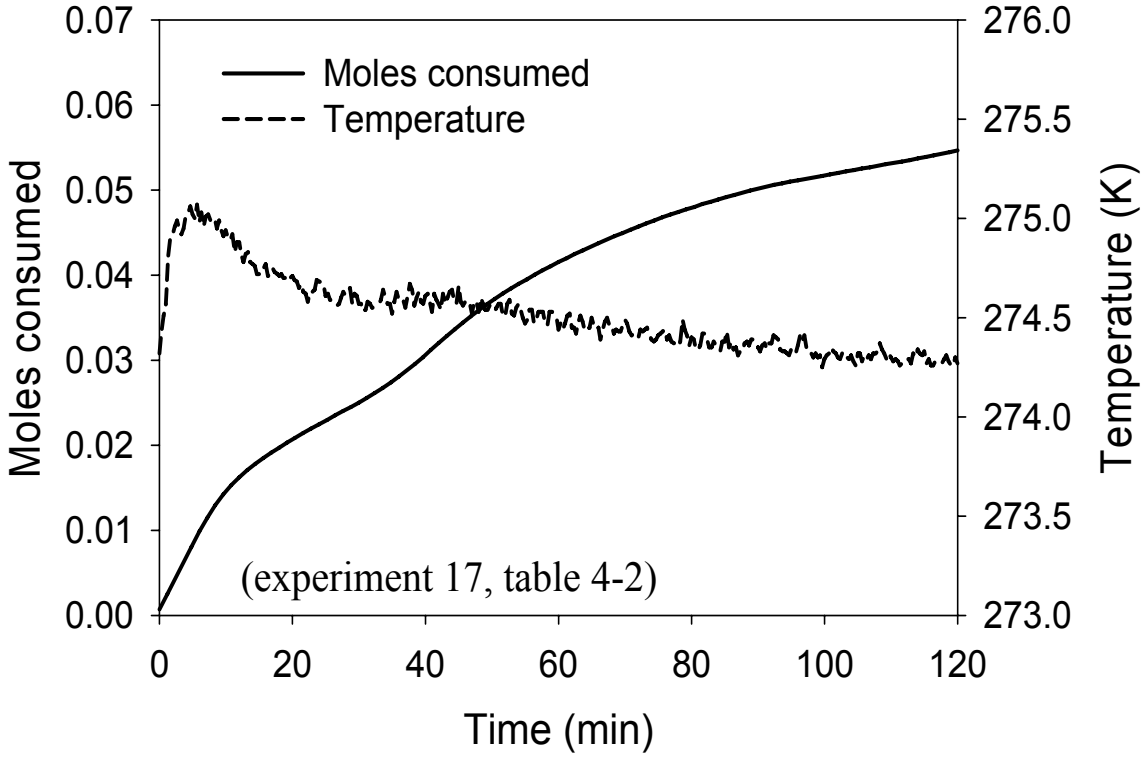

Figure C-17. Gas uptake measurement curve along with temperature profile.

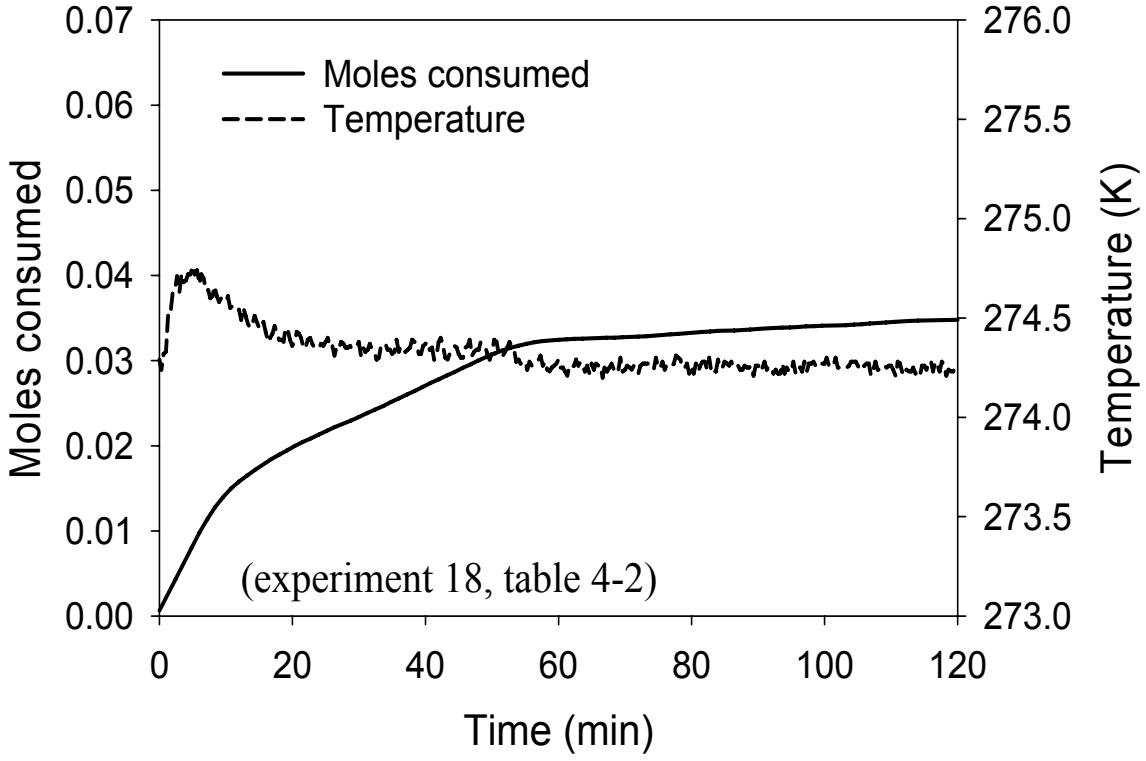

Figure C-18. Gas uptake measurement curve along with temperature profile.

Table C-1. The standard errors and the R^2 values for the calculated rates reported in Table 4-2.

Exp No	Rate (mol/min)	Standard error for rate	R^2
1	0.0008	0.000016	0.9748
2	0.0009	0.000021	0.9712
3	0.0013	0.000033	0.9656
4	0.0014	0.000028	0.9776
5	0.0005	0.000006	0.9919
6	0.0006	0.000008	0.9908
7	0.0010	0.000017	0.9823
8	0.0010	0.000019	0.9781
9	0.0012	0.000017	0.9875
10	0.0016	0.000021	0.9902
11	0.0008	0.000015	0.9826
12	0.0008	0.000012	0.9856
13	0.0007	0.000008	0.9924
14	0.0007	0.000009	0.9896
15	0.0007	0.000029	0.9007
16	0.0008	0.000030	0.9217
17	0.0009	0.000038	0.9220
18	0.0009	0.000043	0.8891

APPENDIX D

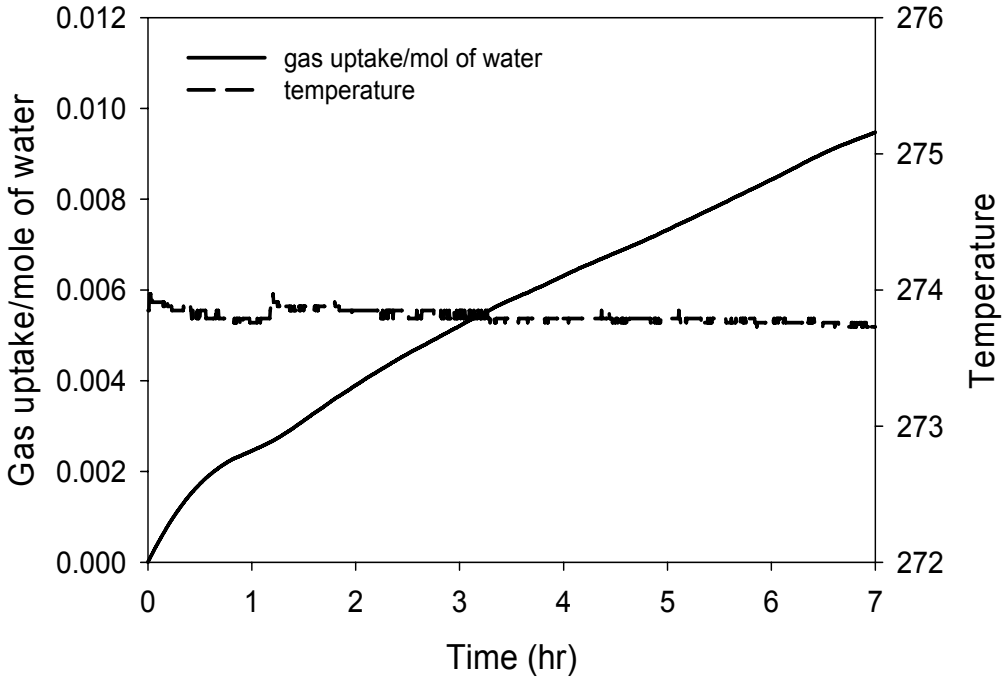

Figure D-1. Gas uptake measurement curve along with temperature profile (experiment 1, table 6-1).

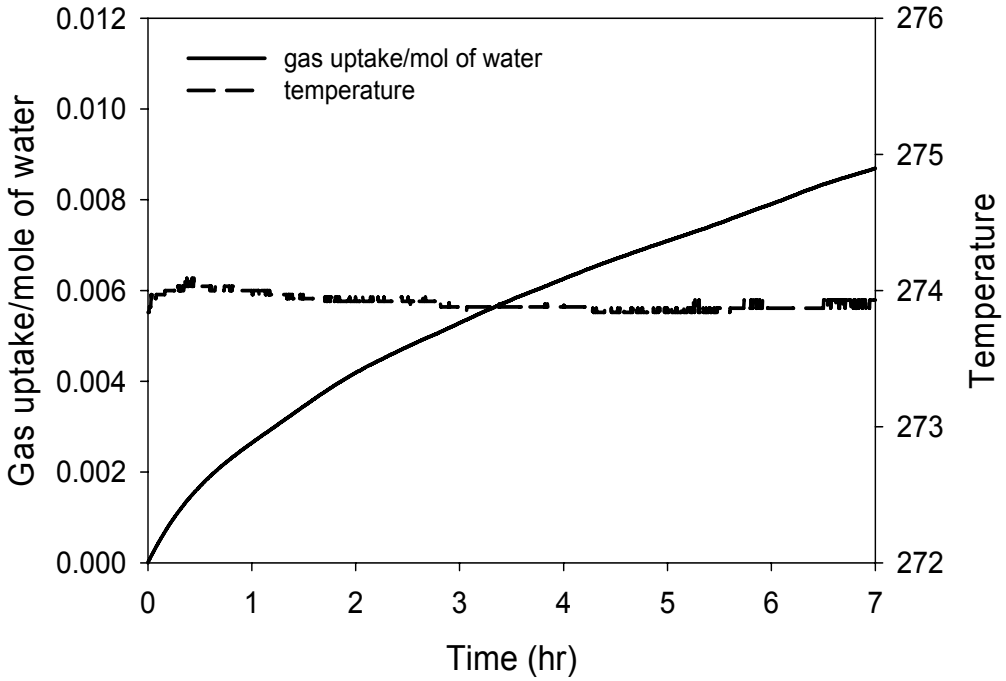

Figure D-2. Gas uptake measurement curve along with temperature profile (experiment 2, table 6-1).

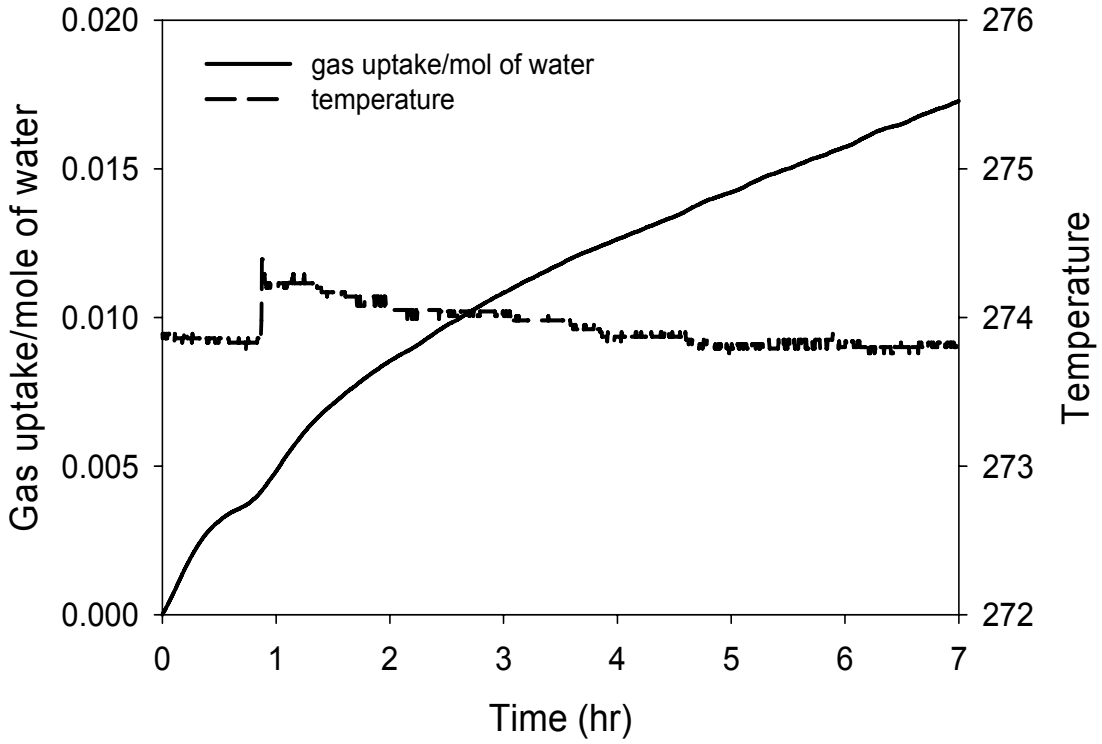

Figure D-3. Gas uptake measurement curve along with temperature profile (experiment 3, table 6-1).

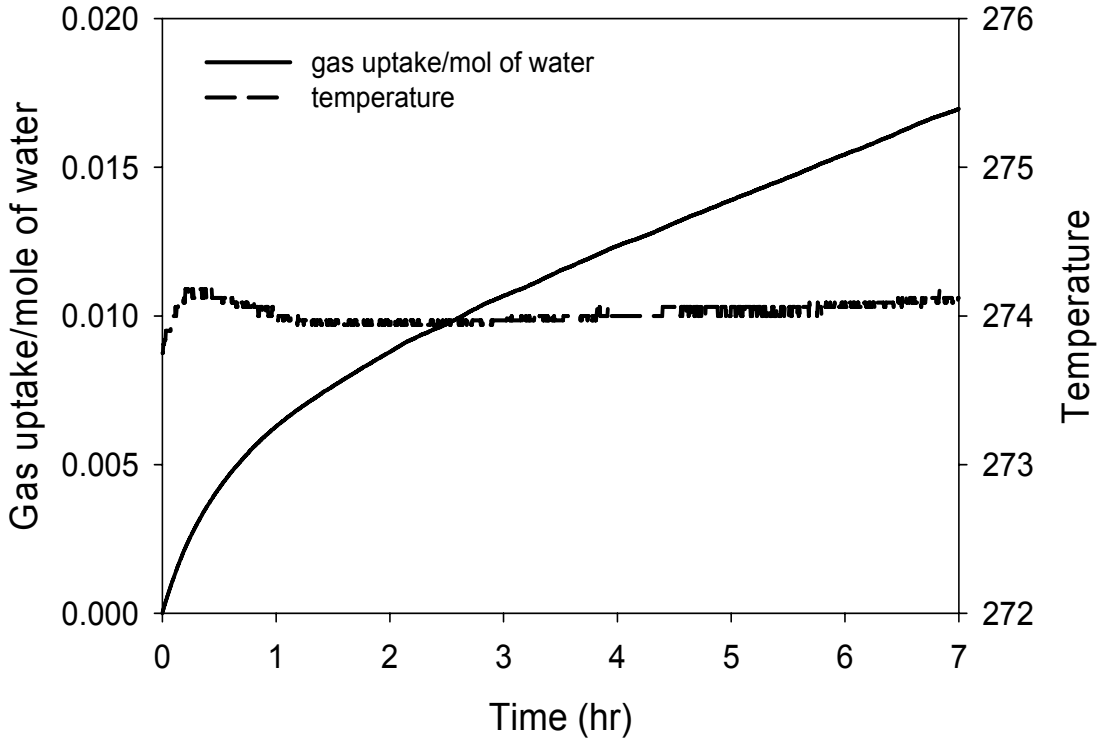

Figure D-4. Gas uptake measurement curve along with temperature profile (experiment 4, table 6-1).

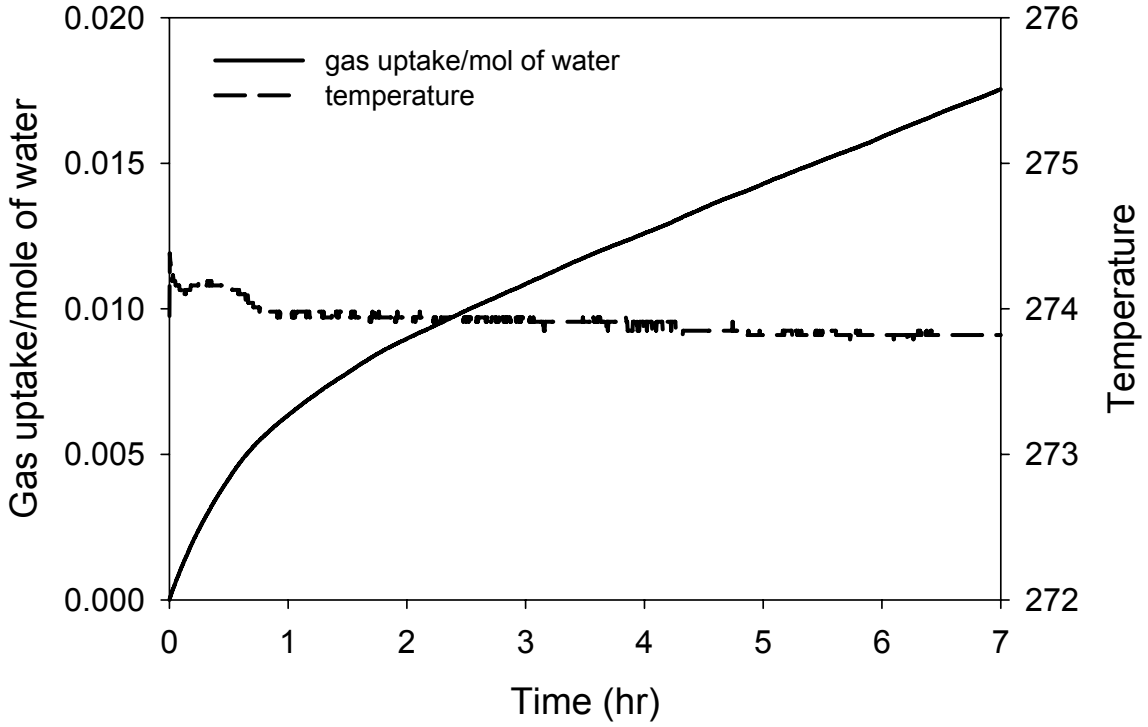

Figure D-5. Gas uptake measurement curve along with temperature profile (experiment 5, table 6-1).

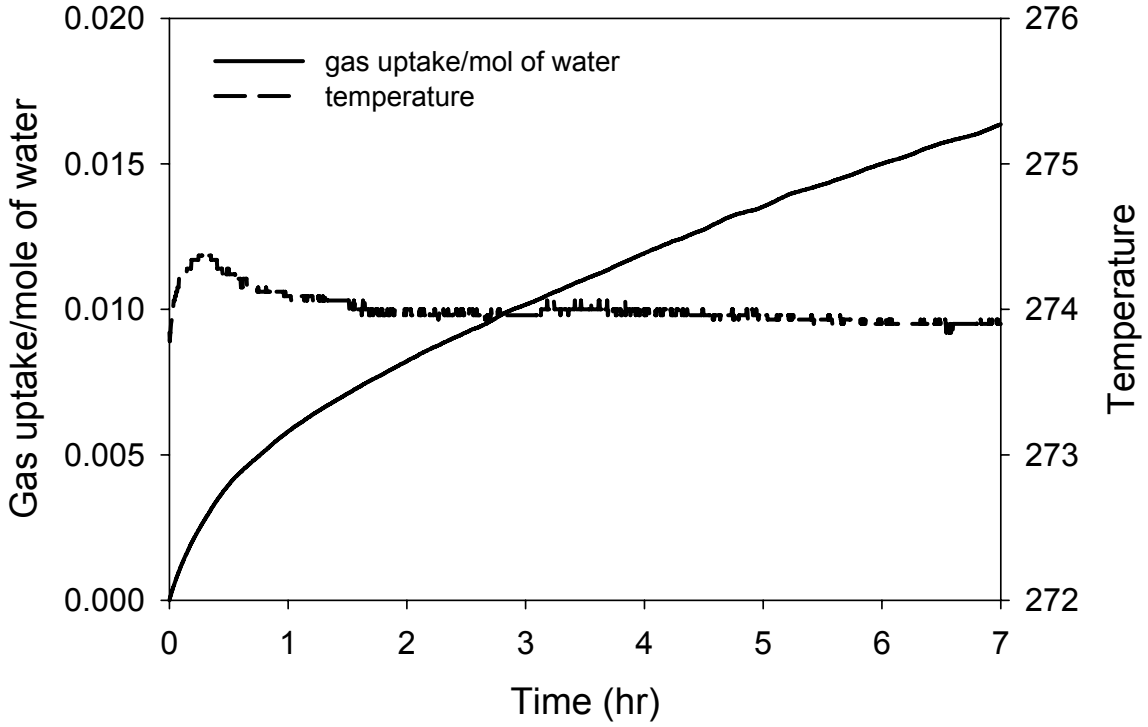

Figure D-6. Gas uptake measurement curve along with temperature profile (experiment 6, table 6-1).

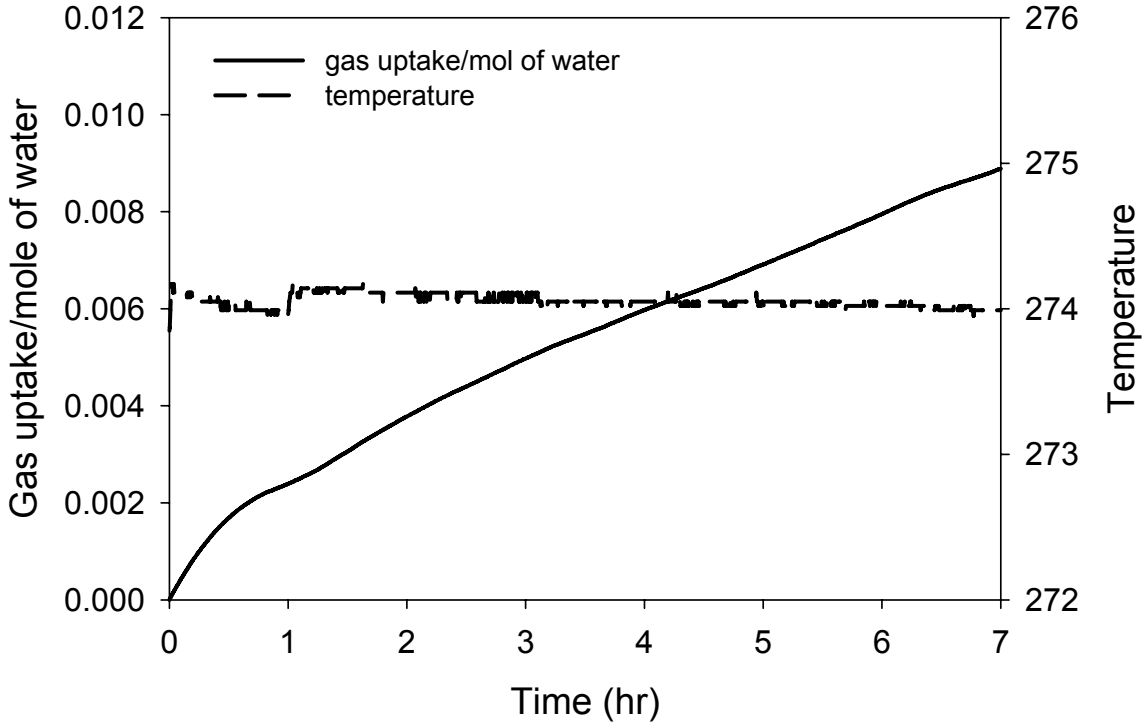

Figure D-7. Gas uptake measurement curve along with temperature profile (experiment 7, table 6-1).

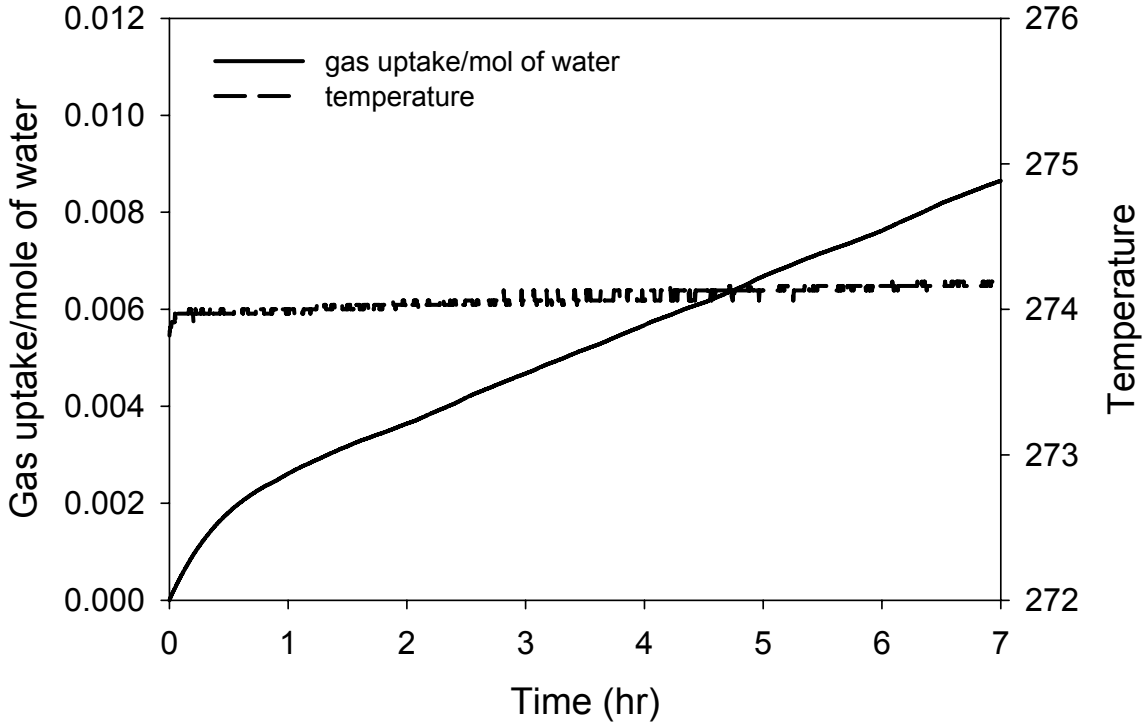

Figure D-8. Gas uptake measurement curve along with temperature profile (experiment 8, table 6-1).

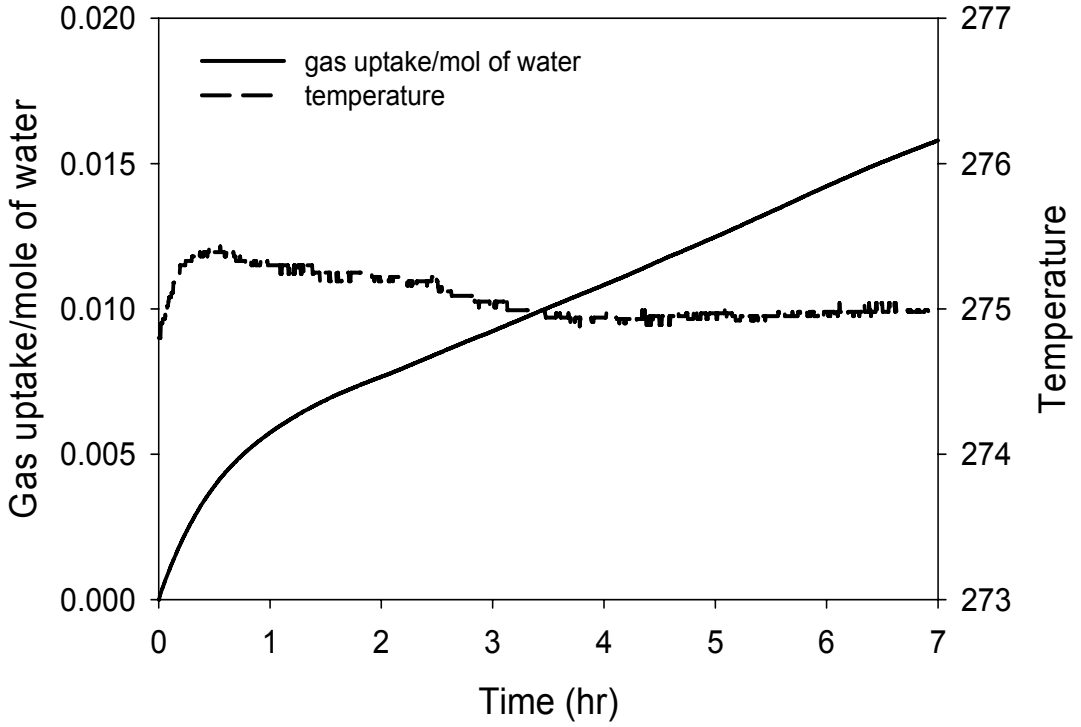

Figure D-9. Gas uptake measurement curve along with temperature profile (experiment 9, table 6-1).

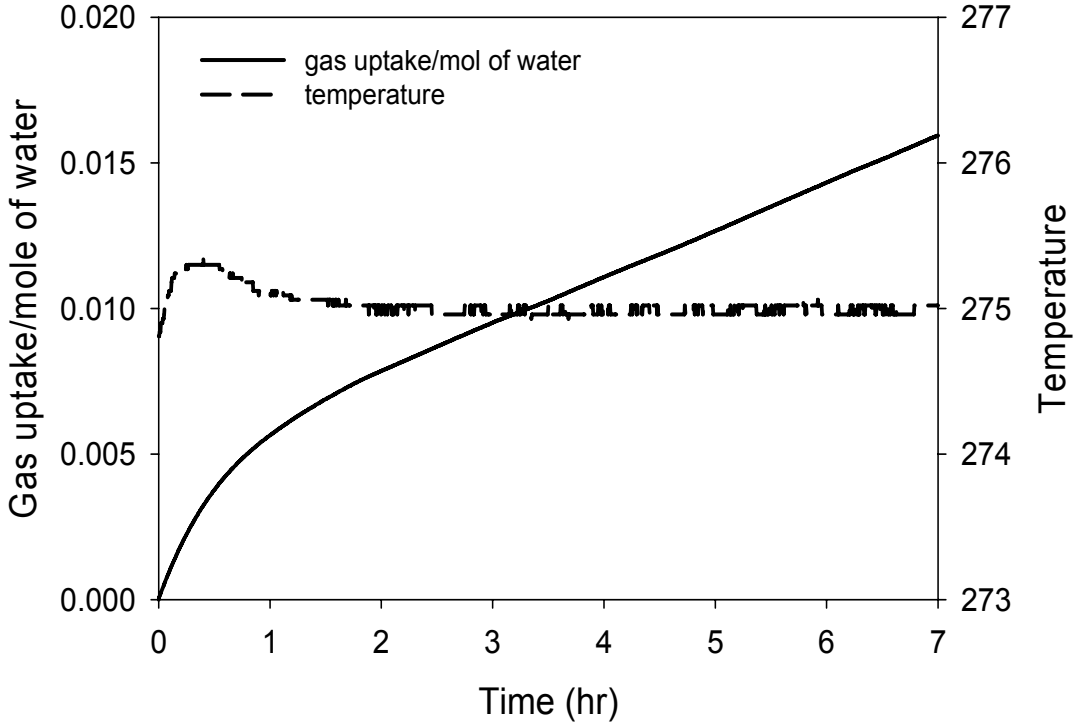

Figure D-10. Gas uptake measurement curve along with temperature profile (experiment 10, table 6-1).